COMPUTER SIMULATION OF SHIP WAVES

SHAOWEN SONG

COMPUTER SIMULATION OF SHIP WAVES

by

©Shaowen Song M. Eng. B. Eng.

A thesis submitted to the School of Graduate Studies

in partial fulfillment of the requirements for the

Degree of Doctor of Philosophy

Faculty of Engineering and Applied Science

Memorial University of Newfoundland

St. John's, Newfoundland, Canada A1B 3X5

January 1993

ISBN 0-315-91576-5

Abstract

In the present study a nonlinear boundary value problem for ship waves is obtained by transforming, through a Taylor's series expansion, the free surface condition of the exact ship wave problem from being satisfied on the actual free surface to being satisfied on the undisturbed fluid free surface. An iterative method based on the direct boundary integral theory and linear element techniques is developed to solve the transformed nonlinear boundary value problem. A numerical towing tank is developed using the iterative method. A visualization and animation system is also implemented in the numerical towing tank to produce the visual simulation effect.

In order to compare the present method with the existing ones and to study the linear models found in literature, a new linearized ship wave problem, as a special case of the present nonlinear ship wave problem, is also derived and solved in this investigation. Algorithms based on both the direct and the indirect boundary integral theories are developed to solve the present linearized ship wave problem.

The theoretical developments in the present study are mainly: the transformation of the free surface condition, the derivation of a new linearized ship wave problem, and the development of an iterative scheme for solving nonlinear boundary value problems. Beside these theoretical achievements, the development in numerical techniques and software design is also an important part of the present study, which includes the development of the algorithm for applying the direct boundary integral theory, the development of the linear element techniques, and the implementation of a visualization and animation system.

ACKNOWLEDGEMENT

I wish to express my sincere thanks to my supervisors Dr. R.E. Baddour, Dr. J.S. Pawlowski, and Dr. D.W. Bass for their valuable advice and continual encouragement.

It has been a great opportunity for me to work closely with Dr. Baddour and Dr. Pawlowski (Head of the Computational Hydrodynamics Laboratory, IMD/NRC) during the development of this work. I am indebted to them for enriching my mind through their broad knowledge on mathematics, naval architecture and computational hydrodynamics.

Special thanks are due to Dr. Bass for taking time to review the final draft of this thesis.

Appreciation is also directed to my friend Qi Xu who provided the offset data file for Series 60 ship hull.

Computations of this work were performed on the mini-supercomputer at the Computational Hydrodynamics Laboratory, IMD/NRC. Support and assistance from my friends and colleagues in the Laboratory Pat Dunphy and Piotr Waclawek are gratefully acknowledged.

TABLE OF CONTENTS

LIST OF FIGURES

LIST OF TABLE

LIST OF SYMBOLS

b	—	beam of the ship;
B_{NT}	—	width of the numerical towing tank;
B_T	—	width of experimental towing tank;
C_b	—	block coefficient, $C_B = U/(L_{pp}bd)$;
C_w	—	wave resistance coefficient, $C_w = R_w/\frac{1}{2}\rho SU^2$;
d	—	draft of the ship;
D_{NT}	—	depth of the numerical towing tank;
D_T	—	depth of the experimental towing tank;
F_n	—	Froude number, $F_n = U/\sqrt{gL}$;
g	—	acceleration due to gravity;
ℓ	—	streamline on $z = 0$;
H	—	nondimensional wave elevation $H = 2\eta g/U^2$;
L	—	length of the body or ship;
L_{NT}	—	length of the simulated section of the tank;
L_{pp}	—	ship length between perpendiculars;
L_T	—	length of experimental towing tank;
L_{wl}	—	design load waterline length;
n	—	unit surface normal;
n_x	—	x component of n;
N_x	—	x component of unit normal to an element;
nb	—	total number of streamlines on the free surface mesh;
ne	—	total number of elements on the body surface mesh;
nn	—	total number of nodes on the body surface mesh;

net	—	total number of elements on both of body surface and fluid free surface meshes;
nnt	—	total number of nodes on both of the body surface and fluid free surface meshes;
P	—	pressure;
p	—	field point;
R_w	—	wave resistance;
U	—	the velocity of the moving body or ship;
U_ℓ	—	fluid velocity along ℓ direction;
$\bar{u}$	—	x component of the velocity of double-body flow;
$\bar{v}$	—	y component of the velocity of double-body flow;
$\bar{w}$	—	z component of the velocity of double-body flow;
u'	—	x component of the velocity of perturbation;
v'	—	y component of the velocity of perturbation;
w'	—	z component of the velocity of perturbation;
u	—	x component of total fluid velocity;
v	—	y component of total fluid velocity;
w	—	z component of total fluid velocity;
x_L	—	nondimensional coordinate along the ship;
x	—	horizontal axis of Cartesian system;
y	—	horizontal axis perpendicular to x;
z	—	vertical (upwards) axis of Cartesian system;
$\bar{\Phi}$	—	double-body potential;
ϕ'	—	velocity potential perturbation;

ϕ	—	total velocity potential;
$\phi_n = \frac{\partial \phi}{\partial n}$	—	normal derivative of total velocity potential;
η	—	surface elevation;
σ	—	single-layer source density;
μ	—	double-layer source density.

1 INTRODUCTION

1.1 Background

The investigation of free surface waves generated by a moving object, floating or submerged, and the corresponding wave resistance to the object, i.e. the ship wave problem, is a classical problem in fluid mechanics and ship hydrodynamics. The subject has caught the interests of hydrodynamists, naval architects and mathematicians for a long time. Although the wave pattern with its distinct structure seems to be well suited to a mathematical treatment, a mathematical solution of the problem is almost impossible to find without introducing simplifications to the problem.

One of the main simplified mathematical models of the ship wave problem is the so-called Neumann-Kelvin problem which is a linear boundary value problem. Except for the fundamental assumption of potential fluid flow, an important assumption of the Neumann-Kelvin ship wave problem is that the ship has to be "thin". Although the Neumann-Kelvin problem is a linear boundary value problem, analytical solutions to the problem are still difficult to find for a real ship which usually involves a complicated curved wetted surface. Further simplifications are, therefore, also introduced with respect to the geometry of the ship surface so that a mathematical solution could be obtained, such as: the thin ship theory which substitutes the real ship surface by a single vertical plane located at the center of the ship, the flat ship theory which simplifies the ship surface into a horizontal plane. A similar idea is also used in the slender ship theory. For the submerged body cases of spheres and ellipsoids analytical solutions could

be obtained by directly satisfying the body surface condition on the real body surface.

Because of the introduction of the above mentioned simplifications the applications of theoretical solutions are extremely limited. Theoretical calculations of the wave-making resistance of ships cannot yet be done with sufficient accuracy to replace model testing. So far, ship designers have to rely on experiment, and the theoretical solutions are valuable to help engineers to analyse and understand the experimental results (Manen and Oossanen, 1988).

With the general availability of computers, the treatment of ship wave problems has been shifting towards methods with large numerical contents that permit lesser simplifications in forming the mathematical model in comparison with the theoretical analyses. Two major mathematical models have been widely used in the numerical modelling of the ship wave problem. They are the Neumann-Kelvin and Dawson's linearized ship wave models. Both of these two models are in the form of linear boundary value problems. The numerical techniques used for solving these two boundary value problems are mainly the boundary element method, the finite difference method and the finite element method, of which the boundary element method also referred to as the boundary integral method or panel method seems to be the most popular and the most successful one (Raven 1988, 1992).

In the numerical treatment of the Neumann-Kelvin problem, the impermeability condition on the ship wetted surface is applied exactly on the ship surface location without any simplification. The fluid free surface condition is the same as the one used in the thin ship theory which requires the ship to be thin. Therefore

the applications of numerical modelling of ship wave problems based on solving the Neumann-Kelvin problem are still limited to thin ships. It is not clear how much the results can be improved in comparison with the thin ship theory by using the exact ship surface condition and keeping the thin ship free surface condition.

A main numerical procedure developed to solve the Neumann-Kelvin linear ship wave problem is the so-called Kelvin source method which could be classified as an indirect boundary integral method (Brebbia 1984, Wardle 1981). Being one of the early numerical modelling methods in ship wave pattern analysis and wave-making resistance computation, the numerical approaches based on solving the Neumann-Kelvin problem have been investigated, developed and applied by many researchers. This resulted in an extensive literature on the subject. These results have provided a huge amount of information contributing to a better understanding of the wave pattern and the wave-making resistance of ships. However problems are also found in the application of this method. One problem is the lack of agreement among the results produced by different formulations of the Green's function used in this method. Large differences were also found in the computations when using the same Green's function to solve the same Neumann-Kelvin problem (see, Baar 1986). The other problem is that the "thin" ship requirement makes the method usually not applicable to practical ship forms.

In order to overcome the thin ship restriction resulting from the fluid free surface condition in the Neumann-Kelvin problem, Dawson (1977) developed a linearized free surface condition based on the double-body flow. This idea had been developed and used in fluid mechanics, and also applied to solve the ship wave

problem by Gadd (1975). By introducing the double-body streamlines, Dawson simplified a three dimensional free surface condition into a two dimensional one which provided opportunities and advantages for the development of numerical approaches to solve the problem. A one-sided four-point finite difference formula was also applied by Dawson to impose the wave radiation condition. These two aspects are considered to be the most important contributions by Dawson.

Since Dawson's free surface condition is more complicated than the one found in the Neumann-Kelvin problem, it is difficult to find a Green's function to satisfy this free surface condition if the Kelvin source method is used to solve the boundary value problem. The Rankine source method, which is also considered as an indirect boundary integral approach, was used by Dawson and many others to solve Dawson's linear ship wave problem.

When the double-body flow perturbation is applied to linearize the free surface condition, two steps are usually involved. Firstly, the free surface condition satisfied on the actual wavy fluid free surface has to be transformed to a condition satisfied on the undisturbed fluid free surface. And secondly, the transformed nonlinear free surface condition satisfied on the undisturbed fluid free surface must be linearized by a perturbation based on the double-body velocity potential. In Dawson's linearization procedure, the fluid free surface condition satisfied on the actual wavy free surface is applied directly on the undisturbed fluid free surface without any treatment before the linearization. This is equivalent, as has been shown by Nakos (1990) and will also be shown in the present study, to keeping only the first term, namely the zero order term in η, in a Taylor's series expansion of the free surface condition about the undisturbed fluid surface

and then performing the linearization. Because of this approximation in Dawson's linear free surface condition, the application of Dawson's linear ship wave problem is still limited to solutions for relatively thin ships. Discussion on Dawson's linearized free surface condition have been presented by Nakos (1990) and Pawlowski (1992a). Comparisons of Dawson's linearized ship wave problem with the linearized ship wave problem developed in the present work and experimental data will be presented in this thesis.

To increase the accuracy of the linearization and fully take advantage of the double-body perturbation, Nakos and Sclavounos (1991) developed a linearized free surface condition by transforming the fluid free surface condition satisfied on the actual fluid free surface to the undisturbed fluid free surface condition through a Taylor's series expansion. Computations have been carried out by Nakos and Sclavounos (1991) and good results have been reported for a modified Wigley hull.

Attempts have been made in the literature to solve the nonlinear ship wave problem by an iteration scheme, such as by Ogiwara (1985), Ni (1987), Jensen, Mi and Soding (1986), Kim (1989), Kim and Lucas (1990), and most recently by Raven (1992). The full theoretical foundation of this approach is not clear and has never been discussed in these studies. The convergence of the iteration has been reported to be a major problem in applications of this method. A so-called relaxation factor had to be used in most of these computations to force the convergence of the iterations.

A new theory for solving the nonlinear ship wave problem by using a one-to-one fluid domain transformation technique has been developed by Pawlowski

(1992a). The transformed nonlinear boundary value problem is solved by a nonlinear perturbation method developed by Pawlowski (1992b). In this theory not only the nonlinearity of the waves has been considered but also the slope of the ship hull, which provides a better modelling of the physical problem. The development of the theory and some of the applications have been reported by Pawlowski (1992a, 1992b). Some applications of this theory are also presented in Chapter 6 of the present thesis.

1.2 The Present Investigation

In the present study, the fluid free surface condition of the exact ship wave problem is transformed from being satisfied at the actual wavy fluid free surface to being satisfied at the undisturbed fluid free surface $z = 0$ by means of a Taylor's series expansion. The transformed nonlinear boundary value problem is then solved by an iterative method developed in the present study. All the cases computed in the present study are convergent and, as will be shown in the following chapters, the computed results are in good agreement with experimental data.

In order to compare the present method with the existing methods and to study the linear models found in the literature, a linear ship wave problem obtained by linearizing the present transformed nonlinear problem is also derived and solved in the present study. Since the present linearized free surface condition is based on the transformed free surface condition which keeps higher order (in η) terms in the Taylor's series expansion, the present linear model gives better results in comparison with Dawson's and other linear models.

To accurately model the ship wave pattern and compute the wave-making resistance, one needs not only a good mathematical model, but also an efficient, robust and accurate numerical approach to solve the mathematical problem. In the present study two numerical approaches are developed. One is based on the direct boundary integral formulation and the other is based on the indirect boundary integral formulation. In both of these approaches the linear element techniques are used. The linear element techniques distribute unknowns (source-densities in the indirect formulation; velocity potentials and their normal derivatives in the direct formulation) at the nodes and linearly vary the unknowns over each panel on the surface mesh. Triangular panels are used in both of these approaches, which give an easy and accurate panelization of surfaces and allow the linear variation of unknowns over each panel.

Because the unknowns are defined at the nodes of the triangular mesh instead of at the centroids of panels, both the fluid free surface condition and the impermeability body surface condition are satisfied on the design load waterline of the considered ship. In the present study these two conditions are satisfied simultaneously at the exact location of the waterline. This has not been studied and applied in the literature.

The idea of linear elements has been discussed in boundary integral theories dealing with the subject of boundary value problems, (see Wardle 1981, for instance). However, the technique has not been applied in the numerical algorithm to solve surface ship wave boundary value problems. Baddour (1989) developed a system of algorithms using three-node triangular linear elements to solve potential problems. Theories and techniques for three-node triangular linear elements

were developed in that work, such as the conectivity system for three-node triangular elements and analytical integrations of linear unknown distributions. The present study is based on Baddour's three-node triangular linear element algorithm. The complexity of the linear element algorithm is much higher than that of the constant element algorithm found in the literature. However, the drawbacks inherent in the constant element algorithm, such as the collocation points being away from the actual boundary, the variables between panels being discontinuous, and the panelization being inaccurate, are overcome. Therefore, more accurate computational results can be obtained by applying the linear element techniques.

The direct boundary integral method relates the velocity potential and its normal derivative on the boundary of the domain under consideration. Since the velocity potential and its normal derivative are the values directly related to the solution of the problem, the method is called the direct method or direct formulation to distinguish it from the indirect formulation which seeks the solution to the problem through an intermediate source density distributed on the boundary. Even though the direct boundary integral formulation has significant advantages for solving the free surface ship wave problem, the method has never been used in the literature. In the present study a numerical towing tank is developed based on the direct boundary integral formulation. In a sense it simulates the process of ship model testing in a towing tank. In particular the wave pattern and the wave-making resistance are computed by including the effects of the existence of the side walls and the bottom of the tank. Therefore the numerical results are directly comparable with laboratory measurements.

In order to enhance the interpretation of the results obtained from the computation, techniques of visualization and animation of ship motion and related physical parameters, such as pressure distribution on the surface of ship hull and velocity field in the fluid, are also developed in the present study based on a software package called Advanced Visual System (AVS). Through the visualization and animation numerically simulated towing tanks give the same or even a better representation of physical effect in comparison with a real towing tank in a laboratory.

1.3 Outline of the Thesis

This thesis is organized into eight chapters. Following this introduction, in Chapter 2, a review is presented on the topics of the linearized ship wave boundary value problems, namely the Neumann-Kelvin problem, Dawson's linear problem and the linear ship wave problem developed by Nakos and Sclavounos (1991). The corresponding numerical methods for solving these linear problems (the Kelvin source and the Rankine source methods) are also presented. A review of the one-to-one domain transformation and nonlinear perturbation theories developed by Pawlowski (1992a, 1992b) is detailed in this chapter. The iterative panel method based on the Rankine source theory developed by several authors is also reviewed in this chapter.

In Chapter 3, the formulations of the problems solved in the present study are presented. These include: the transformation of the free surface condition from being satisfied at the actual fluid free surface to being satisfied at the undisturbed fluid surface by means of a Taylor's series expansion, the derivation of a new

linearized free surface condition based on the present transformed nonlinear free surface condition, and the formulation of an iterative scheme for solving the transformed nonlinear ship wave problem.

A general discussion of the direct and indirect boundary integral formulations and a comparison between these two formulations are presented in Chapter 4 of this thesis.

In Chapter 5, the development of the present indirect and direct boundary integral algorithms for solving the linearized ship wave problem developed in Chapter 3 are presented. Applications and comparisons are also presented in this chapter.

In Chapter 6, an iterative scheme for solving the nonlinear ship wave problem (a nonlinear numerical towing tank) is developed. Comparisons with the linear results obtained in the present study, the nonlinear results found in the literature, and experimental data are also presented.

In Chapter 7, the computer visualization and animation of the computed results are presented.

Finally, in Chapter 8, conclusions and recommendations are presented as the results of the present investigation.

Four appendices are also provided in this thesis to detail some of the contents involved in the development of the present algorithms.

A list of references is attached, which is organized in alphabetical order.

2 LITERATURE REVIEW

2.1 The Exact Ship Wave Problem

Although the generation of ship waves and the corresponding wave resistance depend on both the presence of the gravitational force field and the viscosity of the fluid, investigations of this problem so far are mainly based on potential theory, i.e. the fluid under consideration is regarded as homogeneous, incompressible and inviscid. In other words, it is supposed that the effects of viscosity on the formation of ship waves are negligible and the wave resistance is a function of the Froude number alone. Irrotational flow is also assumed in formulating the problem. The usefulness of the investigation of this simplified problem may be seen as follows. For most ships advancing at a sufficiently low velocity the viscous resistance cannot be significantly reduced by changing the hull form and this leaves the ship designers more or less free to choose a suitable hull form (from a resistance point of view). Optimal ship forms are those which generate the smallest waves and it is therefore highly desirable to develop a theoretical tool to analyse the relationship between wave resistance and the geometry of the ship's hull, (see Baar, 1986). The wave generation problem is also an important part of more advanced problems of ship motions in waves. Therefore it is relevant to a broad range of seakeeping and structural response problems.

It is convenient to describe the steady ship motion by fixing the system of coordinates (x, y, z) with the ship which has a velocity of advance U in space. The coordinate system is located such that axis x is in the ship velocity direction and axis z directs upwards from the design load waterline. The exact or almost exact,

(see Wehausen 1973, Baar 1986), boundary value problem of steady ship waves established by the potential theory is then described by the following equations.

The governing field equation is

$$\nabla^2\phi = 0, \tag{2.1}$$

where $\phi = \phi(x, y, z)$ is the velocity potential within the fluid domain.

The impermeability body surface condition is given as:

$$\vec{n} \cdot \nabla\phi = 0, \tag{2.2}$$

on the wetted body surface, and $\vec{n}$ represents the unit normal vector directed out of the fluid domain.

The boundary conditions to be satisfied on the free surface of the water $z = \eta$, are of the form (Newman 1977, Pawlowski, 1992a) :

$$g\frac{\partial\phi}{\partial z} + \frac{1}{2}\nabla\phi \cdot \nabla(\nabla\phi \cdot \nabla\phi) = 0, \tag{2.3}$$

$$g\eta + \frac{1}{2}[(|\nabla\phi|)^2 - U^2] = 0. \tag{2.4}$$

where U represents the velocity of the ship.

The velocity potential ϕ must also satisfy the condition at infinity. This condition requires that

$$|\nabla\phi| \to -U \quad when \quad z \leq 0, \quad \sqrt{x^2 + y^2 + z^2} \to \infty. \tag{2.5}$$

Finally, to ensure a unique solution, we must also impose the physically acceptable (radiation) condition that no waves are propagated upstream from the body.

To summarize the above equations the exact ship wave problem is written as:

$$\begin{cases} \nabla^2\phi = 0, & \textit{in the fluid domain}; \\ \vec{n}\cdot\nabla\phi = 0, & \textit{on the body surface}; \\ g\frac{\partial\phi}{\partial z} + \frac{1}{2}\nabla\phi\cdot\nabla(\nabla\phi\cdot\nabla\phi) = 0, & \textit{on } z = \eta; \\ |\nabla\phi| \to -U, \quad z \le 0 \textit{ and } \sqrt{x^2+y^2+z^2} \to \infty; & \\ \textit{The radiation condition.} & \end{cases} \tag{2.6}$$

From (2.4) the wave elevation η is given by

$$\eta = -\frac{1}{2g}[(|\nabla\phi|)^2 - U^2], \qquad z = \eta. \tag{2.7}$$

System of equations (2.6) defines a nonlinear boundary value problem with an unknown boundary (free surface) location. It is not easy to find an analytical solution to the problem without introducing simplifications. Those methods which have been applied to solve the problem usually entail some kind of simplifying assumptions, such as thin ship and low speed assumptions. Many mathematicians and naval architects have expended considerable efforts in developing an adequate solution to the problem by applying different methods and simplifications, such as theories developed by Michell, Kelvin, Havelock, Hogner, Peters, Ursell, Kochin, Bessho, Farell, Guttmann, and Guilloton to mention but a few. All their contributions, and many others, form an extensive literature on the analytical treatment of the problem, which has been reviewed comprehensively by Wigley (1949), Lunde (1951), Inui (1962), Sabuncu (1962), Weinblum (1963), Guilloton (1964), Kostyukov (1968), Gadd (1968), Wehausen (1973), Newman (1976), and Baar (1986).

It is the objective of the present review to present a general survey of the formulations of the linear mathematical models of the ship wave problem and of corresponding numerical treatments, as well as the theories and numerical methods for solving nonlinear ship wave problems.

2.2 Neumann-Kelvin Linearized Problem

The procedure for linearization of the exact ship wave problem to obtain the Neumann-Kelvin linearized problem can be explained as follows:

1. Expanding the combined free surface condition (2.3) in a Taylor's series expansion about the undisturbed fluid free surface and keeping only the zero order terms in η, we have

$$g\frac{\partial \phi}{\partial z} + \frac{1}{2}\nabla\phi \cdot \nabla(\nabla\phi \cdot \nabla\phi) = 0, \qquad on\ z = 0. \tag{2.8}$$

2. Assuming the velocity potential ϕ to be composed of a uniform flow $(-U)$ and a perturbation ϕ', that is $\phi = -Ux + \phi'$, and substituting for ϕ into equation (2.8) gives

$$\frac{1}{2}\nabla(-Ux + \phi') \cdot \nabla[\nabla(-Ux + \phi') \cdot \nabla(-Ux + \phi')] + g\frac{\partial}{\partial z}(-Ux + \phi') = 0, \ on\ z = 0. \tag{2.9}$$

3. Dropping the nonlinear terms in ϕ', equation (2.9) becomes:

$$U^2\frac{\partial^2 \phi'}{\partial x^2} + g\frac{\partial \phi'}{\partial z} = 0, \qquad on\ z = 0. \tag{2.10}$$

The exact problem is then represented by a linear boundary value problem which is called the Neumann-Kelvin problem, (see Brard 1971, 1974a,b, Baar

and Price 1988). Expressing the variables in the coordinate system fixed with the moving ship, the Neumann-Kelvin linear problem is then described in terms of ϕ' as:

$$\begin{cases} \nabla^2\phi' = 0, & \textit{in the fluid domain;} \\ \vec{n}\cdot\nabla\phi' = Un_x, & \textit{on the body surface;} \\ U^2\frac{\partial^2\phi'}{\partial x^2} + g\frac{\partial\phi'}{\partial x} = 0, & \textit{on } z = 0; \\ |\nabla\phi'| \to 0, \qquad z \le 0 \ \textit{and} \ \sqrt{x^2+y^2+z^2} \to \infty; & \\ \textit{The radiation condition.} & \end{cases} \tag{2.11}$$

In boundary value problem (2.11), n_x represents the x component of $\vec{n}$.

The wave elevation is given by

$$\eta = \frac{1}{g}U\nabla\phi', \qquad z = 0. \tag{2.12}$$

The body surface condition in boundary value problem (2.11) is of Neumann type. The linear free surface condition in this problem was first investigated by Lord Kelvin in the context of the thin ship theory, (see Thomson 1887). The radiation condition of the exact ship wave problem should also be imposed to ensure a unique solution for this linear boundary value problem.

2.3 Dawson's Linearized Problem

Dawson's linearized free surface condition is obtained by directly applying the kinematic and dynamic free surface conditions on the undisturbed free surface $z = 0$ before the linearization. The combined free surface condition satisfied on $z = 0$ is obtained by eliminating η from the kinematic and dynamic free surface

conditions. And then the combined free surface condition satisfied on $z = 0$ is linearized based on the double-body flow. Although the elimination procedure used by Dawson is inappropriate mathematically (see Newman 1977), the result is correct for the accuracy of zero order in η. This is because of $\partial\bar{\Phi}/\partial z = 0$ on $z = 0$ in this particular case. In this section, the simple steps given by Dawson (1977) to obtain his linearized free surface condition are repeated without any change. The derivation of Dawson's linearized free surface condition through a mathematically consistent approach will be shown in Chapter 3, where a new linearized free surface condition is derived.

We follow the procedure described by Dawson (1977). For a three-dimensional problem, the free surface conditions are linearized in terms of the double-body velocity potential $\bar{\Phi}$, that is, $\phi = \bar{\Phi} + \phi'$ and nonlinear terms in ϕ' are dropped. Also the free surface conditions are applied at $z = 0$, not at the free surface. When η is eliminated, the kinematic and dynamic free surface conditions reduce to:

$$\frac{1}{2}\{\frac{\partial\phi}{\partial x}\frac{\partial}{\partial x}[(\frac{\partial\phi}{\partial x})^2 + (\frac{\partial\phi}{\partial y})^2 + (\frac{\partial\phi}{\partial z})^2] + \frac{\partial\phi}{\partial y}\frac{\partial}{\partial y}[(\frac{\partial\phi}{\partial x})^2 + (\frac{\partial\phi}{\partial y})^2 + (\frac{\partial\phi}{\partial z})^2]\} + g\frac{\partial\phi}{\partial z} = 0. \tag{2.13}$$

Now for any function F

$$\frac{\partial\bar{\Phi}}{\partial x}\frac{\partial F}{\partial x} + \frac{\partial\bar{\Phi}}{\partial y}\frac{\partial F}{\partial y} = \frac{\partial\bar{\Phi}}{\partial \ell}\frac{\partial F}{\partial \ell}. \tag{2.14}$$

where ℓ represents the double-body streamline on $z = 0$.

Thus the free surface condition becomes

$$\begin{aligned}\frac{1}{2}\{\frac{\partial\bar{\Phi}}{\partial\ell}\frac{\partial}{\partial\ell}[(\frac{\partial\bar{\Phi}}{\partial\ell})^2 + 2\frac{\partial\bar{\Phi}}{\partial\ell}\frac{\partial\phi'}{\partial\ell}] + \frac{\partial\phi'}{\partial x}\frac{\partial}{\partial x}[(\frac{\partial\bar{\Phi}}{\partial x})^2 + (\frac{\partial\bar{\Phi}}{\partial y})^2] \\ + \frac{\partial\phi'}{\partial y}\frac{\partial}{\partial y}[(\frac{\partial\bar{\Phi}}{\partial x})^2 + (\frac{\partial\bar{\Phi}}{\partial y})^2]\} + g\frac{\partial\phi'}{\partial z} &= 0, \end{aligned} \tag{2.15}$$

but

$$\frac{1}{2}\{\frac{\partial\phi'}{\partial x}\frac{\partial}{\partial x}[(\frac{\partial\bar{\Phi}}{\partial x})^2+(\frac{\partial\bar{\Phi}}{\partial y})^2]+\frac{\partial\phi'}{\partial y}\frac{\partial}{\partial y}[(\frac{\partial\bar{\Phi}}{\partial x})^2+(\frac{\partial\bar{\Phi}}{\partial y})^2]\}$$

$$= \frac{\partial\bar{\Phi}}{\partial\ell}\frac{\partial}{\partial\ell}(\frac{\partial\bar{\Phi}}{\partial\ell}\frac{\partial\phi'}{\partial\ell})-(\frac{\partial\bar{\Phi}}{\partial\ell})^2\frac{\partial^2\phi'}{\partial\ell^2}$$

$$= \frac{\partial\bar{\Phi}}{\partial\ell}\frac{\partial^2\bar{\Phi}}{\partial\ell^2}\frac{\partial\phi'}{\partial\ell} \tag{2.16}$$

so that

$$(\frac{\partial\bar{\Phi}}{\partial\ell})^2\frac{\partial^2\bar{\Phi}}{\partial\ell^2}+\frac{\partial}{\partial\ell}[(\frac{\partial\bar{\Phi}}{\partial\ell})^2\frac{\partial\phi'}{\partial\ell}]+g\frac{\partial\phi'}{\partial z}=0. \tag{2.17}$$

Now replace ϕ' with $\phi-\bar{\Phi}$ to get

$$\frac{\partial}{\partial\ell}[(\frac{\partial\bar{\Phi}}{\partial\ell})^2\frac{\partial\phi}{\partial\ell}]+g\frac{\partial\phi}{\partial z}=2(\frac{\partial\bar{\Phi}}{\partial\ell})^2\frac{\partial^2\bar{\Phi}}{\partial\ell^2}. \tag{2.18}$$

Rewriting equation (2.18) and combining the rest of the equations in the exact ship wave boundary value problem, Dawson's linearized ship wave problem is then obtained as:

$$\begin{cases} \nabla^2\phi=0, & \textit{in the fluid domain;}\\ \vec{n}\cdot\nabla\phi=0, & \textit{on the body surface;}\\ A_D\frac{\partial^2\phi}{\partial\ell^2}+B_D\frac{\partial\phi}{\partial\ell}+g\frac{\partial\phi}{\partial z}=C_D, & \textit{on } z=0;\\ |\nabla\phi|\to -U, \quad z\le 0, & \textit{and } \sqrt{x^2+y^2+z^2}\to\infty;\\ \textit{The radiation condition;} & \end{cases} \tag{2.19}$$

where

$$A_D = (\frac{\partial\bar{\Phi}}{\partial\ell})^2; \tag{2.20}$$

$$B_D = 2\frac{\partial\bar{\Phi}}{\partial\ell}\frac{\partial^2\bar{\Phi}}{\partial\ell^2}; \tag{2.21}$$

$$C_D = 2(\frac{\partial\bar{\Phi}}{\partial\ell})^2\frac{\partial^2\bar{\Phi}}{\partial\ell^2}. \tag{2.22}$$

In the above equations ℓ represents the coordinate along the streamline of the corresponding double-body flow on $z = 0$; and $\bar{\Phi}$ is the double-body potential which is obtained by solving the double-body problem, (see Fig. 5.1 for the geometry of the double-body model). The double-body flow problem is defined by

$$\begin{cases} \nabla^2\bar{\Phi} = 0, & \textit{in the fluid domain}; \\ \vec{n}\cdot\nabla\bar{\Phi} = 0, & \textit{on the body surface}; \\ \frac{\partial\bar{\Phi}}{\partial z} = 0, & \textit{on } z = 0; \\ |\nabla\bar{\Phi}| \to -U, & \textit{as } \sqrt{x^2+y^2+z^2} \to \infty, \quad z \le 0. \end{cases} \tag{2.23}$$

Dawson's linearized problem is originally written in terms of total velocity potential ϕ, (see boundary value problem (2.19)). However it can also be written in terms of the perturbation potential ϕ' in the same way as expressed in the Neumann-Kelvin linear problem (2.11), (see Ogiwara 1983). In terms of ϕ' problem (2.19) becomes:

$$\begin{cases} \nabla^2\phi' = 0, & \textit{in the fluid domain}; \\ \vec{n}\cdot\nabla\phi' = Un_x, & \textit{on the body surface}; \\ A_O\frac{\partial^2\phi'}{\partial\ell^2} + B_O\frac{\partial\phi'}{\partial\ell} + g\frac{\partial\phi'}{\partial z} = C_O, & \textit{on } z = 0; \\ |\nabla\phi'| \to 0, \quad z \le 0, & \sqrt{x^2+y^2+z^2} \to \infty; \\ \textit{The radiation condition}; \end{cases} \tag{2.24}$$

where the total velocity potential ϕ is defined as:

$$\phi = \bar{\Phi} + \phi', \tag{2.25}$$

and

$$A_O = (\frac{\partial \bar{\Phi}}{\partial \ell})^2; \tag{2.26}$$

$$B_O = 2\frac{\partial \bar{\Phi}}{\partial \ell}\frac{\partial^2 \bar{\Phi}}{\partial \ell^2}; \tag{2.27}$$

$$C_O = -(\frac{\partial \bar{\Phi}}{\partial \ell})^2\frac{\partial^2 \bar{\Phi}}{\partial \ell^2}. \tag{2.28}$$

The radiation condition in Dawson's linearized problem is the same as that for the exact ship wave problem.

As has been discussed above, Dawson's linearized free surface condition is equivalent, as shown by Nakos (1990) and as will be shown in Chapter 3 of this thesis, to the result of keeping only the first term (zero order term in η) in the Taylor's series expansion of the free surface condition about $z = 0$ and then performing the linearization.

The error in the results of solving Dawson's linearized ship wave problem, induced by keeping only one term in the Taylor's series expansion, depends on the block ratio of the ship hull and the curvature of the bow and stern. For thin ships the errors are relatively small. However, for ships with larger block ratios or rounded surfaces at the bow and stern the error could be significantly large. For instance, in the case of a moving floating sphere with its center plane on the undisturbed fluid free surface, it is known, from the theoretical solution, that the fluid velocity $\partial\bar{\Phi}/\partial\ell$ at the stagnation points of the double-body solution

are zero. Therefore it can be seen that the three coefficients A_D, B_D, and C_D in Dawson's free surface condition given by equations (2.20), (2.21), and (2.22) are all equal to zero. Hence, at the stagnation points the solution of Dawson's linearized boundary value problem (2.19) can easily be found to be

$$\partial\phi/\partial\ell = 0, \tag{2.29}$$

and

$$\partial\phi/\partial z = 0. \tag{2.30}$$

The above equation implies that the vertical fluid velocity at the front edge of the sphere is zero. This is obviously wrong. The first order approximation of the vertical fluid velocity at the stagnation points of the sphere can be obtained in terms of the velocity potential ϕ from the linear ship wave problem developed in the present study, (see Chapter 3 for the present linearized free surface condition), which is

$$\frac{\partial\phi}{\partial z} = \frac{\partial\phi'}{\partial z} = \frac{U^2}{2g}\frac{\partial^2\phi}{\partial\ell^2}. \tag{2.31}$$

As will be shown in Chapter 3, the reason why Dawson's linear problem, as given by (2.19) or (2.24), gives wrong predictions at the stagnation points is that the terms produced by the second term (first order term in η) in the Taylor's series expansion are important for rounded surfaces at the stagnation points or large block ratio bodies. These terms are relatively small when $|\tilde{u}'/U|$ is small, where $\tilde{u}'$ is the perturbation component of the fluid velocity due to the double-body, and U is the forward speed, i.e. $\partial\tilde{\Phi}/\partial x = U + \tilde{u}'$. The effect of these terms will increase when the value of $|\tilde{u}'/U|$ increases. For the sphere case at the stagnation points $|\tilde{u}'/U| = 1$, which is the maximum value of $|\tilde{u}'/U|$, and these terms have the maximum effect, resulting in the obviously wrong solution.

As reported by Raven (1992) the vertical component of fluid velocity, obtained by solving Dawson's linearized ship wave problem, at the bow of a Series 60 hull, $C_b = 0.60$, could have 35% error and at the stern could reach up to 65%. The reason that the error at the stern is larger than the error at the bow is that the waterline entrance angle at the stern of Series 60, $C_b = 0.60$, is larger than at the bow, (see Fig. 5.10).

2.4 Nakos and Sclavounos Linearized Problem

A Dawson-like linearized free surface condition has been derived and used by Nakos and Sclavounos (Nakos 1990, Nakos and Sclavounos 1991). In this linearized free surface condition terms up to the first order in η in the Taylor's series expansion are kept. The original linearized free surface condition published by Nakos and Sclavounos is in the form of a vector expression, given by

$$\begin{aligned} & \nabla\bar{\Phi}\cdot\nabla(\nabla\bar{\Phi}\cdot\nabla\phi') + \frac{1}{2}\nabla(\nabla\bar{\Phi}\cdot\nabla\bar{\Phi})\cdot\nabla\phi' + g\frac{\partial\phi'}{\partial z} - \frac{\partial^2\bar{\Phi}}{\partial z^2}(\nabla\bar{\Phi}\cdot\nabla\phi') \\ = \; & -\frac{1}{2}\nabla(\nabla\bar{\Phi}\cdot\nabla\bar{\Phi})\cdot\nabla\bar{\Phi} - \frac{1}{2}(U^2 - \nabla\bar{\Phi}\cdot\nabla\bar{\Phi})\frac{\partial^2\bar{\Phi}}{\partial z^2}, \; on\, z = 0, \end{aligned} \tag{2.32}$$

where $\bar{\Phi}$ is the double-body potential; ϕ' is the potential perturbation for the free surface problem.

Rewriting equation (2.32) in terms of the double-body streamline, we have

$$A_N\frac{\partial^2\phi'}{\partial\ell^2} + B_N\frac{\partial\phi'}{\partial\ell} + g\frac{\partial\phi'}{\partial z} = C_N, \tag{2.33}$$

where

$$A_N = (\frac{\partial\bar{\Phi}}{\partial\ell})^2; \tag{2.34}$$

$$B_N = 3\frac{\partial\bar{\Phi}}{\partial\ell}\frac{\partial^2\bar{\Phi}}{\partial\ell^2}; \tag{2.35}$$

$$C_N = -(\frac{\partial\bar{\Phi}}{\partial\ell})^2\frac{\partial^2\bar{\Phi}}{\partial\ell^2} + \frac{1}{2}(U^2 - \frac{\partial\bar{\Phi}}{\partial\ell})\frac{\partial^2\bar{\Phi}}{\partial\ell^2}. \tag{2.36}$$

Comparing the linearized free surface condition given by equation (2.33), together with equations (2.34), (2.35) and (2.36), with Dawson's linearized free surface condition given in boundary value problem (2.24), together with equations (2.26), (2.27) and (2.28), it can be seen that there are two differences. Firstly B_D in equation (2.27) has a coefficient of 2 and B_N in equation (2.35) has a coefficient of 3 instead of 2. Secondly, on the right-hand side of equation (2.33) there is one extra term, in comparison with Dawson's linearized free surface condition, which appears in the coefficient C_N, given by equation (2.36).

It should be mentioned that an assumption that $\frac{1}{2g}(\nabla\bar{\Phi}\cdot\nabla\bar{\Phi} - U^2)$ is of the order of magnitude of ϕ' was used in obtaining equation (2.32) or (2.33), (Nakos 1990). This resulted in some terms in the Taylor's series expansion of the free surface condition not appearing in (2.32).

The above linearized free surface condition and the rest of the equations described in the exact ship wave problem form a linearized problem which was solved by Nakos (1990), Nakos and Sclavounos (1991) for a modified Wigley hull.

2.5 Pawlowski's Nonlinear Theory

Pawlowski (1992a, 1992b) introduced a new approach of one-to-one domain transformation as a basis of consistent formulations of nonlinear boundary value problems. The theory transforms the real fluid domain with an unknown actual

free surface into a computational domain with a flat free surface in the sense of an approximation series. The transformed boundary value problem in the computational domain is then solved by a nonlinear perturbation approach. The theory considers both the steady case of a ship moving in still water and the unsteady (time dependant) case of a ship moving in waves.

The development of the domain transformation theory has been detailed by Pawlowski (1992a). A perturbation approach for solving the transformed ship wave problem was introduced in that paper and further extended by Pawlowski (1992b). Some assumptions about hypothesised order of magnitude used in the first paper for the perturbation purposes have been relaxed in the second paper, and this resulted in the nonlinear perturbation formulation.

The transformation is given as:

$$exp(\bar{\eta} \cdot \nabla) = 1 + \bar{\eta} \cdot \nabla + \frac{1}{2}(\bar{\eta} \cdot \nabla)^2 + \ldots \ , \tag{2.37}$$

where ∇ denotes the gradient operator and dot indicates the scalar multiplication, and $\bar{\eta}$ represents the vector field of domain transformation which is a function of x, y, z and t.

The transformation (2.37) is applicable to all conditions in the ship wave problem (Pawlowski 1992a), such as Laplace's equation, the free surface condition, the ship impermeability surface condition, the pressure and velocity fields in the fluid domain. Under this transformation, the fluid domain with a wavy free surface is transformed into a computational domain with a flat surface, where the computations are performed.

The governing equation in the computational domain is obtained by applying

transformation (2.37) to Laplace's equation which is given as:

$$exp(\bar{\eta} \cdot \nabla)\nabla^2\Phi = 0 \ , \tag{2.38}$$

where Φ represents the velocity potential.

Similarly, the free surface conditions in the computational domain (i.e. on $z = 0$), are given as:

$$exp(\bar{\eta} \cdot \nabla)(\frac{\partial \Phi}{\partial t} + \frac{1}{2}|\nabla\Phi|^2 + gz) = 0 \ , \tag{2.39}$$

and

$$exp(\bar{\eta} \cdot \nabla)[\frac{\partial^2 \Phi}{\partial t^2} + g\frac{\partial \Phi}{\partial z} + 2\nabla\Phi \cdot \frac{\partial}{\partial t}(\nabla\Phi) + \frac{1}{2}\nabla\Phi \cdot \nabla(\nabla\Phi \cdot \nabla\Phi)] = 0 \ . \tag{2.40}$$

The impermeability condition on the surface of the body becomes

$$[exp(\bar{\eta} \cdot \nabla)\nabla\Phi - \frac{\partial}{\partial t}\bar{\eta}] \cdot (\bar{\bar{I}} + \nabla \otimes \bar{\eta})^{-1} \cdot \bar{n} = 0 \ , \tag{2.41}$$

where $\bar{\bar{I}}$ denotes the unit tensor, and $\otimes$ signifies the tensor multiplication; $\bar{n}$ represents the normal vector to the body surface.

Also, the radiation conditions are obtained by transforming appropriate restriction conditions on a whole boundary depending on the fluid domain under consideration.

The above described transformed boundary value problem is a nonlinear one, but the location of the free surface is known as $z = 0$. In order to solve this nonlinear boundary value problem, the total velocity potential Φ is decomposed into a perturbation series of order n, where n denotes the order of the perturbation under consideration. It gives

$$\Phi = \Phi_U^{(0)} + \bar{\Phi}^{(0)} + \Phi_U^{(1)} + \bar{\Phi}^{(1)} + ... + \Phi_U^{(n)} + \bar{\Phi}^{(n)} \ , \tag{2.42}$$

where $\Phi_U^{(n)}$ represents the *nth* order steady part of the perturbation velocity potential, whereas $\bar{\Phi}^{(n)}$ represents the *nth* order unsteady (time dependent) part of the perturbation velocity potential.

For the steady ship wave problem equation (2.42) can be rewritten as:

$$\Phi = \Phi^{(0)} + \Phi^{(1)} ... + \Phi^{(n)}, \tag{2.43}$$

where $\Phi^{(n)}$ denotes the *nth* order steady fluid velocity potential.

As has been mentioned above, the one-to-one domain transformation theory considers not only the nonlinearity of the free surface condition but also of the impermeability condition on the ship hull. Therefore not only the free surface condition is transformed but also the impermeability condition on the hull surface, see equation (2.41). However, if the theory is applied to a ship with a sufficiently small curvature on the wetted surface, especially at the designed waterline, the impermeability condition (2.41) reduces to the same form as the condition used in the exact ship wave problem (2.6), (Pawlowski 1992a).

Depending on the orders of magnitude assigned to the spatial and temporal derivatives of the velocity potentials in (2.42), or spatial derivatives in (2.43), the perturbation formulations may lead to a series of linear or nonlinear boundary value problems which sequentially determine the velocity potentials. In (Pawlowski 1992b) the concept of a nonlinear perturbation procedure was introduced as the name for a perturbation solution in which nonlinear boundary value problems must be solved.

In the nonlinear perturbation procedure, the free surface condition of the zero order ship wave problem, for the wall-sided ship, is given as (Pawlowski 1992b):

$$\{(\frac{\partial\Phi^{(0)}}{\partial\ell})^2-(\frac{\partial\Phi^{(0)}}{\partial z})^2\}\frac{\partial^2\Phi^{(0)}}{\partial\ell^2}$$
$$+[2\frac{\partial\Phi^{(0)}}{\partial\ell}\frac{\partial^2\Phi^{(0)}}{\partial\ell^2}+g]\frac{\partial\Phi^{(0)}}{\partial z} = 0, \qquad on\ z=0. \tag{2.44}$$

where $\Phi^{(0)}$ represents the fluid velocity potential of the zero order nonlinear ship wave problem; ℓ represents the streamline coordinate on the flat surface $z = 0$ of the computational domain.

From equation (2.38) the governing equation in the computational domain for the zero order problem is obtained as:

$$\nabla^2\Phi^{(0)} = 0. \tag{2.45}$$

The zero order nonlinear ship wave problem is then written as:

$$\begin{cases} \nabla^2\Phi^{(0)} = 0, & in\ the\ fluid\ domain; \\ \vec{n}\cdot\nabla\Phi^{(0)} = 0, & on\ the\ body\ surface; \\ \{(\frac{\partial\Phi^{(0)}}{\partial\ell})^2-(\frac{\partial\Phi^{(0)}}{\partial x})^2\}\frac{\partial^2\Phi^{(0)}}{\partial\ell^2} & \\ +[2\frac{\partial\Phi^{(0)}}{\partial\ell}\frac{\partial^2\Phi^{(0)}}{\partial\ell^2}+g]\frac{\partial\Phi^{(0)}}{\partial x} = 0, & on\ \ z=0; \\ |\nabla\Phi^{(0)}| \to -U, \qquad z\le 0\ \ and\ \ \sqrt{x^2+y^2+z^2}\to\infty; & \\ The\ radiation\ condition. & \end{cases} \tag{2.46}$$

It is important to note that the above zero order ship wave problem is a nonlinear boundary value problem. An exact solution of this nonlinear boundary value problem was obtained by using an iterative procedure.

To produce a more accurate solution, a first order perturbation is considered. The governing equation for the first order problem is also obtained from equation (2.38). It is given as:

$$\nabla^2\Phi^{(1)} = 0. \tag{2.47}$$

Using equations (2.40) and (2.43), the nonlinear free surface condition of the first order nonlinear ship wave problem is given as:

$$
\begin{aligned}
&[\frac{\partial}{\partial \ell}(\Phi^{(0)}+\Phi^{(1)})]^2\frac{\partial^2}{\partial \ell^2}(\Phi^{(0)}+\Phi^{(1)})\\
+\frac{\partial}{\partial z}(\Phi^{(0)}+\Phi^{(1)})\{&g+2\frac{\partial}{\partial \ell}(\Phi^{(0)}+\Phi^{(1)})\frac{\partial^2}{\partial \ell \partial z}(\Phi^{(0)}+\Phi^{(1)})\\
&-\frac{\partial}{\partial z}(\Phi^{(0)}+\Phi^{(1)})\frac{\partial^2}{\partial \ell^2}(\Phi^{(0)}+\Phi^{(1)})\}\\
&+\eta^{(1)}\{-g\frac{\partial^2}{\partial \ell^2}(\Phi^{(0)}+\Phi^{(1)})\\
+2\frac{\partial}{\partial z}(\Phi^{(0)}+\Phi^{(1)})[&(\frac{\partial^2}{\partial \ell \partial z}(\Phi^{(0)}+\Phi^{(1)}))^2\\
&+(\frac{\partial^2}{\partial \ell^2}(\Phi^{(0)}+\Phi^{(1)}))^2\\
&-\frac{\partial}{\partial \ell}(\Phi^{(0)}+\Phi^{(1)})\frac{\partial^3}{\partial \ell^3}(\Phi^{(0)}+\Phi^{(1)})]\\
+\frac{\partial^3}{\partial \ell^2 \partial z}(\Phi^{(0)}+\Phi^{(1)})[&(\frac{\partial}{\partial \ell}(\Phi^{(0)}+\Phi^{(1)}))^2\\
&-(\frac{\partial}{\partial z}(\Phi^{(0)}+\Phi^{(1)}))^2]\} \;=\; 0,\\
&\text{on } z=0. \qquad (2.48)
\end{aligned}
$$

In equation (2.48), $\Phi^{(1)}$ is the first order perturbation based on the zero order solution $\Phi^{(0)}$. The wave elevation $\eta^{(1)}$ is given as:

$$
\eta^{(1)} = -\frac{[\frac{\partial^2}{\partial \ell^2}(\Phi^{(0)}+\Phi^{(1)})]^2+[\frac{\partial^2}{\partial x^2}(\Phi^{(0)}+\Phi^{(1)})]^2-U^2}{2\{g+\frac{\partial}{\partial \ell}(\Phi^{(0)}+\Phi^{(1)})\frac{\partial^2}{\partial \ell \partial z}(\Phi^{(0)}+\Phi^{(1)})-\frac{\partial^2}{\partial \ell^2}(\Phi^{(0)}+\Phi^{(1)})\frac{\partial}{\partial z}(\Phi^{(0)}+\Phi^{(1)})\}}. \qquad (2.49)
$$

The first order nonlinear ship wave problem is accordingly written as:

$$
\begin{cases}
\nabla^2\Phi^{(1)} = 0, & \text{in the fluid domain;} \\
\vec{n}\cdot\nabla\Phi^{(1)} = -\vec{n}\cdot\nabla\Phi^{(0)}, & \text{on the body surface;} \\
(\frac{\partial}{\partial t}(\Phi^{(0)}+\Phi^{(1)}))^2\frac{\partial^2}{\partial t^2}(\Phi^{(0)}+\Phi^{(1)})+ & \\
\frac{\partial}{\partial z}(\Phi^{(0)}+\Phi^{(1)}) & \\
\{g+2\frac{\partial}{\partial t}(\Phi^{(0)}+\Phi^{(1)})\frac{\partial^2}{\partial t\partial z}(\Phi^{(0)}+\Phi^{(1)})- & \\
\frac{\partial}{\partial z}(\Phi^{(0)}+\Phi^{(1)})\frac{\partial^2}{\partial t^2}(\Phi^{(0)}+\Phi^{(1)})\}+ & \\
\eta^{(1)}\{-g\frac{\partial^2}{\partial t^2}(\Phi^{(0)}+\Phi^{(1)})+ & \\
2\frac{\partial}{\partial z}(\Phi^{(0)}+\Phi^{(1)})[(\frac{\partial^2}{\partial t\partial z}(\Phi^{(0)}+\Phi^{(1)}))^2+ & \\
(\frac{\partial^2}{\partial t^2}(\Phi^{(0)}+\Phi^{(1)}))^2- & \\
\frac{\partial}{\partial t}(\Phi^{(0)}+\Phi^{(1)})\frac{\partial^2}{\partial t^2}(\Phi^{(0)}+\Phi^{(1)})]+ & \\
\frac{\partial^2}{\partial t^2\partial z}(\Phi^{(0)}+\Phi^{(1)})[(\frac{\partial}{\partial t}(\Phi^{(0)}+\Phi^{(1)}))^2- & \\
(\frac{\partial}{\partial z}(\Phi^{(0)}+\Phi^{(1)}))^2]\} = 0, & \text{on } z=0; \\
|\nabla\Phi^{(1)}| \to 0, \qquad z\le 0 \text{ and } \sqrt{x^2+y^2+z^2}\to\infty; & \\
\textit{The radiation condition.} &
\end{cases}
\tag{2.50}
$$

System of equations (2.50) describes a nonlinear boundary value problem. The same iterative procedure as the one used to solve the zero order nonlinear problem was applied to solve this nonlinear problem.

The total velocity potential up to the first order perturbation is then written as:

$$\Phi = \Phi^{(0)} + \Phi^{(1)}. \tag{2.51}$$

Through the above described perturbation procedure (Pawlowski, 1992a, 1992b) not only a perturbed nonlinear solution of the ship wave problem can be obtained but also the convergence of the perturbation can be determined, which will be further discussed in Chapter 6 of this thesis where the nonlinear perturbation theory is used to analyse the convergence of the iterative method presented in this thesis.

2.6 Kelvin Source Method

The Kelvin source method, which is considered as an indirect boundary integral method, was recommended by Brard (1971, 1974a, b). In this method the disturbance potential ϕ' is obtained by solving the Neumann-Kelvin linearized problem (2.11). In solving the problem the Kelvin wave source potentials are usually applied. The potentials are defined by a Green's function which is constructed to satisfy the Neumann-Kelvin linear free surface condition and the radiation condition.

Noblesse (1981) demonstrated that the Kelvin wave source potential can be expressed in the form:

$$a\pi G(\vec{\xi},\vec{x};F_n^2)=\frac{-1}{|\vec{\xi}-\vec{x}|}+\{N(\vec{X})+W(\vec{X})\}/F_n^2, \tag{2.52}$$

where $|\vec{\xi}-\vec{x}|$ represents the distance between the field and the source points and the dimensionless vector quantity $\vec{X}(\vec{\xi},\vec{x};F_n^2)$ is defined by

$$\vec{X}=(X,Y,Z\geq 0)=(x-\xi,y-\eta,|z+\zeta|)/F_n^2. \tag{2.53}$$

The vector $F_n^2\vec{X}$ joins the field point $\vec{\xi}$ with the free surface mirror image of the source point $\vec{x}$ (notice that $X<0$ upstream from the source and $X>0$ downstream from the source). F_n is the Froude number which is defined by $F_n=U/\sqrt{gL}$ and L is the length of the object.

Equation (2.52) implies that the Kelvin wave source potential is decomposed into three characteristic components:

1. the potential $-\frac{1}{4\pi}|\vec{\xi}-\vec{x}|$ of a fundamental Rankine source in infinite fluid

(in the absence of the free surface);

2. the potential $N(\vec{X})/(4\pi F_n^2)$ of a localized nonoscillatory nearfield disturbance, symmetric upstream and downstream from the source; and

3. the potential $W(\vec{X})/(4\pi F_n^2)$ of a wave like disturbance which accounts for the waves produced by the source.

Physically the Kelvin wave source potential $G(\vec{\xi}, \vec{x}; F_n^2)$ given by equation (2.52) represents the linearized velocity potential at the field point $\vec{\xi}(\xi, \eta, \zeta \leq 0)$ of the flow produced by a unit source at the source point $\vec{x}(x, y, z)$ in steady rectilinear motion with unit speed at depth $-z$ below the free surface of an otherwise unbounded fluid. In the limiting case when $z = 0$ the source is evidently no longer fully submerged and it may be shown that the unit outflow produced at $(x, y, z = 0)$ now stems from a flux across the free surface, (see Ursell 1960, Noblesse 1981, and Euvrard 1983).

Since the Kelvin wave source potential satisfies only some of the conditions of the boundary value problem, the expression is not unique. It can take many different forms. Baar and Price(1989) classified these expressions found in the literature into the following five alternative representations:

1. an expression implicitly contained in Michell's (1898) paper, rediscovered by Eggers et al.(1967) and modified by Noblesse (1981);

2. an expression originally due to Havelock (1932) and subsequently modified by among others Lunde (1951), Kostyukov (1968), Standing (1975) and Shen and Farell (1977);

3. an expression due to Peters (1949) and modified by Noblesse (1977), see also Eggers et al (1967) and Andersson (1975);

4. an expression obtained by Bessho (1964), re-derived by Ursell (1984) and modified by Simmgen (1986); and

5. an expression proposed by Demanche (1981) and re-derived by Baar (1984).

All these expressions of the Kelvin wave source potential were chosen so that the Neumann-Kelvin linearized free surface condition in boundary value problem (2.11) is satisfied. The source densities distributed on the wetted surface of the object are calculated by forcing the Kelvin wave source potentials to satisfy the body impermeability condition given in boundary value problem (2.11). Unfortunately, large differences were found between the results calculated by these expressions, (see Baar (1986) for a comparison). The reason for the differences is not clear. It is also not clear if the solutions based on these different expressions are the same.

A full comparison and discussion of these expressions is beyond the scope of the present review. But as discussed by Baar and Price (1988) the second expression due to Havelock (1932), which is also quoted in Wehausen and Laitone (1960), has been the most popular. In recent years, however, the third expression due to Peters(1949) has been recognized as the most convenient one from both physical, mathematical and numerical points of views, see for example Noblesse (1981), Euvrard (1983) and Newman (1987). This expression has also been adopted by Baar and Price (1988).

2.7 Rankine Source Method

Since the free surface conditions of Dawson's and Dawson-like linearized problems are more complicated than the one in Neumann-Kelvin problem, it is difficult to find Green's function solutions to satisfy these free surface conditions. The method for solving Dawson's linear problem developed by Dawson and modified by many others is based on the Rankine source theory, which is also considered as an indirect boundary integral method. The solution to the problem in terms of a Rankine source density σ is assumed in the form

$$\phi = -Ux + \int_{BS} \frac{1}{r(p,q)}\sigma(q)dS(q) + \int_{FS} \frac{1}{r(p,q)}\sigma(q)dS(q), \qquad (2.54)$$

where ϕ is the velocity potential of the fluid; BS represents the solid boundary of the body and FS represents the fluid free surface; $\sigma(q)$ is the Rankine source density at source point q with $q \in BS$ or $q \in FS$; $r(p,q)$ is the distance between the field point p and the source point q, which is given by

$$r(p,q) = \sqrt{[x(p)-x(q)]^2 + [y(p)-y(q)]^2 + [z(p)-z(q)]^2}. \qquad (2.55)$$

Equation (2.54) satisfies the governing equation and the condition at infinity in Dawson's linear problem (2.19). By forcing equation (2.54) to satisfy the boundary conditions on the fluid free surface, the body surface condition, and the radiation condition in problem (2.19), the source density $\sigma(q)$ in equation (2.54) can be obtained. Hence the velocity potential of the problem is found. The radiation condition is imposed by applying a down-stream finite difference formula in the free surface condition.

Dawson's free surface condition and the Rankine source scheme have been applied by many authors such as: Van Beek, Piers and Slooff (1985), Ogiwara

and Masuko (1986), Aanesland (1986), Xi and Larsson (1986), Delhommeau and Maisonneuve (1986), Raven (1988, 1991), Kim, Kim and Lucas (1989) and many others. The numerical procedures in these studies may have some differences, but the fundamental strategy is the same, namely applying the Rankine source method to solve Dawson's linearized ship wave problem. All of these studies were based on the constant element techniques, in which the source density is constantly distributed over each quadrilateral element on the surface mesh.

In the Rankine source method, normally, the source densities and the collocation points are on the same mesh. However, it is also possible to distribute the source densities on a separate mesh away from the collocation mesh which is on the surface of the computational domain. This method is called the desingularized method (Cao, 1991), The advantage of this method is to avoid the difficult special treatments needed for the cases when the source density and collocation points are at the same location. The disadvantage of this method is that the source mesh has to be designed carefully with no physical support, or otherwise an ill conditioned matrix system could be generated. This method has been studied by Cao (1991) and also applied by Raven (1992).

To solve Dawson's linearized problem, the radiation condition is usually implemented through numerical schemes. A one-sided finite difference method was introduced by Dawson (1977) and used by many other studies to enforce the radiation condition. A bi-quadratic spline scheme with a proper upstream radiation condition was introduced by Sclavounos and Nakos (1988), Nakos and Sclavounos (1990, 1992), which enjoys distinct numerical advantages relative to the one-sided finite difference scheme, however for practical reasons it was not implemented in the present work.

2.8 Iterative Panel Method

An iterative panel method has been developed to solve the non-linear ship wave problem, see Ogiwara (1985), Ni (1987), Jensen et al (1986, 1989), Kim and Lucas (1990), and most recently Raven (1992). In these studies the fundamental Rankine source method described in Section (2.7) was applied at each iterative step. The iteration schemes used in these studies are basically the same. The iteration starts with solving Dawson's linearized ship wave problem and the free surface condition is re-linearized on the free surface calculated in the previous step. In each step Dawson's linearized ship wave problem is solved. Convergence is the major problem of this method. In most of these studies so-called relaxation factors were used to force the convergence of the solution. These relaxation factors were chosen differently in different studies.

One major problem of this iterative method occurs in the first iteration i- which Dawson's linearized ship wave problem is solved. The solution gives large errors when solving cases considered to be fundamentally nonlinear. The errors generated in the first iteration are likely to be carried into the next iteration since the second iteration is based on the incorrect free surface elevation produced in the first iteration. There is no proof that the errors produced in the first iteration can be corrected in future iterations.

In the most recent study by Raven, a convergence of solution was claimed without using the relaxation factors, even though the same scheme as described above was applied. The desingularized approach (see Cao (1991) for discussions of the desingularized method) was employed at each step of the iteration.

3 FORMULATION OF THE PROBLEM

3.1 A Nonlinear Ship Wave Problem

As has already been discussed in the introduction of this thesis, the procedure of using numerical methods to simulate ship wave patterns and to compute the corresponding wave-making resistances requires, firstly, a mathematical model to represent the physical problem, and secondly, a numerical solver to solve the mathematical problem. The mathematical models which have been developed and used in the ship wave simulation have been reviewed and discussed in the proceeding chapter. In this chapter a nonlinear ship wave boundary value problem is obtained by transforming the free surface condition of the exact ship wave problem from being satisfied at the actual fluid free surface to being satisfied at the undisturbed fluid surface, by means of a Taylor's series expansion. The mathematical formulation of an iterative scheme for solving the transformed nonlinear ship wave problem developed in the present study is also presented in this chapter. In order to compare the present method with the existing ones and to discuss the drawbacks found in the Neumann-Kelvin and Dawson's linear ship wave models, a new linearized ship wave boundary value problem based on the transformed nonlinear ship wave problem developed in the present study is also obtained in this chapter.

The exact ship wave problem has been discussed in the previous chapter. In order to simplify the free surface condition in the exact ship wave boundary value problem (2.6), a name of streamline on the actual free surface is introduced. The streamline on the actual free surface is defined as a spatial curve which lies on

the actual free surface with the velocity of fluid particles on the curve being tangential to this curve. If ℓ is used to represents the the projection of the free surface streamline onto the plane $z = 0$, we write

$$\nabla = \vec{\ell}\frac{\partial}{\partial \ell} + \vec{k}\frac{\partial}{\partial z}, \qquad on\ z = \eta, \tag{3.1}$$

where $\vec{\ell}$ represents a unit vector in the tangential direction to ℓ and $\vec{k}$ represents a unit vector in the vertical direction z.

Using equation (3.1), the exact combined and dynamic free surface conditions can then be written respectively as:

$$(\frac{\partial \phi}{\partial \ell})^2\frac{\partial^2 \phi}{\partial \ell^2} + 2\frac{\partial \phi}{\partial \ell}\frac{\partial \phi}{\partial z}\frac{\partial^2 \phi}{\partial \ell \partial z} + (\frac{\partial \phi}{\partial z})^2\frac{\partial^2 \phi}{\partial z^2} + g\frac{\partial \phi}{\partial z} = 0, \qquad on\ z = \eta, \tag{3.2}$$

and

$$g\eta + \frac{1}{2}[(\frac{\partial \phi}{\partial \ell})^2 + (\frac{\partial \phi}{\partial z})^2 - U^2] = 0, \qquad on\ z = \eta. \tag{3.3}$$

Now expanding the combined free surface condition (3.2) in a Taylor's series expansion about $z = 0$ and keeping the terms up to the first order in η gives

$$[1 + \eta\frac{\partial}{\partial z}][(\frac{\partial \phi}{\partial \ell})^2\frac{\partial^2 \phi}{\partial \ell^2} + 2\frac{\partial \phi}{\partial \ell}\frac{\partial \phi}{\partial z}\frac{\partial^2 \phi}{\partial \ell \partial z} + (\frac{\partial \phi}{\partial z})^2\frac{\partial^2 \phi}{\partial z^2} + g\frac{\partial \phi}{\partial z}] \;=\; 0, \qquad on\ z = 0. \tag{3.4}$$

In the same way, expanding the dynamic free surface condition (3.3) to the first order in η in the Taylor's series expansion, the wave elevation can be obtained as:

$$\eta = \frac{-1}{2(g + \frac{\partial \phi}{\partial \ell}\frac{\partial^2 \phi}{\partial \ell \partial z} - \frac{\partial \phi}{\partial z}\frac{\partial^2 \phi}{\partial \ell^2})}[(\frac{\partial \phi}{\partial \ell})^2 + (\frac{\partial \phi}{\partial z})^2 - U^2], \qquad z = 0. \tag{3.5}$$

Substituting η from equation (3.5) into equation (3.4) and working out the indicated derivatives gives

$$\begin{aligned}
&\{(\frac{\partial\phi}{\partial\ell})^2\frac{\partial^2\phi}{\partial\ell^2}+2\frac{\partial\phi}{\partial\ell}\frac{\partial\phi}{\partial z}\frac{\partial^2\phi}{\partial\ell\partial z}-(\frac{\partial\phi}{\partial z})^2\frac{\partial^2\phi}{\partial\ell^2}+g\frac{\partial\phi}{\partial z}\}\\
&\qquad\{g+\frac{\partial\phi}{\partial\ell}\frac{\partial^2\phi}{\partial\ell\partial z}-\frac{\partial\phi}{\partial z}\frac{\partial^2\phi}{\partial\ell^2}\}\\
&-\frac{1}{2}\{(\frac{\partial\phi}{\partial\ell})^2\frac{\partial^3\phi}{\partial\ell^2\partial z}+2\frac{\partial\phi}{\partial z}(\frac{\partial^2\phi}{\partial\ell\partial z})^2-2\frac{\partial\phi}{\partial\ell}\frac{\partial\phi}{\partial z}\frac{\partial^3\phi}{\partial\ell^3}\\
&\qquad+2\frac{\partial\phi}{\partial z}(\frac{\partial^2\phi}{\partial\ell^2})^2-(\frac{\partial\phi}{\partial z})^2\frac{\partial^3\phi}{\partial\ell^2\partial z}-g\frac{\partial^2\phi}{\partial\ell^2}\}\\
&\qquad\{(\frac{\partial\phi}{\partial\ell})^2+(\frac{\partial\phi}{\partial z})^2-U^2\} \;=\; 0,\ \textit{on}\ z=0. \quad (3.6)
\end{aligned}$$

Equation (3.6) is the free surface condition satisfied at the undisturbed fluid free surface $z = 0$ with an accuracy of order η in the Taylor's series expansion sense. It is noted that the relation $\frac{\partial^2\phi}{\partial x^2} = -\frac{\partial^2\phi}{\partial\ell^2}$ was used in obtaining equation (3.6).

For the hull forms with a sloped shape at the design waterline, the impermeability condition on the surface of the ship hull has to be transformed, see Pawlowski (1992a) for a complete derivation and discussion of the domain transformation which includes the governing equation and all boundary conditions in the ship wave boundary value problem. In the present study wall-sided hull forms at the design waterline are discussed.

The exact ship wave boundary value problem for wall-sided hull surface is then represented by the following approximate nonlinear boundary value problem with the free surface condition being satisfied at the undisturbed fluid free surface $z = 0$.

$$
\begin{cases}
\nabla^2\phi = 0, & \text{in the fluid domain;} \\
\vec{n}\cdot\nabla\phi = 0, & \text{on the body surface;} \\
\\
\{(\frac{\partial\phi}{\partial t})^2\frac{\partial^2\phi}{\partial t^2} + 2\frac{\partial\phi}{\partial t}\frac{\partial\phi}{\partial x}\frac{\partial^2\phi}{\partial t\partial x} - \\
(\frac{\partial\phi}{\partial x})^2\frac{\partial^2\phi}{\partial t^2} + g\frac{\partial\phi}{\partial x}\} \\
\{g + \frac{\partial\phi}{\partial t}\frac{\partial^2\phi}{\partial t\partial x} - \frac{\partial\phi}{\partial x}\frac{\partial^2\phi}{\partial t^2}\} - \\
\frac{1}{2}\{(\frac{\partial\phi}{\partial t})^2\frac{\partial^3\phi}{\partial t^2\partial x} + 2\frac{\partial\phi}{\partial x}(\frac{\partial^2\phi}{\partial t\partial x})^2 - \\
2\frac{\partial\phi}{\partial t}\frac{\partial\phi}{\partial x}\frac{\partial^3\phi}{\partial t^2} + 2\frac{\partial\phi}{\partial x}(\frac{\partial^2\phi}{\partial t^2})^2 - \\
(\frac{\partial\phi}{\partial x})^2\frac{\partial^3\phi}{\partial t^2\partial x} - g\frac{\partial^2\phi}{\partial t^2}\} \\
\{(\frac{\partial\phi}{\partial t})^2 + (\frac{\partial\phi}{\partial x})^2 - U^2\} = 0, & \text{on } z = 0; \\
\\
|\nabla\phi| \to -U, & z \le 0 \text{ and } \sqrt{t^2+z^2} \to \infty; \\
\text{The radiation condition.}
\end{cases}
\tag{3.7}
$$

In the nonlinear boundary value problem (3.7), the free surface condition is more complicated than the one found in the exact ship wave boundary value problem (2.6). However, the location of the boundary is known, which makes it easier to solve the problem. An iterative approach based on the direct boundary integral method and linear element techniques is developed in the present study to solve this nonlinear boundary value problem. The mathematical formulation of the iterative method will be discussed in the next section and the numerical details of the iterative approach will be presented in Chapter 6.

In obtaining the transformed fluid free surface condition (3.6), terms up to the first order in η are kept in the Taylor's series expansion, which is shown to give good accuracy when applied to predict ship waves. There is no theoretical limitation in keeping higher order terms in the Taylor's series expansion of the free surface condition, however the complexity will increase dramatically by keeping more terms. A discussion of the convergence of this Taylor's series expansion by applying Pawlowski's nonlinear perturbation approach will be presented in

Chapter 6, where an iterative scheme to solve boundary value problem (3.7) is developed and implemented.

3.2 Formulation of an Iterative Method

System of equations (3.7) defines a nonlinear boundary value problem, which can not be solved directly by a boundary integral method. An iterative scheme is, therefore, developed in the present study to solve this nonlinear boundary value problem "exactly". So that only one approximation is involved in the formulation of the present method, which is the transformation of the free surface condition from $z = \eta$ to $z = 0$, for wall-sided hull forms.

The basic idea of the present iterative scheme is to seek the solution of a nonlinear boundary value problem by solving iteratively a series of linear boundary value problems. In each iteration the boundary condition is linearized based on the solution of the previous step plus an incremental part. If the iteration is convergent the increment will become smaller with the iteration steps, and the iterative solutions of the linearized boundary value problems will converge to the solution of the nonlinear boundary value problem. To start the iteration, an initial value of the solution is needed which can be chosen arbitrarily.

In this section the linearized boundary value problem solved in each iteration is derived. The details of the iterative scheme will be presented in Chapter 6.

Applying the iterative procedure to solve nonlinear ship wave problem (3.7), only the free surface condition is needed to be linearized since the boundary condition on the surface of the ship is linear. To linearize the free surface condition,

the total velocity potential of the fluid flow ϕ is written as:

$$\phi = \Phi + \phi', \tag{3.8}$$

where Φ represents the sum of the velocity potentials obtained from the previous steps, ϕ' represents an incremental potential, and ϕ is the total velocity potential for the present iteration.

Substituting equation (3.8) into equation (3.6) and dropping the high order terms in ϕ', a linearized free surface condition can be obtained as:

$$\begin{aligned} A\frac{\partial^2}{\partial \ell^2}(\Phi+\phi') + B\frac{\partial}{\partial \ell}(\Phi+\phi') + C\frac{\partial}{\partial z}(\Phi+\phi') \\ +D\frac{\partial^2}{\partial \ell \partial z}(\Phi+\phi') + E\frac{\partial^3}{\partial \ell^2 \partial z}(\Phi+\phi') + F\frac{\partial^3}{\partial \ell^3}(\Phi+\phi') \;=\; H, \;\; on\, z=0. \end{aligned} \tag{3.9}$$

The coefficients A, B, C, D, E, F, and H are coefficients which are functions of Φ. They are given as:

$$\begin{aligned} A \;=\; & 3g[(\frac{\partial\Phi}{\partial\ell})^2 - (\frac{\partial\Phi}{\partial z})^2] - gU^2 + 2(\frac{\partial\Phi}{\partial\ell})^3\frac{\partial^2\Phi}{\partial\ell\partial z} \\ & -8(\frac{\partial\Phi}{\partial\ell})^2\frac{\partial\Phi}{\partial z}\frac{\partial^2\Phi}{\partial\ell^2} - 6\frac{\partial\Phi}{\partial\ell}(\frac{\partial\Phi}{\partial z})^2\frac{\partial^2\Phi}{\partial\ell\partial z} + 4\frac{\partial\Phi}{\partial z}\frac{\partial^2\Phi}{\partial\ell^2}U^2; \end{aligned} \tag{3.10}$$

$$\begin{aligned} B \;=\; & 2[3g\frac{\partial\Phi}{\partial\ell}\frac{\partial^2\Phi}{\partial\ell^2} + 3g\frac{\partial\Phi}{\partial z}\frac{\partial^2\Phi}{\partial\ell\partial z} - 2(\frac{\partial\Phi}{\partial\ell})^3\frac{\partial^3\Phi}{\partial\ell^2\partial z} \\ & +3(\frac{\partial\Phi}{\partial\ell})^2\frac{\partial\Phi}{\partial z}\frac{\partial^3\Phi}{\partial\ell^3} + 3(\frac{\partial\Phi}{\partial\ell})^2\frac{\partial^2\Phi}{\partial\ell^2}\frac{\partial^2\Phi}{\partial\ell\partial z} \\ & -4\frac{\partial\Phi}{\partial\ell}\frac{\partial\Phi}{\partial z}(\frac{\partial^2\Phi}{\partial\ell^2})^2 + 2\frac{\partial\Phi}{\partial\ell}\frac{\partial\Phi}{\partial z}(\frac{\partial^2\Phi}{\partial\ell\partial z})^2 + \frac{\partial\Phi}{\partial\ell}\frac{\partial^3\Phi}{\partial\ell^2\partial z}U^2 \\ & +(\frac{\partial\Phi}{\partial z})^3\frac{\partial^3\Phi}{\partial\ell^3} - 3(\frac{\partial\Phi}{\partial z})^2\frac{\partial^2\Phi}{\partial\ell^2}\frac{\partial^2\Phi}{\partial\ell\partial z} - \frac{\partial\Phi}{\partial z}\frac{\partial^3\Phi}{\partial\ell^3}U^2]; \end{aligned} \tag{3.11}$$

$$\begin{aligned} C \;=\; & 2[g^2 + (\frac{\partial\Phi}{\partial\ell})^3\frac{\partial^3\Phi}{\partial\ell^3} - \frac{\partial\Phi}{\partial\ell}\frac{\partial^3\Phi}{\partial\ell^3}U^2 + (\frac{\partial^2\Phi}{\partial\ell^2})^2U^2 \\ & -2(\frac{\partial\Phi}{\partial\ell})^2(\frac{\partial^2\Phi}{\partial\ell^2})^2 + (\frac{\partial\Phi}{\partial\ell})^2(\frac{\partial^2\Phi}{\partial\ell\partial z})^2 + 3g\frac{\partial\Phi}{\partial\ell}\frac{\partial^2\Phi}{\partial\ell\partial z} \end{aligned}$$

$$
\begin{aligned}
&-3g\frac{\partial\Phi}{\partial z}\frac{\partial^2\Phi}{\partial\ell^2}+3\frac{\partial\Phi}{\partial\ell}(\frac{\partial\Phi}{\partial z})^2\frac{\partial^3\Phi}{\partial\ell^3}\\
&-6\frac{\partial\Phi}{\partial\ell}\frac{\partial\Phi}{\partial z}\frac{\partial^2\Phi}{\partial\ell^2}\frac{\partial^2\Phi}{\partial\ell\partial z}+2(\frac{\partial\Phi}{\partial z})^3\frac{\partial^3\Phi}{\partial\ell^2\partial z}\\
&-3(\frac{\partial\Phi}{\partial z})^2(\frac{\partial^2\Phi}{\partial\ell\partial z})^2-\frac{\partial\Phi}{\partial z}\frac{\partial^3\Phi}{\partial\ell^2\partial z}U^2+(\frac{\partial^2\Phi}{\partial\ell\partial z})^2U^2]; \qquad (3.12)
\end{aligned}
$$

$$
\begin{aligned}
D &= 2[(\frac{\partial\Phi}{\partial\ell})^3\frac{\partial^2\Phi}{\partial\ell^2}+3g\frac{\partial\Phi}{\partial\ell}\frac{\partial\Phi}{\partial z}+2(\frac{\partial\Phi}{\partial\ell})^2\frac{\partial\Phi}{\partial z}\frac{\partial^2\Phi}{\partial\ell\partial z}\\
&\quad -3\frac{\partial\Phi}{\partial\ell}(\frac{\partial\Phi}{\partial z})^2\frac{\partial^2\Phi}{\partial\ell^2}-2(\frac{\partial\Phi}{\partial z})^3\frac{\partial^2\Phi}{\partial\ell\partial z}+2\frac{\partial\Phi}{\partial z}\frac{\partial^2\Phi}{\partial\ell\partial z}U^2]; \qquad (3.13)
\end{aligned}
$$

$$
E = -(\frac{\partial\Phi}{\partial\ell})^2[(\frac{\partial\Phi}{\partial\ell})^2-U^2]-(\frac{\partial\Phi}{\partial z})^2[(\frac{\partial\Phi}{\partial z})^2+U^2]; \qquad (3.14)
$$

$$
F = 2\frac{\partial\Phi}{\partial\ell}\frac{\partial\Phi}{\partial z}[(\frac{\partial\Phi}{\partial\ell})^2+(\frac{\partial\Phi}{\partial z})^2-U^2]; \qquad (3.15)
$$

$$
\begin{aligned}
H &= 2[3g(\frac{\partial\Phi}{\partial\ell})^2\frac{\partial^2\Phi}{\partial\ell^2}+6g\frac{\partial\Phi}{\partial\ell}\frac{\partial\Phi}{\partial z}\frac{\partial^2\Phi}{\partial\ell\partial z}-3g(\frac{\partial\Phi}{\partial z})^2\frac{\partial^2\Phi}{\partial\ell^2}\\
&\quad -2(\frac{\partial\Phi}{\partial\ell})^4\frac{\partial^3\Phi}{\partial\ell^2\partial z}+4(\frac{\partial\Phi}{\partial\ell})^3\frac{\partial\Phi}{\partial z}\frac{\partial^3\Phi}{\partial\ell^3}+4(\frac{\partial\Phi}{\partial\ell})^3\frac{\partial^2\Phi}{\partial\ell\partial z}\frac{\partial^2\Phi}{\partial\ell^2}\\
&\quad +4(\frac{\partial\Phi}{\partial\ell})^2\frac{\partial\Phi}{\partial z}(\frac{\partial^2\Phi}{\partial\ell\partial z})^2-8(\frac{\partial\Phi}{\partial\ell})^2\frac{\partial\Phi}{\partial z}(\frac{\partial^2\Phi}{\partial\ell^2})^2\\
&\quad +(\frac{\partial\Phi}{\partial\ell})^2\frac{\partial^3\Phi}{\partial\ell^2\partial z}U^2+4\frac{\partial\Phi}{\partial\ell}(\frac{\partial\Phi}{\partial z})^3\frac{\partial^3\Phi}{\partial\ell^3}\\
&\quad -12\frac{\partial\Phi}{\partial\ell}(\frac{\partial\Phi}{\partial z})^2\frac{\partial^2\Phi}{\partial\ell\partial z}\frac{\partial^2\Phi}{\partial\ell^2}-2\frac{\partial\Phi}{\partial\ell}\frac{\partial\Phi}{\partial z}\frac{\partial^3\Phi}{\partial\ell^3}U^2\\
&\quad +2(\frac{\partial\Phi}{\partial z})^4\frac{\partial^3\Phi}{\partial\ell^2\partial z}-4(\frac{\partial\Phi}{\partial z})^3(\frac{\partial^2\Phi}{\partial\ell\partial z})^2\\
&\quad -(\frac{\partial\Phi}{\partial z})^2\frac{\partial^3\Phi}{\partial\ell^2\partial z}U^2+2\frac{\partial\Phi}{\partial z}(\frac{\partial^2\Phi}{\partial\ell\partial z})^2U^2+2\frac{\partial\Phi}{\partial z}(\frac{\partial^2\Phi}{\partial\ell^2})^2U^2]. \qquad (3.16)
\end{aligned}
$$

Now the boundary value problem to be solved at each iteration is written as:

$$\begin{cases} \nabla^2\phi' = 0, & \text{in the } fluid \text{ domain;} \\ \vec{n}\cdot\nabla\phi' = -\vec{n}\cdot\nabla\Phi, & \text{on the body } surface; \\ \\ A\frac{\partial^2}{\partial t^2}(\Phi+\phi') + B\frac{\partial}{\partial t}(\Phi+\phi') + \\ C\frac{\partial}{\partial x}(\Phi+\phi') + D\frac{\partial^2}{\partial t\partial x}(\Phi+\phi') + \\ +E\frac{\partial^3}{\partial t^2\partial x}(\Phi+\phi')F\frac{\partial^3}{\partial t^3}(\Phi+\phi') = H, & \text{on } z=0; \\ \\ |\nabla(\Phi+\phi')| \to -U, \quad z\le 0 \text{ and } \sqrt{x^2+y^2+z^2}\to\infty; \\ \text{The radiation condition.} \end{cases} \tag{3.17}$$

It is easy to prove that if the iteration is convergent then the converged $\phi = \Phi + \phi'$ is the solution to the nonlinear boundary value problem (3.7). When the iteration converges, the incremental potential ϕ' becomes zero, i.e. we have $\Phi = \phi$ (see Chapter 6 for details of the iteration scheme). Replacing Φ by ϕ in equations (3.10) to (3.16) and substituting these coefficients into equation (3.9) it can be found that equation (3.9) becomes the original nonlinear free surface condition (3.6), which means that equation (3.6) is satisfied by ϕ, or in other words ϕ obtained through the iteration satisfies the nonlinear free surface condition (3.6). Since ϕ also satisfies the remaining equations in problem (3.7), ϕ is therefore the solution of nonlinear boundary problem (3.7).

When linearized boundary value problem (3.17) is used to form the iteration, the high order derivatives of the total velocity potential $\phi = \Phi + \phi'$, namely $\frac{\partial^2}{\partial t\partial x}(\Phi+\phi')$, $\frac{\partial^3}{\partial t^2\partial x}(\Phi+\phi')$, and $\frac{\partial^3}{\partial t^3}(\Phi+\phi')$, have to be computed. In the boundary integral method these high order derivatives are expressed by finite difference formulas, and are difficult to handle in the computation. However, it can be proved that by dropping the incremental parts of these high order derivatives, namely $\frac{\partial^2}{\partial t\partial x}(\phi')$, $\frac{\partial^3}{\partial t^2\partial x}(\phi')$, and $\frac{\partial^3}{\partial t^3}(\phi')$, and keeping only the major parts, namely $\frac{\partial^2}{\partial t\partial x}(\Phi)$, $\frac{\partial^3}{\partial t^2\partial x}(\Phi)$, and $\frac{\partial^3}{\partial t^3}(\Phi)$ in the linearized free surface condition, the iteration

still converges to the solution of nonlinear boundary value problem (3.7). By dropping the terms in $\frac{\partial^2}{\partial \ell \partial z}(\phi')$, $\frac{\partial^3}{\partial \ell^2 \partial z}(\phi')$, and $\frac{\partial^3}{\partial \ell^3}(\phi')$, the free surface condition in problem (3.17) becomes:

$$\begin{aligned} A\frac{\partial^2}{\partial \ell^2}(\Phi+\phi') + B\frac{\partial}{\partial \ell}(\Phi+\phi') + C\frac{\partial}{\partial z}(\Phi+\phi') \\ +D\frac{\partial^2}{\partial \ell \partial z}(\Phi) + E\frac{\partial^3}{\partial \ell^2 \partial z}(\Phi) + F\frac{\partial^3}{\partial \ell^3}(\Phi) &= H, \ \ on\ z=0. \end{aligned} \tag{3.18}$$

Equation (3.18) can also be written in terms of ϕ as:

$$A\frac{\partial^2 \phi}{\partial \ell^2} + B\frac{\partial \phi}{\partial \ell} + C\frac{\partial \phi}{\partial z} = R, \qquad on\ z=0, \tag{3.19}$$

where coefficients A, B, C are given by equations (3.10), (3.11), and (3.12) respectively; R is given as:

$$\begin{aligned} R \ = \ & 6g(\frac{\partial \Phi}{\partial \ell})^2\frac{\partial^2 \Phi}{\partial \ell^2} + 6g\frac{\partial \Phi}{\partial \ell}\frac{\partial \Phi}{\partial z}\frac{\partial^2 \Phi}{\partial \ell \partial z} \\ & -6g(\frac{\partial \Phi}{\partial z})^2\frac{\partial^2 \Phi}{\partial \ell^2} - 3(\frac{\partial \Phi}{\partial \ell})^4\frac{\partial^3 \Phi}{\partial \ell^2 \partial z} \\ & +6(\frac{\partial \Phi}{\partial \ell})^3\frac{\partial \Phi}{\partial z}\frac{\partial^3 \Phi}{\partial \ell^3} + 6(\frac{\partial \Phi}{\partial \ell})^3\frac{\partial^2 \Phi}{\partial \ell \partial z}\frac{\partial^2 \Phi}{\partial \ell^2} \\ & +4(\frac{\partial \Phi}{\partial \ell})^2\frac{\partial \Phi}{\partial z}(\frac{\partial^2 \Phi}{\partial \ell \partial z})^2 - 16(\frac{\partial \Phi}{\partial \ell})^2\frac{\partial \Phi}{\partial z}(\frac{\partial^2 \Phi}{\partial \ell^2})^2 \\ & +(\frac{\partial \Phi}{\partial \ell})^2U^2\frac{\partial^3 \Phi}{\partial \ell^2 \partial z} + 6\frac{\partial \Phi}{\partial \ell}(\frac{\partial \Phi}{\partial z})^3\frac{\partial^3 \Phi}{\partial \ell^3} \\ & -18\frac{\partial \Phi}{\partial \ell}(\frac{\partial \Phi}{\partial z})^2\frac{\partial^2 \Phi}{\partial \ell \partial z}\frac{\partial^2 \Phi}{\partial \ell^2} - 2\frac{\partial \Phi}{\partial \ell}\frac{\partial \Phi}{\partial z}U^2\frac{\partial^3 \Phi}{\partial \ell^3} \\ & +3(\frac{\partial \Phi}{\partial z})^4\frac{\partial^3 \Phi}{\partial \ell^2 \partial z} - 4(\frac{\partial \Phi}{\partial z})^3(\frac{\partial^2 \Phi}{\partial \ell \partial z})^2 \\ & -(\frac{\partial \Phi}{\partial z})^2U^2\frac{\partial^3 \Phi}{\partial \ell^2 \partial z} + 4\frac{\partial \Phi}{\partial z}U^2(\frac{\partial^2 \Phi}{\partial \ell^2})^2 \ . \end{aligned} \tag{3.20}$$

The boundary value problem to be solved at each iteration is then written as:

$$\begin{cases} \nabla^2\phi = 0, & \textit{in the fluid domain;} \\ \vec{n}\cdot\nabla\phi = 0, & \textit{on the body surface;} \\ A\frac{\partial^2\phi}{\partial t^2} + B\frac{\partial\phi}{\partial t} + C\frac{\partial\phi}{\partial z} = R, & \textit{on } z = 0; \\ |\nabla\phi| \to -U, \quad z \le 0 \textit{ and } \sqrt{x^2+y^2+z^2} \to \infty; & \\ \textit{The radiation condition.} & \end{cases} \tag{3.21}$$

When the linearized boundary value problem given by (3.21) is used to form the iteration (see Chapter 6 for details of the iteration scheme), once the iteration converges, the incremental potential becomes zero, i.e. we have $\Phi = \phi$. Replacing Φ by ϕ in equations (3.10), (3.11), (3.12), (3.20) and substituting these coefficients into equation (3.19) it can be found that equation (3.19) becomes the nonlinear free surface condition (3.6). Thus ϕ obtained through the iteration based on (3.21) is also the solution to nonlinear boundary value problem (3.7).

Both linearized boundary value problems (3.17) and (3.21) can be used to form the iteration to solve nonlinear boundary value problem (3.7). Theoretically, the convergence speed of using (3.17) is faster than the convergence speed of using (3.21). However, the algorithm for using (3.21) is simpler. Therefore it will be used in Chapter 6 of this thesis to form the iterative algorithm to solve the nonlinear ship wave problem (3.7).

3.3 A Linearized Ship Wave Problem

In order to compare the present computation with the numerical results found in the literature and to disc the drawbacks found in the Neumann-Kelvin and Dawson's linearized ship wave models, a new linearized ship wave problem based

on the transformed nonlinear ship wave problem obtained in Section (3.1) is also derived and solved in the present study as a special case of the present iterative approach.

As has been mentioned in Section (3.2), an initial value for Φ is needed in the first step of the iteration, which can be chosen arbitrarily. However, if this initial value Φ is chosen to be the double-body solution, i.e. if we set $\Phi = \bar{\Phi}$, the result of the first iteration becomes a perturbation solution based on the double-body potential $\phi = \bar{\Phi} + \phi'$. In other words, the first iteration gives a linear solution to the nonlinear boundary value problem (3.7).

Using $\frac{\partial \bar{\phi}}{\partial x} = 0$, $\frac{\partial}{\partial x}(\frac{\partial \bar{\phi}}{\partial \ell}) = 0$, $\frac{\partial}{\partial x}(\frac{\partial^2 \bar{\phi}}{\partial \ell^2}) = 0$ for double-body flow in equations (3.10) to (3.16) and dividing these equations by $2g$, a linearized free surface condition of the ship wave problem in terms of the double-body potential $\bar{\Phi}$ is obtained as:

$$A\frac{\partial^2 \phi}{\partial \ell^2} + B\frac{\partial \phi}{\partial \ell} + C\frac{\partial \phi}{\partial z} + D\frac{\partial^2 \phi}{\partial \ell \partial z} + E\frac{\partial^3 \phi}{\partial \ell^2 \partial z} = H, \quad on\ z = 0. \tag{3.22}$$

The coefficients A, B, C, D, E, and H become

$$A = \frac{3}{2}(\frac{\partial \bar{\Phi}}{\partial \ell})^2 - \frac{1}{2}U^2; \tag{3.23}$$

$$B = 3\frac{\partial \bar{\Phi}}{\partial \ell}\frac{\partial^2 \bar{\Phi}}{\partial \ell^2}; \tag{3.24}$$

$$C = g - \frac{1}{g}(\frac{\partial^2 \bar{\Phi}}{\partial \ell^2})^2[2(\frac{\partial \bar{\Phi}}{\partial \ell})^2 - U^2] + \frac{1}{2g}\frac{\partial \bar{\Phi}}{\partial \ell}\frac{\partial^3 \bar{\Phi}}{\partial \ell^3}[(\frac{\partial \bar{\Phi}}{\partial \ell})^2 - U^2]; \tag{3.25}$$

$$D = \frac{1}{g}(\frac{\partial \bar{\Phi}}{\partial \ell})^3\frac{\partial^2 \bar{\Phi}}{\partial \ell^2}; \tag{3.26}$$

$$E = -\frac{1}{2g}[(\frac{\partial\bar{\Phi}}{\partial\ell})^2 - U^2](\frac{\partial\bar{\Phi}}{\partial\ell})^2; \tag{3.27}$$

$$H = 3(\frac{\partial\bar{\Phi}}{\partial\ell})^2\frac{\partial^2\bar{\Phi}}{\partial\ell^2}. \tag{3.28}$$

Equation (3.22) is a linear free surface condition which is satisfied at the undisturbed fluid free surface $z = 0$. The projection of free surface streamline ℓ in this case becomes the double-body streamline. The exact ship wave boundary value problem is, therefore, approximated by the following linearized boundary value problem based on the double-body flow.

$$\begin{cases} \nabla^2\phi = 0, & \textit{in the fluid domain;} \\ \vec{n}\cdot\nabla\phi = 0, & \textit{on the body surface;} \\ A\frac{\partial^2\phi}{\partial\ell^2} + B\frac{\partial\phi}{\partial\ell} + C\frac{\partial\phi}{\partial z} + D\frac{\partial^2\phi}{\partial\ell\partial z} + E\frac{\partial^3\phi}{\partial\ell^2\partial z} = H, & \textit{on } z = 0; \\ |\nabla\phi| \to -U, & z \le 0 \textit{ and } \sqrt{x^2+y^2+z^2} \to \infty; \\ \textit{The radiation condition.} \end{cases} \tag{3.29}$$

Dawson's free surface condition (2.17) can be easily obtained, if only the terms of zero order in η are kept in the Taylor's series expansion (3.4). Two steps can be explained as follows:

1. Keeping only the zero terms in η, equation (3.4) becomes

$$(\frac{\partial\phi}{\partial\ell})^2\frac{\partial^2\phi}{\partial\ell^2} + 2\frac{\partial\phi}{\partial\ell}\frac{\partial\phi}{\partial z}\frac{\partial^2\phi}{\partial\ell\partial z} + (\frac{\partial\phi}{\partial z})^2\frac{\partial^2\phi}{\partial z^2} + g\frac{\partial\phi}{\partial z} = 0, \quad \textit{on } z = 0. \tag{3.30}$$

2. Substituting $\phi = \bar{\Phi} + \phi'$ into equation (3.30) and dropping all non-linear terms in ϕ' gives

$$(\frac{\partial\bar{\Phi}}{\partial\ell})^2\frac{\partial^2\phi'}{\partial\ell^2} + 2\frac{\partial\bar{\Phi}}{\partial\ell}\frac{\partial^2\bar{\Phi}}{\partial\ell^2}\frac{\partial\phi'}{\partial\ell} + g\frac{\partial\phi'}{\partial z} = -(\frac{\partial\bar{\Phi}}{\partial\ell})^2\frac{\partial^2\bar{\Phi}}{\partial\ell^2}, \quad \textit{on } z = 0. \tag{3.31}$$

Equation (3.31) is exactly Dawson's linearized free surface condition given by equation (2.17). It can also be written in terms of the total velocity potential ϕ, as it was originally given by Dawson, in the form:

$$(\frac{\partial\tilde{\Phi}}{\partial\ell})^2\frac{\partial^2\phi}{\partial\ell^2}+2\frac{\partial\tilde{\Phi}}{\partial\ell}\frac{\partial^2\tilde{\Phi}}{\partial\ell^2}\frac{\partial\phi}{\partial\ell}+g\frac{\partial\phi}{\partial z}=2(\frac{\partial\tilde{\Phi}}{\partial\ell})^2\frac{\partial^2\tilde{\Phi}}{\partial\ell^2},\quad on\ z=0. \tag{3.32}$$

Equation (3.32) is Dawson's linearized free surface condition given by equation (2.18) which is in terms of the total velocity potential ϕ.

Comparing the present linearized free surface condition (3.22) with Dawson's linearized free surface condition (2.18) or (3.32), (see Table 3.1), it can be seen that in Dawson's linearized free surface condition some zero and first order terms in ϕ' are missing, because of the neglecting of the terms of order η in the Taylor's series expansion.

When the thin ship condition is satisfied, the present linearized free surface can be reduced to the Neumann-Kelvin linearized free surface condition (while Dawson's linearized free surface condition can not). For a thin ship case, the velocity potential is expressed by a uniform flow plus a perturbation, i.e. we write $\phi=-Ux+\phi'$. Replacing $\tilde{\Phi}$ by $-Ux$ and ℓ by x in equations (3.23) to (3.28) and writing equation (3.22) in terms of perturbation potential ϕ', the Neumann-Kelvin linearized free surface condition (2.10) can be obtained. A comparison between the present linearized free surface and the Neumann-Kelvin free surface is also shown in Table 3.1.

	Present	Dawson	Neumann-Kelvin
A	$\frac{3}{2}(\frac{\partial\hat{\phi}}{\partial t})^2 - \frac{1}{2}U^2$	$(\frac{\partial\hat{\phi}}{\partial t})^2$	U^2
B	$3\frac{\partial\hat{\phi}}{\partial t}\frac{\partial^2\hat{\phi}}{\partial t^2}$	$2\frac{\partial\hat{\phi}}{\partial t}\frac{\partial^2\hat{\phi}}{\partial t^2}$	0
C	$g - \frac{1}{g}(\frac{\partial^2\hat{\phi}}{\partial t^2})^2[2(\frac{\partial\hat{\phi}}{\partial t})^2 - U^2]$ $+\frac{1}{2g}\frac{\partial\hat{\phi}}{\partial t}\frac{\partial^3\hat{\phi}}{\partial t^3}[(\frac{\partial\hat{\phi}}{\partial t})^2 - U^2]$	g	g
D	$\frac{1}{g}(\frac{\partial\hat{\phi}}{\partial t})^3\frac{\partial^2\hat{\phi}}{\partial t^2}$	0	0
E	$-\frac{1}{2g}[(\frac{\partial\hat{\phi}}{\partial t})^2 - U^2](\frac{\partial\hat{\phi}}{\partial t})^2$	0	0
H	$3(\frac{\partial\hat{\phi}}{\partial t})^2\frac{\partial^2\hat{\phi}}{\partial t^2}$	$2(\frac{\partial\hat{\phi}}{\partial t})^2\frac{\partial^2\hat{\phi}}{\partial t^2}$	0

Table 3.1. Comparison of linearized free surface conditions

4 BOUNDARY INTEGRAL METHOD

4.1 Indirect Formulation

The discussions on the boundary integral formulations in this section are focused on a potential boundary value problem in which Laplace's equation is satisfied in the considered domain Ω and a boundary condition is satisfied on its boundary S. The problem under consideration can be expressed as:

$$\begin{cases} \nabla^2\phi(x,y,z) = 0, & in \ \ \Omega; \\ f[\phi(x,y,z), \phi_n(x,y,z)] = 0, & on \ \ S. \end{cases} \tag{4.1}$$

The boundary condition in boundary value problem (4.1) is of a mixed type, and is a function of the potential function ϕ and its normal derivative ϕ_n. When the boundary condition in (4.1) is a function of ϕ only the condition is called of Dirichlet type, while of ϕ_n only it is called of the Neumann type.

In principle, the solution to Laplace's equation can be represented by a combination of single-layer and double-layer source potentials (Wardle, 1981)

$$\phi(p) = \int_S \sigma(q)\psi(p,q)dS(q) + \int_S \mu(q)\frac{\partial\psi(p,q)}{\partial n(q)}dS(q), \tag{4.2}$$

where p represents a field point; q represents the source point; $\phi(p)$ denotes the velocity potential at the field point p; $\sigma(q)$ and $\mu(q)$ are the single-layer and double-layer source densities respectively; and $\psi(p,q)$ is a function of p and q which will be explained later in this section. Here $\frac{\partial}{\partial n}$ is used to denote the normal derivative with respect to the normal to S.

The first integral in equation (4.2) is called single-layer potential which is

formed by distributing simple sources with density $\sigma(q)$ over the surface S. The second integral in equation (4.2) is called double-layer potential which can be generated by two single-layer sources. Considering two surfaces separated by a small distance ϵ, assume each surface has a distribution of attraction of equal magnitude but of opposite sign for neighbouring points and take the magnitude of the attraction to be inversely proportional to ϵ. The potential associated with the point $q(x, y, z)$ and the point $q(x + dx, y + dy, z + dz)$ is given by the limit

$$\lim_{\epsilon \to 0}\{\frac{1}{\epsilon}[\psi(p, q + \epsilon) - \psi(p, q)]\}, \tag{4.3}$$

which can be seen to be the derivative of the function $\psi(p, q)$ in the direction normal to the surface S. Integrating over surface S gives the second integral in equation (4.2) which is the double-layer potential.

For equation (4.2) to be the solution of boundary value problem (4.1), $\psi(p, q)$ has to satisfy Laplace's equation in Ω. This function $\psi(p, q)$ is called the fundamental solution of Laplace's equation. It is easily verified by direct substitution that the functions

$$\frac{1}{r(p, q)}, \qquad \textit{in three dimensions}, \tag{4.4}$$

$$\log[\frac{1}{r(p, q)}], \qquad \textit{in two dimensions}, \tag{4.5}$$

satisfy the respective Laplace's equation in Ω for $r(p, q) \neq 0$ and are called the fundamental solutions of the corresponding Laplace's equations, where $r(p, q)$ is the scalar distance between points p and q.

Since there is only one boundary condition and there are two functions (ψ and $\partial\psi/\partial n$) in equation (4.2), there is a "degree of freedom" in using it to solve potential boundary value problems. This leads to the fact that only one of the

source potentials is needed in solving a given problem. For example, to solve a boundary value problem with Dirichlet type boundary condition (ϕ prescribed on S), the unknown function $\phi(p)$ with $p(x,y,z) \in (\Omega + S)$ may be expressed solely as a double-layer potential of unknown density $\mu(q)$

$$\phi(p) = \int_S \mu(q) \frac{\partial \psi(p,q)}{\partial n(q)} dS(q). \tag{4.6}$$

To solve a boundary value problem with Neumann type boundary condition (ϕ_n prescribed on S), which is the type of boundary value problem solved in fluid flow passing an object (a double-body problem for instance), the unknown function $\phi(p)$ can be expressed solely as a single-layer potential with unknown density $\sigma(q)$

$$\phi(p) = \int_S \sigma(q) \psi(p,q) dS(q), \tag{4.7}$$

for point $p(x,y,z) \in (\Omega + S)$.

To solve a Neumann boundary value problem by using equation (4.7), the normal derivative of ϕ at p is substituted into the boundary condition so that the source density $\sigma(q)$ can be computed. The normal derivative of ϕ at p can be obtained by directly differentiating equation (4.7), which gives

$$\frac{\partial \phi(p)}{\partial n(p)} = \int_S \sigma(q) \frac{\partial \psi(p,q)}{\partial n(p)} dS(q), \tag{4.8}$$

where n is the unit normal to S.

Usually in the literature equation (4.8) is written, for three dimensional cases, by using the limiting behaviour of the integral of equation (4.8) when point p is located at the same point q, in the following form:

$$\frac{\partial \phi(p)}{\partial n(p)} = -2\pi\sigma(p) + \int_S \sigma(q) \frac{\partial}{\partial n(p)} [\frac{1}{r(p,q)}] dS(q). \tag{4.9}$$

It is important to note that, firstly, equation (4.9) is true only for the case when S is a smooth surface, and secondly, the integral in the equation does not include the point p. It should also be noted that for the linear element boundary integral algorithm in which the collocation points are on the nodes of the mesh instead of on its panels, equation (4.9) can not be used, although the unpaneled surface could be a smooth one, because the limit of $\partial\phi/\partial n$ for p approaching q is not $2\pi\sigma(p)$ in this case. To accurately define the normal derivative ϕ_n, a new expression is introduced as

$$\frac{\partial\phi(p)}{\partial n(p)} = -\beta\sigma(p) + \oint\!\!\!\!\!\!\bigcirc_S \sigma(q)\frac{\partial}{\partial n(p)}[\frac{1}{r(p,q)}]dS(q), \tag{4.10}$$

where β is the solid angle at point p subtended by the surface $S - p$. The calculation of β will be further discussed in Chapter 5, where the algorithm of the present study is presented. The new notation introduced here $\oint\!\!\!\!\!\!\bigcirc_S$ is defined as the surface integration over S with point p excluded.

It should be mentioned that the two integral equations (4.6) and (4.7) are not the only possible ones that can be formulated using the single-layer and double-layer potentials. For example, instead of using the double-layer potential for the Dirichlet boundary conditions one could use a single-layer potential.

For mixed boundary value problems, for example the ship wave problem, either the single-layer or the double-layer can be used to solve the problem. In this case a relation between ϕ and its normal derivative ϕ_n is provided by the boundary condition. So far almost without exception, authors of research papers on solving the ship wave problem have only used the single-layer source potential in formulating their algorithms.

4.2 Direct Formulation

A conceptual disadvantage of single-layer and double-layer potentials is the introduction of formal source densities which usually bear no physical relation to the solution of the problem. This can be overcome by using the direct formulation of the boundary integral method, where values of the potential function ϕ and its normal derivative ϕ_n over S play the role of the source densities in generating the solution ϕ in Ω. This formulation can be deduced through Green's third identity, Betti's or similar theorems or principles such as virtual work (Brebbia 1984). According to Green's theorem, if ϕ and ψ are two continuous functions with continuous first order derivatives, the following identity exists

$$\int_{\Omega}(\phi\nabla^2\psi - \psi\nabla^2\phi)d\Omega = \int_S(\phi\frac{\partial\psi}{\partial n} - \psi\frac{\partial\phi}{\partial n})dS. \tag{4.11}$$

The normal direction to S is taken outwards from Ω.

If ϕ is taken to be the unknown harmonic function (satisfies $\nabla^2\phi = 0$) and ψ as the fundamental solution to Laplace's equation, which satisfies the condition of Green's theorem, the integral on the left hand side of equation (4.11) becomes zero, through a limit procedure (Wardle 1981). Equation (4.11) can then be written as:

$$\int_S \phi\frac{\partial\psi}{\partial n}dS = \int_S \psi\frac{\partial\phi}{\partial n}dS. \tag{4.12}$$

Equation (4.12) is an important formulation of the direct boundary integral method for potential problems. It represents a constraint equation between the solution of the problem ϕ and its normal derivative ϕ_n on the boundaries. For Dirichlet boundary condition the left hand side of (4.12) is known and ϕ_n is to be found. For the Neumann boundary conditions the right hand side of the

equation is known. For a mixed boundary condition, a relation between ϕ and ϕ_n is provided by the boundary condition, which allows equation (4.12) to be arranged to compute either ϕ or ϕ_n.

For three dimensional domains, by substituting the fundamental solution to Laplace's equation into equation (4.12), we have

$$\int_S \phi(q)\frac{\partial}{\partial n(q)}[\frac{1}{r(p,q)}]dS(q) = \int_S \frac{1}{r(p,q)}\frac{\partial \phi(q)}{\partial n(q)}dS(q). \tag{4.13}$$

By isolating the singularity arising when p approaches q in the integrals, equation (4.13) can also be written as follows

$$\beta\phi(p) + \oint_S \phi(q)\frac{\partial}{\partial n(q)}[\frac{1}{r(p,q)}]dS(q) = \int_S \frac{1}{r(p,q)}\frac{\partial \phi(q)}{\partial n(q)}dS(q), \tag{4.14}$$

where β is the solid angle at point p subtended by $S - p$; and the notation $\oint_S$ is defined to be the integration through S with point p excluded.

4.3 Direct VS Indirect Formulation

As the unknowns in the integral equation are physical boundary quantities (either ϕ or ϕ_n), equation (4.14) is called the direct boundary integral equation to distinguish it from integral equations that involve an intermediate source density, for example equations (4.6) and (4.7). Formulations based on the source distribution approach are called indirect because the solution can only be obtained through an intermediate source density. It is difficult to explicitly display the relation between the direct and the indirect formulations since both of them are in integral equation forms. However these two approaches have the same theoretical foundation and behaviour.

By isolating the singularity at $p = q$ from the integral over S, and using the notation $\oint\!\!\!\!\!\!\bigcirc_S$, equation (4.2) can be rewritten as:

$$(1-\beta)\phi(p) - \oint\!\!\!\!\!\!\bigcirc_S \mu(q)\frac{\partial \psi(p,q)}{\partial n(q)}dS(q) = \int_S \sigma(p,q)\psi(p,q)dS(q). \qquad (4.15)$$

For three dimensional domains, replacing $\psi(q,p)$ by $1/r(p,q)$ allows equation (4.15) to be rewritten as:

$$(1-\beta)\phi(p) - \oint\!\!\!\!\!\!\bigcirc_S \mu(q)\frac{\partial}{\partial n(q)}[\frac{1}{r(p,q)}]dS(q) = \int_S \sigma(p,q)\frac{1}{r(p,q)}dS(q). \qquad (4.16)$$

Comparing equation (4.16) and the direct integral equation (4.14) it can be seen that if both single- and double-layers are distributed to solve a potential boundary value problem, then the source densities of single-layer and double-layer have to be related, since the number of unknowns are more than the constraint. The relation between these sources can be established, as explained before, by the Green's third identity. In other words, the direct formulation distributes both single-layer and double-layer sources with the double-layer source to be the velocity potential ϕ and the single-layer source the normal derivatives of the potential ϕ_n.

5 NUMERICAL PROCEDURES FOR SOLVING THE LINEAR PROBLEM

5.1 Indirect Boundary Integral Algorithm

5.1.1 The structure of the algorithm

A numerical algorithm based on the indirect boundary integral theory is developed in this section to solve the linearized ship wave problem derived in Section (3.3) of this thesis. The linearized ship wave boundary value problem given by system of equations (3.29) is written here again for convenience:

$$\begin{cases} \nabla^2\phi = 0, & \textit{in the fluid domain;} \\ \vec{n}\cdot\nabla\phi = 0, & \textit{on the body surface;} \\ A\frac{\partial^2\phi}{\partial\ell^2} + B\frac{\partial\phi}{\partial\ell} + C\frac{\partial\phi}{\partial x} + D\frac{\partial^2\phi}{\partial\ell\partial x} + E\frac{\partial^3\phi}{\partial\ell^2\partial x} = H, & \textit{on } z = 0; \\ |\nabla\phi| \to -U, & z \le 0 \textit{ and } \sqrt{x^2+y^2+z^2} \to \infty; \\ \textit{The radiation condition.} \end{cases} \tag{5.1}$$

The coefficients in the fluid free surface condition are given as:

$$A = \frac{3}{2}(\frac{\partial\bar{\Phi}}{\partial\ell})^2 - \frac{1}{2}U^2; \tag{5.2}$$

$$B = 3\frac{\partial\bar{\Phi}}{\partial\ell}\frac{\partial^2\bar{\Phi}}{\partial\ell^2}; \tag{5.3}$$

$$C = g - \frac{1}{g}(\frac{\partial^2\bar{\Phi}}{\partial\ell^2})^2[2(\frac{\partial\bar{\Phi}}{\partial\ell})^2 - U^2] + \frac{1}{2g}\frac{\partial\bar{\Phi}}{\partial\ell}\frac{\partial^3\bar{\Phi}}{\partial\ell^3}[(\frac{\partial\bar{\Phi}}{\partial\ell})^2 - U^2]; \tag{5.4}$$

$$D = \frac{1}{g}(\frac{\partial\bar{\Phi}}{\partial\ell})^3\frac{\partial^2\bar{\Phi}}{\partial\ell^2}; \tag{5.5}$$

$$E = -\frac{1}{2g}[(\frac{\partial\bar{\Phi}}{\partial\ell})^2 - U^2](\frac{\partial\bar{\Phi}}{\partial\ell})^2; \tag{5.6}$$

$$H = 3(\frac{\partial\bar{\Phi}}{\partial\ell})^2\frac{\partial^2\bar{\Phi}}{\partial\ell^2}. \tag{5.7}$$

The present numerical algorithm for solving the above linearized boundary value problem is developed by applying the linear element technique. The linear element technique distributes the unknowns on the nodes of the surface mesh and linearly varies the unknowns over each element (or panel). To accurately panelize the body surface, triangular panels are used on the surface mesh.

In the algorithm, applying the indirect boundary integral theory, the wave elevation and the wave resistance are computed through the following steps:

1. Solving the double-body problem for $\bar{\Phi}$;
2. Generating the streamlines on $z = 0$ by using the potential $\bar{\Phi}$;
3. Computing the coefficients A, B, C, D, E and H;
4. Solving boundary value problem (5.1) for ϕ;
5. Calculating the wave resistance by using ϕ;
6. Evaluating the free surface wave elevation by using ϕ.

Six computer program modules have been developed to perform the tasks of the above mentioned six steps. The program modules are controlled by a control module. Input is read in by the control module. The output is sent to output files for post processing.

5.1.2 Solution of double-body problem

The algorithm begins with solving the double-body problem. The geometry of the double-body problem is shown in Fig. 5.1. The purpose of using the double-body shape is to generate a constant flow around the real body with zero velocity in z direction on $z = 0$ by using the Rankine source method. In other words, the flow generated by the double-body moving steadily in a fluid of infinite extent, is equivalent to the flow generated by a single body moving in a semi-infinite fluid when the free surface disturbance is neglected or $\frac{\partial \bar{\Phi}}{\partial z} = 0$ on $z = 0$.

The double-body problem in the coordinate system fixed with the double-body is written here again as:

$$\begin{cases} \nabla^2 \bar{\Phi} = 0, & \textit{in the fluid domain;} \\ \vec{n} \cdot \nabla \bar{\Phi} = 0, & \textit{on the body surface;} \\ \frac{\partial \bar{\Phi}}{\partial z} = 0, & \textit{on } z = 0; \\ |\nabla \bar{\Phi}| \to -U, & \textit{as } \sqrt{x^2 + y^2 + z^2} \to \infty, \quad z \leq 0. \end{cases} \tag{5.8}$$

In boundary value problem (5.8), U is the velocity of the double-body.

The double-body velocity potential $\bar{\Phi}$ at any point in the fluid domain (including the boundaries) is then expressed in terms of sources distributed linearly over each triangular element of the mesh generated on the body surface. This potential is written as:

$$\bar{\Phi}(p) = -Ux(p) + \sum_{q=1}^{ne} \int_{S(q)} [\frac{1}{r(p,q)} + \frac{1}{r(p,\bar{q})}] \sigma(q) dS(q), \tag{5.9}$$

where p is any point in the fluid field including the body surface, which is called the field point; q refers to the element label; ne is the total number of elements on the body surface (the object body only); $S(q)$ represents the area of element

q; and $r(p,q)$ is the distance from p to the integration point $[x(q), y(q), z(q)]$ on element q, which is defined as:

$$r(p,q) = \sqrt{[x(p) - x(q)]^2 + [y(p) - y(q)]^2 + [z(p) - z(q)]^2}, \tag{5.10}$$

and $r(p,\bar{q})$ is the distance from field point p to the image point $[x(\bar{q}), y(\bar{q}), z(\bar{q})]$ of point $[x(q), y(q), z(q)]$ with respect to the plane $z = 0$, which is given by

$$r(p,\bar{q}) = \sqrt{[x(p) - x(\bar{q})]^2 + [y(p) - y(\bar{q})]^2 + [z(p) - z(\bar{q})]^2}. \tag{5.11}$$

Equation (5.9) expresses the velocity potential as a resultant of the source density distribution $\sigma(q)$ over all elements. In this equation $\sigma(q)$ is the linear function based on $\sigma_1(q)$, $\sigma_2(q)$, $\sigma_3(q)$, where $\sigma_1(q)$, $\sigma_2(q)$, $\sigma_3(q)$ are the source density magnitudes at the three vertices which define panel q. These locally numbered source density values can also be converted to the globally numbered source density values $\sigma(i)$, i=1,2,3, ..., nn, through a connectivity matrix, where nn is the total number of nodes on the body surface mesh.

In order to explain how the linear system of equations is formed to solve for the nn unknowns $\sigma(i)$ $i = 1, 2, 3, ..., nn$, the velocity potential is written in terms of these unknowns $\sigma(i)$. By introducing a tent function $T(j)$ the double-body velocity potential is written as:

$$\bar{\Phi}(i) = -Ux(i) + \sum_{j=1}^{nn} \sigma(j) \int_{S(j)} [\frac{1}{r(i,q)} + \frac{1}{r(i,\bar{q})}] T(j) dS(q), \tag{5.12}$$

where $\bar{\Phi}(i)$ represents the velocity potential at a field point numbered i; $\sigma(j)$ represents the source density at node point j; $T(j)$ is a tent function centered at node j, such that $T(j) = 1$ at node j and $T(j) = 0$ at the nodes surrounding j ; $S(j)$ represents the area of the continuous compact support of $T(j)$, i.e. the

surface area of the elements having a common vertex at node j, (see Fig. A.1 in Appendix A); $r(i,q)$ and $r(i,\bar{q})$ are given as:

$$r(i,q) = \sqrt{[x(i)-x(q)]^2 + [y(i)-y(q)]^2 + [z(i)-z(q)]^2}, \tag{5.13}$$

and

$$r(i,\bar{q}) = \sqrt{[x(i)-x(\bar{q})]^2 + [y(i)-y(\bar{q})]^2 + [z(i)-z(\bar{q})]^2}. \tag{5.14}$$

By letting equation (5.12) satisfy at each node ($i = 1,2,3,...,nn$) the impermeability condition in boundary value problem (5.8), a linear system of nn linear equations can be obtained for the nn unknowns $\sigma(i)$, $i = 1,2,3,...,nn$. The linear system could be written as:

$$[A]\{\sigma\} = U\{n_x\}, \tag{5.15}$$

where

$$[A] = \begin{bmatrix} a(1,1) & a(1,2) & \cdots & a(1,nn) \\ a(2,1) & a(2,2) & \cdots & a(2,nn) \\ & & & \\ & & & \\ a(nn,1) & a(nn,2) & \cdots & a(nn,nn) \end{bmatrix}.$$

$[A]$ is called the influence coefficients matrix. The entry $a(i,j)$ of this matrix represents the influence at node i produced by a unit source density at node j. The unit source density at point j is linearly distributed on all the elements surrounding point j, i.e. the source density at node j is equal to one and is equal to zero at each of the surrounding nodes. The matrix is generated by using the following equation:

$$
\begin{aligned}
a(i,j) \;=\; & \int_{S(j)} \{ \frac{\partial}{\partial x(i)} [\frac{1}{r(i,q)} + \frac{1}{r(i,\bar{q})}] n_x(i) \\
& + \frac{\partial}{\partial y(i)} [\frac{1}{r(i,q)} + \frac{1}{r(i,\bar{q})}] n_y(i) \\
& + \frac{\partial}{\partial z(i)} [\frac{1}{r(i,q)} + \frac{1}{r(i,\bar{q})}] n_z(i) \} T(j) dS(q), \qquad (5.16)
\end{aligned}
$$

where $n_x(i)$, $n_y(i)$, and $n_z(i)$ are the unit normal components of the paneled body surface at node i in the directions of x, y, z respectively.

The partial derivatives with respect to x, y, and z in the integrand of equation (5.16) are given here as follows:

$$
\frac{\partial}{\partial x(i)} [\frac{1}{r(i,q)} + \frac{1}{r(i,\bar{q})}] = -[\frac{x(i) - x(q)}{r^3(i,q)} + \frac{x(i) - x(\bar{q})}{r^3(i,\bar{q})}]; \qquad (5.17)
$$

$$
\frac{\partial}{\partial y(i)} [\frac{1}{r(i,q)} + \frac{1}{r(i,\bar{q})}] = -[\frac{y(i) - y(q)}{r^3(i,q)} + \frac{y(i) - y(\bar{q})}{r^3(i,\bar{q})}]; \qquad (5.18)
$$

$$
\frac{\partial}{\partial z(i)} [\frac{1}{r(i,q)} + \frac{1}{r(i,\bar{q})}] = -[\frac{z(i) - z(q)}{r^3(i,q)} + \frac{z(i) - z(\bar{q})}{r^3(i,\bar{q})}]. \qquad (5.19)
$$

The integration in equation (5.16) is performed by one of two methods depending whether the field point i is on the source point j or not. When the field point i is not on the source point j, i.e. $i \neq j$, a numerical integration routine is used to calculate the integral in equation (5.16), (see Appendix A for details of the numerical integration procedure). When the field point i is on the source point j, i.e. $i = j$, the value of the integral in equation (5.16) is equal to the solid angle at j subtended by the paneled surface, (see also Appendix A for the procedure for computing the solid angle).

The linear system is solved by using the Gaussian elimination method. A standard linear system solver is adopted in the software.

5.1.3 Generation of streamlines

In the present linearized problem, boundary value problem (3.29) or (5.1), the free surface condition is written in terms of the streamlines located on the plane $z = 0$. Therefore these streamlines must be generated and a surface mesh based on these streamlines must be produced. In the present study the streamlines of the double-body flow, on $z = 0$, are generated by solving the ordinary differential equation that describes a streamline on $z = 0$, that is

$$\frac{dx}{\bar{u}} = \frac{dy}{\bar{v}}, \tag{5.20}$$

where x, y are the coordinates of a point on the streamline; $\bar{u}$ and $\bar{v}$ are velocity components of the double-body flow in x and y directions respectively. These velocity components can be expressed in terms of the source densities $\sigma(i)$, $i = 1, 2, 3, ..., nn$, obtained from solving the double-body problem.

In equation (5.20) dx is specified by the element size of the surface mesh which, in turn, is determined according to the Froude number. See Appendix C for details of the relation between the surface mesh size, element size and the Froude number. Therefore dy could be computed by solving the ordinary differential equation (5.20). In the present study a modified Euler-Heun's technique is used. Applying this procedure to equation (5.20) gives

$$x(i+1) = x(i) + dx(i), \tag{5.21}$$

$$y(i+1) = y(i) + \frac{1}{2}[\frac{\bar{v}(i)}{\bar{u}(i)} + \frac{\bar{v}(c)}{\bar{u}(c)}]dx(i), \tag{5.22}$$

where $\bar{u}(i)$, $\bar{v}(i)$ are the fluid velocity components of the double-body flow at point i, and $\bar{u}(c)$, $\bar{v}(c)$ are the corresponding velocity components of the double-body

flow at point c. The coordinates of point c, namely $x(c)$, $y(c)$ are determined by

$$x(c) = x(i) + dx(i), \tag{5.23}$$

$$y(c) = \frac{\tilde{u}(i)}{\tilde{v}(i)} dx(i). \tag{5.24}$$

The velocity components $\tilde{u}(i)$, $\tilde{v}(i)$, $\tilde{u}(c)$, and $\tilde{v}(c)$ are computed by using the double-body velocity potential through the following formulations:

$$\tilde{u}(i) = -U + \sum_{j=1}^{nn} 2\sigma(j) \int_{S(j)} \frac{-[x(i) - x(q)]T(j)}{\{[x(i) - x(q)]^2 + [y(i) - y(q)]^2 + [z(i) - z(q)]^2\}^{3/2}} dS(q); \tag{5.25}$$

$$\tilde{v}(i) = \sum_{j=1}^{nn} 2\sigma(j) \int_{S(j)} \frac{-[y(i) - y(q)]T(j)}{\{[x(i) - x(q)]^2 + [y(i) - y(q)]^2 + [z(i) - z(q)]^2\}^{3/2}} dS(q); \tag{5.26}$$

$$\tilde{u}(c) = -U + \sum_{j=1}^{nn} 2\sigma(j) \int_{S(j)} \frac{-[x(c) - x(q)]T(j)}{\{[x(c) - x(q)]^2 + [y(c) - y(q)]^2 + [z(c) - z(q)]^2\}^{3/2}} dS(q); \tag{5.27}$$

$$\tilde{v}(c) = \sum_{j=1}^{nn} 2\sigma(j) \int_{S(j)} \frac{-[y(c) - y(q)]T(j)}{\{[x(c) - x(q)]^2 + [y(c) - y(q)]^2 + [z(c) - z(q)]^2\}^{3/2}} dS(q); \tag{5.28}$$

where nn is the number of nodes on the real body surface mesh.

It is noted that the integration is performed only on the real body surface, since the symmetric condition is used. A factor of 2 is used in equations (5.25) to (5.28) to account for the effect of the image body. In the submerged case the collocation point i could never be located on the integration element j, in calculating the integrals in equations (5.25) to (5.28), since i is on the free surface mesh and q is on the body surface mesh. Therefore only the numerical integration

is used to compute the values of the integrals. See Appendix A for the details of the numerical integration.

The first node on each streamline and the increments $dx(i)$ in the x direction are predefined by the size of the free surface mesh and the size of the elements, which are Froude Number dependent. See Appendix C for the details. The location of the second node $[x(i=2), y(i=2)]$ is calculated by using equations (5.21) and (5.22) knowing the location of the first node $[x(i=1), y(i=1)]$. Repeatedly using equations (5.21) and (5.22) for $i = 1, 2, 3, ..., n\ell$, a streamline can be obtained, where $n\ell$ is the number of nodes on each streamline. The coordinates of the nodes of the surface mesh are obtained by repeating the same procedure for all streamlines needed to generate the free surface mesh.

5.1.4 Computation of coefficients

In order to compute the coefficients A, B, C, D, E and H in the free surface condition in boundary value problem (5.1) directly from the source densities, the partial derivatives with respect to ℓ, in the expressions of these coefficients have to be converted into partial derivatives with respect to x and y. From the definition of ℓ we can write:

$$\begin{aligned}
\frac{\partial \tilde{\Phi}}{\partial \ell} &= \frac{\partial \tilde{\Phi}}{\partial x}\frac{\partial x}{\partial \ell} + \frac{\partial \tilde{\Phi}}{\partial y}\frac{\partial y}{\partial \ell} \\
&= \tilde{u}\frac{\tilde{u}}{\sqrt{\tilde{u}^2+\tilde{v}^2}} + \tilde{v}\frac{\tilde{v}}{\sqrt{\tilde{u}^2+\tilde{v}^2}} \\
&= \sqrt{\tilde{u}^2+\tilde{v}^2}. \qquad (5.29)
\end{aligned}$$

$\frac{\partial\bar{\Phi}}{\partial\ell}$ at point i is then expressed as:

$$\frac{\partial\bar{\Phi}}{\partial\ell}(i) = \sqrt{\bar{u}^2(i) + \bar{v}^2(i)}, \tag{5.30}$$

where $\bar{u}(i)$ and $\bar{v}(i)$ are the velocity components of the double-body flow in x and y directions respectively, which have been already given by equations (5.25) and (5.26).

The second order derivatives of $\bar{\Phi}$ with respect to ℓ are obtained by applying a five-point centered finite difference operator on the first order derivatives $\partial\bar{\Phi}/\partial\ell$, which is expressed as:

$$\begin{aligned}\frac{\partial^2\bar{\Phi}}{\partial\ell^2}(i) &= F5D1(i)\frac{\partial\bar{\Phi}}{\partial\ell}(im2) \\ &+F5D2(i)\frac{\partial\bar{\Phi}}{\partial\ell}(im1) \\ &+F5D3(i)\frac{\partial\bar{\Phi}}{\partial\ell}(i) \\ &+F5D4(i)\frac{\partial\bar{\Phi}}{\partial\ell}(ip1) \\ &+F5D5(i)\frac{\partial\bar{\Phi}}{\partial\ell}(ip2),\end{aligned} \tag{5.31}$$

where $F5D1(i)$, $F5D2(i)$, $F5D3(i)$, $F5D4(i)$, $F5D5(i)$ are the five coefficients of the five-point centered finite difference operator, (see Appendix D for details). $im2$, $im1$, $ip1$, $ip2$ are the point numbers, which are given as:

$$im2 = i - 2nb; \tag{5.32}$$

$$im1 = i - nb; \tag{5.33}$$

$$ip1 = i + nb; \tag{5.34}$$

$$ip2 = i + 2nb. \tag{5.35}$$

The variable nb represents the number of streamlines on the fluid free surface mesh.

The coefficients in the free surface condition of the present linear ship wave problem given by equations (5.2) to (5.7) are finally obtained as:

$$A(i) = \frac{3}{2}[U_\ell(i)]^2 - \frac{1}{2}U^2; \tag{5.36}$$

$$B(i) = 3U_\ell(i)\frac{\partial U_\ell}{\partial \ell}(i); \tag{5.37}$$

$$\begin{aligned} C(i) = {} & g - \frac{1}{g}[\frac{\partial U_\ell}{\partial \ell}(i)]^2\{2[U_\ell(i)]^2 - U^2\} \\ & + \frac{1}{2g}\{[U_\ell(i)]^2 - U^2\}U_\ell(i)\frac{\partial^2 U_\ell}{\partial \ell^2}(i); \end{aligned} \tag{5.38}$$

$$D(i) = \frac{1}{g}[U_\ell(i)]^3\frac{\partial U_\ell}{\partial \ell}(i); \tag{5.39}$$

$$E(i) = -\frac{1}{2g}\{[U_\ell(i)]^2 - U^2\}[U_\ell(i)]^2; \tag{5.40}$$

$$H(i) = 3[U_\ell(i)]^2\frac{\partial U_\ell}{\partial \ell}(i); \tag{5.41}$$

$$G(i) = U_\ell(i)/\bar{u}(i); \tag{5.42}$$

where $U_\ell(i)$ represents the fluid velocity along ℓ on $z = 0$ at node point i, which is defined as:

$$U_\ell(i) = \frac{\partial \bar{\Phi}}{\partial \ell}(i). \tag{5.43}$$

The fluid velocity of double-body flow $\tilde{u}(i)$ in equation (5.42) is given as:

$$\tilde{u}(i) = \frac{\partial \dot{\Phi}}{\partial x}(i). \tag{5.44}$$

The second order derivative of $U_\ell(i)$, namely $\frac{\partial^2 U_\ell}{\partial t^2}(i)$, in equation (5.38) is also computed by the five-point centered finite different formula.

Coefficient $G(i)$ is a new one which will be used in solving the free surface ship wave problem in the next subsection.

5.1.5 Solution of surface problem

Having solved the double-body problem, generated the streamline-bounded free surface mesh, and computed the coefficients A, B, C, D, E, H, and G, the total velocity potential ϕ could now be obtained by solving the linearized boundary value problem developed in the present study which was obtained in Section (3.3). By using the coefficient G the present linearized free surface condition can be written in terms of fluid velocity components u and w, with $u = \partial\phi/\partial x$ and $w = \partial\phi/\partial z$. The linearized ship wave problem given by boundary value problem (5.1) can then be rewritten as:

$$\begin{cases} \nabla^2\phi = 0, & \text{in the } \textit{fluid domain}; \\ \vec{n} \cdot \nabla\phi = 0, & \text{on the } \textit{body surface}; \\ A\frac{\partial}{\partial x}(Gu) + BGu + Cw + D\frac{\partial}{\partial x}w + E\frac{\partial^2}{\partial x^2}w = H, & \text{on } z = 0; \\ \nabla\phi \to -U, & \text{as } \sqrt{x^2 + y^2 + z^2} \to \infty, z \le 0; \\ \textit{The radiation condition}. \end{cases} \tag{5.45}$$

By satisfying the impermeability condition in the above boundary value problem at all the nodes on the body surface mesh, an number of linear equations

can be obtained as:

$$\frac{\partial \phi}{\partial n}(i) = 0, \qquad i = 1, 2, ..., nn. \tag{5.46}$$

Variable nn is the total number of nodes on the surface mesh of the moving object.

In order to use the fluid free surface condition in boundary value problem (5.45) to obtain the remaining $(nnt - nn)$ number of linear equations to form a system of linear equations, the second order derivatives of w along ℓ in the free surface condition in (5.45) are expressed as:

$$\frac{\partial^2 w}{\partial \ell^2} = \frac{\partial}{\partial \ell}(\frac{\partial w}{\partial \ell}), \tag{5.47}$$

and the first order derivative of w along ℓ which is represented by $w_\ell = \partial w / \partial \ell$ is given as:

$$\begin{aligned} w_\ell(i) \;=\; & F5D1(i)w(im2) \\ & + F5D2(i)w(im1) \\ & + F5D3(i)w(i) \\ & + F5D4(i)w(ip1) \\ & + F5D5(i)w(ip2), \end{aligned} \tag{5.48}$$

where $F5D1(i)$, $F5D2(i)$, $F5D3(i)$, $F5D4(i)$, $F5D5(i)$ are the five coefficients of the five-point centered finite difference operator; $im2$, $im1$, $ip1$, and $ip2$ are the node labels which are calculated by using equations (5.32) to (5.35).

Replacing the partial derivatives $\frac{\partial}{\partial \ell}$ in the fluid free surface condition in boundary value problem (5.45) by a four-point down-stream finite difference operator, the fluid free surface condition in the present linearized ship wave problem given

by boundary value problem (5.45) can be written as:

$$\begin{aligned}
&A(i)[F4D1(i)G(i)u(i)\\
&+F4D2(i)G(im1)u(im1)\\
&+F4D3(i)G(im2)u(im2)\\
&+F4D4(i)G(im3)u(im3)]\\
&+B(i)G(i)u(i)+C(i)w(i)\\
&+D(i)[F4D1(i)w(i)\\
&+F4D2(i)w(im1)\\
&+F4D3(i)w(im2)\\
&+F4D4(i)w(im3)]\\
&+E(i)[F4D1(i)w_\ell(i)\\
&+F4D2(i)w_\ell(im1)\\
&+F4D3(i)w_\ell(im2)\\
&+F4D4(i)w_\ell(im3)] \;=\; H(i),\\
i=(nn+3nb+1),&(nn+3nb+2),...,nnt. \qquad (5.49)
\end{aligned}$$

In equation (5.49) $F4D1(i)$, $F4D2(i)$, $F4D3(i)$ and $F4D4(i)$ are the four coefficients in the four-point down-stream finite difference operator, (see Appendix D for details); nnt is the total number of nodes on the body surface and the fluid free surface meshes; $im3$, $im2$, and $im1$ are the labels of the nodes on the free surface mesh, which are given as:

$$im3 = i - 3nb; \qquad (5.50)$$

$$im2 = i - 2nb; \qquad (5.51)$$

$$iml \quad = \quad i - nb. \tag{5.52}$$

The variable nb represents the number of streamlines on the free surface mesh.

It is noted that the above discretized fluid free surface condition is satisfied at all of the nodes on the free surface mesh except the first $3nb$ nodes on the upstream side of the mesh because of the application of the finite difference formulation. The free surface condition which is satisfied on the first $3nb$ number of nodes on the upstream side of the mesh is a special case of equation (5.49), with $\partial u/\partial \ell = 0$ and $\partial w/\partial \ell = 0$, which is given as:

$$B(i)G(i)u(i) + C(i)w(i) = H(i), \quad i = (nn+1), (nn+2), ..., (nn+3nb). \tag{5.53}$$

In order to express ϕ by the Rankine sources distributed on the body surface and the fluid free surface, and also to satisfy the condition at infinity in boundary value problem (5.45), the total velocity potential ϕ is written as a constant velocity U which is the velocity of the body plus a potential ϕ' which can be generated directly by the source density σ. We have

$$\phi(i) = -Ux(i) + \phi'(i). \tag{5.54}$$

The particle velocity components of the fluid can, accordingly, be written as:

$$u(i) = -U + u'(i), \tag{5.55}$$

and

$$w(i) = w'(i). \tag{5.56}$$

The variables $\phi'(i)$, $u'(i)$, and $w'(i)$ can be expressed in terms of all the sources distributed on the body surface and on the fluid free surface meshes. They are

given by

$$\phi'(i) = \sum_{j=1}^{nn} \sigma(j) \int_{S(j)} [\frac{1}{r(i,q)} + \frac{1}{r(i,\bar{q})}] T(j) dS(q) + \sum_{j=nn+1}^{nnt} \sigma(j) \int_{S(j)} [\frac{1}{r(i,q)}] T(j) dS(q); \quad (5.57)$$

$$u'(i) = -\sum_{j=1}^{nn} \sigma(j) \int_{S(j)} [\frac{x(i)-x(q)}{r^3(i,q)} + \frac{x(i)-x(\bar{q})]}{r^3(i,\bar{q})}) T(j) dS(q) - \sum_{j=nn+1}^{nnt} \sigma(j) \int_{S(j)} [\frac{x(i)-x(q)}{r^3(i,q)}] T(j) dS(q); \quad (5.58)$$

$$w'(i) = -\sum_{j=1}^{nn} \sigma(j) \int_{S(j)} [\frac{z(i)-z(q)}{r^3(i,q)} + \frac{z(i)-z(\bar{q})}{r^3(i,\bar{q})}] T(j) dS(q) - \sum_{j=nn+1}^{nnt} \sigma(j) \int_{S(j)} [\frac{z(i)-z(q)}{r^3(i,q)}] T(j) dS(q). \quad (5.59)$$

Equations (5.46), (5.49) and (5.53) are rewritten, by moving the known terms to their corresponding right hand sides, as:

$$\frac{\partial \phi'}{\partial n}(i) = U n_x(i), \qquad i = 1, 2, ..., nn; \quad (5.60)$$

$$B(i)G(i)u'(i) + C(i)w'(i) = H(i) + B(i)G(i)U, \quad i = (nn+1), (nn+2), ..., (nn+3nb); \quad (5.61)$$

and

$$A(i)[F4D1(i)G(i)u'(i) + F4D2(i)G(im1)u'(im1) + F4D3(i)G(im2)u'(im2) + F4D4(i)G(im3)u'(im3)]$$

$$
\begin{aligned}
&+B(i)G(i)u'(i) + C(i)w'(i) \\
&\quad +D(i)[F4D1(i)w'(i) \\
&\quad\quad +F4D2(i)w'(im1) \\
&\quad\quad +F4D3(i)w'(im2) \\
&\quad\quad +F4D4(i)w'(im3)] \\
&\quad +E(i)[F4D1(i)w'_\ell(i) \\
&\quad\quad +F4D2(i)w'_\ell(im1) \\
&\quad\quad +F4D3(i)w'_\ell(im2) \\
&\quad\quad +F4D4(i)w'_\ell(im3)] \;=\; H(i) \\
&\qquad\qquad\qquad +A(i)U[F4D1(i)G(i) \\
&\qquad\qquad\qquad +F4D2(i)G(im1) \\
&\qquad\qquad\qquad +F4D3(i)G(im2) \\
&\qquad\qquad\qquad +F4D4(i)G(im3)] \\
&\qquad\qquad\qquad +B(i)UG(i),
\end{aligned}
$$

$$
i = (nn + 3nb + 1), (nn + 3nb + 2), ..., nnt. \tag{5.62}
$$

Finally by putting equations (5.60), (5.61) and (5.62) together and writing the result in matrix format a linear system can be obtained as:

$$
\begin{bmatrix} AB \\ \\ AS \end{bmatrix} \begin{bmatrix} \\ \sigma \\ \\ \end{bmatrix} = \begin{bmatrix} RB \\ \\ RS \end{bmatrix}, \tag{5.63}
$$

where

$$[\sigma] = \begin{bmatrix} \sigma(1) \\ \sigma(2) \\ \sigma(3) \\ . \\ . \\ . \\ \sigma(nnt) \end{bmatrix};$$

$$[RB] = \begin{bmatrix} Un_x(1) \\ Un_x(2) \\ Un_x(3) \\ . \\ . \\ . \\ Un_x(nn) \end{bmatrix};$$

$$[RS] = \begin{bmatrix} rs(nn+1) \\ rs(nn+2) \\ rs(nn+3) \\ . \\ . \\ . \\ rs(nnt) \end{bmatrix}.$$

and $rs(i)$ is defined by the right hand side of equations (5.61) and (5.62), which is

$$\begin{aligned} rs(i) &= H(i) + B(i)G(i)U, \\ & \quad i = (nn+1), (nn+2), ..., (nn+3nb); \end{aligned} \tag{5.64}$$

$$\begin{aligned} rs(i) &= H(i) + B(i)G(i)U \\ & \quad + UA(i)[F4D1(i)G(i) + F4D2(i)G(im1) \\ & \quad + F4D3(i)G(im2) + F4D4(i)G(im3) \\ & \quad i = (nn+3nb+1), (nn+3nb+2), .. \ nnt. \end{aligned} \tag{5.65}$$

The upper part of the influence coefficients matrix $[AB]$ in system of equations (5.63) represents the influence coefficients on the surface of the body produced by the sources distributed on the body surface and the free surface meshes. It is given as:

$$[AB] = \begin{bmatrix} ab(1,1) & ab(1,2) & \cdots & ab(1,nnt) \\ ab(2,1) & ab(2,2) & \cdots & ab(2,nnt) \\ & & & \\ & & & \\ ab(nn,1) & ab(nn,2) & \cdots & ab(nn,nnt) \end{bmatrix}. \tag{5.66}$$

The entries to this part of the matrix are computed by the following equation, which is obtained from the body surface impermeability condition (5.60):

$$ab(i,j) = a_u(i,j)n_x(i) + a_v(i,j)n_y(i) + a_w(i,j)n_z(i), \tag{5.67}$$

where $n_x(i)$, $n_y(i)$, and $n_z(i)$ are the components of $\vec{n}(i)$ in x, y, and z direction respectively; $a_u(i,j)$, $a_v(i,j)$, and $a_w(i,j)$ are the elements of the velocity coefficient matrices, which are defined as:

$$\begin{aligned} a_u(i,j) &= -\int_{S(j)} [\frac{x(i)-x(q)}{r^3(i,q)} + \frac{x(i)-x(\bar{q})}{r^3(i,\bar{q})}] T(j) dS(q), \\ & \quad for\ j = 1,2,...,nn; \end{aligned} \tag{5.68}$$

$$\begin{aligned} a_u(i,j) &= -\int_{S(j)} [\frac{x(i)-x(q)}{r^3(i,q)}] T(j) dS(q), \\ & \quad for\ j = (nn+1),(nn+2),...,nnt; \end{aligned} \tag{5.69}$$

$$\begin{aligned} a_v(i,j) &= -\int_{S(j)} [\frac{y(i)-y(q)}{r^3(i,q)} + \frac{y(i)-y(\bar{q})}{r^3(i,\bar{q})}] T(j) dS(q), \\ & \quad for\ j = 1,2,...,nn; \end{aligned} \tag{5.70}$$

$$a_v(i,j) = -\int_{S(j)}[\frac{y(i)-y(q)}{r^3(i,q)}]T(j)dS(q),$$
$$for\ j = (nn+1),(nn+2),...,nnt; \tag{5.71}$$

$$a_w(i,j) = -\int_{S(j)}[\frac{z(i)-z(q)}{r^3(i,q)} + \frac{z(i)-z(\bar{q})}{r^3(i,\bar{q})}]T(j)dS(q),$$
$$for\ j = 1,2,...,nn; \tag{5.72}$$

$$a_w(i,j) = -\int_{S(j)}[\frac{z(i)-z(q)}{r^3(i,q)}]T(j)dS(q),$$
$$for\ j = (nn+1),(nn+2),...,nnt. \tag{5.73}$$

See Appendix A for the computation of the integrals involved in the velocity coefficients $a_u(i,j)$, $a_v(i,j)$, and $a_w(i,j)$.

The lower part of the influence coefficients matrix in linear system (5.63) represents the influence coefficients at the nodes on the free surface mesh produced by the sources on the body surface and on the free surface meshes. It is in the form:

$$[AS] = \begin{bmatrix} as(nn+1,1) & as(nn+1,2) & \cdots & as(nn+1,nnt) \\ as(nn+2,1) & as(nn+2,2) & \cdots & as(nn+2,nnt) \\ & & & \\ & & & \\ as(nnt,1) & as(nnt,2) & \cdots & as(nnt,nnt) \end{bmatrix}. \tag{5.74}$$

The entries to this part of the matrix are computed by using the free surface boundary condition equations (5.61) and (5.62), such that:

$$as(i,j) = B(i)G(i)a_u(i,j)+C(i)a_w(i,j), \quad i = (nn+1),(nn+2),...,3nb; \tag{5.75}$$

$$as(i,j) = A(i)[F4D1(i)G(i)a_u(i,j)$$

$$
\begin{aligned}
&+F4D2(i)G(im1)a_u(im1,j)\\
&+F4D3(i)G(im2)a_u(im2,j)\\
&+F4D4(i)G(im3)a_u(im3,j)]\\
&+B(i)G(i)a_u(i,j)+C(i)a_w(i,j)\\
&+D(i)[F4D1(i)a_w(i,j)\\
&+F4D2(i)a_w(im1,j)\\
&+F4D3(i)a_w(im2,j)\\
&+F4D4(i)a_w(im3,j)]\\
&+E(i)[F4D1(i)a_{w\ell}(i,j)\\
&+F4D2(i)a_{w\ell}(im1,j)\\
&+F4D3(i)a_{w\ell}(im2,j)\\
&+F4D4(i)a_{w\ell}(im3,j)],\\
&i=(nn+3nb+1),(nn+3nb+2),...,nnt. \qquad (5.76)
\end{aligned}
$$

In equation (5.76) $a_{w\ell}(i,j)$ is calculated by applying the five-point centered finite difference operator on $a_w(i,j)$.

The routine for solving the linear system of the double-body problem is also used here to solve the system of linear equations (5.63).

5.1.6 Free surface wave evaluation

The free surface elevation can be evaluated by using the velocity components $u(i)$, $v(i)$, $w(i)$ on the plane $z=0$. The free surface elevation at each node of the

free surface mesh $\eta(i)$, $i = (nn+1),(nn+2),...,nnt$, is given as:

$$\eta(i) = \frac{U^2 - [u_\ell^2(i) + w^2(i)]}{2[g + u_\ell(i)\frac{\partial w}{\partial \ell}(i) - w(i)\frac{\partial u_\ell}{\partial \ell}(i)]}, \quad i = (nn+1),(nn+2),...,nnt. \quad (5.77)$$

where i refers to a node on the free surface mesh; $u_\ell(i) = [u^2(i) + v^2(i)]^{1/2}$ represents the fluid velocity along the streamline ℓ; The velocity components $u(i)$, $v(i)$, $w(i)$ could be calculated directly from the source densities obtained by solving the linear system (5.63) and the velocity coefficient matrices $a_u(i,j)$, $a_v(i,j)$, $a_w(i,j)$.

$$u(i) = -U + \sum_{j=1}^{nnt} a_u(i,j)\sigma(j); \quad (5.78)$$

$$v(i) = \sum_{j=1}^{nnt} a_v(i,j)\sigma(j); \quad (5.79)$$

$$w(i) = \sum_{j=1}^{nnt} a_w(i,j)\sigma(j). \quad (5.80)$$

The velocity coefficient matrices $a_u(i,j)$, $a_v(i,j)$, and $a_w(i,j)$ have already been defined by equations (5.68) to (5.73), respectively.

5.1.7 Wave resistance calculation

The wave resistance can be calculated by integrating the pressure over the wetted area of the solid body surface. It is expressed as:

$$R_w = -\sum_{q=1}^{ne} \int_{S(q)} P(q)N_x(q)dS(q), \quad (5.81)$$

where $N_x(q)$ represents the unit normal component in x direction to element q; $P(q)$ is the pressure distribution on element q, it is the linear function of the pressure interpolated by the values $P(q_1)$, $P(q_2)$ and $P(q_3)$ of P at the three

vertices of element q. These locally numbered pressure values $P(q_1)$, $P(q_2)$ and $P(q_3)$ can be converted into the globally numbered pressure values $P(i)$ in the same way as are the source densities σ. The pressure at each node is calculated by

$$P(i) = \frac{1}{2}\rho\{U^2 - [u^2(i) + v^2(i) + w^2(i)]\}; \quad i = 1, 2, 3, ..., nn, \tag{5.82}$$

where $u(i)$, $v(i)$, and $w(i)$ are calculated by using equations (5.78), (5.79), and (5.80), while here $i = 1, 2, 3, ..., nn$.

The wave resistance coefficient C_w is computed by

$$C_w = R_w / \frac{1}{2}\rho U^2 S, \tag{5.83}$$

where S is the total surface area of the body and ρ is the fluid density. For a prolate spheroid, S is given by

$$S = \frac{1}{2}\pi L^2 \epsilon[(sin^{-1}\delta)/\delta + \epsilon], \tag{5.84}$$

where $\epsilon = D/L$, $\delta^2 = 1 - \epsilon^2$, D and L are the minor and major axes of the ellipsoid, respectively.

5.2 Direct Boundary Integral Algorithm

5.2.1 Direct integral method and numerical towing tank

As has already been discussed in Section (4.2), the fundamental integral equation of the direct boundary integral method, in the three dimensional case, is given as:

$$\int_S \phi(q)\frac{\partial}{\partial n(q)}[\frac{1}{r(p,q)}]dS(q) = \int_S \frac{1}{r(p,q)}\frac{\partial \phi(q)}{\partial n(q)}dS(q), \tag{5.85}$$

where q is a point on S; S is the boundary or boundaries of the considered fluid domain; $\phi(q)$ represents the velocity potential at point q; p is a field point; and $r(p,q)$ is the distance between p and q, which is defined as:

$$r(p,q) = \sqrt{[x(p) - x(q)]^2 + [y(p) - y(q)]^2 + [z(p) - z(q)]^2}. \tag{5.86}$$

Equation (5.85) represents a constraint relation between the Dirichlet boundary conditions (ϕ defined) and the Neumann boundary conditions (ϕ_n defined, ϕ_n used here denotes the normal derivative of ϕ, that is $\phi_n = \partial\phi/\partial n$,with n the normal to S directed out of the fluid). For Neumann boundary conditions the right hand side of equation (5.85) is known, giving a Fredholm equation of the second kind for the unknown boundary values of function $\phi(q)$. For the Dirichlet problem equation (5.85) becomes a Fredholm equation of the first kind for the unknown boundary values ϕ_n. For the mixed boundary condition, which is the case of the fluid free surface condition of the ship wave problem, both ϕ and ϕ_n are unknowns but a relation between ϕ and ϕ_n is provided by the boundary condition which allows that an arrangement can be made to solve for either ϕ or ϕ_n.

Except for very simple geometries, analytical solutions to the boundary integral equations are unavailable and numerical methods must be used. By assuming that the boundary is divided into surface elements over which the data has a prescribed polynomial variation we can reduce the problem to solving a linear system of equations for some unknown coefficients.

In solving the ship wave problem, boundaries have to be defined before the numerical procedure is started. Theoretically, the fluid domain considered in the ship wave problem is of infinite extent. However in the case of model testing in a

towing tank, the boundaries of the tank and the surface of the ship plus the fluid free surface form a closed surface covering the fluid domain, which just satisfies the condition of integral equation (5.85). By paneling the boundaries of the tank, the surface of the ship and the fluid free surface, numerical integration for equation (5.85) can be obtained which allows to solve for either ϕ or ϕ_n according to the given conditions. This forms exactly a numerical simulation of a potential flow towing tank experiment. Once a ship model and the dimensions of a towing tank are given, numerical results in terms of potential function ϕ can be obtained by solving the integral equation (5.85) numerically. The wave profile and the wave-making resistance can then be computed from ϕ.

Unlike a towing tank model testing, in which the size of the model is limited because of the size of the tank, a numerical towing tank can perform full scale testing by simply using a prototype ship, instead of a ship model, and enlarge the tank proportionally. Further more, by extending the dimension of the tank such that the side walls of the tank do not effect the waves, the case of a ship in open sea can also be simulated.

In this section, the algorithm of a numerical towing tank based on solving the linearized ship wave problem derived in Section (3.3) , i.e. a linear numerical towing tank, is developed. The algorithm developed in this section will also be used in Chapter 6 in the iteration procedure developed to solve the nonlinear problem. As has been used in the indirect boundary integral algorithm in the previous section, the linear element technique is also used in the present numerical towing tank algorithm.

5.2.2 Panelization and boundary conditions

As for a real towing tank in a laboratory, a numerical towing tank is formed by four impermeable walls and a bottom. One wall is located on the upstream side, and one wall is on the downstream side of the tank. And two walls are on the lateral sides of the tank.

In the numerical algorithm of the present numerical towing tank the symmetrical condition of the tank is used advantageously to save computer memory and to reduce the amount of computations. Also, in order to save more computer memory an image tank is introduced to avoid the panelization on the bottom of the tank, by paying the price of increasing a certain amount of computations. Because of the implementation of the image tank the amount of computations is increased by about 20%. In return, the size of memory is reduced by about 200% in the present algorithm.

In order to identify the boundaries, a label is given to each of them. The wall on the upstream (in front of the ship) is labelled 1; one half of the ship hull surface (since the symmetrical condition is used) is labelled 2; the wall on the downstream side of the tank (behind the ship) is labelled 3; the side wall of the tank (only one side since the application of the symmetrical condition) is labelled 4. Finally, the free surface of the fluid is labelled 5. All these boundaries are paneled by triangular panels. Fig. 5.11 shows the panelization of the tank with a Wigley hull intersecting the fluid free surface. Fig. 5.12 shows the panelization of the tank and the ship hull of a Series 60, block $C_b = 0.60$.

It is noted that the panels on the fluid free surface, boundary 5, are bounded by streamlines. These streamlines are generated through the indirect boundary

integral method which has been discussed in the previous section. Streamlines can also be generated by using the direct boundary integral method which is being discussed in the present section. But it is not as convenient as applying the Rankine source method discussed in Section (5.1). It is also expensive to use the direct boundary integral method to generate these streamlines.

To simulate a towing tank, the boundary conditions on the side walls of the tank have to be specified to replace the boundary condition at infinity in boundary value problem (3.29). This defines a towing tank boundary value problem. If the size of the tank is big enough, the boundary condition on the walls of the tank will be equivalent to the condition at infinity. The boundary value problem in this case then defines a problem of a ship moving in open sea. The boundary conditions on fixed walls of a tank can easily be expressed by $\phi_n = 0$, based on the impermeability property of these boundaries. However, this will make the boundary value problem to be solved a Neumann problem (ϕ_n given on all of the boundaries), since the boundary conditions on the ship surface and on the fluid free surface are also specified through ϕ_n . As it is known that the solution to a Neumann boundary value problem is not unique (there is a constant difference between solutions). This could lead to situations that involve very big or very small values in the numerical solution of the problem. The accuracy of the solution could, consequently, be affected. In order to avoid the above mentioned situations, the boundary condition on boundary 1 of the present numerical towing tank is prescribed by specifying the velocity potential function ϕ which is known when the Froude number of the test is preassigned.

In order to use limited computer resources to produce the best simulation

results. only the section of the tank which contains the ship model is simulated in the present study. This can easily be achieved by specifying the conditions on boundaries #1 and #3 by a radiation condition and replacing the length of the tank by the length of the section to be simulated. The radiation condition is defined here as the waves going through the boundary without reflections. As has been discussed, to avoid the boundary value problem becoming a Neumann type, the radiation condition on boundary #1 is defined by ϕ and the radiation condition on boundary #3 is given by ϕ_n. Finally, by fixing the coordinate on the ship, the boundary value problem for a linear numerical towing tank is given as:

$$\begin{cases} \nabla^2\phi = 0, & \textit{in the fluid domain;} \\ \phi = 0, & \textit{on boundary \# 1;} \\ \vec{n}\cdot\nabla\phi = 0, & \textit{on boundary \# 2;} \\ \vec{n}\cdot\nabla\phi = -U, & \textit{on boundary \# 3;} \\ \vec{n}\cdot\nabla\phi = 0, & \textit{on boundary \# 4;} \\ A\frac{\partial^2\phi}{\partial t^2} + B\frac{\partial\phi}{\partial t} + C\frac{\partial\phi}{\partial x} + D\frac{\partial^2\phi}{\partial t\partial x} + E\frac{\partial^2\phi}{\partial t^2\partial x} = H, & \textit{on boundary \# 5;} \\ \textit{The radiation condition.} \end{cases} \tag{5.87}$$

The coefficients A, B, C, D, E and H have been defined by equations (5.2) to (5.6), respectively. The Cartesian coordinate system is placed such that xoz is in the center plane of the ship with the origin o in the plane of the designed waterline. Axis x is in the direction of the ship velocity U and axis z is directed vertically upwards.

It has been discussed in Section (3.3) that coefficients A, B, C, D, E, and H in the fluid free surface condition of boundary value problem (5.87) are functions of the double-body potential $\bar{\Phi}$. In the numerical towing tank case $\bar{\Phi}$ can be obtained by simply imposing the fluid free surface condition to be $\partial\bar{\Phi}/\partial n = 0$. The boundary value problem to be solved for $\bar{\Phi}$ is then given as:

$$\begin{cases} \nabla^2\bar{\Phi} = 0, & in\ the\ fluid\ domain; \\ \bar{\Phi} = 0, & on\ boundary\ \#\ 1; \\ \vec{n}\cdot\nabla\bar{\Phi} = 0, & on\ boundary\ \#\ 2; \\ \vec{n}\cdot\nabla\bar{\Phi} = -U, & on\ boundary\ \#\ 3; \\ \vec{n}\cdot\nabla\bar{\Phi} = 0, & on\ boundary\ \#\ 4; \\ \vec{n}\cdot\nabla\bar{\Phi} = 0, & on\ boundary\ \#\ 5. \end{cases} \tag{5.88}$$

System of equations (5.88) defines a towing tank with the fluid free surface being restricted so that the vertical fluid velocity at the surface $z = 0$ is forced to be zero. Since there is no image body considered here, $\bar{\Phi}$ is called the zero order solution for the numerical towing tank.

It is clear now that to obtain the solution of the towing tank boundary value problem (5.87), the zero order tank problem (5.88) has first to be solved so that the coefficients A, B, C, D, E, H can be computed and then the free surface towing tank problem can be solved following the same procedure with a more complicated free surface condition.

5.2.3 Zero order numerical towing tank

System of equations (5.88) defines a zero order numerical tank problem, in which the fluid free surface is restricted to generate a fundamental fluid flow in the tank to be used in the perturbation procedure to solve the linear or first order free surface towing tank problem.

To solve the boundary value problem (5.88), by applying the direct boundary integral method, the fundamental equation (5.85) is written in terms of $\bar{\Phi}$ in a discretized form as:

$$\sum_{q=1}^{net}\int_{S(q)}\bar{\Phi}(q)\frac{\partial}{\partial n(q)}[\frac{1}{r(p,q)}]dS(q) = \sum_{q=1}^{net}\int_{S(q)}\frac{1}{r(p,q)}\frac{\partial\bar{\Phi}(q)}{\partial n(q)}dS(q), \tag{5.89}$$

where $S(q)$ represents the area of element q and net represents the total number of elements on the boundary surface mesh.

The integrals in equation (5.89) are over each element on the surface mesh. Since $\tilde{\Phi}(q)$ and $\partial\tilde{\Phi}(q)/\partial n$ are linear functions of their values at the three vertices of element q, equation (5.89) could be written in terms of nodes in the form:

$$\sum_{j=1}^{nnt}\{\tilde{\Phi}(j)\int_{S(j)}\frac{\partial}{\partial n(j)}[\frac{1}{r(p,q)}]T(j)dS(q)\} = \sum_{j=1}^{nnt}\{\tilde{\Phi}_n(j)\int_{S(j)}\frac{1}{r(p,q)}T(j)dS(q)\}, \tag{5.90}$$

where p represents the field point; j represents a node number; q denotes the location of the integration element area $dS(q)$; $\phi(j)$ is the velocity potential at node j; $n(j)$ represents the unit normal to the paneled surface at point j directed out of the fluid; nnt represents the total number of nodes on the surface mesh of the tank. The variable $r(p,j)$ represents the distance between point p and the integration element area $dS(q)$, which is defined as:

$$r(p,q) = \sqrt{[x(p)-x(q)]^2+[y(p)-y(q)]^2+[z(p)-z(q)]^2}. \tag{5.91}$$

By satisfying equation (5.90) at all the nodes of the surface mesh, a linear system of equations can be obtained, and written in matrix form as:

$$[A]\{\tilde{\Phi}\} = [B]\{\tilde{\Phi}_n\}, \tag{5.92}$$

where A and B are $nnt \times nnt$ matrices which are called the matrices of influence coefficients. They are defined by

$$[A] = \begin{bmatrix} a(1,1) & a(1,2) & \cdots & a(1,nnt) \\ a(2,1) & a(2,2) & \cdots & a(2,nnt) \\ & & & \\ & & & \\ a(nnt,1) & a(nnt,2) & \cdots & a(nnt,nnt) \end{bmatrix};$$

and

$$[B] = \begin{bmatrix} b(1,1) & b(1,2) & \cdots & b(1,nnt) \\ b(2,1) & b(2,2) & \cdots & b(2,nnt) \\ & & & \\ & & & \\ b(nnt,1) & b(nnt,2) & \cdots & b(nnt,nnt) \end{bmatrix};$$

where

$$a(i,j) = \int_{S(j)} \frac{\partial}{\partial n(j)} [\frac{1}{r(i,q)}] T(j) dS(q); \tag{5.93}$$

$$b(i,j) = \int_{S(j)} \frac{1}{r(i,q)} T(j) dS(q). \tag{5.94}$$

To calculate the integrals in equations (5.93) and (5.94), two cases have to be considered. They are

1). The field point i is not on the collocation point j;

2). The field point i is on the collocation point j.

The integrations for these two cases are detailed in Appendices A and B. In the algorithm of the present numerical towing tank, an image wave tank is used to eliminate the panelization on the bottom of the tank. Therefore the integrations in equations (5.93) and (5.94) are not only going through the tank boundary surface itself but also going through the image tank. The influence coefficient matrices A and B are, therefore, further written as:

$$a(i,j) = \int_{S(j)} \frac{\partial}{\partial n(j)} [\frac{1}{r(i,q)} + \frac{1}{r(i,\bar{q})}] T(j) dS(q); \tag{5.95}$$

$$b(i,j) = \int_{S(j)} [\frac{1}{r(i,q)} + \frac{1}{r(i,\bar{q})}] T(j) dS(q). \tag{5.96}$$

By rearranging the influence coefficient matrices A and B into sub-matrices according to the five boundaries of the tank, #1, #2, #3, #4, #5, the matrix

system given by equation (5.92) becomes

$$\begin{bmatrix} A_{11} & A_{12} & A_{13} & A_{14} & A_{15} \\ A_{21} & A_{22} & A_{23} & A_{24} & A_{25} \\ A_{31} & A_{32} & A_{33} & A_{34} & A_{35} \\ A_{41} & A_{42} & A_{43} & A_{44} & A_{45} \\ A_{51} & A_{52} & A_{53} & A_{54} & A_{55} \end{bmatrix} \begin{bmatrix} \bar{\Phi}_1 \\ \bar{\Phi}_2 \\ \bar{\Phi}_3 \\ \bar{\Phi}_4 \\ \bar{\Phi}_5 \end{bmatrix} = \begin{bmatrix} B_{11} & B_{12} & B_{13} & B_{14} & B_{15} \\ B_{21} & B_{22} & B_{23} & B_{24} & B_{25} \\ B_{31} & B_{32} & B_{33} & B_{34} & B_{35} \\ B_{41} & B_{42} & B_{43} & B_{44} & B_{45} \\ B_{51} & B_{52} & B_{53} & B_{54} & B_{55} \end{bmatrix} \begin{bmatrix} \bar{\Phi}_{n1} \\ \bar{\Phi}_{n2} \\ \bar{\Phi}_{n3} \\ \bar{\Phi}_{n4} \\ \bar{\Phi}_{n5} \end{bmatrix} \tag{5.97}$$

In system (5.97), A_{ij} and B_{ij} represent the sub-influence coefficient matrices of boundary number j to boundary number i. For example, A_{23} represent the influence of boundary #3 to boundary #2.

According to the boundary conditions described in boundary value problem (5.88), on boundary #1 the values of $\bar{\Phi}$ are given and the values of $\bar{\Phi}_n$ are to be calculated, on boundaries #2, #3, #4 and #5 values of $\bar{\Phi}_n$ are given and values of $\bar{\Phi}$ need to be calculated. By moving the unknown variables to the left hand side and the known values to the right hand side, a linear system of equations to be solved for nnt unknowns is obtained. On boundary #1, solve for $\bar{\Phi}_n$, on boundaries #2 to #5 solve for $\bar{\Phi}$. Matrix system (5.97) becomes

$$\begin{bmatrix} B_{11} & A_{12} & A_{13} & A_{14} & A_{15} \\ B_{21} & A_{22} & A_{23} & A_{24} & A_{25} \\ B_{31} & A_{32} & A_{33} & A_{34} & A_{35} \\ B_{41} & A_{42} & A_{43} & A_{44} & A_{45} \\ B_{51} & A_{52} & A_{53} & A_{54} & A_{55} \end{bmatrix} \begin{bmatrix} \bar{\Phi}_{n1} \\ \bar{\Phi}_2 \\ \bar{\Phi}_3 \\ \bar{\Phi}_4 \\ \bar{\Phi}_5 \end{bmatrix} = \begin{bmatrix} A_{11} & B_{12} & B_{13} & B_{14} & B_{15} \\ A_{21} & B_{22} & B_{23} & B_{24} & B_{25} \\ A_{31} & B_{32} & B_{33} & B_{34} & B_{35} \\ A_{41} & B_{42} & B_{43} & B_{44} & B_{45} \\ A_{51} & B_{52} & B_{53} & B_{54} & B_{55} \end{bmatrix} \begin{bmatrix} \bar{\Phi}_1 \\ \bar{\Phi}_{n2} \\ \bar{\Phi}_{n3} \\ \bar{\Phi}_{n4} \\ \bar{\Phi}_{n5} \end{bmatrix} \tag{5.98}$$

By solving the above matrix system the unknowns on all of the boundaries are obtained.

5.2.4 First order numerical towing tank

Having solved the zero order towing tank problem, values of $\tilde{\Phi}$ on the fluid free surface $z = 0$ are obtained at all the nodes on the surface mesh. The coefficients A, B, C, D, E and H in the free surface condition of boundary value problem (5.87) can then be computed through $\tilde{\Phi}$. The derivatives of $\tilde{\Phi}$ along ℓ are calculated by a three-point finite difference formulation, (see Appendix D for the details about the finite difference formulations).

From the experience gained from the computations of the indirect formulation it is found that the last two terms in the left hand side of the free surface condition in the ship wave problem (3.29) or the towing tank problem (5.87) are small relative to the other terms. They are, therefore, neglected in the algorithm of the present linear numerical towing tank. The third term in the expression of coefficient C, equation (3.25), is also dropped since it is also small. The boundary value problem defining the linear or first order numerical towing tank is then written in the form

$$\begin{cases} \nabla^2\phi = 0, & \textit{in the fluid domain}; \\ \phi = 0, & \textit{on boundary \# 1}; \\ \vec{n}\cdot\nabla\phi = 0, & \textit{on boundary \# 2}; \\ \vec{n}\cdot\nabla\phi = -U, & \textit{on boundary \# 3}; \\ \vec{n}\cdot\nabla\phi = 0, & \textit{on boundary \# 4}; \\ A\frac{\partial^2\phi}{\partial\ell^2} + B\frac{\partial\phi}{\partial\ell} + C\frac{\partial\phi}{\partial x} = H, & \textit{on boundary \# 5}; \\ \textit{The radiation condition}; \end{cases} \tag{5.99}$$

where

$$A = \frac{3}{2}(\frac{\partial\tilde{\Phi}}{\partial\ell})^2 - \frac{1}{2}U^2; \tag{5.100}$$

$$B = 3\frac{\partial\tilde{\Phi}}{\partial\ell}\frac{\partial^2\tilde{\Phi}}{\partial\ell^2}; \tag{5.101}$$

$$C = g - \frac{1}{g}(\frac{\partial^2\bar{\Phi}}{\partial\ell^2})^2[2(\frac{\partial\bar{\Phi}}{\partial\ell})^2 - U^2]; \tag{5.102}$$

$$H = 3(\frac{\partial\bar{\Phi}}{\partial\ell})^2\frac{\partial^2\bar{\Phi}}{\partial\ell^2}. \tag{5.103}$$

In the condition imposed on boundary #5, both ϕ and ϕ_n are unknown. However this condition defines a relation between ϕ and ϕ_n. It is noted that since the normal to boundary #5 is in the direction of z, we have $\phi_n = \phi_z$. ϕ_n can then be expressed in terms of ϕ on boundary #5 as:

$$\phi_n = C_H + C_A\frac{\partial}{\partial\ell}(\frac{\partial\phi}{\partial\ell}) + C_B\frac{\partial\phi}{\partial\ell}, \tag{5.104}$$

where

$$C_A = -A/C; \tag{5.105}$$

$$C_B = -B/C; \tag{5.106}$$

$$C_H = H/C. \tag{5.107}$$

Expressing $\partial\phi/\partial\ell$ by a three-point centered finite difference, and expressing the second order derivative $\partial(\partial\phi/\partial\ell)/\partial\ell$ in equation (5.104) by a four-point downstream finite difference in terms of $\partial\phi/\partial\ell$, equation (5.104) becomes

$$\begin{aligned}\phi_n(j) = {} & C_H(j) \\ & + C_{M4}(j)\phi(jm4) \\ & + C_{M3}(j)\phi(jm3) \\ & + C_{M2}(j)\phi(jm2) \\ & + C_{M1}(j)\phi(jm1)\end{aligned}$$

$$+C_{M0}(j)\phi(j)$$
$$+C_{P1}(j)\phi(jP1), \qquad (5.108)$$

where

$$C_{M4} = C_A(j)F4D1(j)F3D1(jm3); \qquad (5.109)$$

$$C_{M3} = C_A(j)[F4D1(j)F3D2(jm3)$$
$$+F4D2(j)F3D1(jm2)]; \qquad (5.110)$$

$$C_{M2} = C_A(j)[F4D1(j)F3D3(jm3)$$
$$+F4D2(j)F3D2(jm2)$$
$$+F4D3(j)F3D1(jm1)]; \qquad (5.111)$$

$$C_{M1} = C_A(j)[F4D2(j)F3D3(jm2)$$
$$+F4D3(j)F3D2(jm1)$$
$$+F4D4(j)F3D1(j)]$$
$$+CB(j)F3D1(j); \qquad (5.112)$$

$$C_{M0} = C_A(j)[F4D3(j)F3D3(jm1)$$
$$+F4D4(j)F3D2(j)]$$
$$+C_B(j)F3D2(j); \qquad (5.113)$$

$$C_{P1} = C_A(j)F4D4(j)F3D3(j)$$
$$+C_B(j)F3D3(j). \tag{5.114}$$

And $F4D1(j)$, $F4D2(j)$, $F4D3(j)$, $F4D4(j)$ are the four coefficients of the four-point downstream finite difference formula. $F3D1(j)$, $F3D2(j)$, $F3D3(j)$ are the three coefficients in the three-point centered finite difference formula, (see Appendix D for details). Also

$$jm4 = j - 4nb; \tag{5.115}$$
$$jm3 = j - 3nb; \tag{5.116}$$
$$jm2 = j - 2nb; \tag{5.117}$$
$$jm1 = j - nb; \tag{5.118}$$
$$jp1 = j + nb. \tag{5.119}$$

Again, nb is the number of streamlines on boundary #5. j is the label of the nodes on boundary #5, which varies from $(nnt - nn5)$ to nnt, $nn5$ is the total number of nodes on the fluid free surface mesh #5.

The only difference between the zero and first order numerical towing tank problems given by (5.88) and (5.99) is in the conditions on boundary #5. In the zero order numerical towing tank problem (5.88) the condition on boundary #5 is prescribed by $\phi_n = 0$ at all the nodes on the mesh. In the first order numerical towing tank problem (5.99) the condition on boundary #5 is given by a linear relation between the velocity potential ϕ and its normal derivative ϕ_n. This relation is given in a discretized form by equation (5.108). Therefore, the

linear system for solving the first order towing tank problem (5.99), similar to linear system (5.98), is given as:

$$\begin{bmatrix} B_{11} & A_{12} & A_{13} & A_{14} & A_{15} \\ B_{21} & A_{22} & A_{23} & A_{24} & A_{25} \\ B_{31} & A_{32} & A_{33} & A_{34} & A_{35} \\ B_{41} & A_{42} & A_{43} & A_{44} & A_{45} \\ B_{51} & A_{52} & A_{53} & A_{54} & A_{55} \end{bmatrix} \begin{bmatrix} \phi_{n1} \\ \phi_2 \\ \phi_3 \\ \phi_4 \\ \phi_5 \end{bmatrix} = \begin{bmatrix} A_{11} & B_{12} & B_{13} & B_{14} & B_{15} \\ A_{21} & B_{22} & B_{23} & B_{24} & B_{25} \\ A_{31} & B_{32} & B_{33} & B_{34} & B_{35} \\ A_{41} & B_{42} & B_{43} & B_{44} & B_{45} \\ A_{51} & B_{52} & B_{53} & B_{54} & B_{55} \end{bmatrix} \begin{bmatrix} \phi_1 \\ \phi_{n2} \\ \phi_{n3} \\ \phi_{n4} \\ \phi_{n5} \end{bmatrix} \tag{5.120}$$

By substituting $\phi_n(j)$ on boundary #5 expressed by (5.108) into matrix system (5.120) and working out the numbering relations, a linear system to be solved for $\{\phi_n\}$ on boundary #1, and for $\{\phi\}$ on boundaries #2 to #5 is obtained as:

$$\begin{aligned} &\sum_{j=1}^{nnstop1} b(i,j)\phi_n(j) \\ &+ \sum_{j=nnstart2}^{nnstop2} a(i,j)\phi(j) \\ &+ \sum_{j=nnstart3}^{nnstop3} a(i,j)\phi(j) \\ &+ \sum_{j=nnstart4}^{nnstop4} a(i,j)\phi(j) \\ &+ \sum_{j=nnstart5}^{nnt} a(i,j)\phi(j) \\ &- \sum_{j=nnstop4+1}^{nnt-5nb} C_{M4}(jp4)b(i,jp4)\phi(j) \\ &- \sum_{j=nnstop4+nb+1}^{nnt-4nb} C_{M3}(jp3)b(i,jp3)\phi(j) \\ &- \sum_{j=nnstop4+2nb+1}^{nnt-3nb} C_{M2}(jp2)b(i,jp2)\phi(j) \\ &- \sum_{j=nnstop4+3nb+1}^{nnt-2nb} C_{M1}(jp1)b(i,jp1)\phi(j) \end{aligned}$$

$$
\begin{aligned}
&- \sum_{j=nnstop4+4nb+1}^{nnt-nb} C_{M0}(j) b(i,j) \phi(j) \\
&- \sum_{j=nnstop4+5nb+1}^{nnt} C_{P1}(jm1) b(i,jm1) \phi(j) \\
&= - \sum_{j=nnstart3+1}^{nnstop3} b(i,j) U \\
&+ \sum_{j=nnstop4+1}^{nnstop4+4nb} b(i,j) [C_H(i) - C_B(i) U] \\
&+ \sum_{j=nnstop4+4nb+1}^{nnt-nb} b(i,j) C_H(j) \\
&+ \sum_{j=nnt-nb+1}^{nnt} b(i,j) [C_H(i) - C_B(i) U] \\
&\qquad i = 1, 2, ..., nnt \quad , \qquad (5.121)
\end{aligned}
$$

where

$$nnstart1 = 1 ; \qquad (5.122)$$

$$nnstart2 = nn1 + 1 ; \qquad (5.123)$$

$$nnstart3 = nn1 + nn2 + 1 ; \qquad (5.124)$$

$$nnstart4 = nn1 + nn2 + nn3 + 1 ; \qquad (5.125)$$

$$nnstart5 = nn1 + nn2 + nn3 + nn4 + 1 ; \qquad (5.126)$$

$$nnstop1 = nn1 ; \qquad (5.127)$$

$$nnstop2 = nn1 + nn2 ; \qquad (5.128)$$

$$nnstop3 = nn1 + nn2 + nn3 ; \qquad (5.129)$$

$$nnstop4 = nn1 + nn2 + nn3 + nn4 ; \qquad (5.130)$$

$$nnstop5 = nn1 + nn2 + nn3 + nn4 + nn5 . \qquad (5.131)$$

The above linear system of equations contains nnt numbers of unknowns.

There are $nn1$ values of ϕ_n and $(nnt - nn1)$ values of velocity potential ϕ. The linear system is solved by using a Gaussian elimination linear system solver, which has been used in the indirect method of the present study.

The wave elevation is calculated from the vertical velocity and the horizontal velocity components along the stream line ℓ on the fluid free surface mesh. It is given by

$$\eta(i) = \frac{U^2 - [u_\ell^2(i) + w^2(i)]}{2[g + u_\ell(i)\frac{\partial w}{\partial \ell}(i) - w(i)\frac{\partial u_\ell}{\partial \ell}(i)]} , \quad i = (nnstart5{+}1), (nnstart5{+}2), ..., nnt , \tag{5.132}$$

where $u_\ell(i)$ represents the horizontal fluid velocity component along ℓ at node i; $w(i)$ represents the vertical component of fluid velocity at i.

The vertical component of the fluid velocity $w(i)$ is calculated by using the relation between ϕ_n, $\partial\phi/\partial\ell$, and $\partial^2\phi/\partial\ell^2$ which is given by equation (5.104). We have

$$w(i) = C_H(i) + C_A(i)\frac{\partial^2\phi}{\partial\ell^2}(i) + C_B(i)\frac{\partial\phi}{\partial\ell}(i) . \tag{5.133}$$

The first order derivative of ϕ along ℓ is calculated by applying the five-point centered finite difference operator, giving:

$$\begin{aligned} u_\ell(i) = \frac{\partial\phi}{\partial\ell}(i) \;=\; & F5D1(i)\phi(im2) \\ & + F5D2(i)\phi(im1) \\ & + F5D3(i)\phi(i) \\ & + F5D4(i)\phi(ip1) \\ & + F5D5(i)\phi(ip2), \end{aligned} \tag{5.134}$$

where $im2$, $im1$, $ip1$, and $ip2$ are given by equations (5.32) to (5.35).

The second order derivatives in equation (5.133) is generated by using u_ℓ through the three-point centered finite difference operator, which is

$$\frac{\partial^2 \phi}{\partial \ell^2}(i) = F3D1(i)u_\ell(im1) + F3D2(i)u_\ell(i) + F3D3(i)u_\ell(ip1). \qquad (5.135)$$

See Appendix D for the coefficients of the finite difference operators.

The wave-making resistance is calculated by integrating the pressure over the wetted area of the hull surface. It is given as:

$$R_w = -\sum_{q=1}^{nc} \int_{S(q)} P(q) N_x(q) dS(q), \qquad (5.136)$$

where $N_x(q)$ represents the unit normal component in x direction to element q; $P(q)$ is the pressure on element q, expressed as the linear function of the pressures at node $P(i)$, (see Section (5.1.7)). The pressure $P(i)$ is calculated from two orthogonal tangential velocity components at node i, since the normal velocity components on the hull are zero. $P(i)$ is given as:

$$P(i) = \frac{1}{2}\rho\{U^2 - [u_t^2(i) + v_t^2(i)]\}, \qquad (5.137)$$

where $u_t(i)$ and $v_t(i)$ denote two orthogonal velocity components. Both $u_t(i)$ and $v_t(i)$ are calculated by applying the three-point centered finite difference formula for the points off the edge, and a two-point finite difference formula is used to compute these two velocity components for the points on the edge of the ship surface mesh.

The wave resistance coefficient C_w is calculated by using equation (5.83) which has been used in the indirect algorithm of the present study. The surface area S in equation (5.83) is calculated by adding up the areas of all panels on the wetted ship hull surface.

5.3 Applications and Comparisons

5.3.1 Submerged ellipsoid: Indirect method

The method based on the indirect boundary integral theory developed in the foregoing sections is presently applied to analyse the wave pattern and to compute the wave-making resistance for a submerged prolate ellipsoid advancing with a constant speed in water. The reason for choosing an ellipsoid is that theoretical and numerical results are available for comparison purposes. A steady flow passing an ellipsoid has been studied through theoretical analyses by Havelock (1931a, 1931b), and Farell (1973). The same problem has also been solved by Doctors and Beck (1987) through a numerical procedure based on the Kelvin source method. Both the theoretical analyses, by Havelock and Farell, and the numerical analysis, by Doctors and Beck (1987), are based on solving the Neumann-Kelvin problem. Therefore, these results can not be directly used for comparison with the present computation, since the present computation solves a new linearized ship wave problem in which the free surface condition is different from the one found in the Neumann-Kelvin linear ship wave problem. In order to compare with the existing results, the present algorithm is also applied to solve the Neumann-Kelvin problem, since the Neumann-Kelvin linear ship wave problem is a special case of the present linearized ship wave problem. When the thin ship condition is satisfied, the double-body flow $\partial\bar{\Phi}/\partial\ell$ becomes the constant flow on which the Neumann-Kelvin linear free surface condition is based. By substituting $\partial\bar{\Phi}/\partial\ell = -U$ into the expressions of the coefficients in the present linearized free surface condition

given by equations (5.2) to (5.7), we have

$$A = U^2, \tag{5.138}$$

$$B = 0, \tag{5.139}$$

$$C = g, \tag{5.140}$$

$$D = 0, \tag{5.141}$$

$$E = 0, \tag{5.142}$$

$$H = 0. \tag{5.143}$$

The present free surface condition then reduces to the Neumann-Kelvin free surface condition. By simply using the above six lines, equations (5.138) to (5.143), in the computer program of the present algorithm instead of computing them by using equations (5.2) to (5.7), the solution to the Neumann-Kelvin problem by using the present algorithm is obtained. If the results obtained by solving the Neumann-Kelvin problem through the present method match the theoretical solution and the numerical results by Havelock (1931a, 1932b), Farell (1973), Doctors and Beck (1987), the conclusion can be drawn that the present algorithm and the corresponding numerical techniques are accurate and the computer program is robust. Furthermore, if the present method solving the present linearized problem gives different results from those obtained by solving the Neumann-Kelvin problem, a conclusion can also be drawn that the extra terms in the present condition (in comparison with the Neumann-Kelvin free surface condition, see Table 3.1) do contribute to the solution of the problem. To prove that the present free surface condition is more accurate in modelling the physical problem than the Neumann-Kelvin problem, comparisons with experimental data have to be

made. This will be shown in the next section where the surface ship cases are discussed, since many reliable experimental measurements are available on wave pattern and wave-making resistance for surface ships.

In order to give a general idea of how much difference between the results given by Dawson's linearized problem from the present linearized problem, Dawson's linearized problem is also solved by using the present method. It is very easy to convert the present computer program to solve Dawson's linear problem, which is simply to change the six lines for calculating the coefficients given by (5.2) to (5.7) into

$$A = (\frac{\partial \bar{\Phi}}{\partial \ell})^2; \tag{5.144}$$

$$B = 2\frac{\partial \bar{\Phi}}{\partial \ell}\frac{\partial^2 \bar{\Phi}}{\partial \ell^2}; \tag{5.145}$$

$$C = g; \tag{5.146}$$

$$D = 0; \tag{5.147}$$

$$E = 0; \tag{5.148}$$

$$H = 2(\frac{\partial \bar{\Phi}}{\partial \ell})^2\frac{\partial^2 \bar{\Phi}}{\partial \ell^2}; \tag{5.149}$$

where $\bar{\Phi}$ is the double-body potential, and ℓ is the double-body streamline.

The numerical procedure of the present indirect method has been discussed in Section (5.1). Applying the method to solve the submerged prolate ellipsoid advancing with constant speed follows exactly the six steps explained in that section. The dimensions of the prolate ellipsoid considered in this example are $a = 5.0m$, $b = 1.0m$, where a represents the semi-major axis and b represents the semi-minor axis of the ellipsoid. The streamline bounded triangular panels on the fluid free surface mesh and the triangular panels on the body surface mesh

are shown in Fig. 5.3. Since the application of the symmetrical condition is considered, only half of the body and half of the free surface are paneled. Fig. (5.3.a) shows the free surface mesh with the body underneath it, which gives the dimensional relation between the ellipsoid and the free surface mesh. The size of the free surface mesh and the size of the panels are determined by the Froude number, (see Appendix C for details). Fig. (5.3.b) shows the free surface mesh only, from which the streamlines can be clearly seen. The total number of panels on the free surface is 2880. The total node number, which represents the number of unknowns distributed on the free surface, is 1573. Fig. (5.3.c) shows the panelization on the surface of the ellipsoid. There are 228 panels and 138 nodes on the mesh of the body surface. The total number of panels on the body surface and the free surface is 3108. The total number of nodes, which is the number of unknowns, is 1711. From these numbers it can be seen that the present algorithm using triangular panelization and linear unknown distribution over elements (linear element techniques) reduces the number of unknowns in comparison with methods using quadrilateral panelization and constant source distribution (constant element techniques), under the condition of the same size of panels.

The wave resistance coefficient C_w for high Froude number and low Froude number cases computed by the present method solving the present linear problem, Dawson's problem and the Neumann-Kelvin problem along with the theoretical results by Farell (1973) and the numerical results by Doctors and Beck (1987) are presented in Fig. 5.4 to Fig. 5.7. Two cases of submerged depth $d/c = 0.3266$ and $d/c = 0.5$ are involved in these computations, where $c = (a^2 - b^2)^{1/2}$. The results

are presented by different type of curves which are explained in the figures, where "Present" means the present method for solving the present linearized problem, "Present-DS" means the present method for solving Dawson's linear problem, and "Present-NK" means the present method for solving the Neumann-Kelvin problem. From these figures it can be seen that the results of using the present method for solving the Neumann-Kelvin problem match very well the numerical results by Doctors and Beck (1987), which match the theoretical solution by Farell (1973) for most cases except one case. Fig. 5.6 shows the case in which the results by Doctors and Beck (1987) do not match the ones by Farell (1973). But the present computation and the computation by Doctors and Beck (1987) are in good agreement.

The results produced by the present method (present algorithm solves the present linearized free surface problem) are close to the solution of Neumann-Kelvin problem for high Froude number cases, but they are different for the low Froude number cases. These differences are believed to be due to the contributions of the double-body streamline effect and the extra terms (in comparison with the Neumann-Kelvin free surface condition, see Table 3.1) in the present free surface condition.

One example of a surface wave pattern generated by the motion of the ellipsoid is presented in Fig. 5.8.

The results obtained by solving Dawson's linear problem are close to those obtained by solving the present linearized problem. This is because the terms missed in Dawson's free surface condition are relatively small in these submerged cases. Differences will appear in the surface ship cases.

5.3.2 The numerical towing tank: Direct method

A. Hull and tank data

The linear numerical towing tank developed in the present study by using the direct boundary integral theory and the linear element techniques is presently used to analyse the flow parameters for two ship hulls, one mathematically defined ship hull — the Wigley hull, and one realistic ship hull — Series 60 ship hull with block ratio $C_b = 0.60$.

Wigley's parabolic hull form has been the subject of extensive experimental, theoretical and numerical studies, (see Chen and Noblesse (1983) and McCarthy (1985) for reviews). The offsets of the Wigley hull are given by the equation

$$y = \frac{b}{2}[1 - (\frac{2x}{L})^2][1 - (\frac{z}{d})^2], \tag{5.150}$$

where b, L and d represent the beam, the length, and the draft respectively, which are chosen, in the present computations, as:

$$\begin{aligned} L &= 4.0m; \\ b &= 0.4m; \\ d &= 0.25m. \end{aligned}$$

The triangular panelization of the Wigley hull is shown in Fig. 5.9, viewing from top, side, and 3-D respectively. A rendered surface of the Wigley hull is shown in Fig. 7.1.

The Series 60 ship hull, $C_b = 0.6$, has been the most popular realistic ship hull in wave resistance studies, (see Todd (1953) for the details of the ship forms

and offset tables). The model dimensions used in the present computations are given as:

$$\begin{aligned} L &= 4.0m; \\ b &= 0.5332m; \\ d &= 0.2133m. \end{aligned}$$

The panelization of Series 60 hull is shown in Fig. 5.10 with top, side, and 3-D views. In this figure only the hull surface below the design load waterline (the ship wetted surface), which is the part of the ship surface used in the computation, is plotted. A rendered surface of the Series 60 ship hull is also shown in Fig. 7.2.

As has been discussed in Section (5.2.1), the size of a numerical towing tank is flexible. It can be chosen to model any specific real towing tank found in a laboratory. Since several experiments are used for comparison purposes, an approximately averaged size of these real towing tanks is selected to be the size of the numerical towing tank in the present numerical experiments. However, because of the limitation of the computer memory only the section of the tank close to the model is simulated. The length of the section was chosen 4 times the length of the ship to be tested, both for Wigley hull and Series 60 ship hull.

The dimensions of the present numerical towing tank for the Wigley hull are given as:

$$\begin{aligned} L_{NT} &= 16.0m, \\ B_{NT} &= 14.4m, \\ D_{NT} &= 2.0m, \end{aligned}$$

where L_{NT} represents the length of the tank section to be simulated, B_{NT} and

D_{NT} represent the width, and the depth of the tank respectively. In the computation only half of the tank is paneled and the width of the half tank is $\frac{1}{2}B_{NT}$. The panelization of the present numerical towing tank along with the Wigley hull are shown in Fig. 5.11. The panel numbers on the tank and on the Wigley hull are 2432 and 288 respectively, which make 2720 the total number of panels used.

The dimensions of the numerical towing tank for the Series 60 ship hull are given as:

$$\begin{aligned} L_{NT} &= 16.0m, \\ B_{NT} &= 12.8m, \\ D_{NT} &= 3.2m. \end{aligned}$$

The panelization of the numerical towing tank along with the Series 60 ship hull are shown in Fig. 5.12. The panel numbers on the tank and on the ship hull are 2048 and 320 respectively, which make 2368 the total number of panels used.

B. Computations and comparisons for Wigley hull

Experimental testing for the wave elevation and wave resistance for Wigley hull has a long history. Chen and Noblesse (1983) investigated the experimental data and concluded that considerable variations generally existed among the experiments. Recently new experiments have been carried out at the University of Iowa (Ju 1983), the University of Tokyo (Kajitani,1983), Ship Research Institute (Tanaka, 1983), and Bulgarian Ship Hydrodynamics Center (Kostov 1983). Good agreement has been obtained by these experimental measurements. These experimental data are used in the present comparisons.

The models used in the above mentioned experiments are listed as:

	SRI	UT	IOWA	BSHC
L (m)	4.0	2.5	3.048	6.096
b (m)	0.4	0.25	0.3048	0.610
d (m)	0.25	0.156	0.1905	0.381

Table 5.1 Dimensions of the Wigley hull models used in the experiments

In Table 5.1, SRI represents Ship Research Institute(Japan), UT University of Tokyo, IOWA University of Iowa and BSHC Bulgarian Ship Hydrodynamics Center.

The dimensions of the tanks used in the above mentioned experiments are listed as:

	SRI	UT	IOWA	BSHC
L_T (m)			91.44	200.0
B_T (m)	18.0	3.5	3.048	16.0
D_T (m)	10.0	2.35	3.14	6.5

Table 5.2 Dimensions of the tanks used for Wigley hull experiments

In Table 5.2 L_T, B_T and D_T are respectively the length, width and depth of the tank. Some data were not specified in the source references. They are kept empty in the table.

Comparisons between the measured and the computed wave profiles for four Froude numbers, $F_n = 0.250$, $F_n = 0.267$, $F_n = 0.289$, and $F_n = 0.316$, are shown in Fig. 5.13 to Fig. 5.16, where x_L is a nondimensional coordinate along the ship length with the bow at -1.0 and stern at $+1.0$, H is a nondimensional wave elevation which is defined as $H = 2\eta g/U^2$, η represents the wave elevation, and U represents the model speed. The Froude number is defined as $F_n = U^2/\sqrt{gL}$, again L is the length of the ship. In these figures, the solid line represents the

present computational results, the dash-dotted line represents the experimental results obtained at the University of Tokyo, the dashed line represents the experimental results of Ship Research Institute(Japan).

From Fig. 5.13 to Fig. 5.16 it can be seen that the wave elevations obtained by the present numerical towing tank match the experimental results fairly well and for all the Froude numbers which have been tested. Some differences are found at the bow, with the numerical waves lower than the ones obtained by the experimental measurements. This is mainly due to the linear property of the present algorithm as will be shown in the next chapter.

Fig. 5.17 gives a 3-D view of the wave pattern generated by the Wigley hull at Froude number $F_n = 0.267$, in which the pattern of diverging and transverse waves are shown clearly.

Fig. 5.18 shows the wave resistance coefficient C_w obtained by the present numerical computation and the experimental results by UT(Kajitani, 1983) SRI(Kajitani, 1983), IOWA (Ju, 1983), and BSHC(Kostov 1983). From this figure it can be seen that the experimental results are in good agreement and the numerical results by the present computation match them well too.

In order to compare Dawson's free surface condition with the present free surface condition, Dawson's free surface condition is also implemented in the present linear numerical towing tank. As has been discussed in Section (5.3.1) the implementation of Dawson's free surface condition is very simple. It only necessary to change the coefficients in the computer program, which is just a matter of six lines. The results of solving Dawson's linear problem by the present direct algorithm are plotted in Fig. 5.19 along with the results of the present

method and the experimental data. Comparisons show that Dawson's free surface condition give almost the same results as the ones obtained by the present method and all of them match the experimental data for the Wigley hull case.

Many numerical computations can be found in the literature for calculating the wave-making resistance for Wigley hull. These mainly fall into two groups. One group is based on solving the Neumann-Kelvin linear problem to compute the wave-making resistance, and the other is based on solving Dawson's linear problem to compute the wave-making resistance. In order to compare these two linear ship wave problems and also compare their results with the present computations, the Neumann-Kelvin free surface condition is also implemented in the present computation. The wave resistances obtained by solving the Neumann-Kelvin problem are plotted in Fig. 5.20 along with the results of solving Dawson's linear problem, the results solving the present linear problem, the experimental results as well as the thin ship theory solution. The comparison shows that the results solving the Neumann-Kelvin linear problem matches the results solving Dawson's linear problem, the results solving the present linear problem and the results experiments as well. Fig. 5.20 also shows that the thin ship theory gives a reasonable prediction of the wave-making resistance for Wigley hull.

It should be mentioned that the Neumann-Kelvin free surface condition used in the present numerical towing tank is satisfied along the streamlines and is expressed as:

$$U^2\frac{\partial^2\phi'}{\partial\ell^2}+g\frac{\partial\phi'}{\partial z}=0. \tag{5.151}$$

In the original Neumann-Kelvin free surface condition, the streamlines for the main flow are parallel to the x-axis, and are penetrating the hull surface, (see

Aanesland 1986). It is the simplest kind of flow and easy to use in the Kelvin source method. But at the same time it is obviously in conflict with the physics of the flow going around the ship hull. Although equation (5.151) has some small differences with the original Neumann-Kelvin free surface condition, the difference should bring the results closer to the real physical problem. Equation (5.151) has been used by Raven (1991).

Fig. 5.21 gives a comparison between the results obtained by solving Dawson's linear problem using the present method with five computational results found in the literature which were published by Dawson (1979), Mori and Murata (1983), Ogiwara (1983), Aanesland (1986), and Xia (1986) respectively. These four computations all solved Dawson's linear problem and all applied the Rankine source method. Good agreements are found in the comparisons.

Fig. 5.22 shows a comparison between C_w obtained by solving the Neumann-Kelvin linear problem using the present method and the C_w computed by solving the same Neumann-Kelvin linear problem by Chang (1979), Hong (1979), Tsai et al (1983), and Baar (1986) respectively. Good agreements are also found in these comparisons.

Finally, results for C_w by solving the Neumann-Kelvin linear problem, by solving Dawson's linear problem, and by solving the present linear ship wave problem obtained in the present computation and the computational results found in the literature of solving Dawson's linear problem and the Neumann-Kelvin problem are plotted in Fig. 5.23. This comparison shows that fairly good agreements are obtained by the computations and they match the experimental results.

In the above mentioned comparisons, all the data, computational or exper-

imental, are for model fixed, since in the present computation the sinkage and trim of the ship are not considered.

One more remark should be mentioned. Some computations found in the literature, such as the ones by Tsutsumi (1979, solving the Neumann-Kelvin linear problem), by Suzuki(1979, solving the Neumann-Kelvin linear problem), and by Nakatake(see Baba 1979, solving Dawson's linear problem), do not match any of the other computations and do not match any experimental results. These computations were not included in the present comparison. Baar (1986) investigated these computations and concluded that the discrepancy must be mainly ascribed to the errors occurring in these evaluations.

C. Computations and comparisons for Series 60 ship hull

Series 60, block 0.60, hull has been one of the most important hull form for evaluating computational methods and also the model testing procedures. Many efforts have been made to produce reliable measurements. In 1983, the ITTC resistance Committee organized a co-operative effort between its member organizations to produce a comprehensive data base of hull flow and resistance components. Results have been collected in the report " Collected Experimental Resistance Component and Flow Data For Three Surface Ship Model Hulls" by the David W. Taylor Naval Ship Research and Development Center (McCarthy 1985). These results are believed to be the most recent and reliable experimental data. All (except only one by Huang 1972) the experimental data for Series 60 used in the present study are from this report. Since the sinkage and trim of the ship are not modeled in the present study, the experimental data used

for comparison are all those data obtained under the condition of model fixed (without sinkage and trim).

A list of the names of the institutions whose experimental data are used in the present study is given as:

Bulgarian Ship Hydrodynamics Center (BSHC), (Kostov, 1983);

China Ship Scientific Research Center (CSSRC), (Zhang, 1983);

David Taylor Naval Ship Research and Development Center (DTNSRDC), (Kim, 1981);

Marine Design and Research Institute of China (MARIC), (Du, 1983);

Shanghai Chiao Tong University (CTU), (Liu, 1983);

Ship Research Station (SRS, Korea), (Lee, 1983);

Shanghai Ship and Shipping Research Institute (SSSRI), (Chen, 1983).

The experimental equipment used in these experiments are summarized as follows:

Model size:

	BSHC	CSSRC	CTU	MARIC	DTNSRDC	SRS	SSSRI
L_{wl} (m)	7.117	6.1	2.5	2.5	6.2	4.9585	1.83
L_{pp} (m)	7.000	6.0			6.1	4.8768	1.80
b (m)	0.933	0.8	0.3333	0.3333		0.6502	0.24
d (m)	0.373	0.32	0.1333	0.1333		0.2601	0.096

Table 5.3 Dimensions of the Series 60 hull models used in the experiments

In Table 5.3, L_{wl} represents the designed load waterline length, L_{pp} represents the length between perpendiculars, b represents the beam at midship of the model, and d is the draft of the ship model.

Tank size:

	BSHC	CSSRC	CTU	MARIC	DTNSRDC	SRS	SSSRI
L_T (m)	200.0	474.0	110.0	70.0		200.0	50.0
B_T (m)	16.0	14.0	6.0	5.0	15.54	16.0	6.0
D_T (m)	6.5	7.0	3.0	2.5	6.7	7.0	2.0

Table 5.4 Dimensions of the tanks used for Series 60 hull experiments

Comparisons between the measured and computed wave profiles are shown in Fig. 5.24 to Fig. 5.29. From these figures it can be seen that the measured wave profiles are quite close to each other, and the computed wave profiles match the experimental measurements fairly well. Some small discrepancies are found between the computational and the experimental results at the bow waves. This is mainly due to the nonlinearity of the bow wave. Improvement will be seen in the next chapter where the nonlinear computations of the present study are presented. For high Froude number cases, see Fig. 5.27 to 5.29, discrepancies are also noticed at the stern waves. This can be explained as the effect on the waves by the hull surface at the designed load water line. In experiments the waves are affected by the ship hull at the designed load water line, because the hull is not vertically walled. In the algorithm of the present study the slope of the ship hull below the designed load water line is taken care, but the slope effect of the ship hull at the water line is not taken into account. In other words, the ship hull at the designed load water line is considered to be vertical.

A 3-D view of the surface waves generated by the constant motion of a Series 60 ship hull is presented in Fig. 5.30. Two frames of rendered surface waves generated by Series 60 ship hull taken from the animation series are also shown in Fig. 7.13. There is no 3-D measurement available for comparison, but the wave patterns shown in these figures appear very much like the Kelvin wave pattern.

A comparison between the measured and computed wave resistance coefficients is shown in Fig. 5.31. The solid line in this figure represents the present computational wave resistance coefficient C_w, and the seven different marks represent the experimental results measured, respectively, by Chen (1983), Du (1983), Kim (1981), Kostov (1983), Lee (1983), Liu (1983), and Zhang (1983). The comparison shows that the present linear model gives good prediction for the wave resistance.

In order to compare Dawson's linear free surface condition with the present linear free surface condition, Dawson's linear ship wave problem is also solved for the Series 60 hull. The results are plotted in Fig. 5.32. In this figure the solid line represents the results of solving the present linear ship wave problem and the dash-dotted line represents the results of solving Dawson's linear ship wave problem by using the present algorithm. Unlike the Wigley hull case, Dawson's linear problem gives different predictions from those results obtained by solving the present linear ship wave problem and the experimental measurements.

In Fig. 5.33 the wave resistance coefficients C_w predicted by solving the Neumann-Kelvin problem along with the results of solving the present linear problem and Dawson's linear problem are presented. The thin ship theory prediction and the experimental data are also plotted in this figure. From this figure it can be seen that the Neumann-Kelvin linear ship wave model predicts much higher resistance than the experimental measurements. The Neumann-Kelvin linear ship wave model does not give good predictions in wave resistance, but it is better than the thin ship theory, because the ship surface condition of Neumann-Kelvin linear ship wave model is improved while the fluid free surface condition

is the same as in the thin ship theory.

Fig. 5.34 presents a comparison between the results of solving Dawson's linear ship wave problem by the present algorithm for a Series 60 hull and the results found in the literature for solving the same problem. Two computations of solving Dawson's linear ship wave problem for Series 60 ship hull were found in the literature, by Dawson (1979) and by Xia (1986). Both Dawson (1979) and Xia (1986) solved the same Dawson's linear ship wave problem, and different solutions were obtained. However, the present computational results and the results published by Xia (1986) are in good agreement.

In Fig. 5.35 the wave resistance coefficients of the present computation by solving the Neumann-Kelvin problem and the results of solving the same Neumann-Kelvin problem by Adee(1979), Chang (1979), and Tsai et al (1983) are plotted. A fairly good agreement is found in this comparison. All the results of solving the Neumann-Kelvin problem, by the present method, by Adee (1979), Chang (1979), and Tsai et al (1983) are out of the envelope of the experimental data. This can be seen in Fig. 5.36.

In this chapter two algorithms for solving the linearized ship wave problem obtained in Section (3.3) are developed. The algorithms are based on the direct and the indirect boundary integral theories respectively. Linear element techniques are used in both algorithms. The indirect algorithm has been applied to a submerged prolate ellipsoid. The direct algorithm has been applied to the Wigley hull and the Series 60, $C_b = 0.6$, ship hull. The direct algorithm will also be used in the next chapter to form an iterative method for solving the transformed nonlinear ship wave problem obtained in Section (3.1).

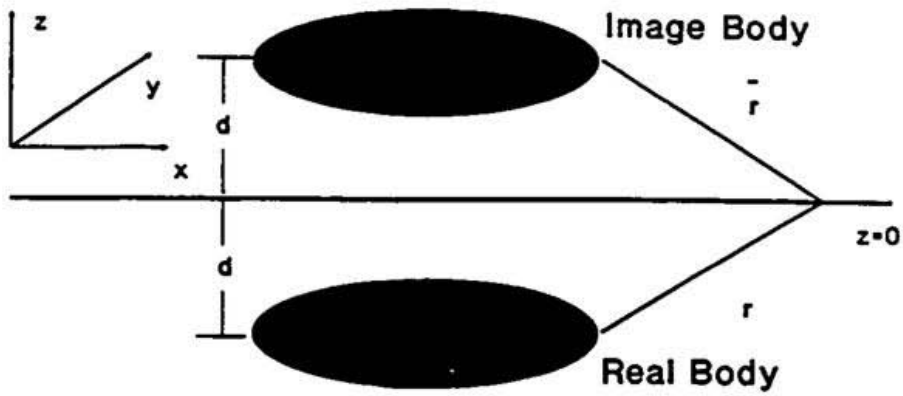

Fig. 5.1 The geometry of double-body problem

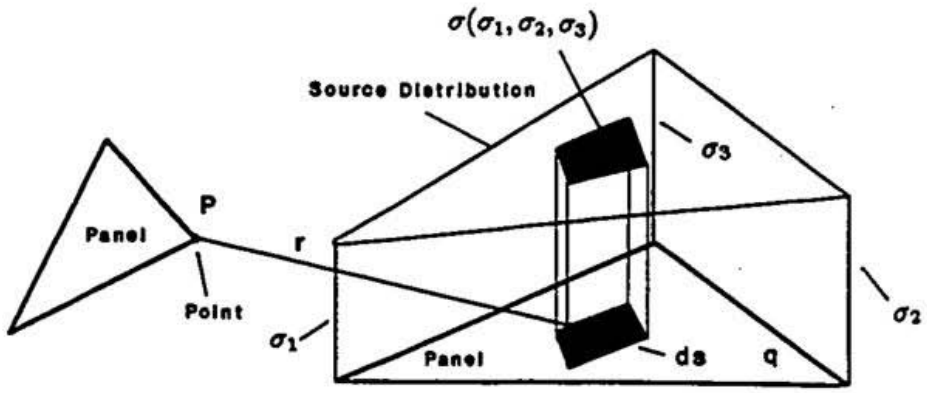

Fig. 5.2 Triangular panels and linear source distribution

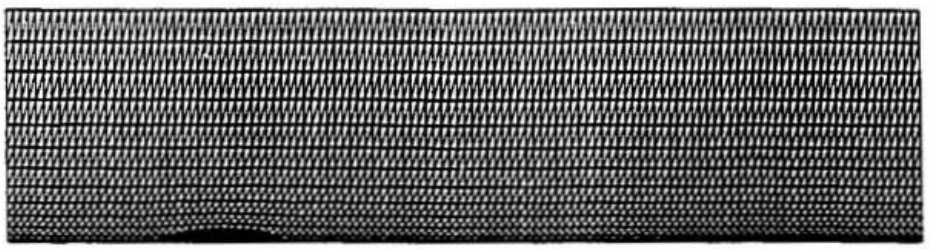

5.3.a Free surface mesh with the ellipsoid underneath it

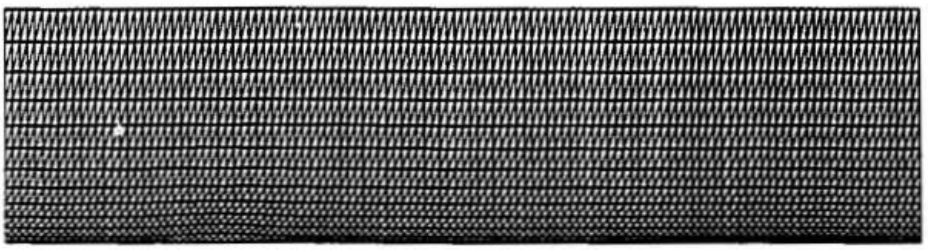

5.3.b Streamline bounded free surface panelization

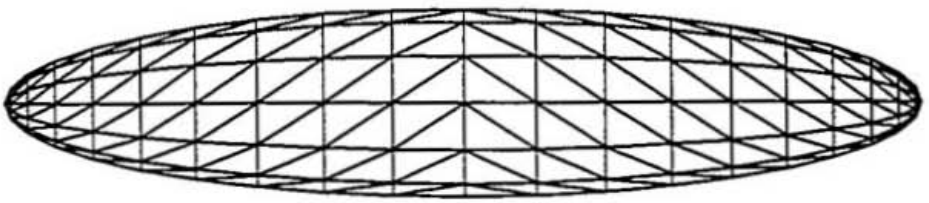

5.3.c Triangular panelization on the surface of ellipsoid

Fig. 5.3 Free surface and body surface panelization

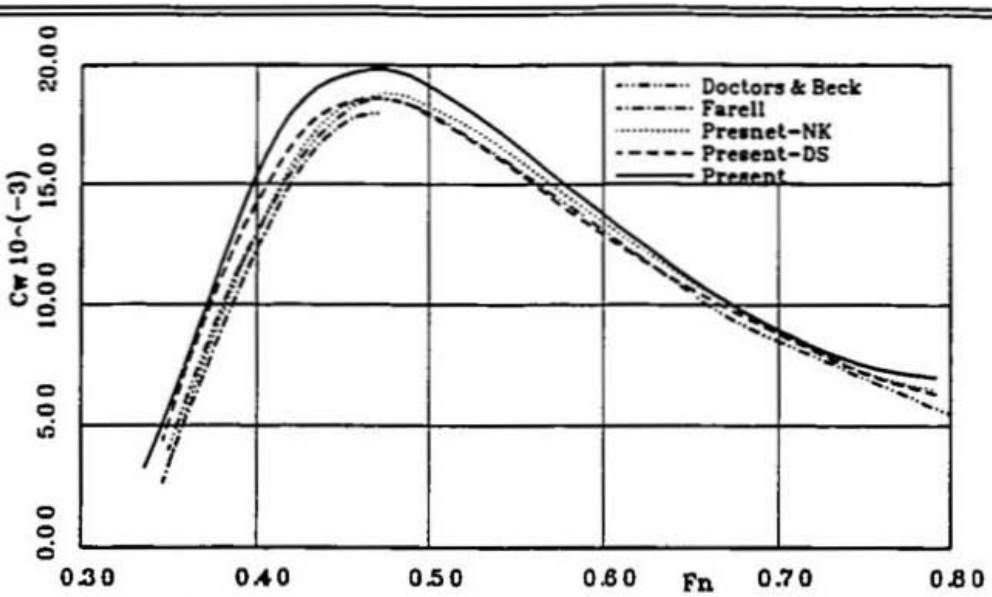

Fig. 5.4 Wave resistance coefficient C_w of submerged ellipsoid (High Froude number, d/c=0.3266)

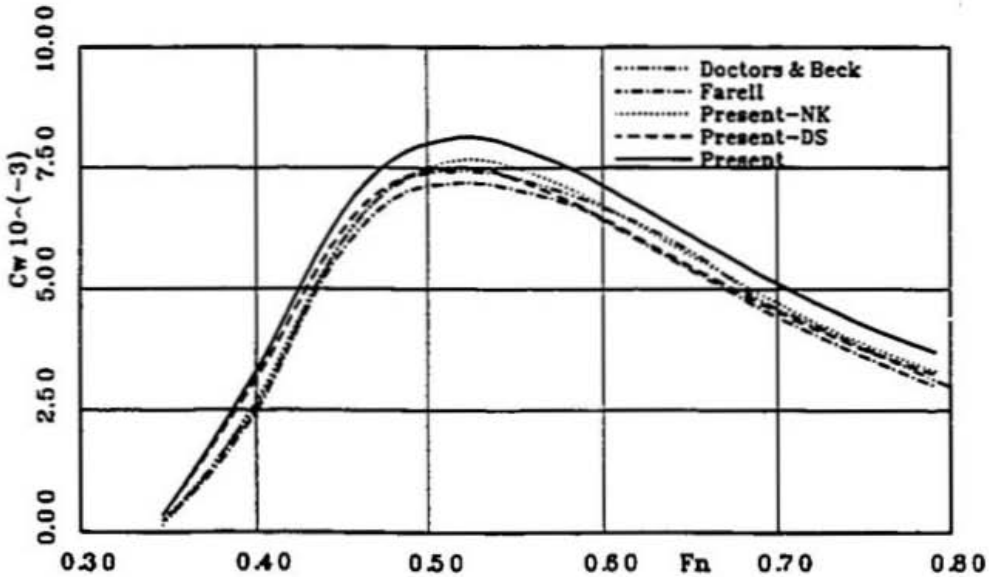

Fig. 5.5 Wave resistance coefficient C_w of submerged ellipsoid (High Froude number, d/c=0.5)

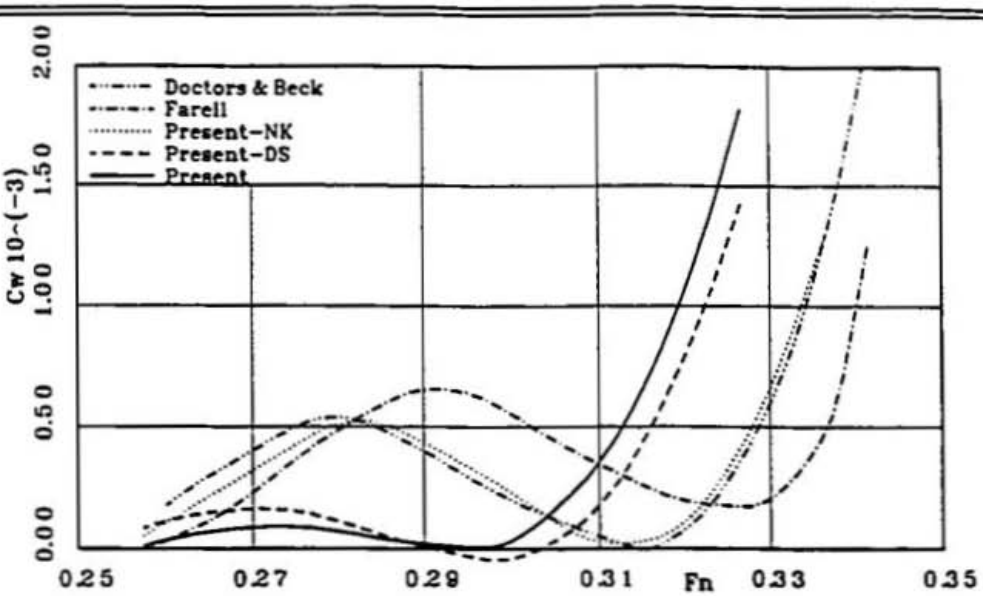

Fig. 5.6 Wave resistance coefficient C_w of submerged ellipsoid (Low Froude number, d/c=0.3266)

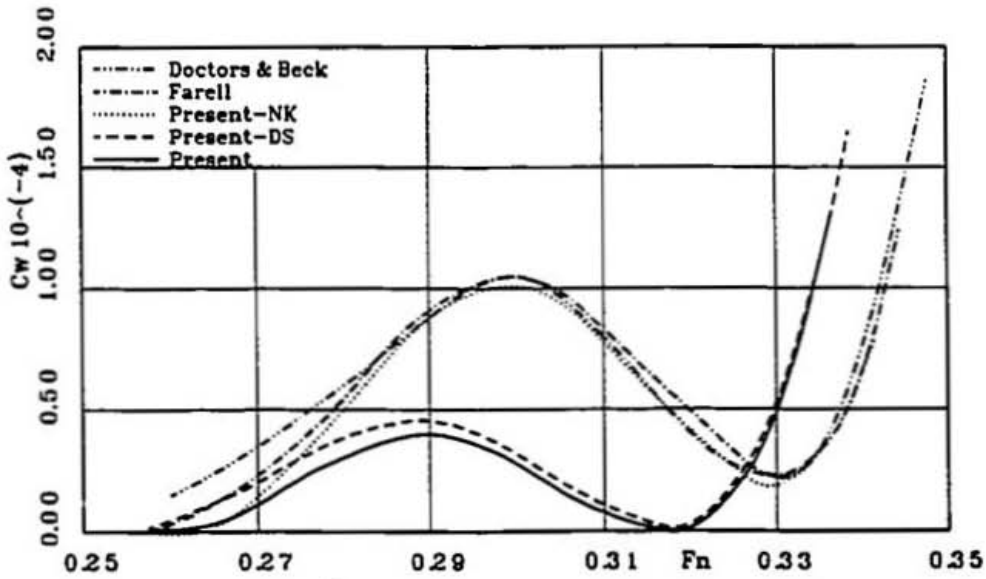

Fig. 5.7 Wave resistance coefficient C_w of submerged ellipsoid (Low Froude number, d/c=0.5)

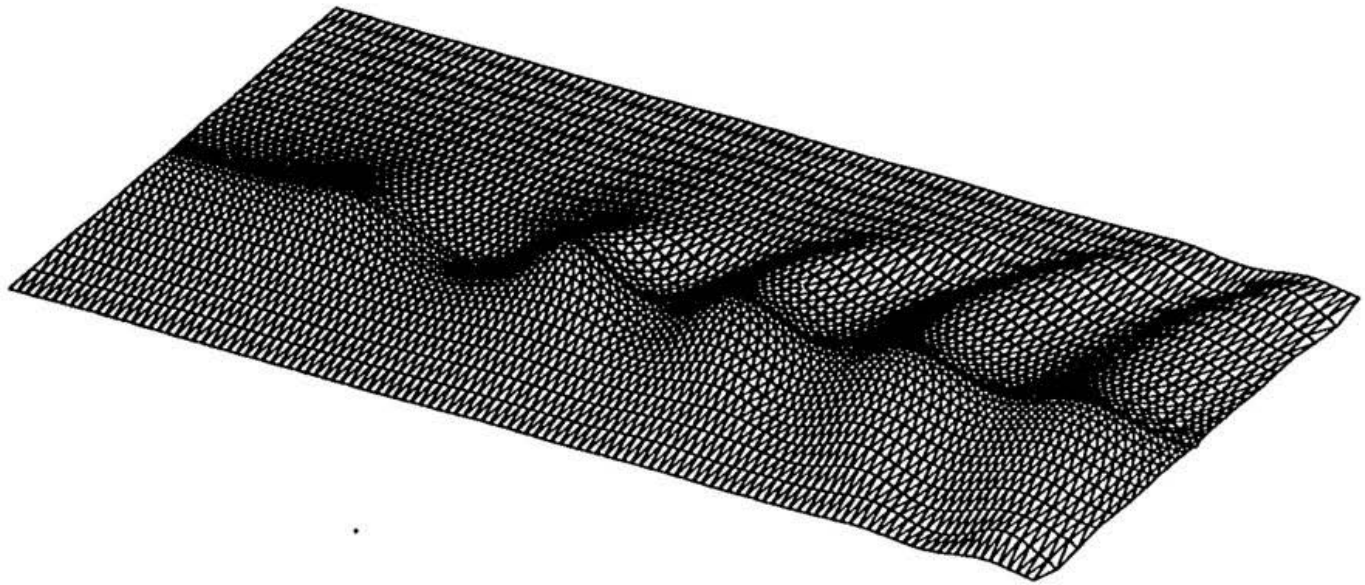

Fig. 5.8 Surface wave pattern generated by the submerged ellipsoid(Fn=0.34,d/c=0.3266)

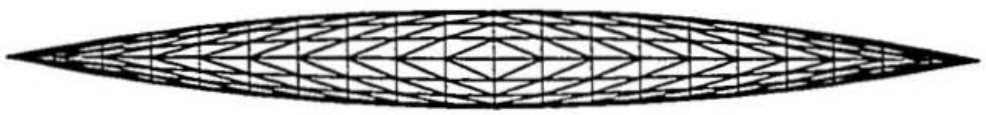

5.9.a Top view

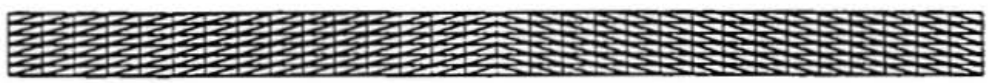

5.9.b Side view

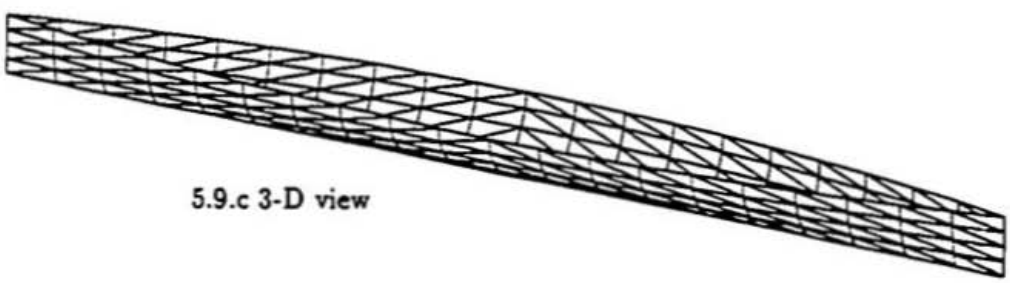

5.9.c 3-D view

Fig. 5.9 Panelization of Wigley hull

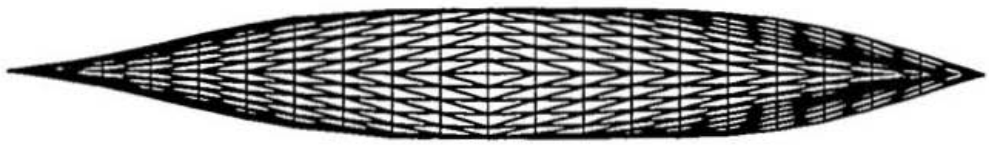

5.10.a Top view

5.10.b Side view

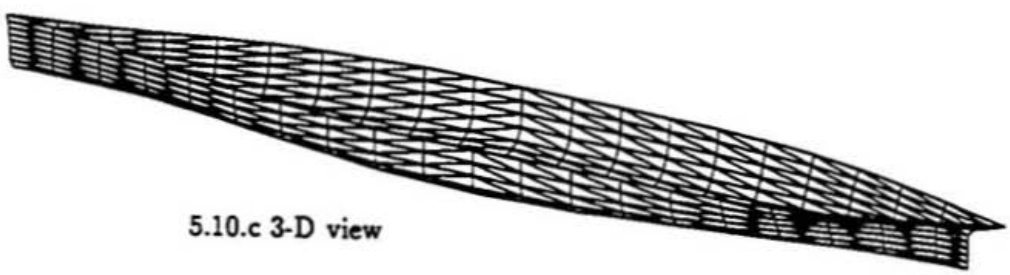

5.10.c 3-D view

Fig. 5.10 Panelization of Series 60 ship hull

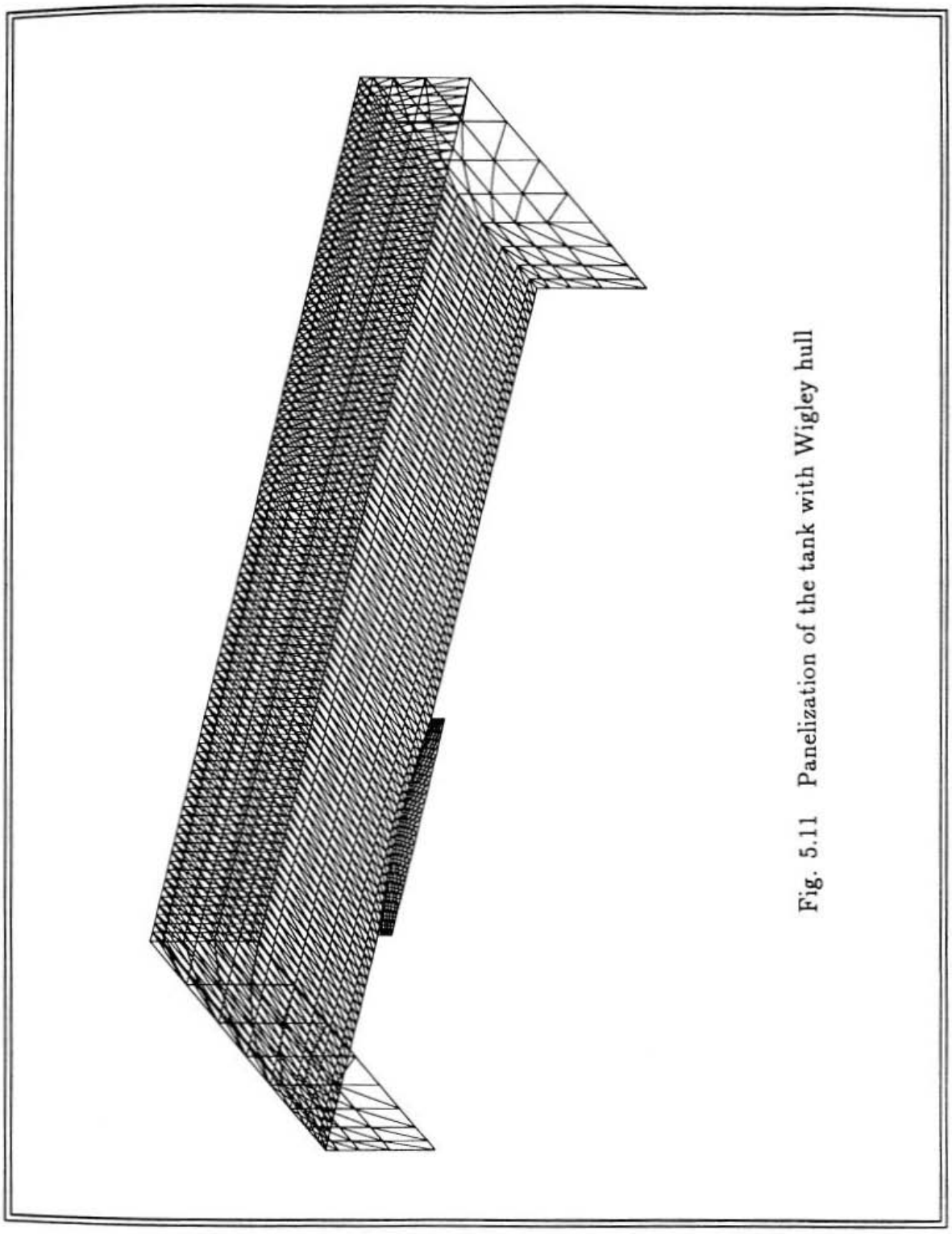

Fig. 5.11 Panelization of the tank with Wigley hull

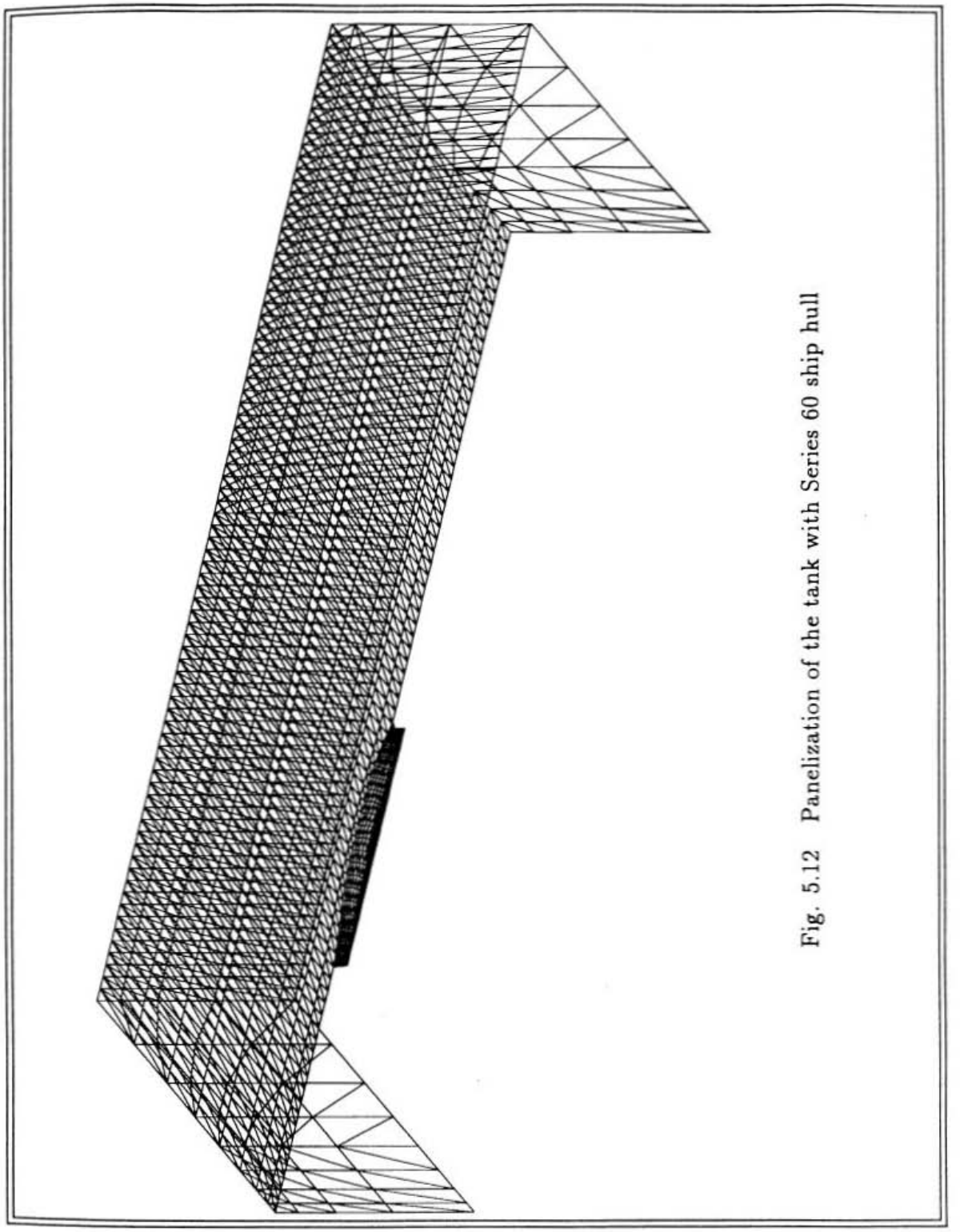

Fig. 5.12 Panelization of the tank with Series 60 ship hull

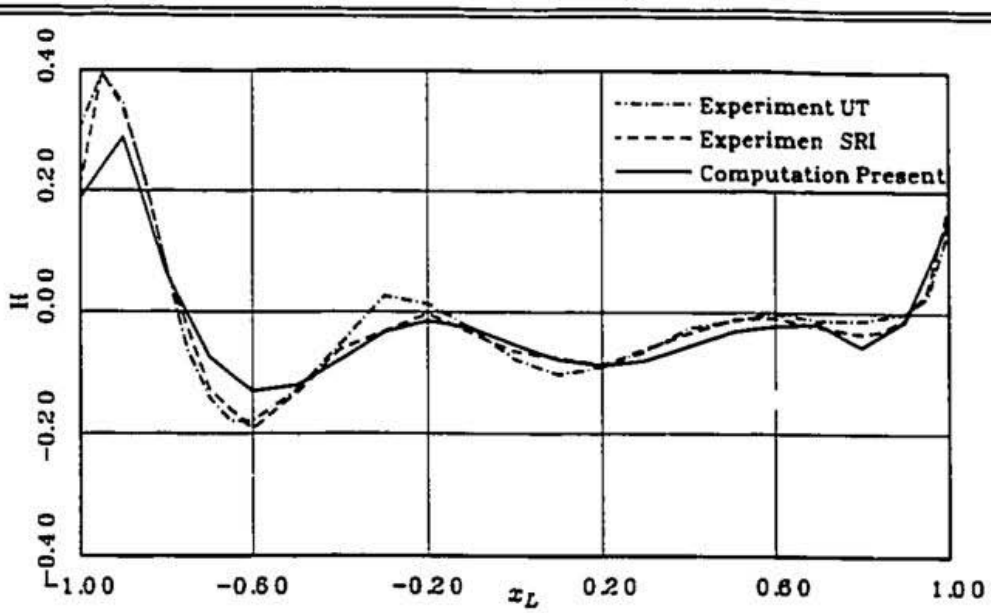

Fig. 5.13 Comparison of wave profiles for Wigley hull (Fn=0.250)

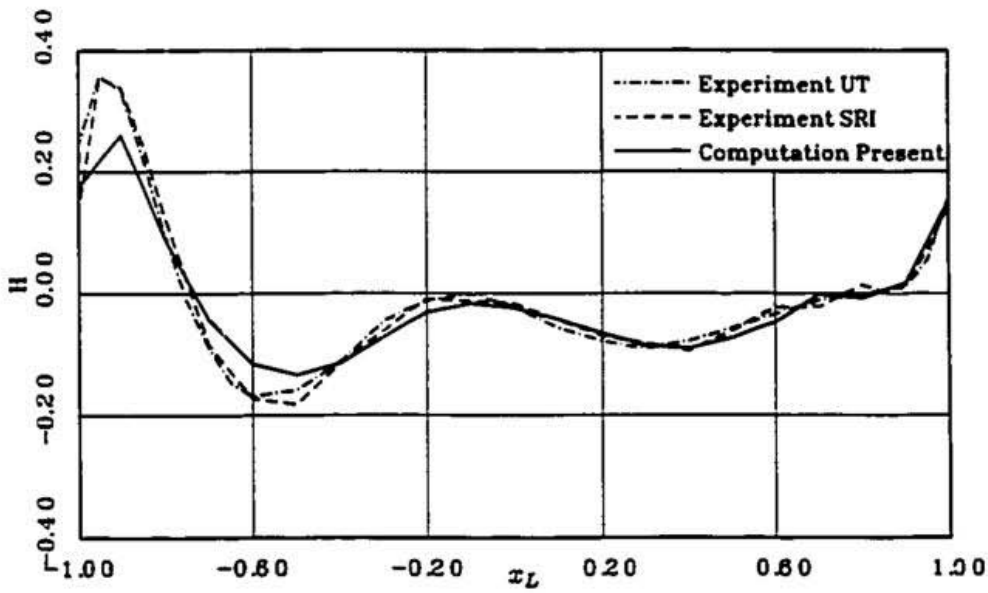

Fig. 5.14 Comparison of wave profiles for Wigley hull (Fn=0.267)

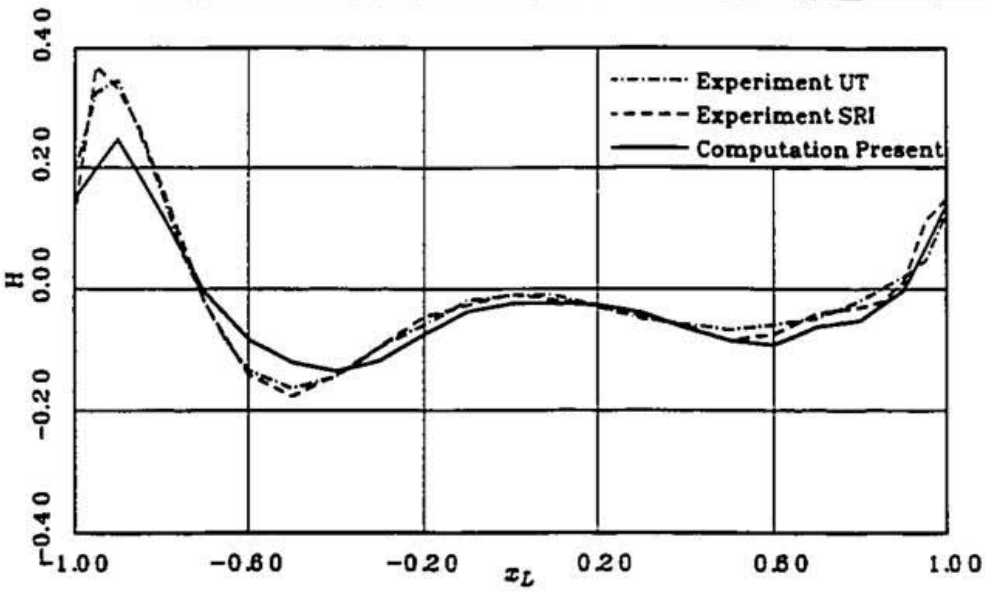

Fig. 5.15 Comparison of wave profiles for Wigley hull (Fn=0.289)

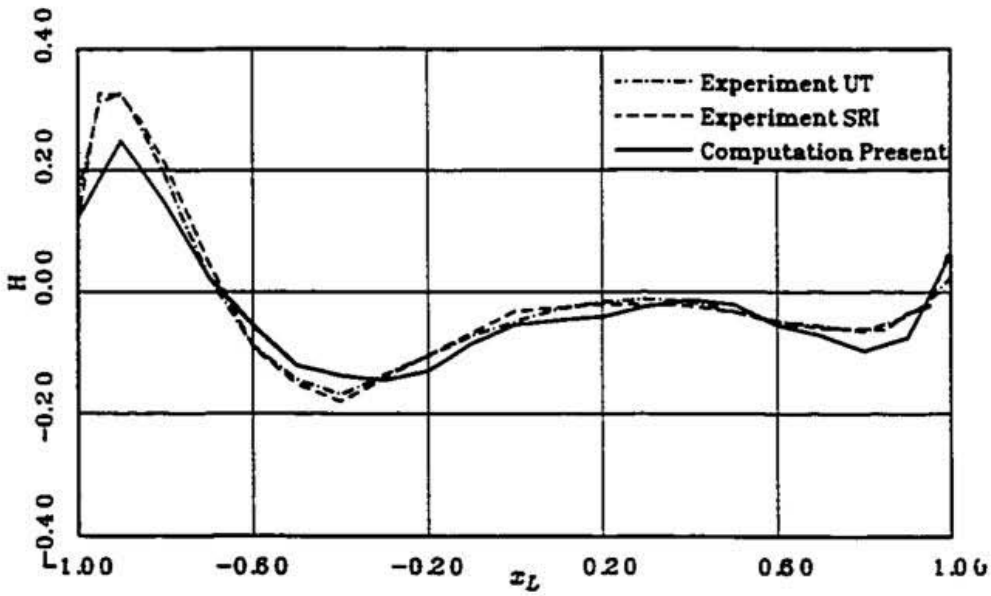

Fig. 5.16 Comparison of wave profiles for Wigley hull (Fn=0.316)

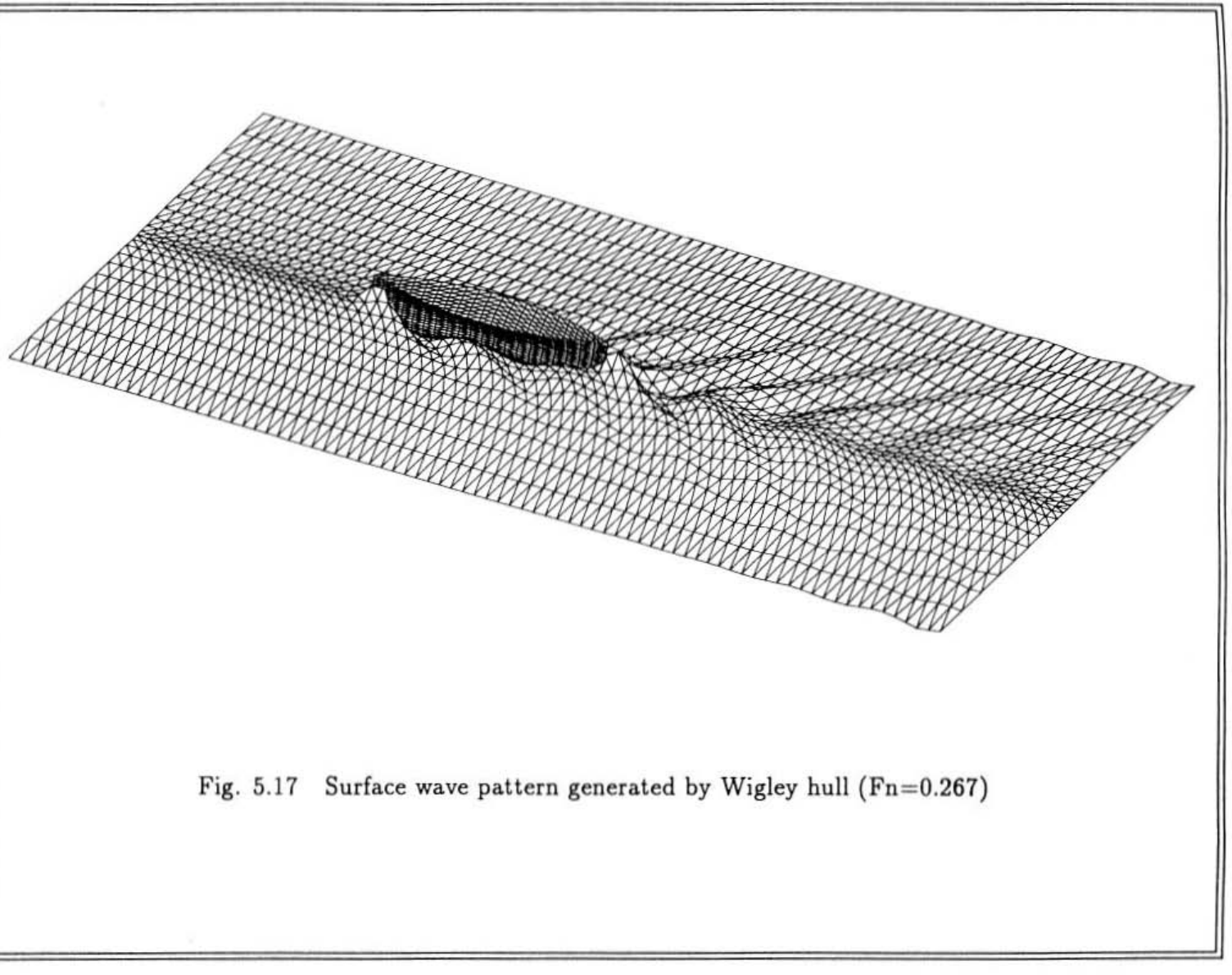

Fig. 5.17 Surface wave pattern generated by Wigley hull (Fn=0.267)

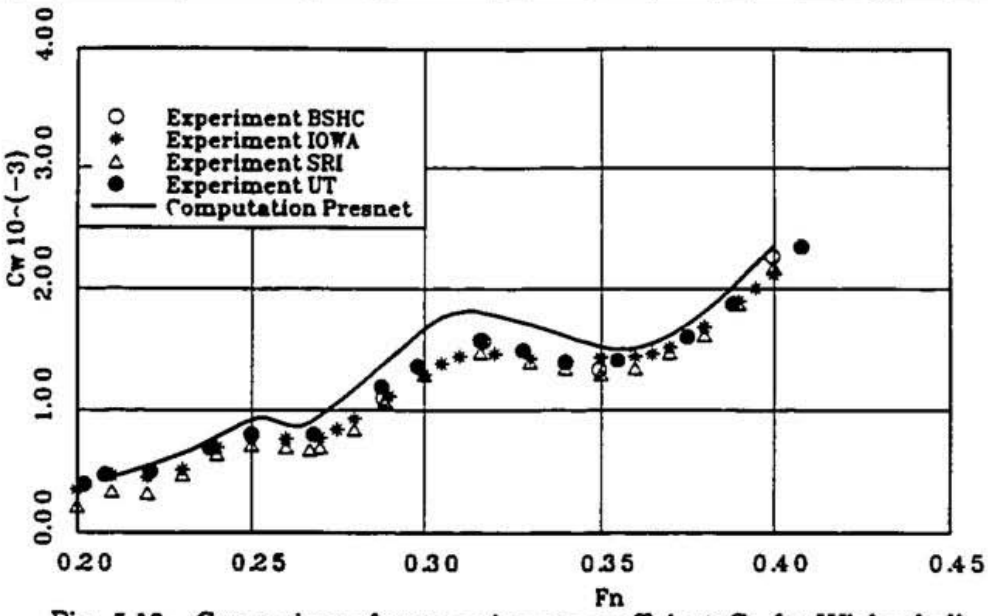

Fig. 5.18 Comparison of wave resistance coefficient C_w for Wigley hull

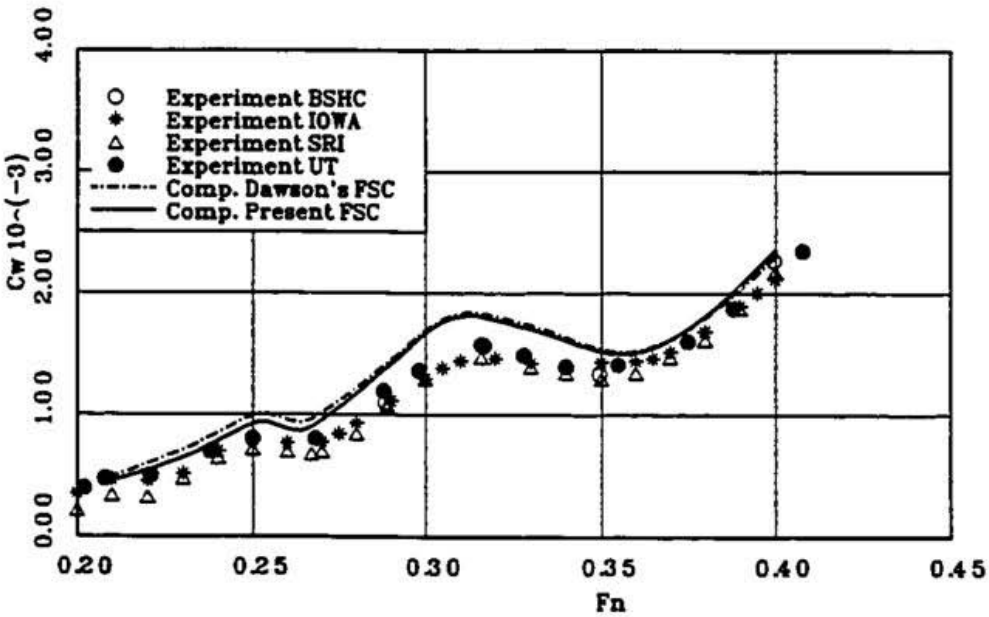

Fig. 5.19 Comparison of wave resistance coefficient C_w for Wigley hull

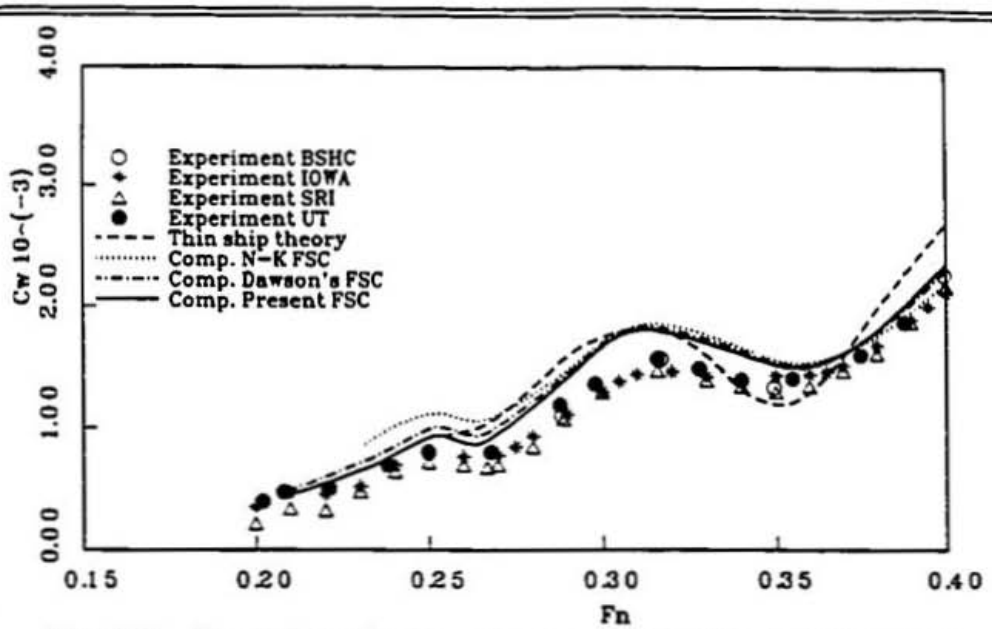

Fig. 5.20 Comparison of wave resistance coefficient C_w for Wigley hull

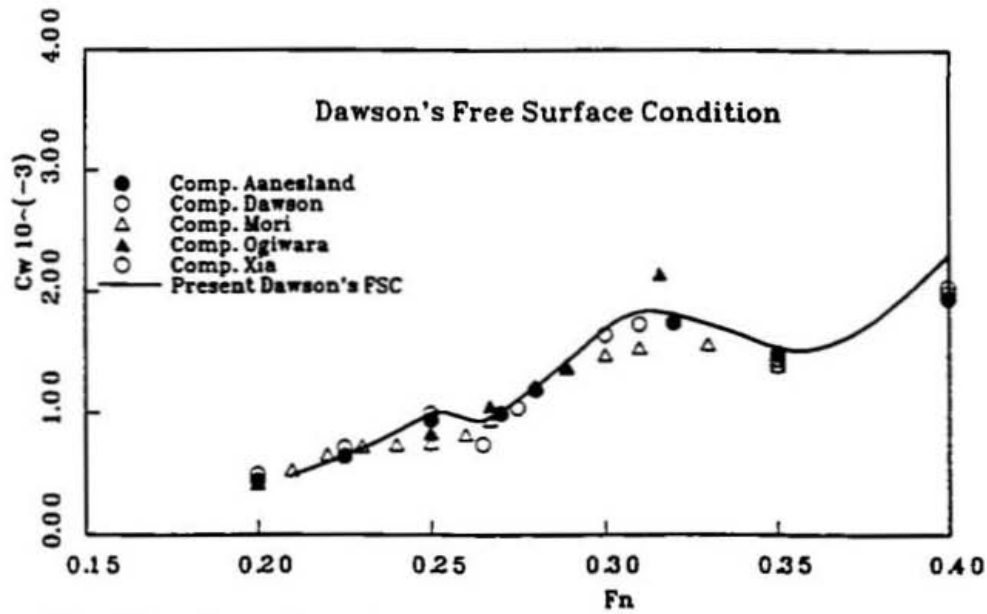

Fig. 5.21 Comparison of wave resistance coefficient C_w for Wigley hull

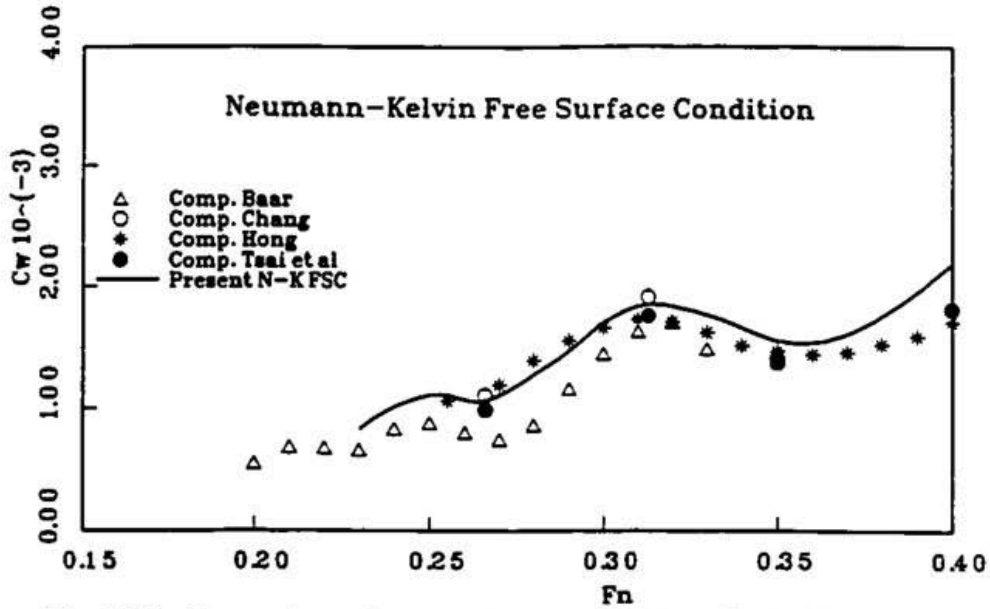

Fig. 5.22 Comparison of wave resistance coefficient C_w for Wigley hull

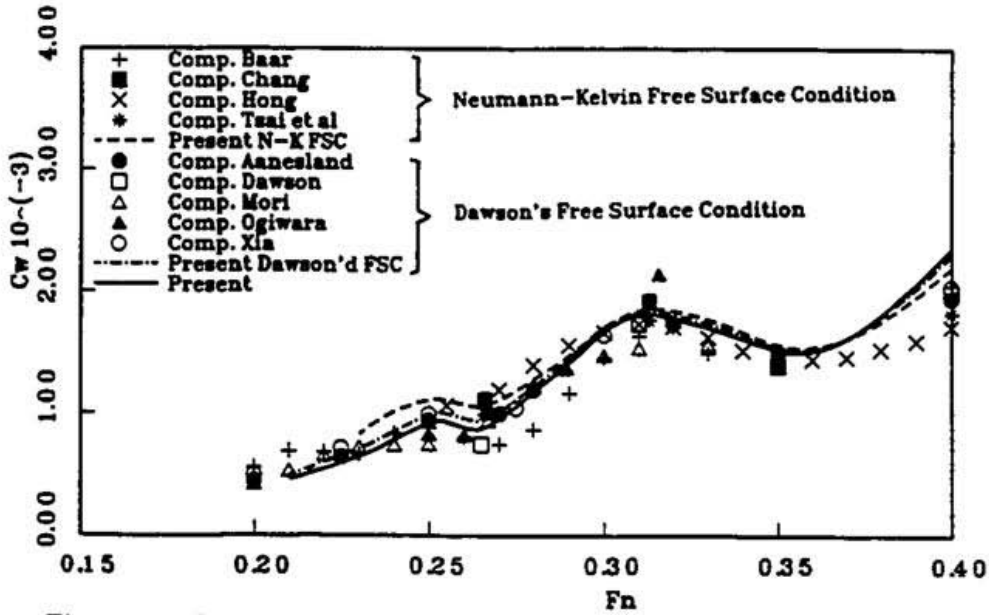

Fig. 5.23 Comparison of wave resistance coefficient C_w for Wigley hull

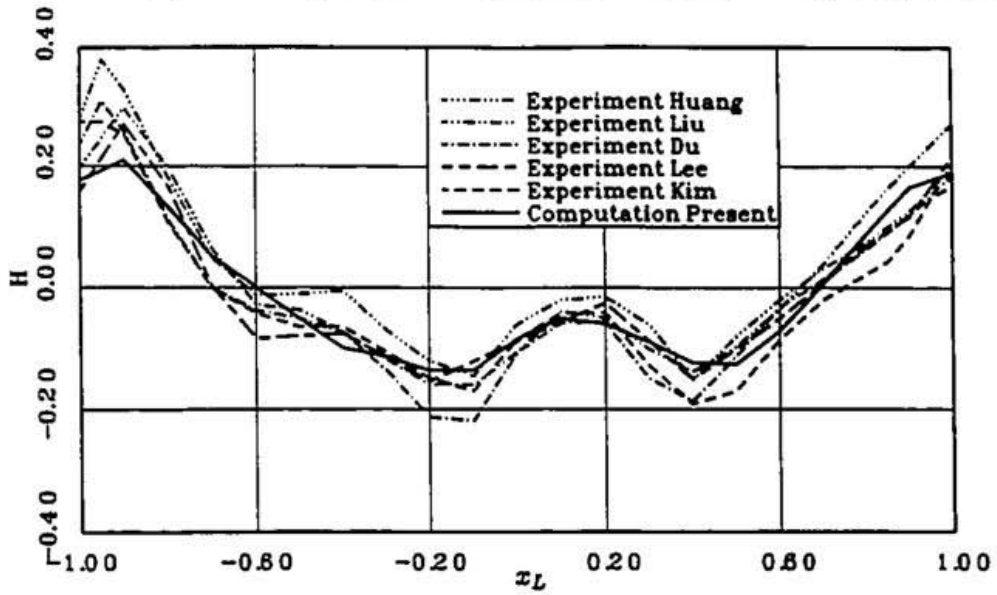

Fig. 5.24 Comparison of wave profiles for Series 60 hull (Fn=0.22)

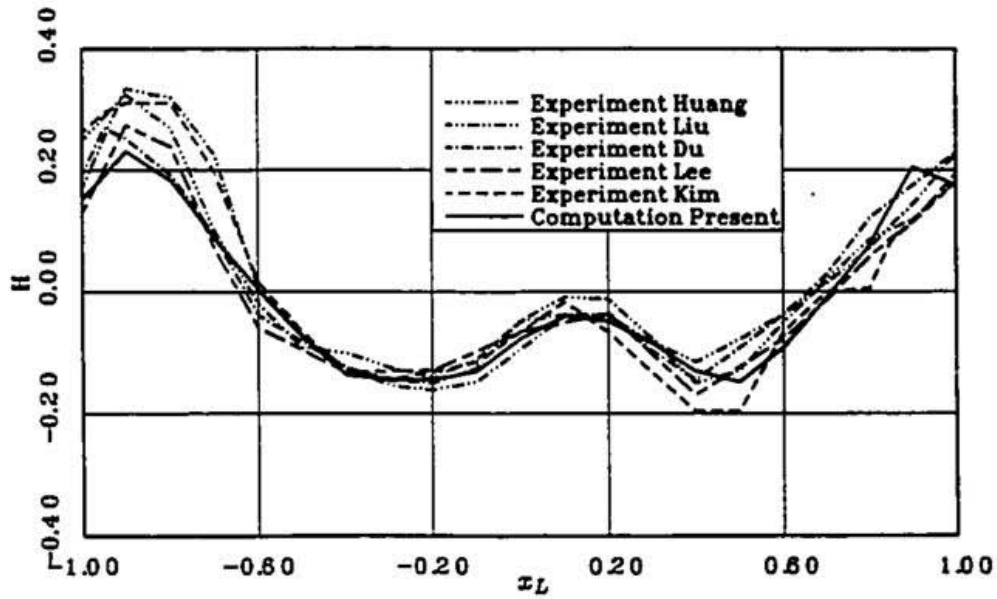

Fig. 5.25 Comparison of wave profiles for Series 60 hull (Fn=0.25)

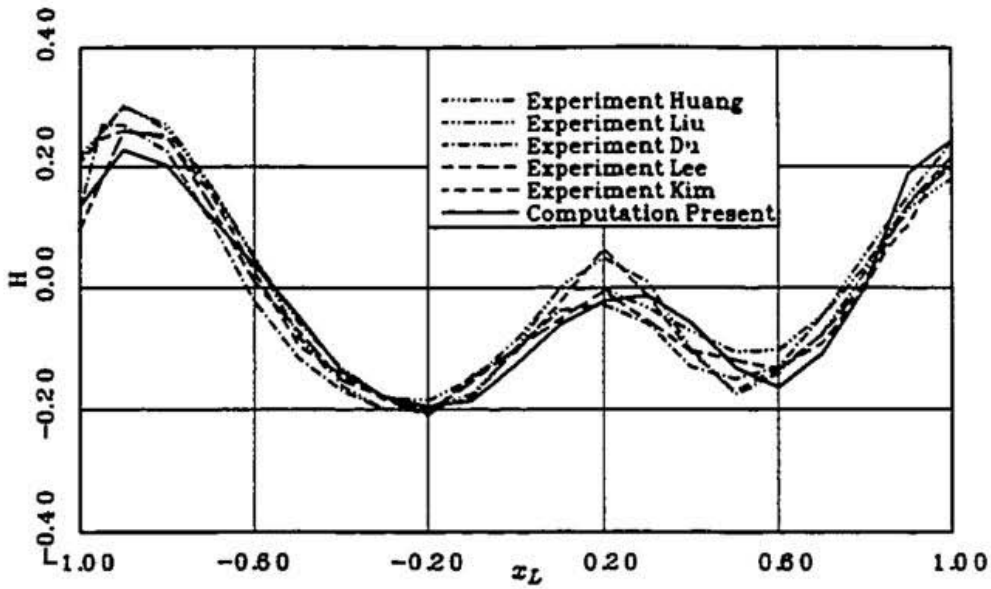

Fig. 5.26 Comparison of wave profiles for Series 60 hull (Fn=0.28)

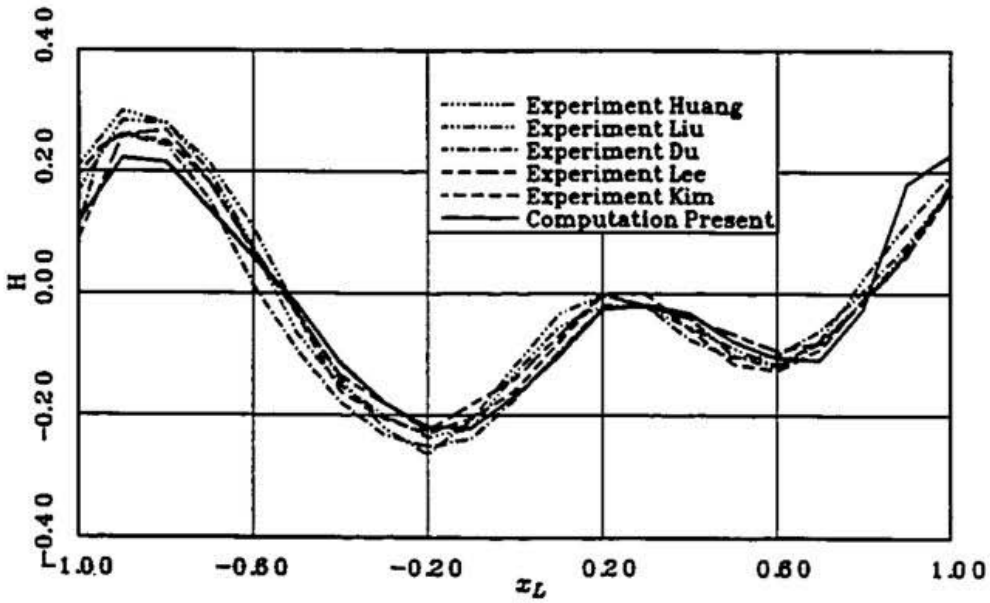

Fig. 5.27 Comparison of wave profiles for Series 60 hull (Fn=0.30)

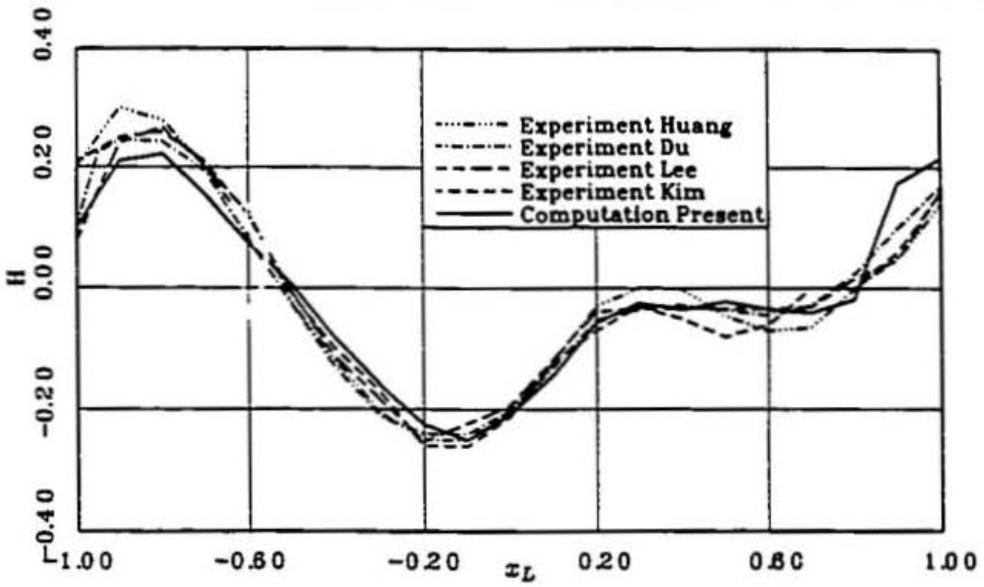

Fig. 5.28 Comparison of wave profiles for Series 60 hull (Fn=0.32)

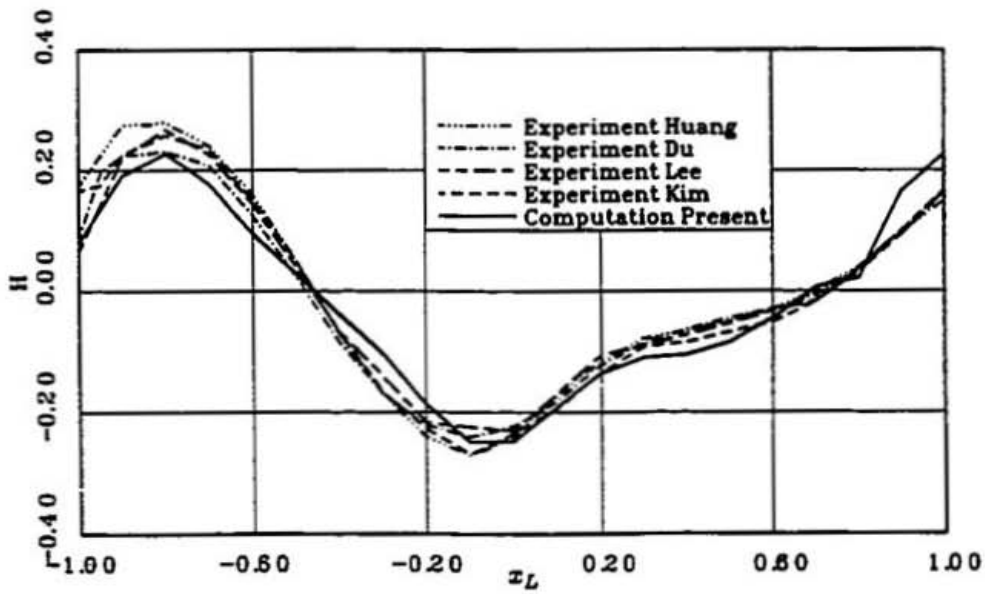

Fig. 5.29 Comparison of wave profiles for Series 60 hull (Fn=0.35)

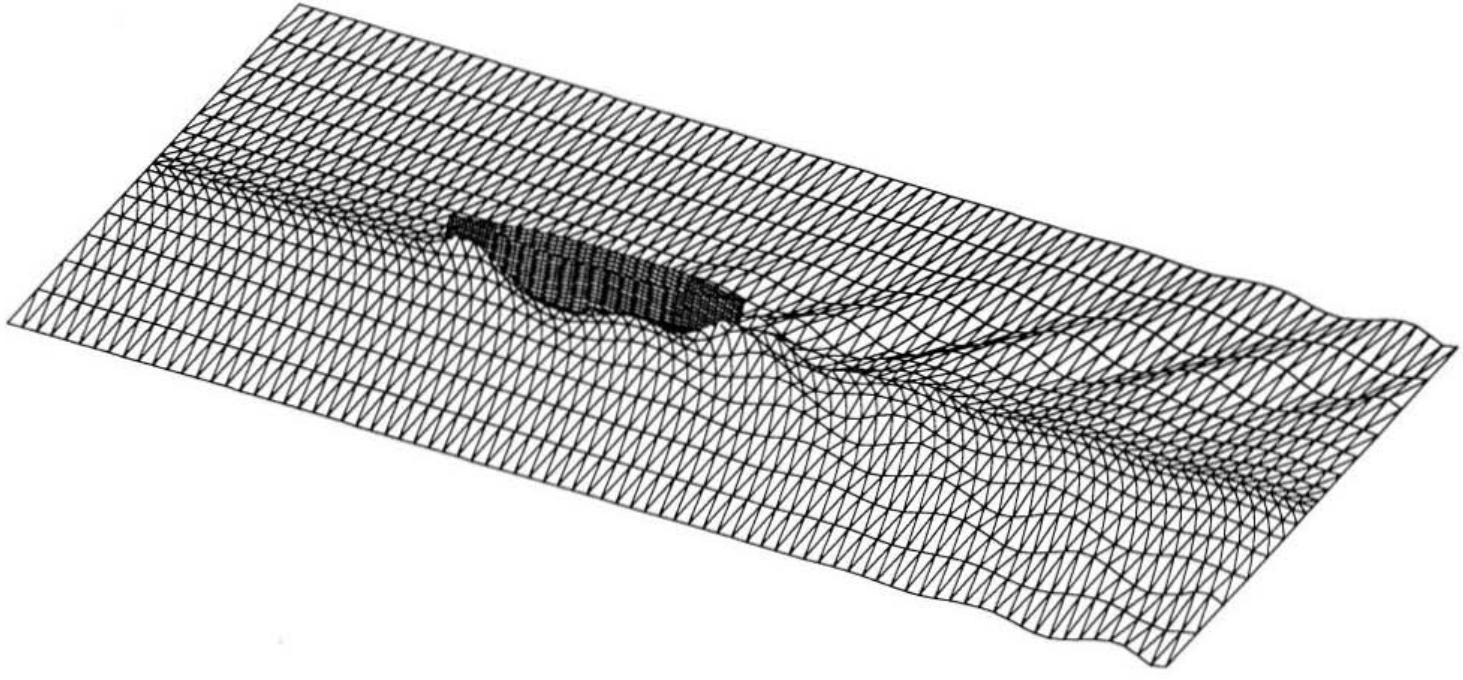

Fig. 5.30 Surface wave pattern generated by Series 60 hull (Fn=0.30)

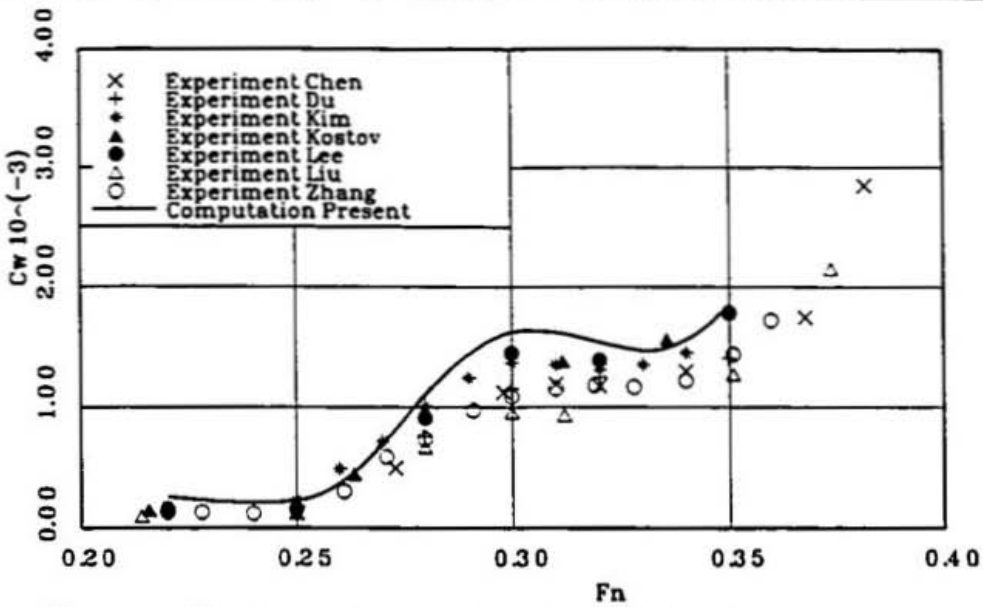

Fig. 5.31 Comparison of wave resistance coefficient C_w for Series 60 hull

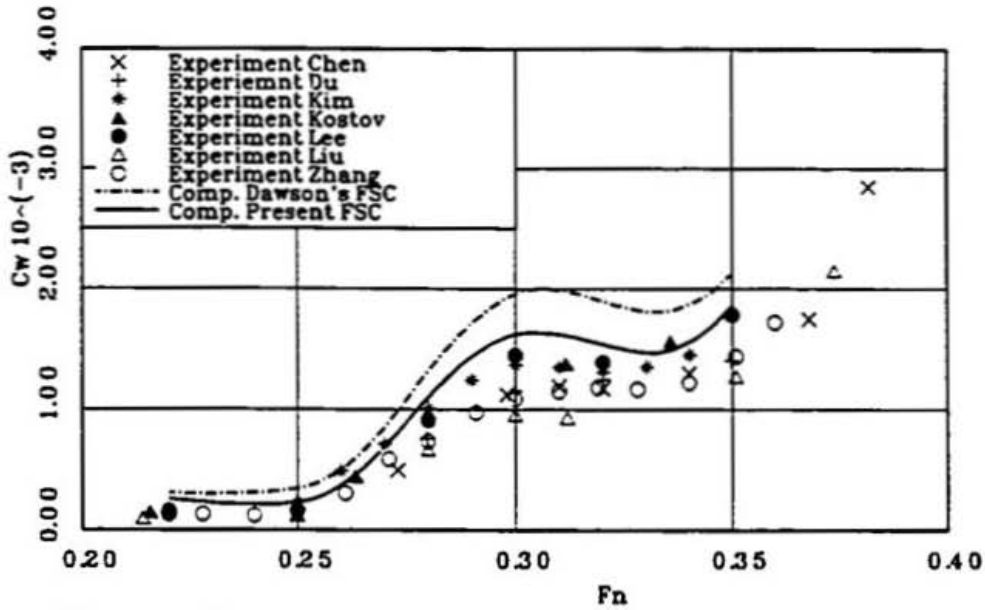

Fig. 5.32 Comparison of wave resistance coefficient C_w for Series 60 hull

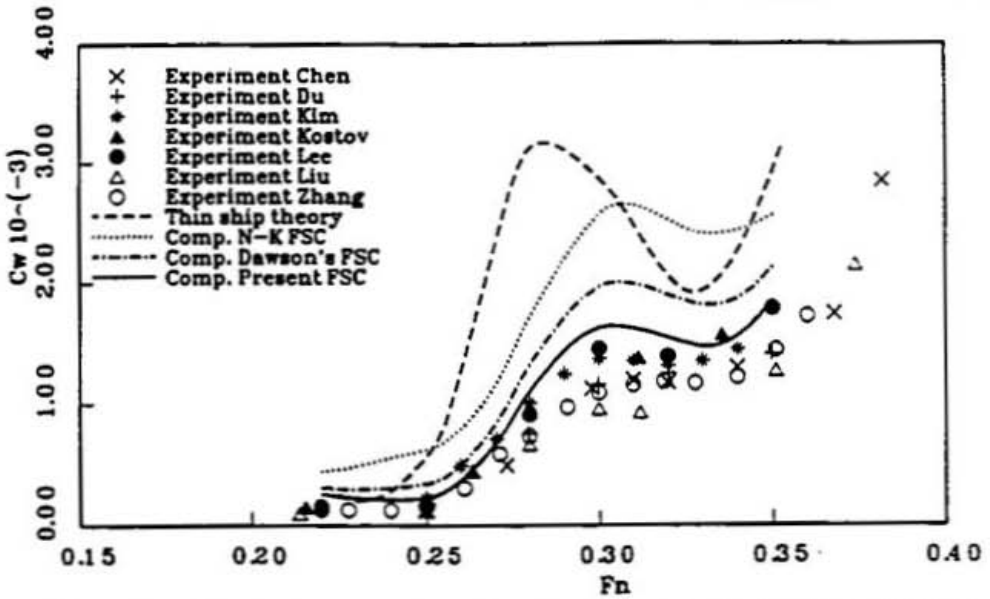

Fig. 5.33 Comparison of wave resistance coefficient C_w for Series 60 hull

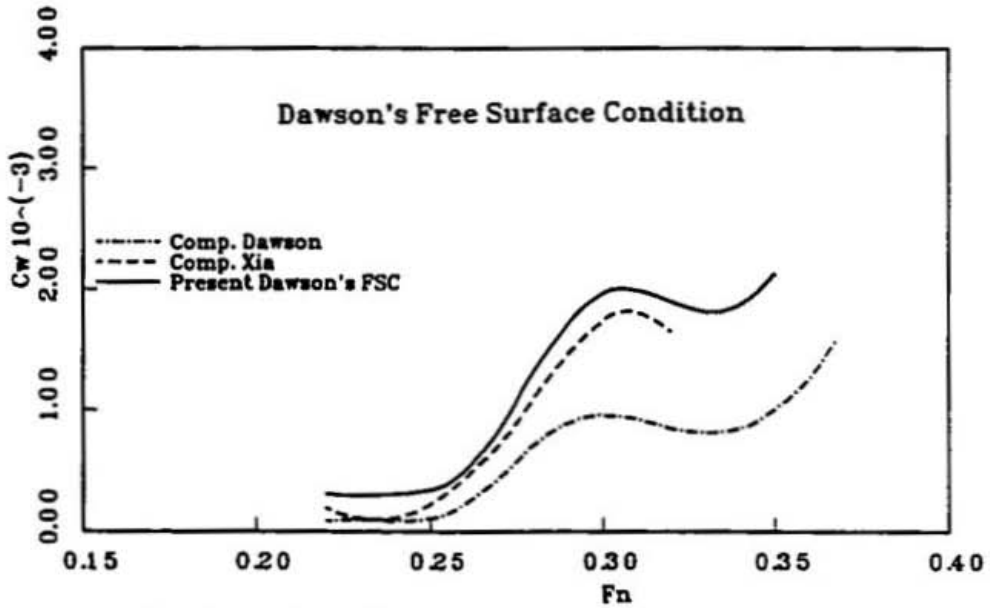

Fig. 5.34 Comparison of wave resistance coefficient C_w for Series 60 hull

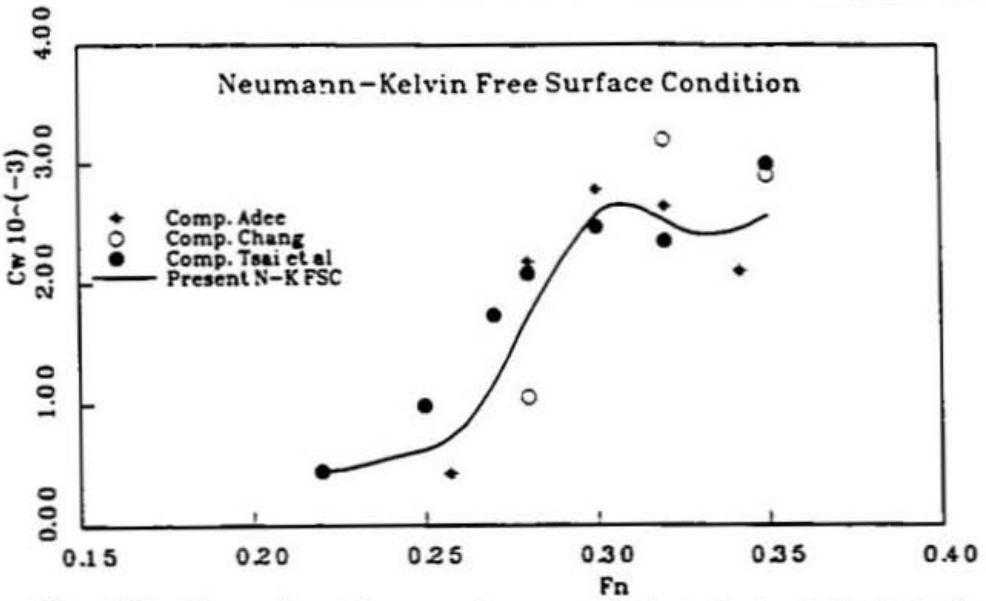

Fig. 5.35 Comparison of wave resistance coefficient C_w for Series 60 hull

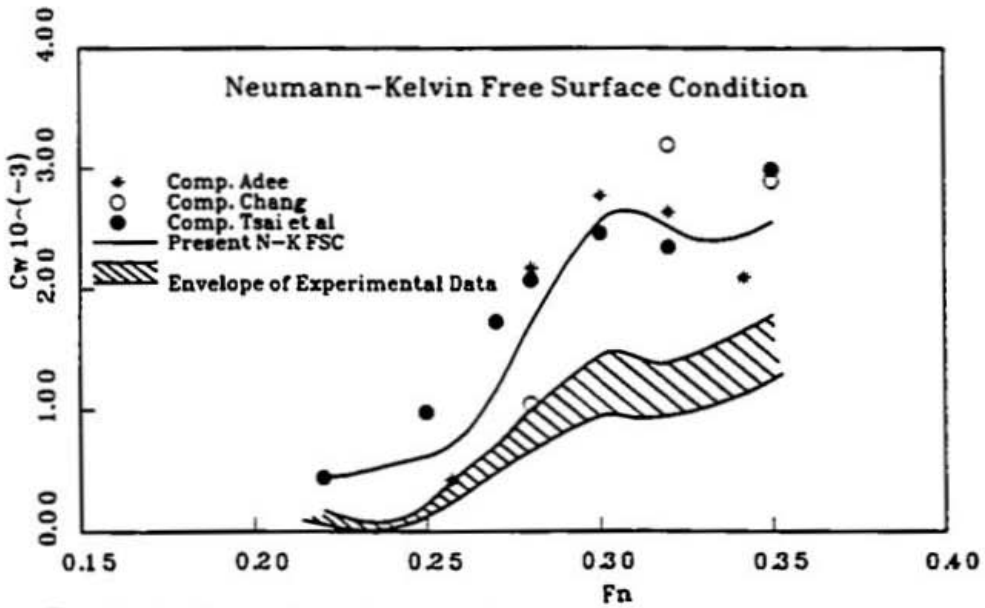

Fig. 5.36 Comparison of wave resistance coefficient C_w for Series 60 hull

6 ITERATIVE METHOD FOR SOLVING THE NONLINEAR PROBLEM

6.1 A Nonlinear Numerical Towing Tank

In the previous chapter the algorithm and applications of a linear numerical towing tank have been discussed. Although the present linear model gives better predictions in wave resistance and wave elevation in comparison with the linear models found in the literature, the nonlinearity of ship waves still can not be simulated by the linear model. The computed bow waves are still lower and the wave resistance is still slightly higher in comparison with the corresponding experimental data. It is the purpose of this chapter to develop an algorithm of a nonlinear numerical towing tank based on the nonlinear ship wave problem given by system of equations (3.7) obtained by transforming the free surface condition of the exact ship wave problem from being satisfied at the actual free surface to the undisturbed fluid free surface. As has been discussed in Section (5.2), to simulate a towing tank the boundary condition at infinity in boundary value problem (3.7) has to be replaced by the boundary conditions on the side walls and on the bottom of the tank. The nonlinear towing tank boundary value problem is, therefore, written as:

$$
\begin{cases}
\nabla^2\phi = 0, & \text{in the fluid domain;} \\
\phi = 0, & \text{on boundary \# 1;} \\
\vec{n}\cdot\nabla\phi = 0, & \text{on boundary \# 2;} \\
\vec{n}\cdot\nabla\phi = -U, & \text{on boundary \# 3;} \\
\vec{n}\cdot\nabla\phi = 0, & \text{on boundary \# 4;} \\
\{(\frac{\partial\phi}{\partial t})^2\frac{\partial^2\phi}{\partial t^2} + 2\frac{\partial\phi}{\partial t}\frac{\partial\phi}{\partial x}\frac{\partial^2\phi}{\partial t\partial x} - \\
(\frac{\partial\phi}{\partial x})^2\frac{\partial^2\phi}{\partial t^2} + g\frac{\partial\phi}{\partial x}\} & \\
\{g + \frac{\partial\phi}{\partial t}\frac{\partial^2\phi}{\partial t\partial x} - \frac{\partial\phi}{\partial x}\frac{\partial^2\phi}{\partial t^2}\} - & \\
\frac{1}{2}\{(\frac{\partial\phi}{\partial t})^2\frac{\partial^3\phi}{\partial t^2\partial x} + 2\frac{\partial\phi}{\partial x}(\frac{\partial^2\phi}{\partial t\partial x})^2 - \\
2\frac{\partial\phi}{\partial t}\frac{\partial\phi}{\partial x}\frac{\partial^2\phi}{\partial t^2} + 2\frac{\partial\phi}{\partial x}(\frac{\partial^2\phi}{\partial t^2})^2 - \\
(\frac{\partial\phi}{\partial x})^2\frac{\partial^3\phi}{\partial t^2\partial x} - g\frac{\partial^2\phi}{\partial t^2}\} & \\
\{(\frac{\partial\phi}{\partial t})^2 + (\frac{\partial\phi}{\partial x})^2 - U^2\} = 0, & \text{on boundary \# 5;} \\
\textit{The radiation condition.} &
\end{cases}
\tag{6.1}
$$

In the above boundary value problem ϕ, as usual, represents the total velocity potential of fluid motion, U represents the speed of the ship, $\vec{n}$ denotes the unit normal to the boundaries directed out of the fluid, and the coordinate system and the numbering system for the boundaries of the tank are the same as explained in Section (5.2.2).

The fundamental idea of the iterative method for solving the above nonlinear boundary value problem, and the linearized free surface condition to be solved at each iteration have been discussed and derived in Section (3.2). In this chapter the iterative mechanism and the algorithm are detailed together with applications. Both the direct and the indirect boundary integral methods discussed in Chapter 5 can be used to solve the linearized boundary value problem which needs to be solved in each iteration. However only the direct boundary integral algorithm developed in Section (5.2) is applied in the present study to develop a nonlinear towing tank which will be used to model surface ship towing tank experiments.

Replacing the boundary condition at infinity in boundary value problem (3.21) by the conditions on the boundaries of the tank, the linear towing tank boundary

value problem which needs to be solved in the iterations is written as:

$$\begin{cases} \nabla^2\phi = 0, & \textit{in the fluid domain;} \\ \phi = 0, & \textit{on boundary \# 1;} \\ \vec{n}\cdot\nabla\phi = 0, & \textit{on boundary \# 2;} \\ \vec{n}\cdot\nabla\phi = -U, & \textit{on boundary \# 3;} \\ \vec{n}\cdot\nabla\phi = 0, & \textit{on boundary \# 4;} \\ A\frac{\partial^2\phi}{\partial t^2} + B\frac{\partial\phi}{\partial t} + C\frac{\partial\phi}{\partial x} = R, & \textit{on boundary \# 5;} \\ \textit{The radiation condition.} \end{cases} \tag{6.2}$$

The coefficients A, B, C, and the right hand side R in the free surface condition are given again as:

$$\begin{aligned} A &= 3g[(\frac{\partial\Phi}{\partial\ell})^2 - (\frac{\partial\Phi}{\partial z})^2] - gU^2 \\ &\quad +2(\frac{\partial\Phi}{\partial\ell})^3\frac{\partial^2\Phi}{\partial\ell\partial z} - 8(\frac{\partial\Phi}{\partial\ell})^2\frac{\partial\Phi}{\partial z}\frac{\partial^2\Phi}{\partial\ell^2} \\ &\quad -6\frac{\partial\Phi}{\partial\ell}(\frac{\partial\Phi}{\partial z})^2\frac{\partial^2\Phi}{\partial\ell\partial z} + 4\frac{\partial\Phi}{\partial z}\frac{\partial^2\Phi}{\partial\ell^2}U^2; \end{aligned} \tag{6.3}$$

$$\begin{aligned} B &= 2[3g\frac{\partial\Phi}{\partial\ell}\frac{\partial^2\Phi}{\partial\ell^2} + 3g\frac{\partial\Phi}{\partial z}\frac{\partial^2\Phi}{\partial\ell\partial z} \\ &\quad -2(\frac{\partial\Phi}{\partial\ell})^3\frac{\partial^3\Phi}{\partial\ell^2\partial z} + 3(\frac{\partial\Phi}{\partial\ell})^2\frac{\partial\Phi}{\partial z}\frac{\partial^3\Phi}{\partial\ell^3} \\ &\quad +3(\frac{\partial\Phi}{\partial\ell})^2\frac{\partial^2\Phi}{\partial\ell^2}\frac{\partial^2\Phi}{\partial\ell\partial z} - 4\frac{\partial\Phi}{\partial\ell}\frac{\partial\Phi}{\partial z}(\frac{\partial^2\Phi}{\partial\ell^2})^2 \\ &\quad +2\frac{\partial\Phi}{\partial\ell}\frac{\partial\Phi}{\partial z}(\frac{\partial^2\Phi}{\partial\ell\partial z})^2 + \frac{\partial\Phi}{\partial\ell}\frac{\partial^3\Phi}{\partial\ell^2\partial z}U^2 \\ &\quad +(\frac{\partial\Phi}{\partial z})^3\frac{\partial^3\Phi}{\partial\ell^3} - 3(\frac{\partial\Phi}{\partial z})^2\frac{\partial^2\Phi}{\partial\ell^2}\frac{\partial^2\Phi}{\partial\ell\partial z} - \frac{\partial\Phi}{\partial z}\frac{\partial^3\Phi}{\partial\ell^3}U^2]; \end{aligned} \tag{6.4}$$

$$\begin{aligned} C &= 2[g^2 + (\frac{\partial\Phi}{\partial\ell})^3\frac{\partial^3\Phi}{\partial\ell^3} - \frac{\partial\Phi}{\partial\ell}\frac{\partial^3\Phi}{\partial\ell^3}U^2 \\ &\quad +(\frac{\partial^2\Phi}{\partial\ell^2})^2U^2 - 2(\frac{\partial\Phi}{\partial\ell})^2(\frac{\partial^2\Phi}{\partial\ell^2})^2 \\ &\quad +(\frac{\partial\Phi}{\partial\ell})^2(\frac{\partial^2\Phi}{\partial\ell\partial z})^2 + 3g\frac{\partial\Phi}{\partial\ell}\frac{\partial^2\Phi}{\partial\ell\partial z} \end{aligned}$$

$$
\begin{aligned}
&-3g\frac{\partial\Phi}{\partial z}\frac{\partial^2\Phi}{\partial\ell^2}+3\frac{\partial\Phi}{\partial\ell}(\frac{\partial\Phi}{\partial z})^2\frac{\partial^3\Phi}{\partial\ell^3}\\
&-6\frac{\partial\Phi}{\partial\ell}\frac{\partial\Phi}{\partial z}\frac{\partial^2\Phi}{\partial\ell^2}\frac{\partial^2\Phi}{\partial\ell\partial z}+2(\frac{\partial\Phi}{\partial z})^3\frac{\partial^3\Phi}{\partial\ell^2\partial z}\\
&-3\frac{\partial\Phi}{\partial z}^2(\frac{\partial^2\Phi}{\partial\ell\partial z})^2-\frac{\partial\Phi}{\partial z}\frac{\partial^3\Phi}{\partial\ell^2\partial z}U^2+(\frac{\partial^2\Phi}{\partial\ell\partial z})^2U^2];
\end{aligned}
\tag{6.5}
$$

$$
\begin{aligned}
R \;=\; & 6g(\frac{\partial\Phi}{\partial\ell})^2\frac{\partial^2\Phi}{\partial\ell^2}+6g\frac{\partial\Phi}{\partial\ell}\frac{\partial\Phi}{\partial z}\frac{\partial^2\Phi}{\partial\ell\partial z}\\
&-6g(\frac{\partial\Phi}{\partial z})^2\frac{\partial^2\Phi}{\partial\ell^2}-3(\frac{\partial\Phi}{\partial\ell})^4\frac{\partial^3\Phi}{\partial\ell^2\partial z}\\
&+6(\frac{\partial\Phi}{\partial\ell})^3\frac{\partial\Phi}{\partial z}\frac{\partial^3\Phi}{\partial\ell^3}+6(\frac{\partial\Phi}{\partial\ell})^3\frac{\partial^2\Phi}{\partial\ell\partial z}\frac{\partial^2\Phi}{\partial\ell^2}\\
&+4(\frac{\partial\Phi}{\partial\ell})^2\frac{\partial\Phi}{\partial z}(\frac{\partial^2\Phi}{\partial\ell\partial z})^2-16(\frac{\partial\Phi}{\partial\ell})^2\frac{\partial\Phi}{\partial z}(\frac{\partial^2\Phi}{\partial\ell^2})^2\\
&+(\frac{\partial\Phi}{\partial\ell})^2U^2\frac{\partial^3\Phi}{\partial\ell^2\partial z}+6\frac{\partial\Phi}{\partial\ell}(\frac{\partial\Phi}{\partial z})^3\frac{\partial^3\Phi}{\partial\ell^3}\\
&-18\frac{\partial\Phi}{\partial\ell}(\frac{\partial\Phi}{\partial z})^2\frac{\partial^2\Phi}{\partial\ell\partial z}\frac{\partial^2\Phi}{\partial\ell^2}-2\frac{\partial\Phi}{\partial\ell}\frac{\partial\Phi}{\partial z}U^2\frac{\partial^3\Phi}{\partial\ell^3}\\
&+3(\frac{\partial\Phi}{\partial z})^4\frac{\partial^3\Phi}{\partial\ell^2\partial z}-4(\frac{\partial\Phi}{\partial z})^3(\frac{\partial^2\Phi}{\partial\ell\partial z})^2\\
&-(\frac{\partial\Phi}{\partial z})^2U^2\frac{\partial^3\Phi}{\partial\ell^2\partial z}+4\frac{\partial\Phi}{\partial z}U^2(\frac{\partial^2\Phi}{\partial\ell^2})^2.
\end{aligned}
\tag{6.6}
$$

Comparing the above linear boundary value problem with the linear boundary value problem (5.99) solved in Section (5.2) it can be seen that the differences between them are in the expressions of the coefficients A, B, C, and the right hand side R. Therefore the algorithm of the linear towing tank developed in Section (5.2) can directly be used in each iteration to solve the linear boundary value problem (6.2). The changes needed in the iterations are the computations of A, B, C and R. In the linear towing tank algorithm these coefficients were computed by using equations (5.100), (5.101), (5.102) respectively, and the right hand side (H was used to represents the right side in the linear towing tank

problem) was computed by (5.103). In the iteration discussed in the present section the coefficients A, B, C, and the right hand side R are calculated by using equations (6.3), (6.4), (6.5) and (6.6) respectively.

In each iteration the same boundary value problem is solved with A, B, C, and R upgraded by using the results of the previous iteration. The procedure can be explained as follows:

Step 1:

In the first iteration (step 1), the total velocity potential ϕ is set to be

$$\phi = \phi_1 = \phi_0 + \phi_1', \tag{6.7}$$

where ϕ_1 represents the total velocity potential to be solved in the present step, ϕ_0 is the initial value which can be chosen arbitrarily, and ϕ_1' denotes the potential increment of the present iteration.

Then the boundary value problem to be solved in this step is written as:

$$\begin{cases} \nabla^2\phi_1 = 0, & \textit{in the fluid domain;} \\ \phi_1 = 0, & \textit{on boundary \# 1;} \\ \vec{n}\cdot\nabla\phi_1 = 0, & \textit{on boundary \# 2;} \\ \vec{n}\cdot\nabla\phi_1 = -U, & \textit{on boundary \# 3;} \\ \vec{n}\cdot\nabla\phi_1 = 0, & \textit{on boundary \# 4;} \\ A\frac{\partial^2\phi_1}{\partial\ell^2} + B\frac{\partial\phi_1}{\partial\ell} + C\frac{\partial\phi_1}{\partial z} = R, & \textit{on boundary \# 5;} \\ \textit{The radiation condition.} \end{cases} \tag{6.8}$$

The coefficients A, B, C, and the right hand side R are computed by replacing Φ by ϕ_0 in equations (6.3), (6.4), (6.5), and (6.6), which gives:

$$\begin{aligned} A \;=\; & 3g[(\frac{\partial\phi_0}{\partial\ell})^2 - (\frac{\partial\phi_0}{\partial z})^2] - gU^2 \\ & +2(\frac{\partial\phi_0}{\partial\ell})^3\frac{\partial^2\phi_0}{\partial\ell\partial z} - 8(\frac{\partial\phi_0}{\partial\ell})^2\frac{\partial\phi_0}{\partial z}\frac{\partial^2\phi_0}{\partial\ell^2} \\ & -6\frac{\partial\phi_0}{\partial\ell}(\frac{\partial\phi_0}{\partial z})^2\frac{\partial^2\phi_0}{\partial\ell\partial z} + 4\frac{\partial\phi_0}{\partial z}\frac{\partial^2\phi_0}{\partial\ell^2}U^2; \end{aligned} \tag{6.9}$$

$$
\begin{aligned}
B &= 2[3g(\frac{\partial\phi_0}{\partial\ell})\frac{\partial^2\phi_0}{\partial\ell^2} + 3g\frac{\partial\phi_0}{\partial z}\frac{\partial^2\phi_0}{\partial\ell\partial z} \\
&\quad -2(\frac{\partial\phi_0}{\partial\ell})^3\frac{\partial^3\phi_0}{\partial\ell^2\partial z} + 3(\frac{\partial\phi_0}{\partial\ell})^2\frac{\partial\phi_0}{\partial z}\frac{\partial^3\phi_0}{\partial\ell^3} \\
&\quad +3(\frac{\partial\phi_0}{\partial\ell})^2\frac{\partial^2\phi_0}{\partial\ell^2}\frac{\partial^2\phi_0}{\partial\ell\partial z} - 4\frac{\partial\phi_0}{\partial\ell}\frac{\partial\phi_0}{\partial z}(\frac{\partial^2\phi_0}{\partial\ell^2})^2 \\
&\quad +2\frac{\partial\phi_0}{\partial\ell}\frac{\partial\phi_0}{\partial z}(\frac{\partial^2\phi_0}{\partial\ell\partial z})^2 + \frac{\partial\phi_0}{\partial\ell}\frac{\partial^3\phi_0}{\partial\ell^2\partial z}U^2 \\
&\quad +(\frac{\partial\phi_0}{\partial z})^3\frac{\partial^3\phi_0}{\partial\ell^3} - 3(\frac{\partial\phi_0}{\partial z})^2\frac{\partial^2\phi_0}{\partial\ell^2}\frac{\partial^2\phi_0}{\partial\ell\partial z} - \frac{\partial\phi_0}{\partial z}\frac{\partial^3\phi_0}{\partial\ell^3}U^2]; \qquad (6.10)
\end{aligned}
$$

$$
\begin{aligned}
C &= 2[g^2 + (\frac{\partial\phi_0}{\partial\ell})^3\frac{\partial^3\phi_0}{\partial\ell^3} - \frac{\partial\phi_0}{\partial\ell}\frac{\partial^3\phi_0}{\partial\ell^3}U^2 \\
&\quad +(\frac{\partial^2\phi_0}{\partial\ell^2})^2U^2 - 2(\frac{\partial\phi_0}{\partial\ell})^2(\frac{\partial^2\phi_0}{\partial\ell^2})^2 \\
&\quad +(\frac{\partial\phi_0}{\partial\ell})^2(\frac{\partial^2\phi_0}{\partial\ell\partial z})^2 + 3g\frac{\partial\phi_0}{\partial\ell}\frac{\partial^2\phi_0}{\partial\ell\partial z} \\
&\quad -3g\frac{\partial\phi_0}{\partial z}\frac{\partial^2\phi_0}{\partial\ell^2} + 3\frac{\partial\phi_0}{\partial\ell}(\frac{\partial\phi_0}{\partial z})^2\frac{\partial^3\phi_0}{\partial\ell^3} \\
&\quad -6\frac{\partial\phi_0}{\partial\ell}\frac{\partial\phi_0}{\partial z}\frac{\partial^2\phi_0}{\partial\ell^2}\frac{\partial^2\phi_0}{\partial\ell\partial z} + 2(\frac{\partial\phi_0}{\partial z})^3\frac{\partial^3\phi_0}{\partial\ell^2\partial z} \\
&\quad -3(\frac{\partial\phi_0}{\partial z})^2(\frac{\partial^2\phi_0}{\partial\ell\partial z})^2 - \frac{\partial\phi_0}{\partial z}\frac{\partial^3\phi_0}{\partial\ell^2\partial z}U^2 + (\frac{\partial^2\phi_0}{\partial\ell\partial z})^2U^2]; \qquad (6.11)
\end{aligned}
$$

$$
\begin{aligned}
R &= 6g(\frac{\partial\phi_0}{\partial\ell})^2\frac{\partial^2\phi_0}{\partial\ell^2} + 6g\frac{\partial\phi_0}{\partial\ell}\frac{\partial\phi_0}{\partial z}\frac{\partial^2\phi_0}{\partial\ell\partial z} \\
&\quad -6g(\frac{\partial\phi_0}{\partial z})^2\frac{\partial^2\phi_0}{\partial\ell^2} - 3(\frac{\partial\phi_0}{\partial\ell})^4\frac{\partial^3\phi_0}{\partial\ell^2\partial z} \\
&\quad +6(\frac{\partial\phi_0}{\partial\ell})^3\frac{\partial\phi_0}{\partial z}\frac{\partial^3\phi_0}{\partial\ell^3} + 6(\frac{\partial\phi_0}{\partial\ell})^3\frac{\partial^2\phi_0}{\partial\ell\partial z}\frac{\partial^2\phi_0}{\partial\ell^2} \\
&\quad +4(\frac{\partial\phi_0}{\partial\ell})^2\frac{\partial\phi_0}{\partial z}(\frac{\partial^2\phi_0}{\partial\ell\partial z})^2 - 16(\frac{\partial\phi_0}{\partial\ell})^2\frac{\partial\phi_0}{\partial z}(\frac{\partial^2\phi_0}{\partial\ell^2})^2 \\
&\quad +(\frac{\partial\phi_0}{\partial\ell})^2U^2\frac{\partial^3\phi_0}{\partial\ell^2\partial z} + 6\frac{\partial\phi_0}{\partial\ell}(\frac{\partial\phi_0}{\partial z})^3\frac{\partial^3\phi_0}{\partial\ell^3} \\
&\quad -18\frac{\partial\phi_0}{\partial\ell}(\frac{\partial\phi_0}{\partial z})^2\frac{\partial^2\phi_0}{\partial\ell\partial z}\frac{\partial^2\phi_0}{\partial\ell^2} - 2\frac{\partial\phi_0}{\partial\ell}\frac{\partial\phi_0}{\partial z}U^2\frac{\partial^3\phi_0}{\partial\ell^3}
\end{aligned}
$$

$$+3(\frac{\partial\phi_0}{\partial z})^4\frac{\partial^3\phi_0}{\partial\ell^2\partial z} - 4(\frac{\partial\phi_0}{\partial z})^3(\frac{\partial^2\phi_0}{\partial\ell\partial z})^2$$
$$-(\frac{\partial\phi_0}{\partial z})^2U^2\frac{\partial^3\phi_0}{\partial\ell^2\partial z} + 4\frac{\partial\phi_0}{\partial z}U^2(\frac{\partial^2\phi_0}{\partial\ell^2})^2. \tag{6.12}$$

Having calculated the coefficients A, B, C, and the right hand side R, the boundary value problem can then be solved by applying the direct boundary integral algorithm (the linear towing tank) developed in Section (5.2). It is noted that in this process the total velocity potential ϕ is directly solved for instead of the potential increment ϕ_1', which makes the iteration and the computation simpler and easier.

Step 2:

In the second iteration (step 2), the total velocity potential is set to be

$$\phi = \phi_2 = \phi_1 + \phi_2', \tag{6.13}$$

where ϕ_2 is the total velocity potential to be solved in the present step, ϕ_1 is the velocity potential obtained in the previous step, (step 1), and ϕ_2' is the increment to the velocity potential in the present iteration.

Then the linear boundary value problem to be solved in this step is written as:

$$\begin{cases} \nabla^2\phi_2 = 0, & \textit{in the fluid domain;} \\ \phi_2 = 0, & \textit{on boundary \# 1;} \\ \vec{n}\cdot\nabla\phi_2 = 0, & \textit{on boundary \# 2;} \\ \vec{n}\cdot\nabla\phi_2 = -U, & \textit{on boundary \# 3;} \\ \vec{n}\cdot\nabla\phi_2 = 0, & \textit{on boundary \# 4;} \\ A\frac{\partial^2\phi_2}{\partial t^2} + B\frac{\partial\phi_2}{\partial t} + C\frac{\partial\phi_2}{\partial x} = R, & \textit{on boundary \# 5;} \\ \textit{The radiation condition.} \end{cases} \tag{6.14}$$

The coefficients A, B, C, and the right hand side R in the free surface (boundary #5) condition are defined by the following equations:

$$
\begin{aligned}
A &= 3g[(\frac{\partial\phi_1}{\partial\ell})^2-(\frac{\partial\phi_1}{\partial z})^2]-gU^2\\
&+2(\frac{\partial\phi_1}{\partial\ell})^3\frac{\partial^2\phi_1}{\partial\ell\partial z}-8(\frac{\partial\phi_1}{\partial\ell})^2\frac{\partial\phi_1}{\partial z}\frac{\partial^2\phi_1}{\partial\ell^2}\\
&-6\frac{\partial\phi_1}{\partial\ell}(\frac{\partial\phi_1}{\partial z})^2\frac{\partial^2\phi_1}{\partial\ell\partial z}+4\frac{\partial\phi_1}{\partial z}\frac{\partial^2\phi_1}{\partial\ell^2}U^2; \qquad (6.15)
\end{aligned}
$$

$$
\begin{aligned}
B &= 2[3g(\frac{\partial\phi_1}{\partial\ell})\frac{\partial^2\phi_1}{\partial\ell^2}+3g\frac{\partial\phi_1}{\partial z}\frac{\partial^2\phi_1}{\partial\ell\partial z}\\
&-2(\frac{\partial\phi_1}{\partial\ell})^3\frac{\partial^3\phi_1}{\partial\ell^2\partial z}+3(\frac{\partial\phi_1}{\partial\ell})^2\frac{\partial\phi_1}{\partial z}\frac{\partial^3\phi_1}{\partial\ell^3}\\
&+3(\frac{\partial\phi_1}{\partial\ell})^2\frac{\partial^2\phi_1}{\partial\ell^2}\frac{\partial^2\phi_1}{\partial\ell\partial z}-4\frac{\partial\phi_1}{\partial\ell}\frac{\partial\phi_1}{\partial z}(\frac{\partial^2\phi_1}{\partial\ell^2})^2\\
&+2\frac{\partial\phi_1}{\partial\ell}\frac{\partial\phi_1}{\partial z}(\frac{\partial^2\phi_1}{\partial\ell\partial z})^2+\frac{\partial\phi_1}{\partial\ell}\frac{\partial^3\phi_1}{\partial\ell^2\partial z}U^2\\
&+(\frac{\partial\phi_1}{\partial z})^3\frac{\partial^3\phi_1}{\partial\ell^3}-3(\frac{\partial\phi_1}{\partial z})^2\frac{\partial^2\phi_1}{\partial\ell^2}\frac{\partial^2\phi_1}{\partial\ell\partial z}-\frac{\partial\phi_1}{\partial z}\frac{\partial^3\phi_1}{\partial\ell^3}U^2]; \qquad (6.16)
\end{aligned}
$$

$$
\begin{aligned}
C &= 2[g^2+(\frac{\partial\phi_1}{\partial\ell})^3\frac{\partial^3\phi_1}{\partial\ell^3}-\frac{\partial\phi_1}{\partial\ell}\frac{\partial^3\phi_1}{\partial\ell^3}U^2\\
&+(\frac{\partial^2\phi_1}{\partial\ell^2})^2U^2-2(\frac{\partial\phi_1}{\partial\ell})^2(\frac{\partial^2\phi_1}{\partial\ell^2})^2\\
&+(\frac{\partial\phi_1}{\partial\ell})^2(\frac{\partial^2\phi_1}{\partial\ell\partial z})^2+3g\frac{\partial\phi_1}{\partial\ell}\frac{\partial^2\phi_1}{\partial\ell\partial z}\\
&-3g\frac{\partial\phi_1}{\partial z}\frac{\partial^2\phi_1}{\partial\ell^2}+3\frac{\partial\phi_1}{\partial\ell}(\frac{\partial\phi_1}{\partial z})^2\frac{\partial^3\phi_1}{\partial\ell^3}\\
&-6\frac{\partial\phi_1}{\partial\ell}\frac{\partial\phi_1}{\partial z}\frac{\partial^2\phi_1}{\partial\ell^2}\frac{\partial^2\phi_1}{\partial\ell\partial z}+2(\frac{\partial\phi_1}{\partial z})^3\frac{\partial^3\phi_1}{\partial\ell^2\partial z}\\
&-3(\frac{\partial\phi_1}{\partial z})^2(\frac{\partial^2\phi_1}{\partial\ell\partial z})^2-\frac{\partial\phi_1}{\partial z}\frac{\partial^3\phi_1}{\partial\ell^2\partial z}U^2+(\frac{\partial^2\phi_1}{\partial\ell\partial z})^2U^2]; \qquad (6.17)
\end{aligned}
$$

$$
\begin{aligned}
R &= 6g(\frac{\partial\phi_1}{\partial\ell})^2\frac{\partial^2\phi_1}{\partial\ell^2}+6g\frac{\partial\phi_1}{\partial\ell}\frac{\partial\phi_1}{\partial z}\frac{\partial^2\phi_1}{\partial\ell\partial z}\\
&-6g(\frac{\partial\phi_1}{\partial z})^2\frac{\partial^2\phi_1}{\partial\ell^2}-3(\frac{\partial\phi_1}{\partial\ell})^4\frac{\partial^3\phi_1}{\partial\ell^2\partial z}
\end{aligned}
$$

$$
\begin{aligned}
&+6(\frac{\partial\phi_1}{\partial\ell})^3\frac{\partial\phi_1}{\partial z}\frac{\partial^3\phi_1}{\partial\ell^3}+6(\frac{\partial\phi_1}{\partial\ell})^3\frac{\partial^2\phi_1}{\partial\ell\partial z}\frac{\partial^2\phi_1}{\partial\ell^2}\\
&+4(\frac{\partial\phi_1}{\partial\ell})^2\frac{\partial\phi_1}{\partial z}(\frac{\partial^2\phi_1}{\partial\ell\partial z})^2-16(\frac{\partial\phi_1}{\partial\ell})^2\frac{\partial\phi_1}{\partial z}(\frac{\partial^2\phi_1}{\partial\ell^2})^2\\
&+(\frac{\partial\phi_1}{\partial\ell})^2U^2\frac{\partial^3\phi_1}{\partial\ell^2\partial z}+6\frac{\partial\phi_1}{\partial\ell}(\frac{\partial\phi_1}{\partial z})^3\frac{\partial^3\phi_1}{\partial\ell^3}\\
&-18\frac{\partial\phi_1}{\partial\ell}(\frac{\partial\phi_1}{\partial z})^2\frac{\partial^2\phi_1}{\partial\ell\partial z}\frac{\partial^2\phi_1}{\partial\ell^2}-2\frac{\partial\phi_1}{\partial\ell}\frac{\partial\phi_1}{\partial z}U^2\frac{\partial^3\phi_1}{\partial\ell^3}\\
&+3(\frac{\partial\phi_1}{\partial z})^4\frac{\partial^3\phi_1}{\partial\ell^2\partial z}-4(\frac{\partial\phi_1}{\partial z})^3(\frac{\partial^2\phi_1}{\partial\ell\partial z})^2\\
&-(\frac{\partial\phi_1}{\partial z})^2U^2\frac{\partial^3\phi_1}{\partial\ell^2\partial z}+4\frac{\partial\phi_1}{\partial z}U^2(\frac{\partial^2\phi_1}{\partial\ell^2})^2. \qquad (6.18)
\end{aligned}
$$

Step 3:

In the third iteration (third step), the total velocity potential is set to be

$$\phi=\phi_3=\phi_2+\phi_3', \qquad (6.19)$$

where ϕ_3 is the total velocity potential to be solved in the present step, ϕ_2 is the velocity potential obtained in the previous step (it is the sum of first and second iterations), and ϕ_3' is the increment to the velocity potential in the present iteration.

Repeating the same procedure as explained in step 2 until the differences between the velocity potentials of two consecutive iterations becomes small enough, i.e

$$(\phi_i-\phi_{i+1})<\Delta\phi, \qquad (6.20)$$

where ϕ_i and ϕ_{i+1} denote the velocity potentials of ith and $(i+1)th$ iterations respectively, and $\Delta\phi$ is the error tolerance which is determined by the accuracy requirement of the computation.

Once equation (6.20) is satisfied, ϕ_{i+1} is the solution of the nonlinear boundary value problem (6.1).

6.2 A Discussion on the Convergence of the Method

There are two convergence problems that need to be discussed in the present iterative approach. They are the convergence of the iterations and the convergence of the Taylor's series expansion of the free surface condition. As has been discussed in Section (3.2), there is no theoretical foundation for the present iterative scheme to be convergent for any kind of nonlinear boundary value problems, but it has been proved that if the iteration is convergent, the converged solution will be the solution of the original nonlinear boundary value problem. Numerical experiments show that the present iterative scheme is stable and efficient in solving the nonlinear ship wave problem. All the computations in the present study have converged without any difficulty.

It is the major purpose of this section to discuss the convergence of the Taylor's series expansion of the free surface condition which has been presented in Section (3.1). As it is noted only the terms up to the first order in η in the Taylor' series are kept in the free surface condition of the nonlinear ship wave problem solved in the present study. Theoretically there is no limitation for the number of orders to be kept in the Taylor's series expansion of the free surface condition. However, practically it is very difficult to keep higher order terms, because of not only the complexity of the problem, but also because of the higher order derivatives in the Taylor's series which usually create difficulties in their numerical treatments. It is difficult directly to analyse the convergence speed of Taylor's series expansion of the free surface condition in the nonlinear ship wave problem. The nonlinear perturbation theory developed by Pawlowski (1992b) is, therefore, used here to discuss the convergence of the Taylor's series of the free surface condition.

As has been reviewed in Section (2.5), the one-to-one domain transformation theory developed by Pawlowski (1992a) considers not only the nonlinearity of the free surface condition but also the slope of the ship hull. Therefore not only the free surface condition is transformed but also the impermeability condition on the hull surface. However, if the theory is applied to the cases considered in the present study, i.e. the ship hull at the design load waterline is assumed to be wall-sided, the impermeability condition in Pawlowski's theory reduces to the same condition used in the present study. Therefore, the free surface in the computational domain obtained through the domain transformation can be directly used to compare with the present nonlinear free surface condition obtained through the Taylor's series expansion.

Through the domain transformation (Pawlowski 1992a), the nonlinear ship wave problem with an unknown free surface is transformed into the computational domain with a known flat surface. The nonlinear boundary value problem in the computational domain is solved by a nonlinear perturbation approach (Pawlowski 1992b). The details of the domain transformation theory and the nonlinear perturbation approach have presented in Section (2.5) of this thesis. Up to the first order nonlinear perturbation, the total velocity potential is the sum of zero order solution and the first order solution, which is given by equation (2.51).

Through the nonlinear perturbation procedure developed by Pawlowski (1992a, 1992b) not only a perturbed nonlinear solution of a ship wave problem can be obtained but also the convergence of the perturbation procedure can be determined. The purpose of the present section is to apply this theory to discuss the

convergence of the Taylor's series expansion of the free surface condition used in the present study.

By substituting equations (2.49) and (2.51) into the first order nonlinear free surface condition (2.48) and comparing with the nonlinear free surface condition in the nonlinear ship wave problem solved in the present study given by system of equations (6.1), it can be found that they are the same. This means that the present study solves the same problem as the nonlinear perturbation theory developed by Pawlowski(1992a, 1992b) up to the first order perturbation for the wall-sided ships. Therefore the convergence of Taylor's series of the free surface condition used in the present study can be determined through the nonlinear perturbation theory.

The convergence of the nonlinear perturbation can be approximately determined by studying the relation between $\Phi^{(0)}$ and $\Phi^{(1)}$. If $\Phi^{(0)}$ is the major contribution to the total velocity potential Φ and $\Phi^{(1)}$ represents only a small portion of Φ, then it can be concluded that the perturbation up to the first order is accurate enough for solving the problem, otherwise higher order terms have to be considered in the perturbation. For this purpose the relation between $\Phi^{(0)}$ and $\Phi^{(1)}$ can be expressed by the wave resistances to the ship produced by these two potentials which represent the overall effect, and by the velocity components along the waterline also produced by these two velocity potentials which represent the local effect.

The wave resistance coefficient C_w computed by the zero order solution $\Phi^{(0)}$ and the total velocity potential up to the first order $\Phi = \Phi^{(0)} + \Phi^{(1)}$ are plotted in Fig. 6.1. The C_w computed through solving Dawson's linear ship wave problem

and the experimental data are also plotted in this figure. It can be seen that the zero order C_w of the nonlinear perturbation theory predicts the major part of the wave resistance. It is higher than the experimental data, but it is still slightly better than the one predicted by Dawson's linear model. The total wave resistance coefficient predicted by including the contribution of the first order perturbation matches very well with the experimental data. The difference between the total wave resistance computed by $\Phi = \Phi^{(0)} + \Phi^{(1)}$ and zero order wave resistance computed by $\Phi^{(0)}$ is the contribution of $\Phi^{(1)}$. From this figure it can be seen that the contribution of $\Phi^{(1)}$ is much smaller than the contribution of $\Phi^{(0)}$.

In Fig. 6.2 the nondimensional vertical fluid velocity components $w^{(0)}/U$ and $w^{(1)}/U$ produced respectively by $\Phi^{(0)}$ and $\Phi^{(1)}$ along the waterline are plotted. In this figure the solid line represents the vertical velocity corresponding to $\Phi^{(0)}$ and the dashed line represents the vertical velocity corresponding to $\Phi^{(1)}$. From this figure it can be seen that the first order perturbation contributes only a small portion in terms of vertical fluid velocity.

In Fig. 6.3 and Fig. 6.4 the nondimensional horizontal fluid velocity components $u^{(0)}/U$ and $u^{(1)}/U$ produced respectively by $\Phi^{(0)}$ and $\Phi^{(1)}$ along the waterline are plotted for two Froude numbers. In these figures the solid lines represent the horizontal velocity component corresponding to $\Phi^{(0)}$ and the dashed lines represent the horizontal velocity component corresponding to $\Phi^{(1)}$. From these figures it can also be seen that the first order perturbation contributes only a small portion in terms of horizontal fluid velocity.

From the above analyses and the comparisons with the experimental results, a conclusion can be made that by considering up to the first order nonlinear per-

turbation in the nonlinear perturbation theory developed by Pawlowski (1992b), good computational results can be obtained and it is accurate enough for practical applications. Since the Taylor's series used in the present study is equivalent to considering up to the first order nonlinear perturbation, the present approach based on the free surface condition obtained by keeping the terms up to the first order in η in the Taylor's series expansion should be accurate enough in the applications.

6.3 Applications and Comparisons

The present nonlinear numerical towing tank based on the iterative method has been used to compute the wave elevation and the wave resistance for the Wigley hull and Series 60, block 0.6, ship hull which have been used in the applications of the linear numerical towing tank in Section (5.3.2). The same range of Froude numbers have been computed. All the considered cases converge without any difficulty. In these computations the initial values of ϕ are chosen to be the corresponding double-body potential $\bar{\Phi}$ on the undisturbed fluid free surface which makes the first iteration exactly the linear solution presented in Section (5.2). In Table 6.1. the wave resistance coefficients of Wigley hull for 6 iterations are listed. The differences between the linear and the nonlinear solutions are also listed in this table which show that the differences are relatively small for the Wigley hull. In Table 6.2 the results of 10 iterations for Series 60 ship hull are listed, which shows the difference are large for some Froude numbers.

From Table 6.1 and Table 6.2 it can be seen that the convergence of the iteration is stable and fast for both ship hulls and all of the Froude numbers. The

wave resistance coefficients versus Froude numbers for the Wigley hull and Series 60 ship hull listed in Table 6.1 and Table 6.2 are plotted in Fig. 6.5 and Fig. 6.6 respectively. In these figures the solid lines represent the nonlinear results and the dashed lines represent the linear results. Experimental data are also plotted in these two figures which are represented by different marks. Fig. 6.5 shows for Wigley hull the linear predictions are accurate enough since the hull is thin. However, for Series 60 ship hull the nonlinear results are improved in comparison with the linear ones which are shown in Fig. 6.6.

It should be mentioned that the wave resistance in the nonlinear algorithm is calculated by integrating the pressure over the ship surface under the actual fluid free surface, which is written as:

$$R_w = -\int_{WS} P N_x dS$$

where WS is the actual wetted ship surface.

In Fig. 6.7 to Fig. 6.12 the wave profiles along the waterline of Series 60 ship hull for Froude number 0.22, 0.25, 0.28, 0.30, 0.32, and 0.35 are presented. In these figures the solid lines represent the computational results of the present nonlinear model, the dashed lines represent the experimental data which have been used in the comparisons presented in Section (5.3.2) . From these figures it can be seen that the computed bow waves are closer to the experimental measurements than those linear predictions. Fig. 6.13 and Fig. 6.14 are the comparison of wave profiles between linear and nonlinear computations.

A comparison between the present iterative method and the nonlinear theory developed by Pawlowski (1992b) was also carried out in the present study. Fig. 6.15 shows the comparison of the wave resistance coefficients. In this figure

the solid line represents the present nonlinear results of C_w for Series 60 ship hull and the dashed line represents the nonlinear results obtained by applying Pawlowski's nonlinear theory. This comparison shows good agreement between the two nonlinear predictions. Small differences of order 4% are found in high Froude number cases.

In Fig. 6.17 and Fig. 6.18 the comparisons of wave profiles along the ship waterline are presented. Again the solid lines represent the wave profile obtained by the present nonlinear numerical towing tank and the dashed lines represent the wave profile predicted by Pawlowski's nonlinear theory (Pawlowski 1992b). Good agreements are found in these cases with Froude number $Fn = 0.25$, and $Fn = 0.35$. As it happens, for the wave resistance, small differences are found in high Froude number cases, which is also of order 4%.

In Fig. 6.16 a comparison of the present nonlinear computations with other nonlinear predictions found in the literature is presented. In this figure, the solid line represents the present nonlinear results, the dash-dotted line represents the nonlinear results obtained by Pawlowski's nonlinear perturbation theory, the dashed line represents the results by Y.H. Kim (1990) through the iterative panel method, the dash-two-dotted and dash-three-dotted lines represent the nonlinear results by K.J. Kim (1989), the short-long-dashed line represents the nonlinear results by Jensen (1989). The results obtained by Jensen, Y.H. Kim and K.J. Kim were based on the same iterative approach, but as it can be seen from this figure they are diverse. Jensen's predictions on the wave resistances are too high. They are even higher than the solutions based on Dawson's linear model. The two computations given by K.J. Kim do not follow the trend of the

experimental data. The results by Y.H. Kim match the experimental data. The present nonlinear predictions and the ones using Pawlowski's nonlinear theory are in good agreement and they agree with the experimental measurements very well.

One more remark should be mentioned. The panelization in the computation is one of the essential factors for the accuracy of the results. Numerical experiments have shown that a minimum of 16 panels per wave-length are required in applying the linear element algorithm in order to achieve reasonable accurate computations. In the present study about 20 panels per wave length are used in the computations. Also the panels on the free surface are arranged such that their dimensions in the transverse direction are smaller in the area closed to the ship.

Iteration number	Fn=0.230 Cw 10^{-3}	Fn=0.250 Cw 10^{-3}	Fn=0.267 Cw 10^{-3}	Fn=0.289 Cw 10^{-3}	Fn=0.300 Cw 10^{-3}
1 (linear)	0.651670	0.928677	0.902482	1.397664	1.675338
2	0.596459	0.884951	0.861314	1.353375	1.639415
3	0.594294	0.884493	0.861500	1.357514	1.645500
4	0.594056	0.884245	0.861351	1.356726	1.643971
5	0.594048	0.884243	0.861350	1.356801	1.644115
6(nonlinear)	0.594048	0.884242	0.861350	1.356808	1.644131
Diff.(%)	9.7	5.0	4.8	3.0	1.9

Iteration number	Fn=0.316 Cw 10^{-3}	Fn=0.330 Cw 10^{-3}	Fn=0.350 Cw 10^{-3}	Fn=0.400 Cw 10^{-3}
1 (linear)	1.809747	1.705472	1.522358	2.359163
2	1.760773	1.647841	1.469928	2.397774
3	1.762377	1.645854	1.467664	2.344974
4	1.760332	1.643083	1.461152	2.319648
5	1.760590	1.643293	1.460916	2.313525
6(nonlinear)	1.760593	1.643273	1.460969	2.314252
Diff.(%)	2.8	3.8	4.2	1.9

Table 6.1 Cw for Wigley hull of 6 iterations

Iteration number	Fn=0.22 Cw 10^{-3}	Fn=0.23 Cw 10^{-3}	Fn=0.24 Cw 10^{-3}	Fn=0.25 Cw 10^{-3}	Fn=0.26 Cw 10^{-3}	Fn=0.27 Cw 10^{-3}
1 (linear)	0.264291	0.226254	0.212484	0.232415	0.374085	0.692893
2	0.258048	0.214740	0.189040	0.185487	0.267175	0.480963
3	0.250831	0.206806	0.182218	0.182202	0.275875	0.528240
4	0.250375	0.205810	0.180369	0.179070	0.270882	0.521501
5	0.250268	0.205674	0.180190	0.178802	0.270494	0.520910
6	0.250261	0.205660	0.180166	0.178760	0.270422	0.521076
7	0.250259	0.205657	0.180163	0.178758	0.270422	0.521022
8	0.250259	0.205657	0.180162	0.178756	0.270421	0.521018
9	0.250259	0.205657	0.180162	0.178756	0.270421	0.521027
10(nonlinear)	0.250259	0.205657	0.180162	0.178756	0.270421	0.521024
Diff. (%)	5.6	10.0	19.9	30.0	38.4	1.4

Iteration number	Fn=0.28 Cw 10^{-3}	Fn=0.30 Cw 10^{-3}	Fn=0.31 Cw 10^{-3}	Fn=0.33 Cw 10^{-3}	Fn=0.34 Cw 10^{-3}	Fn=0.35 Cw 10^{-3}
1 (linear)	1.109442	1.626606	1.621662	1.471720	1.563397	1.857368
2	0.826920	1.555022	1.790382	1.781375	1.811362	2.016574
3	0.935733	1.543085	1.542183	1.334934	1.378793	1.577141
4	0.928234	1.551340	1.582203	1.465533	1.536093	1.775833
5	0.925373	1.557606	1.631392	1.527786	1.579928	1.800696
6	0.927293	1.555797	1.597957	1.452146	1.506726	1.719218
7	0.926721	1.554996	1.602484	1.476632	1.532691	1.746204
8	0.926707	1.555358	1.607080	1.485688	1.543801	1.776300
9	0.926788	1.555559	1.604875	1.474650	1.530684	1.744211
10(nonlinear)	0.926753	1.555346	1.604363	1.477077	1.533179	1.754451
Diff. (%)	19.7	4.6	1.1	-0.4	2.0	5.9

Table 6.2 Cw for Series 60 hull of 10 iterations

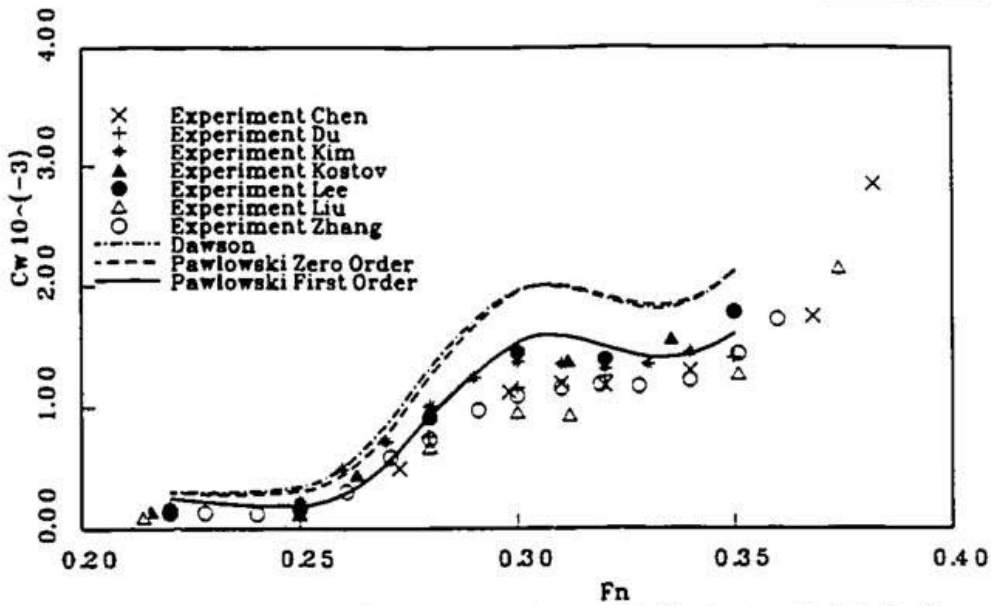

Fig. 6.1 Zero and first order nonlinear C_w for Series 60 ship hull

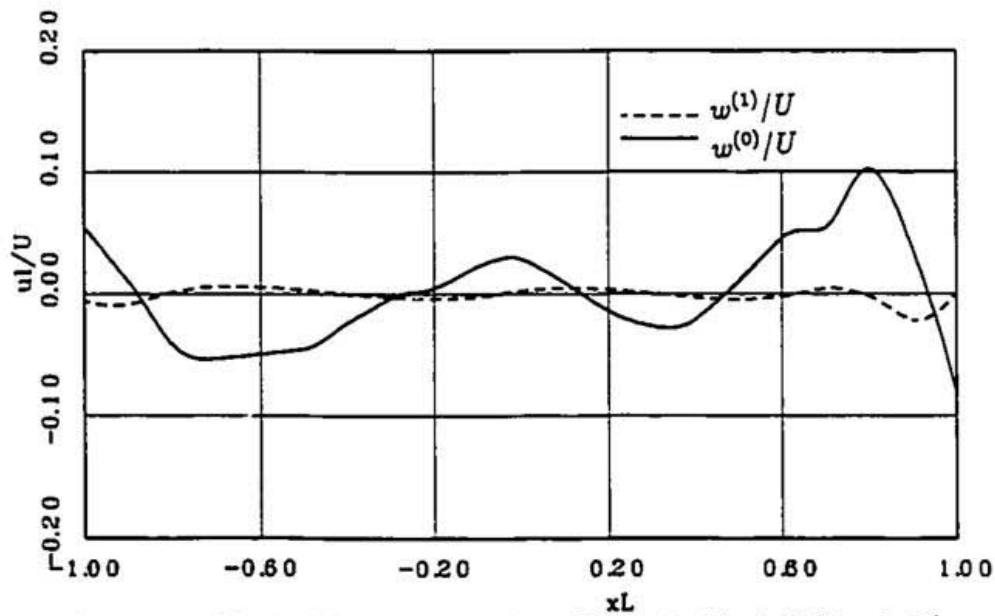

Fig. 6.2 Vertical fluid velocity along Series 60 ship hull (Fn=0.25)

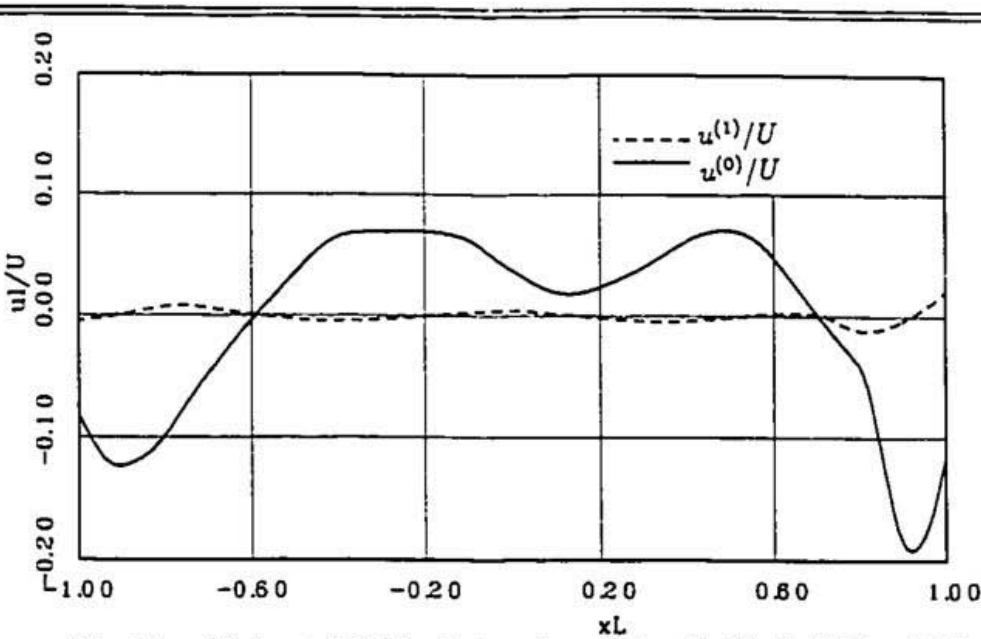

Fig. 6.3 Horizontal fluid velocity along Series 60 ship hull (Fn=0.25)

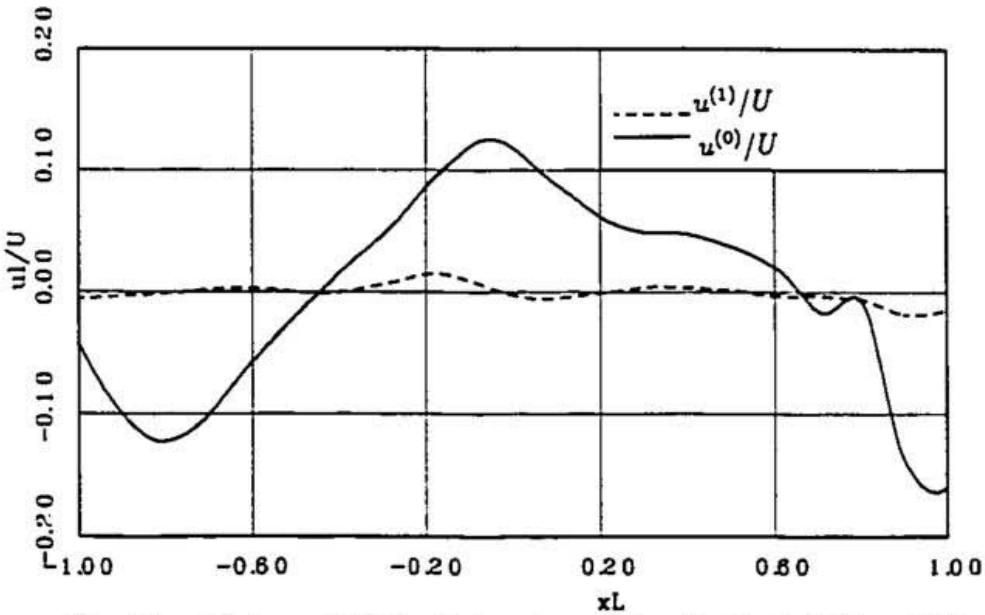

Fig. 6.4 Horizontal fluid velocity along Series 60 ship hull (Fn=0.35)

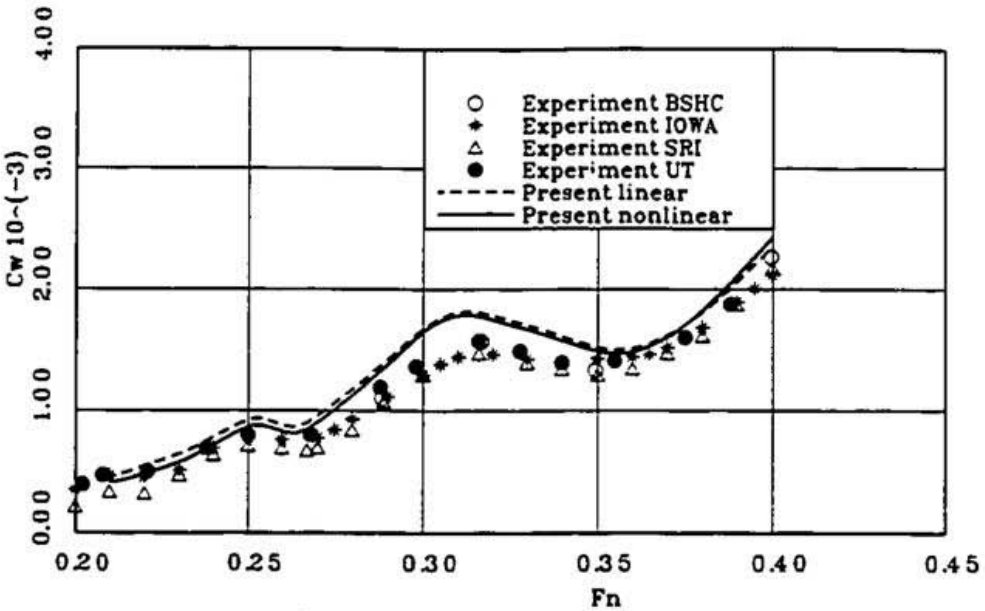

Fig. 6.5 Comparison of nonlinear C_w for Wigley 60 hull

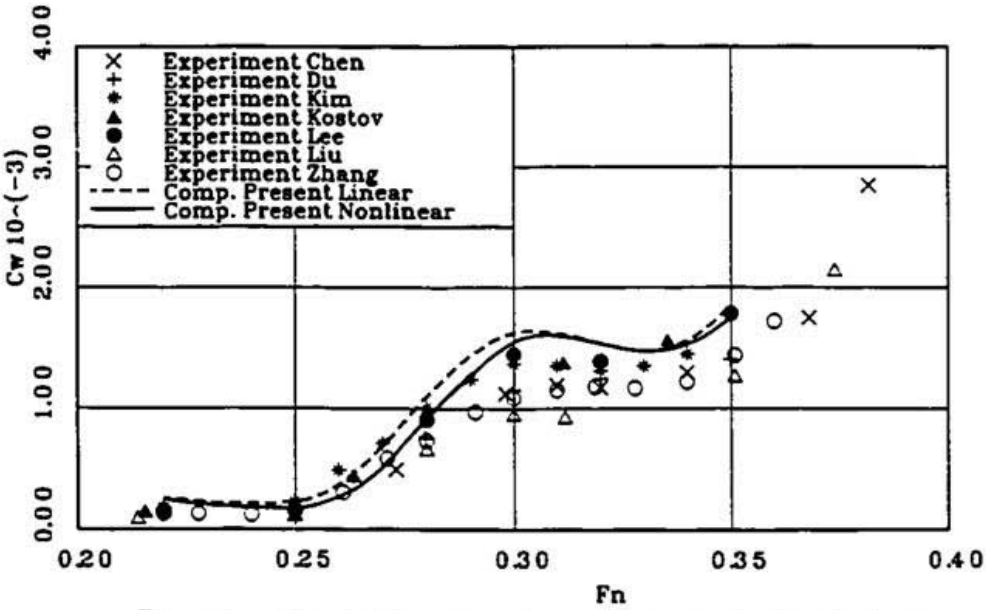

Fig. 6.6 Comparison of nonlinear C_w for Series 60 ship hull

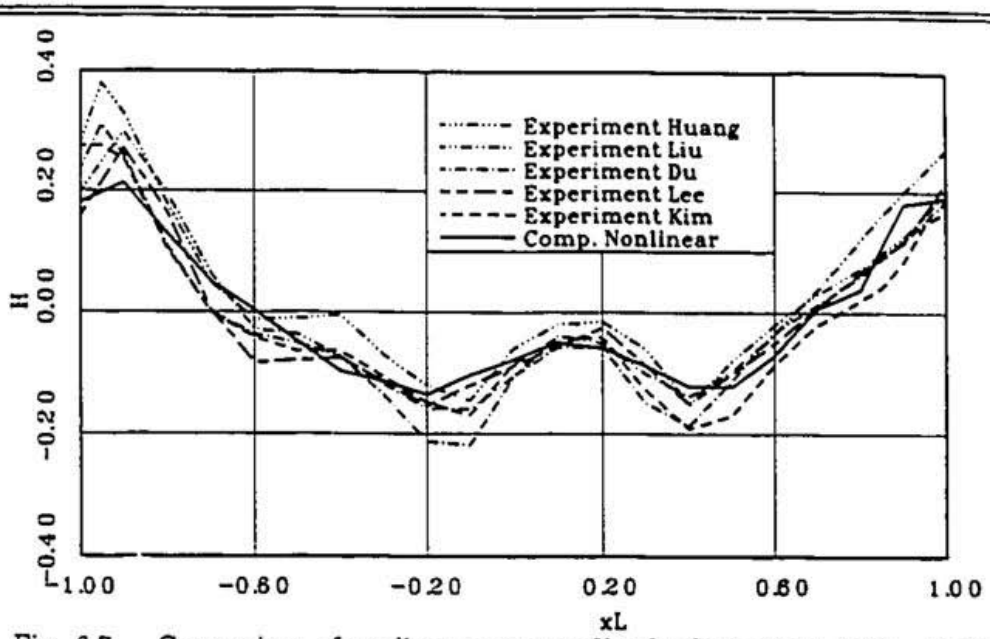

Fig. 6.7 Comparison of nonlinear wave profiles for Series 60 hull (Fn=0.22)

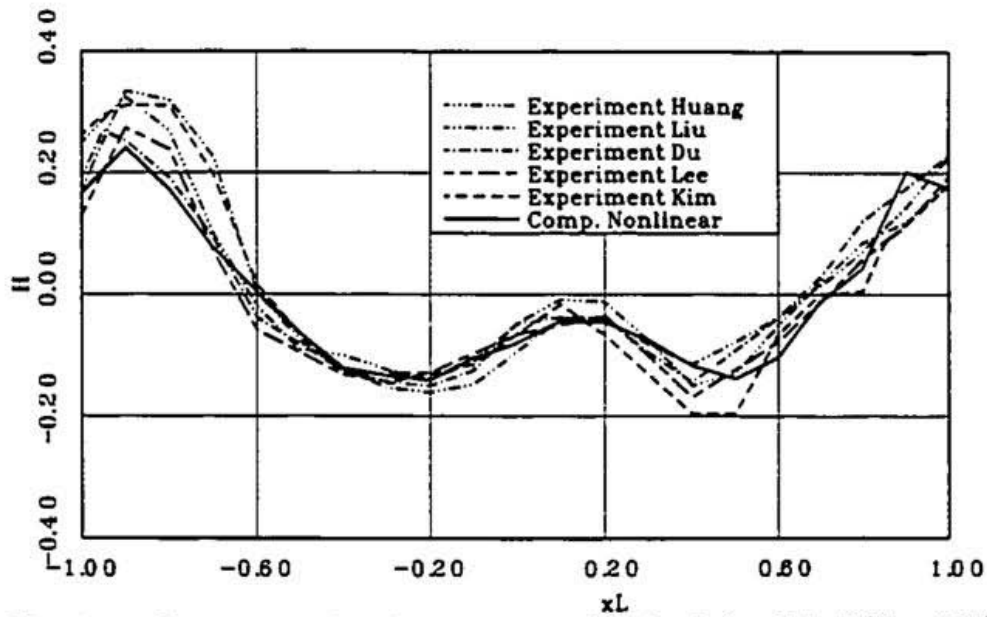

Fig. 6.8 Comparison of nonlinear wave profiles for Series 60 hull (Fn=0.25)

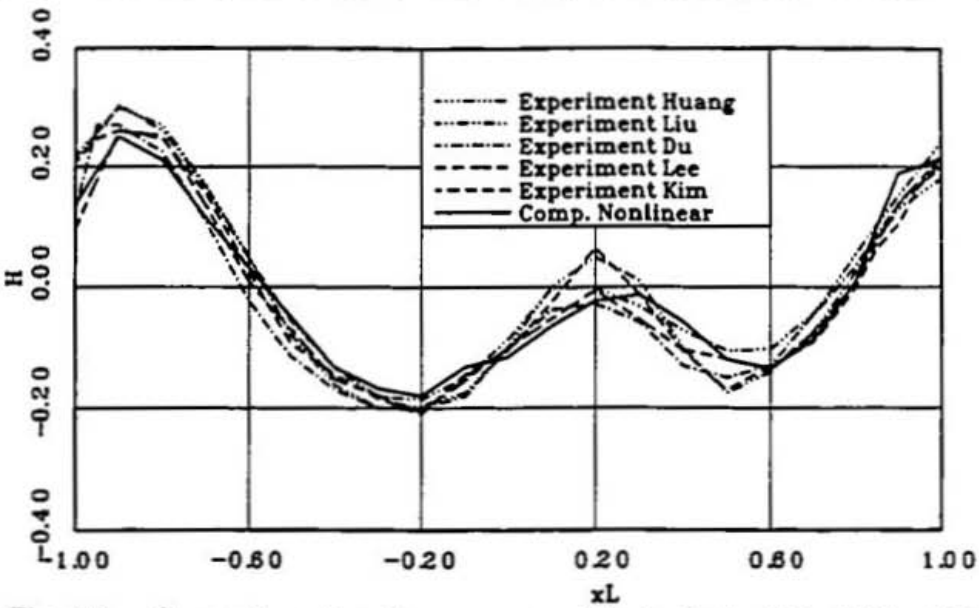

Fig. 6.9 Comparison of nonlinear wave profiles for Series 60 hull (Fn=0.28)

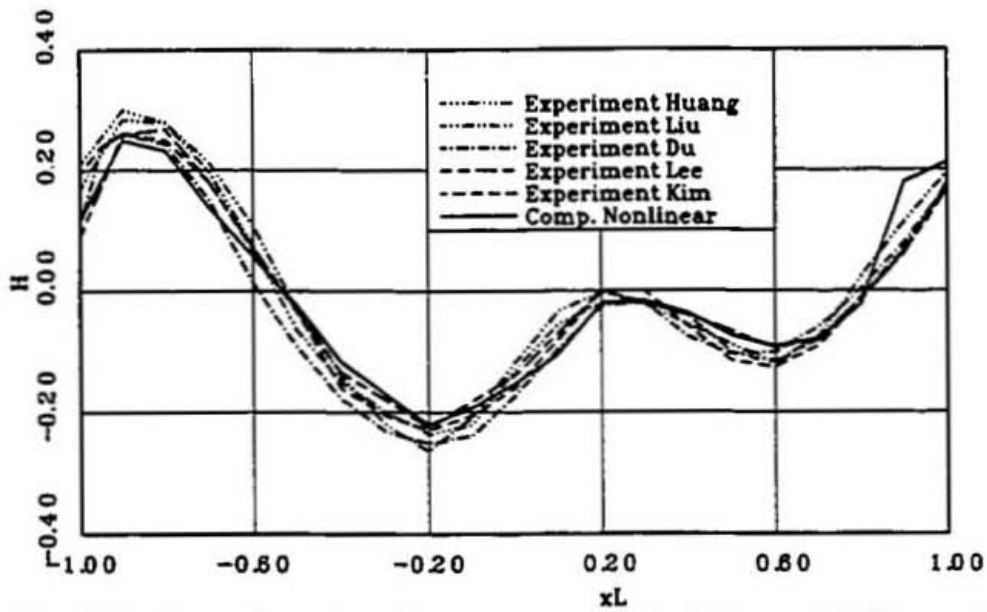

Fig. 6.10 Comparison of nonlinear wave profiles for Series 60 hull (Fn=0.30)

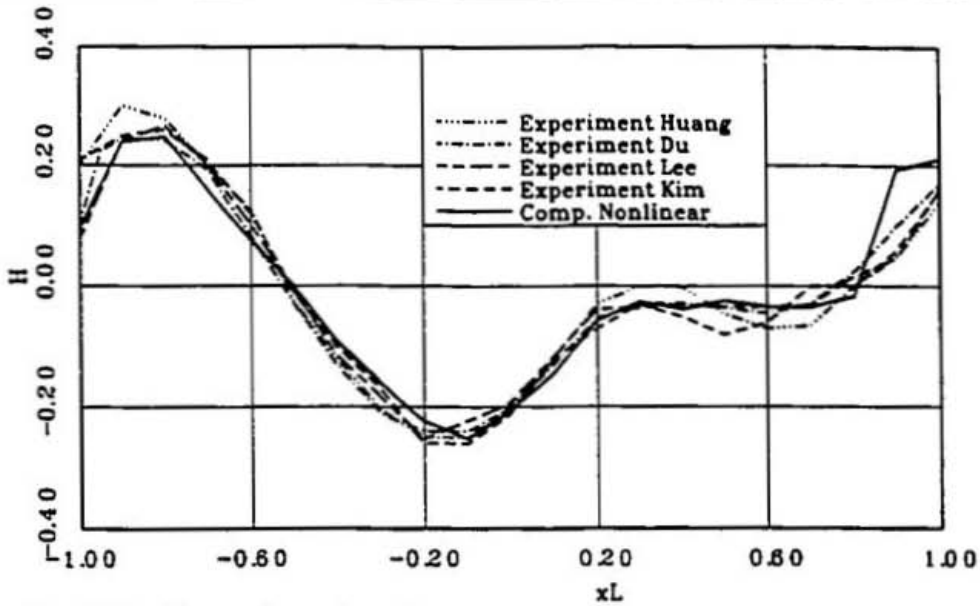

Fig. 6.11 Comparison of nonlinear wave profiles for Series 60 hull (Fn=0.32)

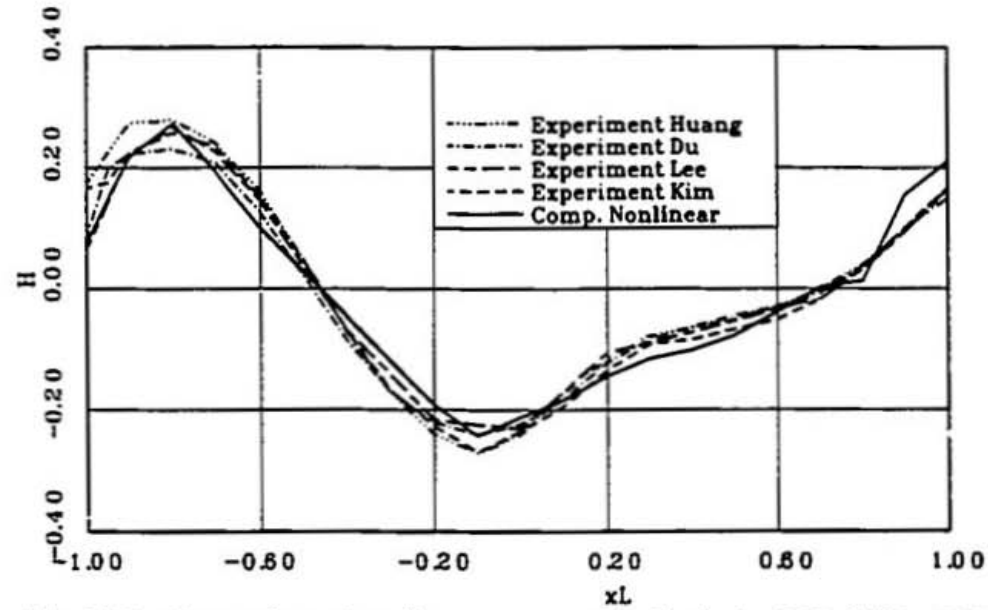

Fig. 6.12 Comparison of nonlinear wave profiles for Series 60 hull (Fn=0.35)

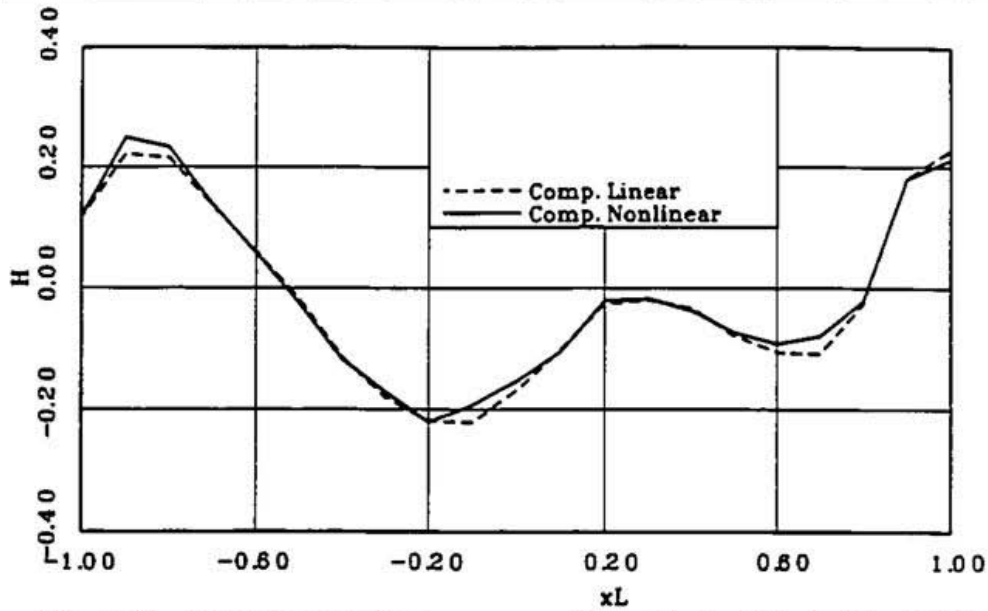

Fig. 6.13 Linear and nonlinear wave profiles of Series 60 hull (Fn=0.30)

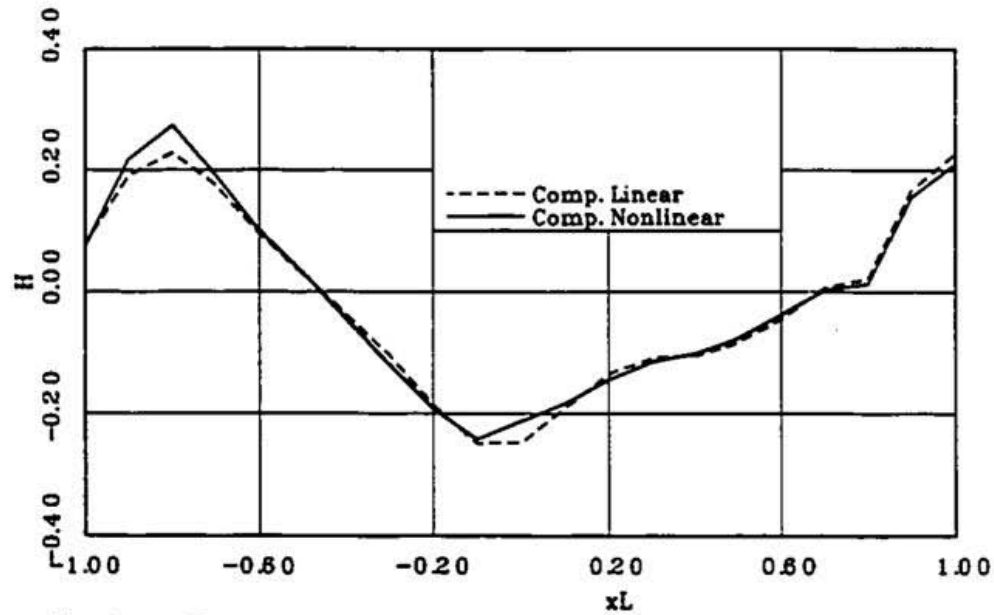

Fig. 6.14 Linear and nonlinear wave profiles of Series 60 hull (Fn=0.35)

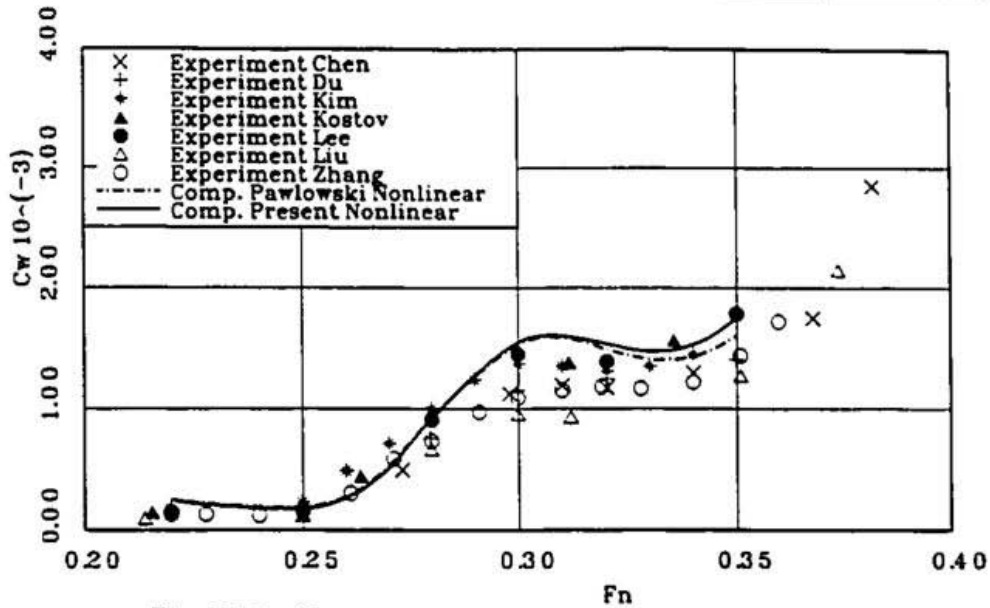

Fig. 6.15 Comparison of nonlinear C_w for Series 60 hull

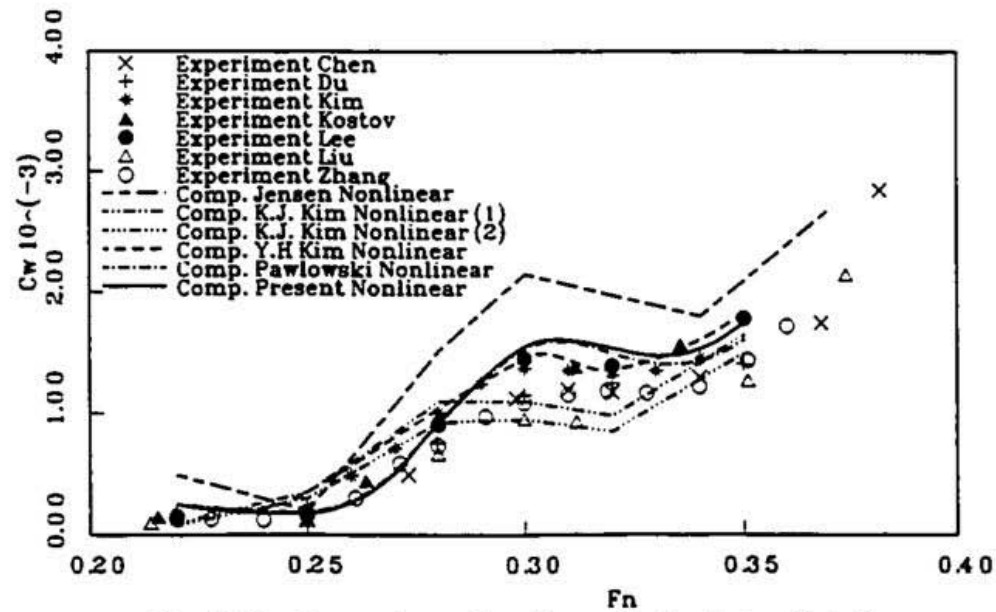

Fig. 6.16 Comparison of nonlinear C_w for Series 60 hull

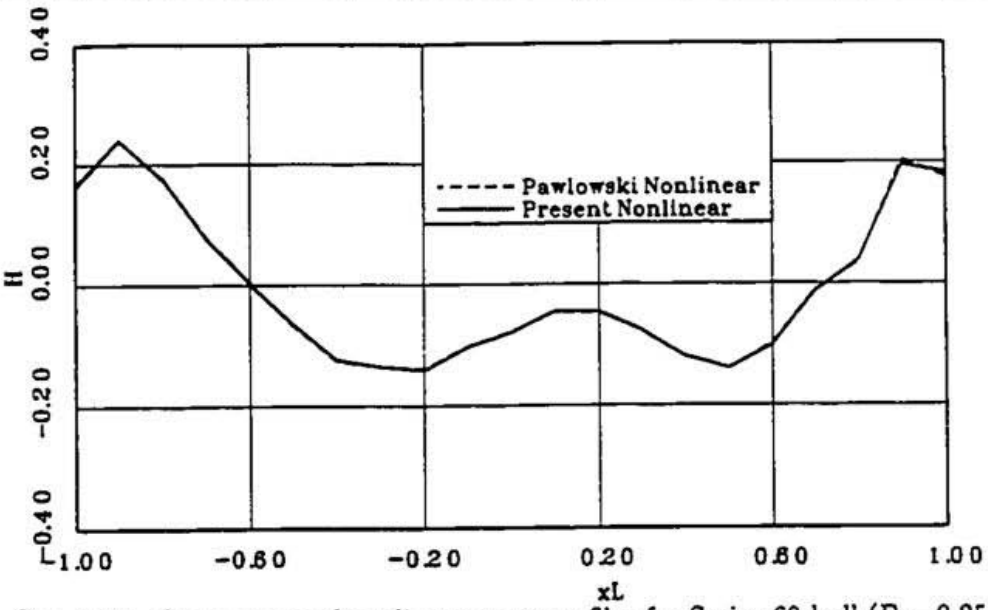

Fig. 6.17 Comparison of nonlinear wave profiles for Series 60 hull (Fn=0.25)

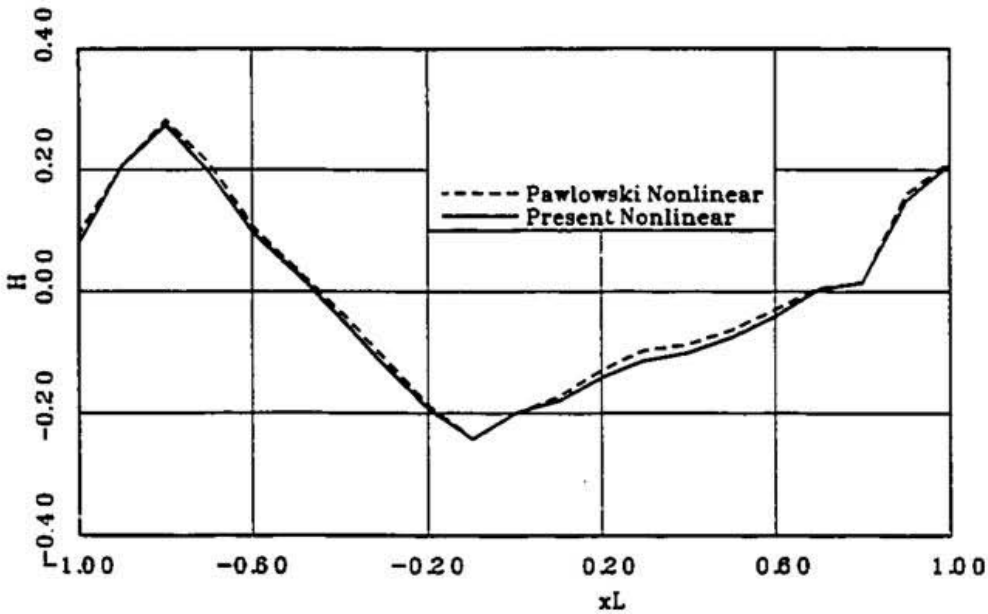

Fig. 6.18 Comparison of nonlinear wave profiles for Series 60 hull (Fn=0.35)

7 VISUALIZATION AND ANIMATION

In order to enhance the interpretation of the results obtained from the computations, a visualization and animation system is also implemented in the present numerical towing tank. Through this system not only the physical motions of a towing tank experiment, such as the ship motion and wave propagation, can be produced but also some properties which can not be easily seen in a towing tank experiment, such as the velocity field in the fluid and the pressure distribution on the ship hull could be visualized.

The principle of computer visualization or animation is simple. Techniques of applying the hardware, software and the development of application software based on existing software to produce the best effect are the major tasks of this kind of work. Today, there is no need to develop the basic visualization and animation tools, such as a render or a color mapper, since software is available for this purpose. However, application interfaces or programs are usually need to be developed to use the existing software to produce a specific visualization or animation. In the present numerical towing tank visualization and animation system, a software package called Advanced Visual System (AVS) is used and run on a mini-supercomputer at the Computational Hydrodynamics Laboratory of NRC. AVS is an application visualization software which was built based on the software called Dynamic Object Rendering Environment (DORE). Some application modules were developed in the present study to meet the needs of the numerical tank visualization and animation.

Fig. 7.1 and Fig. 7.2 show the rendering surface of Wigley hull and Series 60

ship hull respectively.

In Fig. 7.3 to Fig. 7.8 the pressure distribution on the Wigley hull and Series 60 ship hull viewing from 3-D and front are presented. In these figures the pressure is represented by colors. The red color represents the high pressure and the blue color represents the low pressure on the surface of the hull. A color legend is placed in each figure which can be used to determine the pressure for a particular point on the hull surface. Two Froude numbers, $F_n = 0.25$ and $F_n = 0.35$, are presented in these figures which show different pressure distributions on the hull.

In Fig. 7.9 to Fig. 7.12 the velocity fields on the mean water surface are presented. Fig. 7.9 and Fig. 7.10 show the fluid velocity pattern generated by the motion of the Series 60 ship hull at Froude numbers $F_n = 0.25$ and $F_n = 0.35$. Fig. 7.11 and Fig. 7.12 show the fluid velocity pattern generated by the Wigley hull for the same two Froude numbers as show in Fig. 7.9 and Fig. 7.10.

An animation of the surface waves generation by the constant motion of a Series 60 ship is also developed in the present work. Fig. 7.13 shows two frames taken from the animation Series viewed from top and 3-D. The surface wave pattern and the wake are shown clearly in this figure.

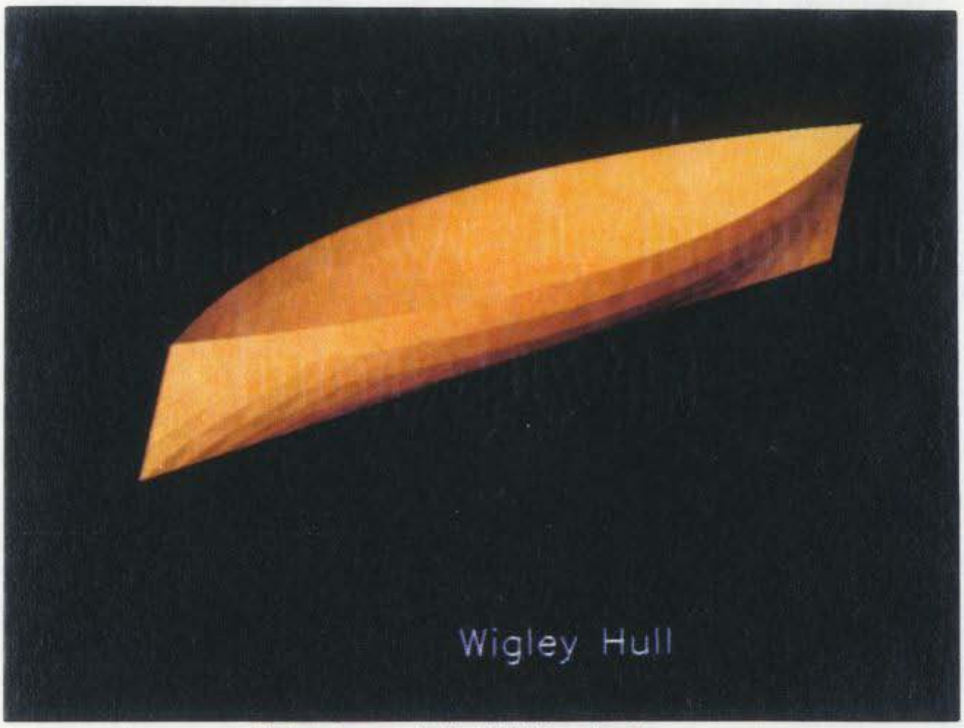

Fig. 7.1 The Wigley hull

Fig. 7.2 Series 60 ship hull (C_b=0.60)

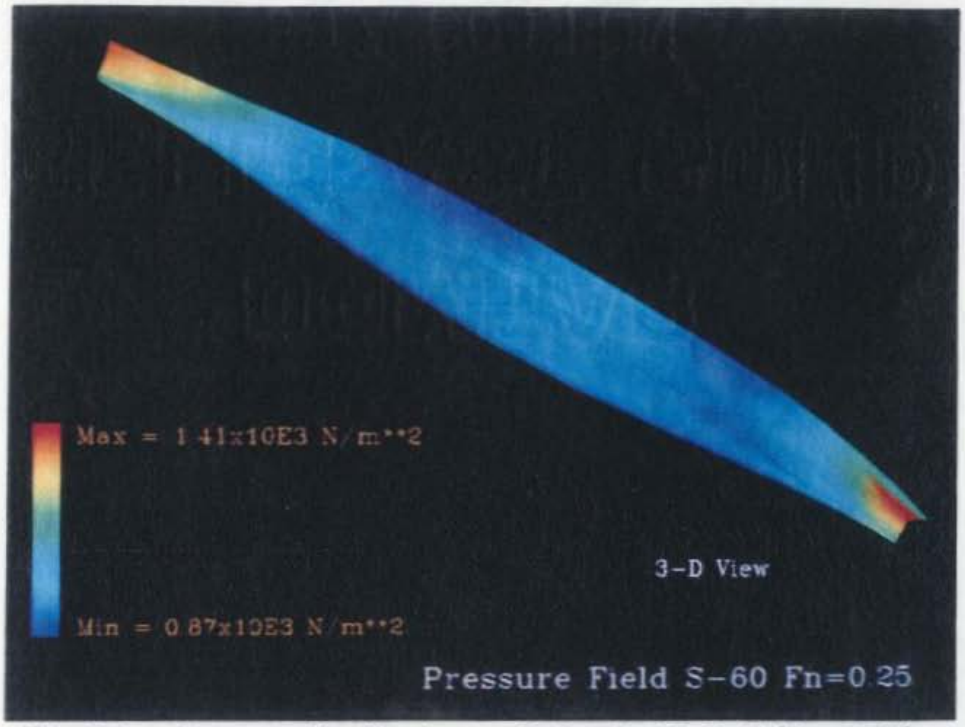

Fig. 7.3 Pressure distribution on Series 60 ship hull (Fn=0.25)

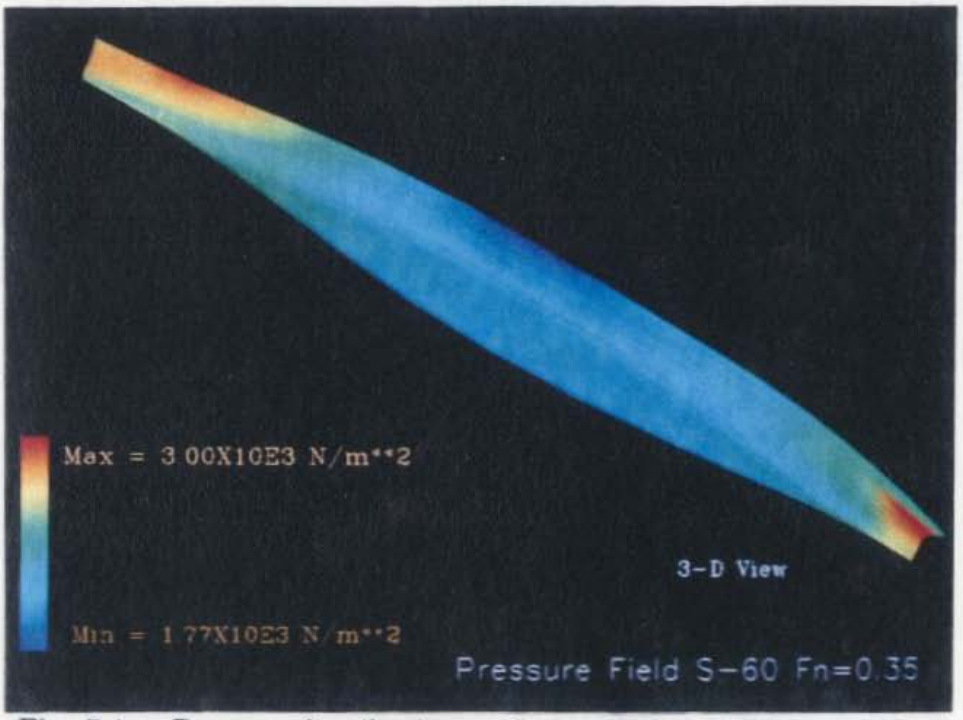

Fig. 7.4 Pressure distribution on Series 60 ship hull (Fn=0.35)

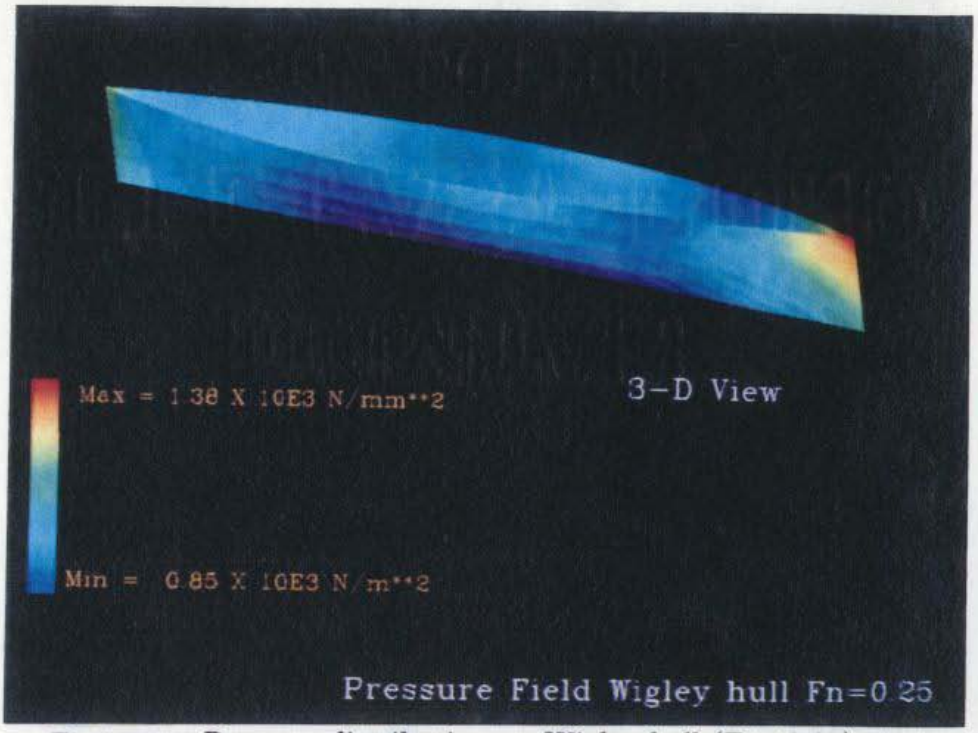

Fig. 7.5 Pressure distribution on Wigley hull (Fn=0.25)

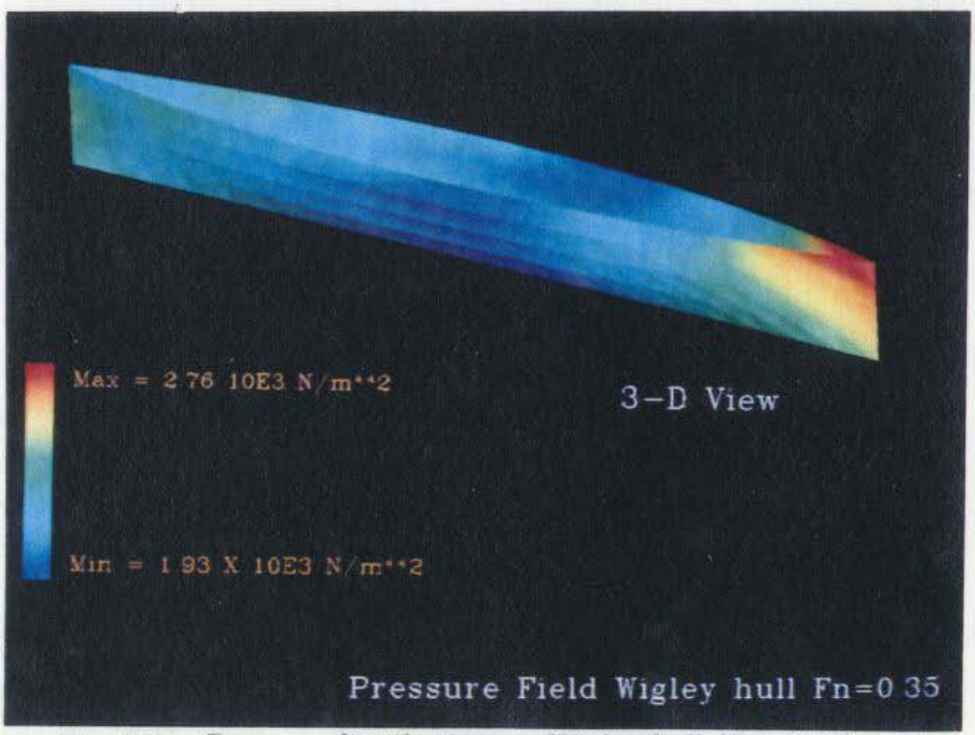

Fig. 7.6 Pressure distribution on Wigley hull (Fn=0.35)

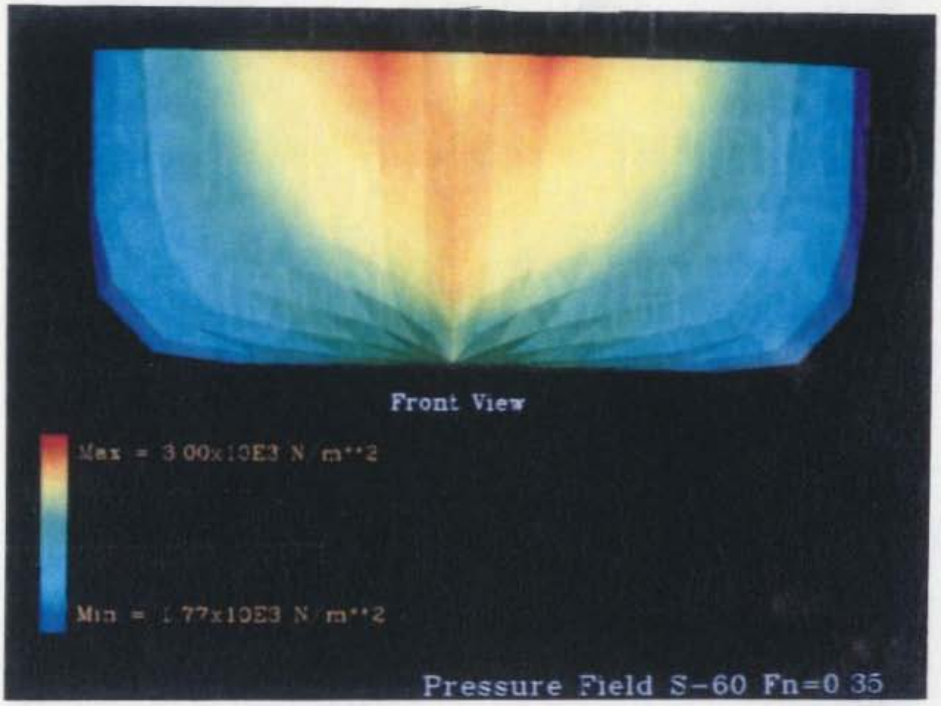

Fig. 7.7 Pressure distribution on Series 60 ship hull (Fn=0.35)

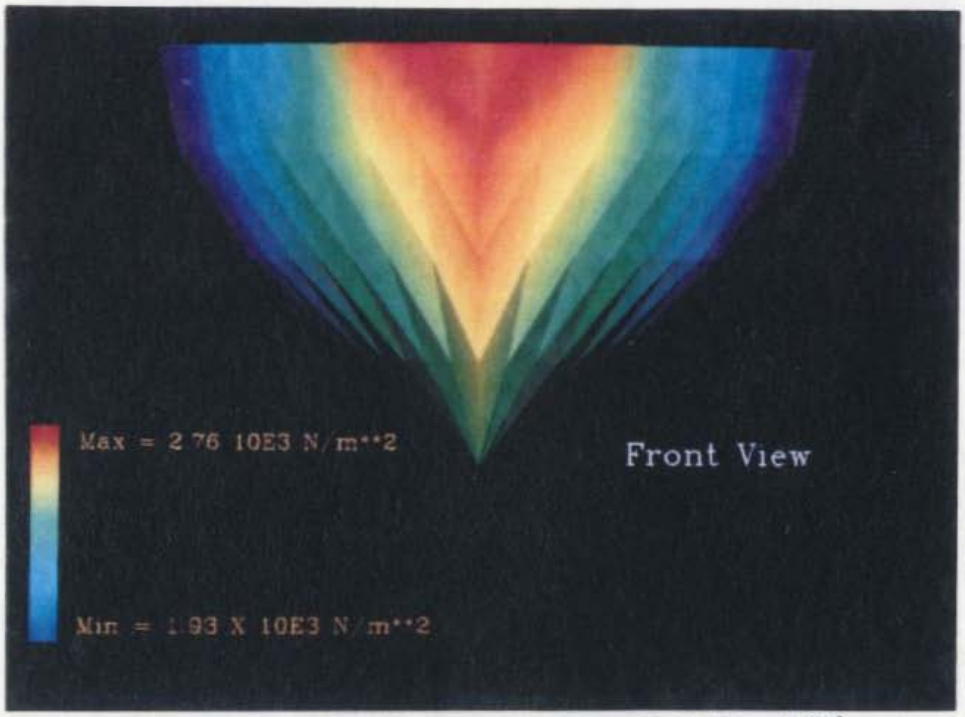

Fig. 7.8 Pressure distribution on Wigley hull (Fn=0.35)

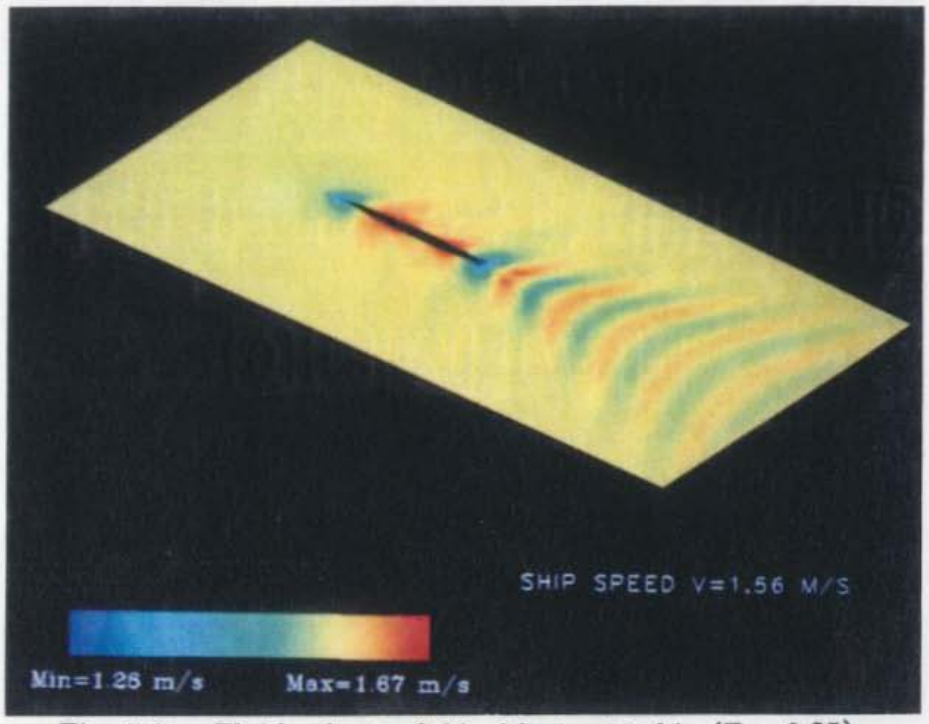

Fig. 7.9 Fluid velocity field of Series 60 ship (Fn=0.25)

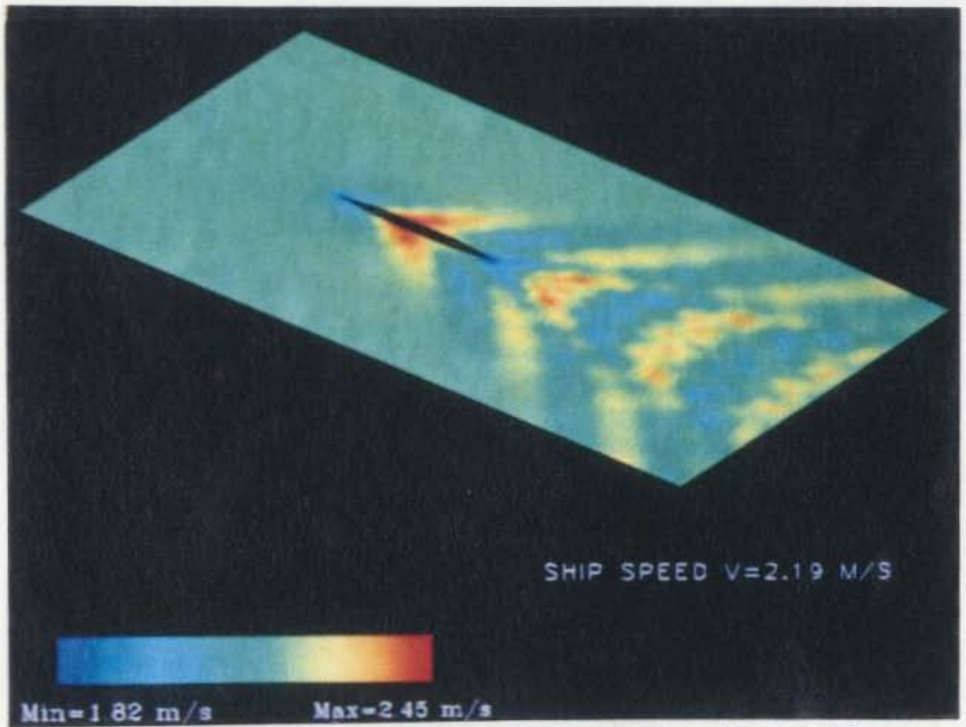

Fig. 7.10 Fluid velocity field of Series 60 ship (Fn=0.35)

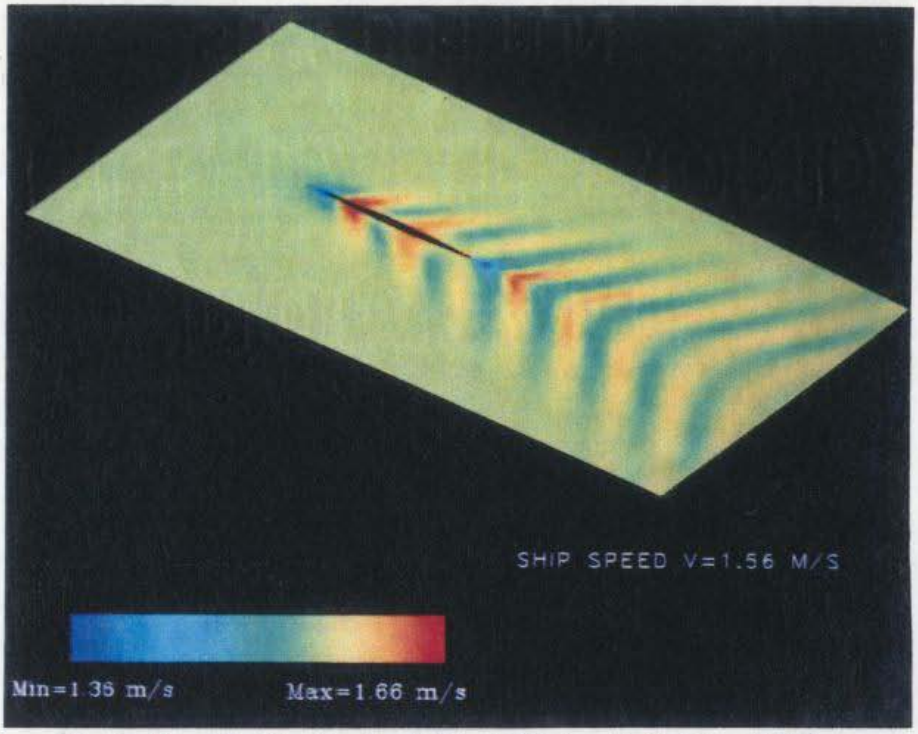

Fig. 7.11 Fluid velocity field of Wigley hull (Fn=0.25)

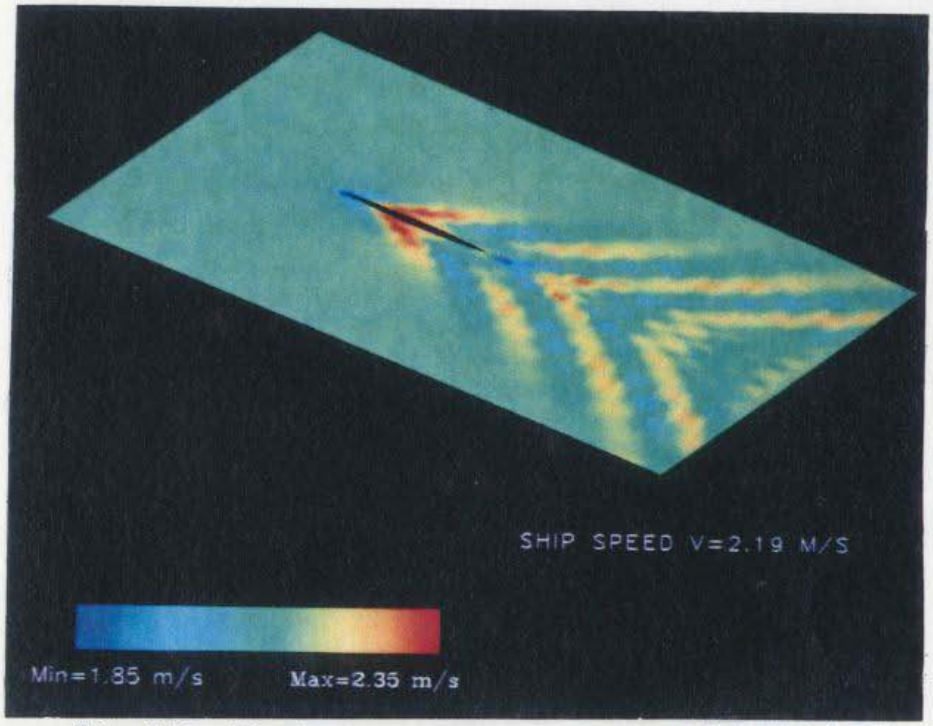

Fig. 7.12 Fluid velocity field of Wigley hull (Fn=0.35)

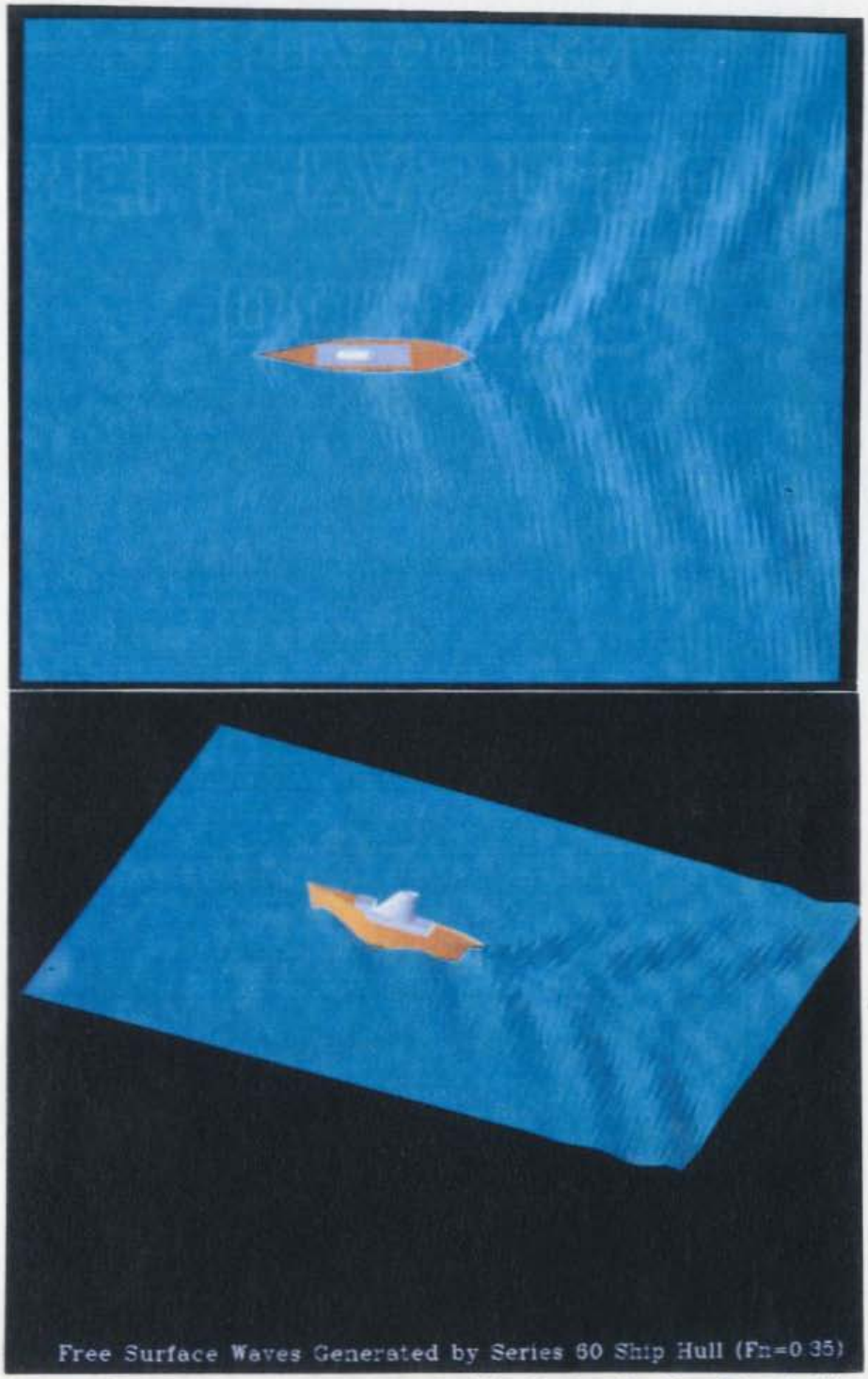

Fig. 7.13 Surface waves generated by Series 60 ship (Fn=0.35)

8 CONCLUSIONS AND RECOMMENDATIONS

In the present study a nonlinear boundary value problem for ship waves was obtained by transforming, through a Taylor's series expansion, the free surface condition of the exact ship wave problem from being satisfied on the actual free surface to being satisfied on the undisturbed fluid free surface. An iterative method based on the direct boundary integral theory and the linear element techniques was developed to solve the transformed nonlinear boundary value problem. A numerical towing tank has been developed using the nonlinear ship wave problem and the iterative scheme developed in the present study. Good agreement has been obtained between the present computational results and the results based on Pawlowski's nonlinear theory and they all match the experimental data of wave resistance measured in towing tanks.

The free surface condition in the present transformed nonlinear ship wave problem is satisfied at the undisturbed fluid free surface. Therefore, the flat free surface mesh stays in the plane of $z = 0$ in the iteration. This brings many advantages for the numerical processing and also benefits the computations in terms of accuracy in comparison with the iterative panel method found in the literature, in which the surface mesh is renewed on the computed wave surface in each iteration.

In order to compare the present method with the existing ones and to study the linear models found in the literature, a new linearized ship wave problem, as a special case of the present nonlinear ship wave problem, was also derived

and solved in the present investigation. Algorithms based on both the indirect and the direct boundary integral theories (linear numerical towing tank) were developed to solve the present linearized ship wave problem.

The theoretical developments in the present study are mainly: the transformation of the free surface condition, the derivation of a new linearized ship wave problem, and the development of an iterative scheme for solving nonlinear boundary value problems. Beside these theoretical achievements, the development of numerical techniques and software design is also an important part of the present study. This includes the development of the algorithm for applying the direct boundary integral theory, the development of the linear element techniques, and the implementation of visualization and animation systems. Vectorization and parallelization were also considered in the computer programing for the algorithms developed in this study.

As a result of this investigation the following conclusions are drawn:

1. The Neumann-Kelvin linear ship wave problem can only be used as an approximation for significantly thin ships, for example a Wigley hull. The results obtained by the Neumann-Kelvin linear model are better than those obtained by the thin ship theory but they are still too much different from the experimental data. It is, therefore, not recommended to apply the Neumann-Kelvin linear model to realistic ships.

2. Dawson's free surface condition contains only the linearized terms of zero order in η in the Taylor's series expansion of the exact free surface condition. Therefore it is still applicable to relatively thin ships. Although Dawson's linear model is better than the Neumann-Kelvin linear model,

errors produced by applying Dawson's linear model for realistic ships are still too high.

3. The present linear free surface condition is obtained by a Taylor's series expansion. It is more accurate than the free surface condition found in Dawson's linear model. The results obtained by solving the present linear ship wave problem are close to experimental data.

4. The free surface condition of the present nonlinear ship wave problem is satisfied at the undisturbed free surface, which brings many advantages for numerical processing, especially for iterative algorithms. Numerical experiments show that the present nonlinear ship wave boundary value problem accurately models the physical problem. The use of the condition can also be justified by a perturbation formulation of the problem (Pawlowski 1992b).

5. The iterative scheme developed in the present study is based on the direct integral theory and linear element techniques. It is stable, accurate, and efficient in solving the nonlinear ship wave problem. It can also be used to solve nonlinear boundary value problems other than the ship wave problem.

6. The numerical towing tank developed in the present investigation gives accurate results for simulating towing tank experiments. With the visualization and animation systems, the present numerical towing tank can produce the effects analogous to the physical effects observed in a laboratory.

From the experience of this investigation the following recommendations are

also presented:

1. Both the direct and the indirect boundary integral formulations can be used to solve the ship wave problem. Although they are used to solve the same problem, the numerical algorithm of the formulations are different. Different numerical considerations are needed in the development of the two algorithms.

2. The numerical algorithm applying the linear element techniques are more complicated than the one using the constant element techniques. Special treatments have to be applied at the nodes of the surface mesh in the linear element algorithm, since they are all singularity points. The linear element techniques give better accuracy than the constant element techniques.

3. It is convenient to use the direct boundary integral formulation to simulate a towing tank. Since the unknowns distributed on the boundary of the computational domain are the velocity potentials and their normal derivatives, which are the direct values of the solution to the problem, the direct formulation is easier in the development of the computer programs than working with source distribution concept.

4. In many studies of solving the ship wave problem, a radiation condition that no waves are propagated upstream from the body is imposed by using a downstream one-sided finite difference formulation, which is also used in the present study. This is because the radiation condition is not entirely mathematically defined. Further studies on a mathematical definition of the radiation condition are needed in future research.

5. The sinkage and the trim were not considered in the algorithm developed in the present study. Further developments are needed to include the effect of the sinkage and trim.

6. The ship hull was assumed to be wall-sided at the design waterline in the present method. Further studies are needed to consider the slope of this part of the ship hull.

REFERENCES

Aanesland, V. (1986): "A theoretical and numerical study of ship wave resistance". *Report, Norwegian Hydrodynamic Laboratories.*

Adee, B.H. (1979): "The calculation of ship wave resistance using surface source distribution". *DTNSRDC Workshop on Ship Wave-Resistance Computations, David W. Taylor Naval Ship Research and Development Center, Bethesda, Maryland, USA, pp. 232–255.*

Andersson, B.J. (1975): "Notes on the theory of ship waves. *Department of Hydromechanics ". Royal Institute of Technology, Stockholm.*

Baar, J.J.M. (1984): "On the use of Green's functions in marine hydromechanics". *Part 2. Translating, Pulsating source in shallow water. Mechanical Engineering Department, Brunel University, Uxbridge.*

Baar. J.J.M. (1986): "A three-dimensional linear analysis of steady ship motion in deep water". *Ph.D. Thesis, Brunel University, U.K.*

Baar, J.J.M. and Price, W.G. (1988): "Developments in the calculation of the wavemaking resistance of ship". *Proc. of the Royal Society, Lond., A 416, pp. 115–147.*

Baba, E. (1979): On the free-surface conditions used by Nakatake et al. and Dawson". *DTNSRDC Workshop on Ship Wave-Resistance Computations, David W. Taylor Naval Ship Research and Development Center, Bethesda, Maryland, USA, pp. 504–510.*

Baddour R.E. (1989): "Three dimensional, three-node triangular elements for potential problems". *NRC-IMD Research Contract Report, St. John's.*

Baddour R.E. , Pawlowski, J.S. and Song, S.W. (1991): "The computation of wave patterns and wave resistance induced by submerged bodies advancing with steady forward speed". *Symp. on Selected Topics of Marine Hydrodynamics, St. John's, Newfoundland, Canada, pp. 1–8.*

Bai, K.J. (1975): "A localized finite-element method for steady, two dimensional free-surface flow problem". *Proc. First Int. Conf. on Nume. Ship Hydrodynamics .*

Bai, K.J. (1977): "A localized finite-element method for steady, three dimensional free-surface flow problems". *Proc. Second Int. Conf. on Nume. Ship Hydrodynamics, Berkeley, pp. 78–87.*

Bai, K.J. (1978): "A localized finite-element method for two dimensional steady potential flow with a free surface". *J. of Ship Research, Vol. 22, No. 4, pp. 216-230.*

Bai, K.J. (1979): "Blockage correction with a free surface". *J. of Fluid Mech., Vol. 94, pp. 433-452.*

Bai, K.J. (1979): "Wave resistance in a restricted water by the localized finite-element method". *DTNSRDC Workshop on Ship Wave-Resistance Computations, David W. Taylor Naval Ship Research and Development Center, Bethesda, Maryland, USA, pp. 407-411.*

Beek C.M., Piers, W.J. and Slooff, J.W. (1985): "Boundary integral method for the computation of the potential flow about ship configurations with lift and free surface effects". *Report, National Aerospace Laboratory NLR, Amsterdam, the Netherlands.*

Bessho, M. (1964): "The fundamental function in the theory of the wavemaking resistance of ships". *Mem. Dep. Acad. Japan 4, pp. 99-199.*

Bessho, M. (1961): "On the wave-making resistance of submerged prolate spheroids". *J. Zosen Kiokai , Vol. 109, pp. 59-72.*

Brard, R. (1971): "The Neumann-Kelvin problem for surface ships". *Bassin d'Essais Carènes, Paris, Rept. No. 11 CST.*

Brard, R. (1974a): "Le problème de Neumann-Kelvin". *C. R. Acad. Sci., Paris, Series A 278, pp. 169-167.*

Brard, R. (1974b): "Compléments sur le Problème de Neumann-Kelvin". *C. R. Acad. Sci., Paris, Series A 278, pp. 379-384.*

Brebbia, C.A. , Telles, J.C.F. and Wrobel, L.C. (1984): "Boundary Element Techniques): Theory and applications in Engineering". *Springer-Verlag.*

Burden, R.L. and Faires, J.D (1989): "Numerical analysis". *Fourth Edition, PWS-KENT Publishing Company, Boston.*

Calisal, S.M., Goren, O. and McGreer, D.E. (1991): "Numerical studies for the calculation of wave resistance for fishing vessels". *Symp. on Selected Topics of Marine Hydrodynamics, St. John's, Newfoundland, Canada, pp. 9-19.*

Cao, Y. (1991): "Computations of nonlinear gravity waves by a desingularized boundary integral method". *Technical Report, Department of Naval Architecture and Marine Engineering, The University of Michigan, USA.*

Chang, M.S. (1979): "Wave resistance predictions by using a singularity method". *DTNSRDC Workshop on Ship Wave-Resistance Computations, David W. Taylor Naval Ship Research and Development Center, Bethesda, Maryland, USA, pp. 232-255.*

Chen. C.Y. and Noblesse, F. (1983): "Comparison between theoretical predictions of wave resistance and experimental data for the Wigley hull". *J. of Ship Research, Vol. 27, pp. 215-226.*

Chen, F.S. and Xu, T.Q. (1983): "Contribution to resistance Committee of 17th ITTC wave pattern resistance of model of series 60, $C_b = 0.60$". *Shanghai Ship and Shipping Research Institute, Shanghai, China.*

Daube, O. and Dulieu, A. (1981): "A numerical approach of the nonlinear wave resistance problem". *Proc. 3rd Int. Conf. on Nume. Ship Hydrodynamics, Paris, pp. 73-80.*

Dawson, C.W. (1977): "A practical computer method for solving ship-wave problems". *Proc. 2nd Int. Conf. on Nume. Ship Hydrodynamics, Berkeley, pp. 30-38.*

Dawson, C.W. (1979): "Calculation with the XYZ free surface program for five ship models". *DTNSRDC Workshop on Ship Wave-Resistance Computations, David W. Taylor Naval Ship Research and Development Center, Bethesda, Maryland, USA, pp. 232-255.*

Delhommeau, G. and Maisonneuve, J.J. (1986): "Application de la méthode des singularités de Rankine au calau de la résistance de vagues de différents types de carènes". *Association Technique Maritime et A é ronantigue 47 rue de Monceau 7500B, Paris, pp. 237-264.*

Demanche, J.F. (1981): "Potential of a moving pulsating source". *Proc. 3rd. Int. Conf. on Nume. Ship Hydrodynamics, Paris, pp. 27-36.*

Doctors L.J. and R.F. Beck (1987): " Convergence properties of the Neumann-Kelvin problem for a submerged body". *J. of Ship Research, Vol. 31, No. 4, pp. 227-234.*

Du, S. , Li, Y. and Wang, H. (1983): "Some experimental results for resistance and wave pattern measurements with series 60, block 0.60 model in MARIC tank". *Report, Marine Design and Research Institute of China, Shanghai, China.*

Eggers, K.W.H. , Sharma, S.D. and Ward, L.W. (1967): "An assessment of some experimental methods for determining the wavemaking characteristics of a ship form". *Annual Meeting The Society of Naval Architects and Marine Engineers, N.Y. 75, pp. 112-144.*

Euvrard, D. (1983): "Les mille et une facéties de la fonction de Green du problème de la résistance de vagues". *Ecole Nationale Superieure de Techiques Avancées, Paris, No. 144.*

Farell, C. (1973): "On the wave resistance of a submerged spheroid". *J. of Ship Research, Vol. 17, No. 1, 1-11.*

Fournier, A. and Reeves, W. (1986): "A simple model of ocean waves". *Computer Graphics, Vol. 20, No. 3.*

Fritts, M. (1990): "Hydro-numeric design: performance prediction and impact on hull design". *Annual Meeting The Society of Naval Architects and Marine Engineers, pp. 15-1-15-18.*

Froude, W. (1876): "The fundamental principles of the resistance of ship". *Proc. Roy. Inst. Gt. Brit., Vol. 8, pp. 188-213.*

Gadd, G.E. (1968): "On understanding ship resistance mathematically". *J. Inst. Math. Appl., Vol. 4, pp. 43-57.*

Gadd, G.E. (1975): "A method of computing the flow and surface wave pattern around hull forms". *The Royal Institution of Naval Architects, Vol. 118, pp. 207-219.*

Guilloton, R. (1964): "L'etude théorique et numérique du bateau en fluide parfait". *Bell. Ass. Tech. Mar. Aeron., Vol. 64, pp. 538-561.*

Guttmann. C. (1983): "Etude therique el numerique du probleme de Neumann-Kelvin tridimensionnal pour un corps totalement immerge". *Ecole Nationale Superieure de Techniques Avancees, Paris, Rep. No. 177.*

Haussling, H.J. and Coleman, R.M. (1979): "Nonlinear water waves generated by an accelerated circular cylinder". *J. of Fluid Mech. Vol. 29, Pt. 4, pp. 767-781.*

Havelock, T.H. (1908): "The Propagation of groups of wave in dispersive media, with application to waves on water produced by a travelling disturbance". *Proc. of the Royal Society, Lond., A. Vol. 81, pp. 398-430.*

Havelock, T.H. (1931a): "The wave resistance of a spheroid". *Proc. of the Royal Society, Lond., A Vol. 131, pp. 275-285.*

Havelock, T.H. (1931b): "The wave resistance of an ellipsoid". *Proc. of the Royal Society, Lond., A Vol. 132, pp. 480-486.*

Havelock, T.H. (1932): "The theory of wave resistance". *Proc. of the Royal Soceity, Lond., A 138, pp. 339-348.*

Hess, J.L. and Smith, A.M.O. (1962): "Calculation of non-lifting potential flow about arbitrary three-dimensional bodies". *Douglas Aircraft Company Report, No. 40622.*

Hess, J.L. and Smith, A.M.O. (1964): " Calculation of nonlifting potential flow about arbitrary three-dimensional bodies". *J. of Ship Research, Vol. 8, No 2, pp. 22-44.*

Hess, J.L. and Smith, A.M.O. (1966): "Calculation of potential flow about arbitrary bodies". *Progress in Aeronautical Science, Vol. 8, pp. 1-138.*

Hess, J.L. (1977): "Progress in the calculation of nonlinear free-surface problems by surface-singularity techniques". *Proc. 2nd. Int. Conf. Nume. Ship Hydrodynamics, Berkeley, pp. 278-284.*

Hideakimiyata and Nishimura, S. (1985): "Finite-difference simulation of nonlinear ship waves". *J. Fluid Mech. Vol. 157, pp. 327-357.*

Hong, Y.S. (1979): "Numerical calculation of second-order wave resistance using Lagrangian coordinates". *DTNSRDC Workshop on Ship Wave-Resistance Computations, David W. Taylor Naval Ship Research and Development Center, Bethesda, Maryland, USA, pp. 370-382.*

Huang, T.T. and von Kerczek, C.H.(1972): " Shear stress and pressure distribution on a surface ship model: Theory and experiment". *Proc. 9th Symp. of Naval Hydrodynamics, Paris, pp. 1969-2010.*

Inui, T. (1962): "Wave-making resistance of ships". *The Society of Naval Architects and Marine Engineers, Trans., Vol. 70, pp. 282-326.*

Issacs, P. and Cohen, M. (1987): "Controlling dynamic simulation with kinematic constraints, behavior functions, and dynamics". *Computer Graphics, Vol. 21, No. 4, pp. 215-224.*

Jensen, G., Soding, H. and Mi, Z.X. (1986): "Rankine source method for numerical solution of the steady wave resistance problem". *Proc. the 16th Symp. on Naval Hydrodynamics, Berkeley, pp. 575-582.*

Jensen, G., and Soding, H. (1989): "Ship wave-resistance computations". *Proc. 15th Int. Conf. on Nume. Ship Hydrodynamics. Hiroshima, Japan. pp. 216-229.*

Johnson, F.T. (1980): "A general panel method for the analysis and design of arbitrary configurations in incompressible flows". *NASA Contractor Report 3079, Boeing Commercial Airplane Company, Seattle, Washington, USA.*

Ju, S. (1983): "Study of total and viscous resistance for the Wigley parabolic ship form". *DTNSRDC Workshop on Ship Wave-Resistance Computations, David W. Taylor Naval Ship Research and Development Center, Bethesda, Maryland, USA, pp. 36-49.*

Kajitani, H. , Miyata, H. , Ikehata, M. , Tanaka, H. , Adachi, H. , Namimatsu, M. , and Ogiwara, S. (1983): " The summary of the coorperative experiment on Wigley parabolic model in Japan". *DTNSRDC Workshop on Ship Wave-Resistance Computations, David W. Taylor Naval Ship Research and Development Center, Bethesda, Maryland, USA, pp. 5-35.*

Kim, K.J. (1989): "Ship flow calculations and resistance minimization". *SSPA Report, Chalmers University of Technology, Goteborg, Sweden.*

Kim, Y.H. and Jenkins, D. (1981): "Trim and sinkage effects on wave resistance with series 60, $C_b = 0.6$". *DTNSRDC Report, DTNSRDC/SPD-1013-01, Bethesda, USA.*

Kim, Y.H. and Lucas, T.R. (1990): "Nonlinear ship waves". *Proc. the 18th on Symp. on Naval Hydrodynamics.*

Kostov, D. and St. Kyulevcheliev (1983): "Resistance tests and wave pattern measurements of Wigley hull and series 60, $C_b = 0.60$". *BSHC Report 6.6-2/03, Varna, Bulgaria.*

Kostyukov, A.A. (1968): "Theory of ship waves and wave resistance". *Iowa: Effective Communications Inc. (English transl.).*

Lamb, H. (1932): "Hydrodynamics". *6th edn. Cambridge University Press.*

Lee, Y.G. and Hyun, B.S. (1983): "Experimental report for 17th ITTC resistance committee coorperative experimental program". *Ship Research Station, Korea Institute of Machinery and Metals, Daeduck Science Town, Daejeon, Korea.*

Lewis, E.U. (1988): "Principles of Naval Architecture". *Vol. 2. Soc. of Naval Architects and Marine Engineers, Jersey City, NJ.*

Liu, Y. , Sheng, Z. and Yan, A. (1983): "Experimental results for resistance, wave pattern measurements and wake survey with series 60, $C_b = 0.60$ model". *Chiao Tong University, Ship Hydro. Lab., Shanghai, China.*

Lunde, J.K. (1951): "On the linearized theory of wave resistance for displacement ships in steady and accelerated motion". *Trans. Soc. Naval Archit. Mar. Engrs., Vol. 59, pp. 25-76.*

Manen, J.D. and Oossanen, P. (1988): "Chapter 5. Resistance". *Principles of*

Naval Architecture, Vol. II. Resistance, Propulsion and Vibration, pp. 1–125.

Maruo, H. and Ogiwara, S. (1985): "A method of computation for steady ship waves with nonlinear free surface conditions". *Proc. 4th Int. Conf. on Nume. Ship Hydrodynamics, pp. 218–233.*

McCarthy, J.H. (1985): "Collected experimental resistance component and flow data for three surface ship model hulls". *Members of the resistance committee of the 17th international towing conference. David Taylor Naval Ship Research and Development Center, Bethesda, Maryland, USA.*

Michell, J.H. (1898): "The wave resistance of a ship". *Phil. Mag. (5) 45, 106–123.*

Mori, K. and Murata, K. (1983): "Wave resistance calculation by modified Rankine source method". *DTNSRDC Workshop on Ship Wave-Resistance Computations, David W. Taylor Naval Ship Research and Development Center, Bethesda, Maryland, USA, pp. 321–340.*

Musker, A.J. (1988): "A panel method for predicting ship wave resistance". *Proc. the 17th Symp. on Naval Hydrodynamics, pp. 143–150.*

Nakos, D.E. (1990): "Ship wave patterns and motions by a three dimensional Rankine panel method". *Ph.D. Thesis, Massachusetts Institute of Technology, Cambridge, Massachusetts.*

Nakos, D.E. and Sclavounos, P.D. (1991): "Ship motions by a three-dimensional Rankine panel method ". *Proc. the 18th Symp. on Naval Hydrodynamics, pp. 21–40.*

Newman, J.N. (1976): "Linearized wave resistance theory". *Proc. Int. Sem. wave Resistance, Tokyo and Osaka , pp. 31–43.*

Newman, J.N. (1977): "Marine Hydrodynamics". *The MIT Press. Cambridge, Massachusetts.*

Newman, J.N. (1985): "The evaluation of free surface Green functions". *Proc. 4th Int. Conf. on Nume. Ship Hydrodynamics, Washington, pp. 4–19.*

Newman, J.N. (1988): "Evaluation of the wave-resistance Green function. Part1. The double integral". *J. of Ship Research, Vol. 31, pp. 79–90.*

Ni, S.Y. (1987): "A higher order panel method for double model linearized free surface potential flows". *SSPA Report 2912-5, Sweden.*

Ni, S.Y. (1987): "Higher order panel methods for potential flows with linear or

non-linear free surface boundary conditions". *SSPA Report ISBN 91-7032-323-2, Sweden.*

Noblesse. F. (1977): "The fundamental solution of the theory of steady motion of a ship". *J. of Ship Research, Vol. 21, pp. 82–88.*

Noblesse, F. (1981): "Alternative integral representations for the green function of the theory of ship wave resistance". *J. Eng. Math., Vol. 15, pp. 241–265.*

Noblesse, F. (1983): "A slender-ship theory of wave resistance". *J. of Ship Research, Vol. 27, pp. 13–33.*

Ogiwara, S. (1983): "Numerical calculation of free surface flow by means of modified Rankine source method". *DTNSRDC Workshop on Ship Wave-Resistance Computations, David W. Taylor Naval Ship Research and Development Center, Bethesda, Maryland, USA, pp. 321–340.*

Ogiwara, S. (1985): "A numerical method of non-linear solution for steady wave around ships (in Japanese)". *J. of the Society of Architects of Japan Vol. 157, pp. 34–46.*

Ogiwara, S. and Masuko, A. (1986): "A method of computation for steady ship waves by means of Rankine source and its application to hull form design". *Int. Conf. CADMO 86, pp. 97–116.*

Oomen, A.(1979): "A finite element method for ship wave resistance computation". *DTNSRDC Workshop on Ship Wave-Resistance Computations, David W. Taylor Naval Ship Research and Development Center, Bethesda, Maryland, USA, pp. 396–406.*

Pawlowski, J.S. (1992a): "A nonlinear theory of ship motion in waves". *Proc. 19th Symp. on Naval Hydrodynamics, pp. 21–42 (Preprintings).*

Pawlowski, J.S. (1992b): "A perturbation formulation of the ship wave resistance problem". *To appear*

Peachey, D.R. (1986): "Modeling waves and surf". *Computer Graphics , Vol. 20, No. 4, pp. 65–74.*

Peters, A.S. (1949): "A new treatment of the ship wave problem". *Communs Pure Appl. Math. 2, pp. 123– 148.*

Raven, H.C. (1988): "Variations on a theme by Dawson". *Proc. the 17th Symp. on Naval Hydrodynamics, pp. 151–172.*

Raven, H.C. (1991): "Adequacy of free surface conditions for the wave resistance

problem". *Proc. the 18th Symp. on Naval Hydrodynamics, pp. 375-395.*

Raven, H.C. (1992): "A practical nonlinear method for calculating ship wavemaking and wave resistance ". *Proc. 19th Symp. on Naval Hydrodynamics, pp. 60-75 (Preprintings).*

Sabuncu, T. (1962): "Some predictions of the value of the wave resistance and moment concerning the Rankine solid under interfacial wave conditions". *Norw. Ship Model Exp. Trondheim, Publ. 65, pp. ii+ii+38.*

Saunders, H.E. (1957): "Hydrodynamics in ship design". *Trans. Soc. Naval Archit. Mar. Engrs., Vol. 2.*

Sclavounos, P.D. (1984a): " The diffraction of free-surface waves by a slender ship". *J. of Ship Research, Vol. 28, No. 1, pp. 29-47.*

Sclavounos, P.D. and Nakos, D.E. (1988): "Stability analysis of panel methods for free-surface flows with forward speed". *Proc. the 17th Symp. on Naval Hydrodynamics, pp. 173-193.*

Scragg, C. and Talcott, J. (1991): "Numerical solution of the "Dawson". free-surface problem using Havelock singularities" *Proc. the 18th Symp. on Naval Hydrodynamics, pp. 259-271.*

Shearer, J.R. and Cross, J.J. (1965): "The experimental determination of the components of ship resistance for a mathematical model". *Transaction of the Royal Institute of Naval Architects, Vol. 107, pp. 459-479.*

Shen, H.T. and Farell, C. (1977): "Numerical calculation of the wave integrals in the linearized theory of water waves". *J. of Ship Research, Vol. 21, pp. 1-10.*

Simmgen, M. (1968): "Ein Beitrag zur linearisierten theorie des preiodisch instationar angestromten unterwassertragflugels". *Z. Ang. Math. Mech. Vol. 48, pp. 255-264.*

Standing, R.G. (1975): "Experience in the computing the wavemaking of source/sink models". *National Physical Laboratory, Teddington, NPL Rep. Ship 190.*

Suzuki, K. (1979): "Calculation of ship wave resistance with special reference to sinkage". *DTNSRDC Workshop on Ship Wave-Resistance Computations, David W. Taylor Naval Ship Research and Development Center, Bethesda, Maryland, USA, pp. 256-281.*

Thomson, W. (Lord Kelvin) (1887): "On the ship waves". *Proc. Inst. Mech. Eng., Vol. 3, pp. 409-434.*

Thomson, W. (Lord Kelvin) (1904): "Deep water ship waves". *Proc. of the Royal Society (Edinb) Vol. 25, pp. 562-587.*

Tood, F.H. (1953): "Some further experiments on single-screw merchant ship forms—series 60". *The Society of Naval Architects and Marine Engineers, Trans. Vol. 61, pp. 516-589.*

Tsai, W.T. , Lin, Y.J. and Liao, C.C. (1983): " Numerical solution of the Neumann-Kelvin problem and its application to ship wave-resistance computations". *DTNSRDC Workshop on Ship Wave-Resistance Computations, David W. Taylor Naval Ship Research and Development Center, Bethesda, Maryland, USA, pp. 233-280.*

Tsutsumi, T. (1979): "Calculation of the wave resistance of ships by the numerical solution of the Neumann-Kelvin problem". *DTNSRDC Workshop on Ship Wave-Resistance Computations, David W. Taylor Naval Ship Research and Development Center, Bethesda, Maryland, USA, pp. 162-201.*

Ursell, F. (1960): "On Kelvin's ship-wave pattern". *J. Fluid Mech. Vol. 8, pp. 418-431.*

Ursell, F. (1984): "Mathematical note on the fundamental solution(Kelvin source) in ship hydrodynamics". *IMA J. Appl. Math. 32, pp. 335-351.*

Wardle, L.J. (1981): "An introduction to the boundary element method". *Numerical Solutions of Partial Differential Equations. Proc. of the 1981 Conf. on the Numerical Solutions of Partial Differential Equations, Held at Queen's College, Melbourne University, Australia, Edited by John Noye, Published by North-Holland Publishing Company, pp. 289-312.*

Wehausen, J.V. (1973): "The wave resistance of ships". *Adv. Appl. Mech., Vol. 13, pp. 93-245.*

Wehausen, J.V. and Laitone, E.V. (1960): "Surface waves". *In Handbuch der Physik, Springer-Verlag, Berlin, Bd. IX, Vol. 9, pp. 446-778.*

Weinblum, G. (1963): "On problems of wave resistance research". *Int. Sem. Theor. Wave Resistance, Ann. Arbor., pp. 1-44.*

Wigley, W.C.S. (1949): "L'Etat actuel des calculs de resistance de vagues". *Bell. Ass. Tech. Mar. Aeron., Vol. 48, pp. 533-564.*

Xia, F. (1986): "Numerical calculation of flows, with special emphasis on the free surface potential flow". *Ph.D. Thesis, Chalmers University of Technology, Sweden.*

Xia, F. and Larsson, L. (1986): "A calculation method for the lifting potential flow around yawed surface piercing 3-D bodies". *Proc. the 16th Symp. on Naval Hydrodynamics, Berkeley, pp. 583–595.*

Xu Q. and Mori (1988): "Numerical simulation of 3-D nonlinear water waves by boundary element method (In the case of submerged bodies)". *J. of the Soc. of Navel Architects of Japan, Vol. 165, pp. 9–15.*

Zhang, J. , Feng, Y. , Lu, G. , Zeng, Q. , Lin, J. and Wu, G. (1983): "Report on ITTC Cooperative experiments for series 60, C_b = 0.60 hull form". *China Ship Scientific Research Center, Wuxi, China.*

Sclavounos, P.D. (1992): "On the quadratic effect of random gravity waves on a vertical boundary". *J. of Fluid Mech., Vol. 242, pp. 475–489.*

APPENDICES

A. Integration of $[x(i) - x(q)]T(j)/r^3(i,q)$

In the application of linear element techniques in the boundary integral method, the following integrals have to be computed.

$$a_u(i,j) = \int_{S(j)} \frac{-[x(i) - x(q)]}{r^3(i,q)} T(j) dS(q); \tag{A.1}$$

$$a_v(i,j) = \int_{S(j)} \frac{-[y(i) - y(q)]}{r^3(i,q)} T(j) dS(q); \tag{A.2}$$

and

$$a_w(i,j) = \int_{S(j)} \frac{-[z(i) - z(q)]}{r^3(i,q)} T(j) dS(q); \tag{A.3}$$

where $a_u(i,j)$, $a_v(i,j)$, and $a_w(i,j)$ are the elements of the velocity coefficient matrices used in both the direct and indirect boundary integral formulations. In the above equations i is a field point on the mesh; j represents the collocation point; $S(j)$ represent the area of all the panels surrounding j (they all have one vertex at j, see Fig. A.1); and r is the distance between i and the integral element area $dS(q)$, which is

$$r(i,q) = \sqrt{[x(i) - x(q)]^2 + [y(i) - y(q)]^2 + [z(i) - z(q)]^2} \,. \tag{A.4}$$

It is noted that $[x(q), y(q), z(q)]$ represents the integration point on the elements surrounding j. $x(q)$, $y(q)$, and $z(q)$ are variables of integration.

The integration is performed by considering two cases, which are the case of field point i being not on the collocation point j, i.e. $i \neq j$, and the case of i being on j, i.e. $i = j$. It is the object of the present appendix to discuss both the numerical integration algorithm for case 1 and the analytical formula for case 2.

Case 1. i not on j

Since all the integrals given by equations (A.1), (A.2) and (A.3) are computed in the same way, (A.1) is used as an example for the discussion in this appendix.

The integration of equation (A.1) goes through all the panels surrounding node point j. Let $ne(j)$ represents the number of panels surrounding j, equation (A.1) can be rewritten as:

$$a_u(i,j) = -\sum_{q=1}^{ne(j)} \int_{S(q)} \frac{[x(i)-x(q)]}{r(i,q)} T(j,q) dS(q), \tag{A.5}$$

where $S(q)$ represents the area of element q; $T(j,q)$ represents part of the tent $T(j)$, which covers only panel q, (see Fig. A.1). By introducing a local numbering system $T(j,q)$ can be explained more clearly. Giving three numbers q(1), q(2),and q(3) to the three vertices of panel q with numbering q(1) at j, and q(2), g(3) anti-clockwise numbering the rest of the two vertices of q, $T(j,q)$ takes the values

$$T[j,q(1)] = 1; \tag{A.6}$$

$$T[j,q(2)] = 0; \tag{A.7}$$

$$T[j,q(3)] = 0. \tag{A.8}$$

Now, the computation of the integral (A.1) becomes the computations of $ne(j)$ number of integrals given in equation (A.5). We have

$$I_u(i,j) = \int_{S(q)} [\frac{x(i)-x(q)}{r(i,q)}] T(j,q) dS(q). \tag{A.9}$$

In the present procedure a mapping technique is used instead of using the global coordinate system. Through the mapping, a triangular element q defined by its vertices at $q(1) = [x(1), y(1), z(1)]$, $q(2) = [x(2), y(2), z(2)]$, and $q(3) =$

$[x(3), y(3), z(3)]$ is mapped into a right-angle triangle in the plane (ξ, ζ) with its three vertices at $(\xi_1, \zeta_1) = (1,0)$, $(\xi_2, \zeta_2) = (0,1)$, $(\xi_3, \zeta_3) = (0,0)$. The linear mapping is in the form:

$$x(q) = [x(1) - x(3)]\xi + [x(2) - x(3)]\zeta + x(3)\,; \tag{A.10}$$

$$y(q) = [y(1) - y(3)]\xi + [y(2) - y(3)]\zeta + y(3)\,; \tag{A.11}$$

$$z(q) = [z(1) - z(3)]\xi + [z(2) - z(3)]\zeta + z(3)\,. \tag{A.12}$$

The linear mapping maps $q(1)$, the number 1 vertex of q, on to $[\xi(1), \zeta(1)] = (1,0)$; $q(2)$, the number 2 vertex of q, on to $[\xi(2), \zeta(2)] = (0,1)$; and $q(3)$, the number 3 vertex of q, on to $[\xi(3), \zeta(3)] = (0,0)$. The linear mapping also maps the tent function $T(j,q)$ into

$$T(\xi, \zeta) = \xi\,. \tag{A.13}$$

Applying the linear mapping to expression (A.9) gives

$$I_u[i; (\xi = 1, \zeta = 0)] = \int_0^1 \int_0^{\zeta - 1} -\frac{\{x(i) - [x(1) - x(3)]\xi - [x(2) - x(3)]\zeta - x(3)\}}{r^3(i; \xi, \zeta)} \xi\, d\xi\, d\zeta, \tag{A.14}$$

where, $r(i; \xi, \zeta)$ is given as:

$$\begin{aligned} r(i; \xi, \zeta) \;=\; & \{[x(i) - (x(1) - x(3))\xi - (x(2) - x(3))\zeta - x(3)]^2 \\ & + [y(i) - (y(1) - y(3))\xi - (y(2) - y(3))\zeta - y(3)]^2 \\ & + [x(i) - (z(1) - z(3))\xi - (z(2) - z(3))\zeta - z(3)]^2\}^{(1/2)}\,. \end{aligned} \tag{A.15}$$

The integration in expression (A.14) is performed numerically by using the Gauss-Kronrod integration formula.

Then $I_u(i,j)$ is obtained by remapping $I_u(i;\xi,\zeta)$ back to the original coordinate system, which is

$$I_u(i,j) = |J| I_u[i;(\xi = 1, \zeta = 0)]\,. \tag{A.16}$$

where $|J|$ is the Jacobian transformation, which is given as:

$$|J| = \sqrt{J_1^2 + J_2^2 + J_3^2}\,, \tag{A.17}$$

with

$$J_1 = [y(1) - y(3)][z(2) - z(3)] - [y(2) - y(3)][z(1) - z(3)]\,; \tag{A.18}$$

$$J_2 = [x(2) - x(3)][z(1) - z(3)] - [x(1) - x(3)][z(2) - z(3)]\,; \tag{A.19}$$

$$J_3 = [x(1) - x(3)][y(2) - y(3)] - [x(2) - x(3)][y(1) - y(3)]\,. \tag{A.20}$$

It is note that in the mapping procedure from equation (A.9) to equation (A.14), $x(i)$, $y(i)$ and $z(i)$ were not changed. This is because they are treated as constants in the integrals.

Case 2. i on j

When the field point i is on the collocation point j, the integration of equations (A.1), (A.2), (A.3) becomes special cases, since $r(i,j) = 0$. The integrands in these integrals are infinity at node point j. The numerical integration scheme for Case 1 can not be sued to computed the integrals.

It is known that the total velocity induced by a unit source at j is

$$\vec{V} = \lim_{r \to 0} \int_S \frac{1}{r^2} [\vec{n}(j) \cdot \vec{n}(S)] dS\,, \tag{A.21}$$

where S is the unwetted part of the surface area of a sphere of diameter $2r$ and centered at j. Consider a sphere with its diameter of $2r$ centered at j, which is called here the covering sphere, this sphere is cut into two parts by the paneled surface. S is the area of one of these two parts which is inside the body or the unwetted part. The reason of define S to be the area of the unwetted part of the sphere is because of the definition of $r(i,j)$. When $r(i,j)$ is defined as:

$$r(i,j) = \sqrt{[x(i) - x(j)]^2 + [y(i) - y(j)]^2 + [z(i) - z(j)]^2}\,, \qquad \text{(A.22)}$$

S should be chosen the unwetted part, while $r(i,j)$ is defined as:

$$r(i,j) = \sqrt{[x(j) - x(i)]^2 + [y(j) - y(i)]^2 + [z(j) - z(i)]^2}\,, \qquad \text{(A.23)}$$

S should then be chosen the wetted part. Physically, S is determined by the direction of the source. When the source goes into the body S should be defined by the unwetted part, otherwise the wetted part. And the definition of $r(i,j)$ determines the direction of the source.

Also in Equation (A.21), $\vec{n}(j)$ is the inside unit normal vector to the paneled body surface at j, and $\vec{n}(S)$ represents the outside unit surface normal vector to the covering sphere; The velocity component in x direction induced by a unit source at point j which is equal to $a_u(j,j)$ can then be given as:

$$a_u(j,j) = \vec{V} n_x = n_x(j) \lim_{r \to 0} \int_S \frac{1}{r^2} dS\,, \qquad \text{(A.24)}$$

where $n_x(j)$ is the component of $\vec{n}(j)$ in the x direction.

Now the problem of calculating $a_u(j,j)$ becomes calculating the limit integration which is the solid angle

$$\beta = \lim_{r \to 0} \int_S \frac{1}{r^2} dS\,, \qquad \text{(A.25)}$$

and

$$a_u(j,j) = n_x(j)\beta\,. \tag{A.26}$$

β represent the solid angle at node point j subtended by the panels surrounding j which is the surface area of the unwetted part of a unit covering sphere.

To compute the solid angle, a local coordinate system (x'', y'', z'') is adopted with z'' in the direction of $\vec{n}(j)$, where $\vec{n}(j)$ represents the inside normal at point j of the paneled surface. The relation between the local coordinate system and the global coordinate system is found to be

$$x'' = n_{yz}x' - n_x z'; \tag{A.27}$$

$$y'' = y'; \tag{A.28}$$

$$z'' = n_x + n_{yz}z'; \tag{A.29}$$

where

$$x' = x - x(j); \tag{A.30}$$

$$y' = \frac{1}{n_{yz}}[n_x(y - y(j)) - n_y(z - z(j))]; \tag{A.31}$$

$$z' = \frac{1}{n_{yz}}[n_y(y - y(j)) - n_x(z - z(j))]\,. \tag{A.32}$$

And

$$n_{yz} = \sqrt{n_y^2 + n_z^2}\,. \tag{A.33}$$

n_x, n_y and n_z are the components of $\vec{n}(j)$ in the directions of x, y, and z, respectively.

By expressing coordinates of all the panels surrounding j in the local coordinate system, the intersecting points of the panels and the unit covering sphere

can be found in terms of local coordinate system. Each panel has two intersecting points with the unite covering sphere. These two points plus the intersecting point q_n of the normal $\vec{n}$ with the unit sphere, three points on the unit covering sphere are determined for each panel. The sphere area between these three points is calculated from spherical trigonometry we have

$$\beta(q) = 4 \arctan \sqrt{\tan(\frac{\alpha}{2}) \tan(\frac{\alpha - \alpha_1}{2}) \tan(\frac{\alpha - \alpha_2}{2}) \tan(\frac{\alpha - \alpha_3}{2})}, \qquad (A.34)$$

where $\alpha = (\alpha_1 + \alpha_2 + \alpha_3)/2$, and α_i is the plane angle at q_n subtended by side i of the triangular panel q, $i = 1, 2, 3$.

The unwetted solid angle is then calculated by

$$\beta = \sum_{q=1}^{ne(j)} \beta(q). \qquad (A.35)$$

where $ne(q)$ is the total number of panels surrounding the collocation point j.

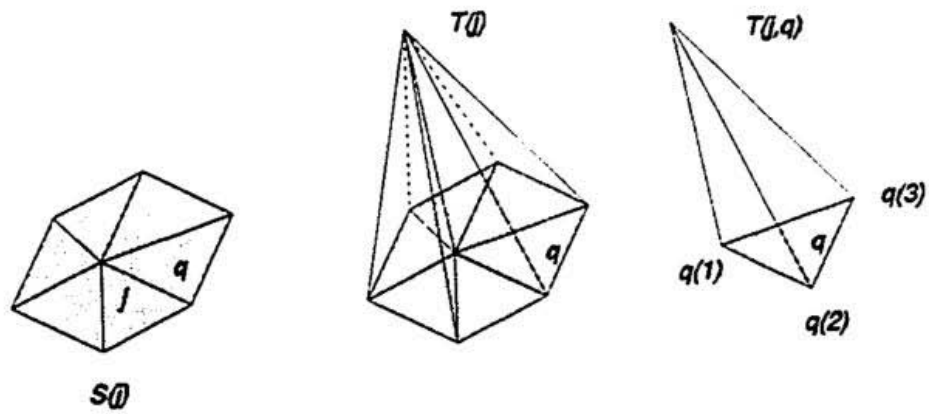

Fig. A.1 The tent function and it supporting elements

B. Integration of $T(j)/r(i,q)$

In applying the direct boundary integral theory by using the linear element techniques, the follc·ving integral is one the most important integrals need to be computed.

$$b(i,j) = \int_{S(j)} \frac{1}{r(i,q)} T(j) dS(q), \tag{B.1}$$

where $b(i,j)$ are the elements of the influence coefficient matrix B. Equation (B.1) is further written as the summary of panels surrounding j as:

$$b(i,j) = \sum_{q=1}^{ne(j)} \int_{S(q)} \frac{1}{r(i,q)} T(j,q) dS(q), \tag{B.2}$$

Now the problem becomes calculating the integral of

$$I(i,j) = \int_{S(q)} \frac{1}{r(i,q)} T(j,q) dS(q). \tag{B.3}$$

The computation of this integral for the case of $i \neq j$ is the same as the computation of equation (A.1) discussed in Appendix A. The same routines of computing integral (A.1) were used to compute this integral by simply changing the integrand. In this appendix the theoretical integration for the case of $i = j$ is detailed.

By introducing a local polar coordinate system with its original at j, (see Fig. B.1), the tent function $T(j,q)$ can be written as:

$$T(j,q) = T(r,\theta) = 1 - \frac{r\cos\theta}{S_{12}} - [\frac{1}{S_{13}\sin\alpha} - \frac{\cos\alpha}{S_{12}\sin\alpha}] r\sin\theta. \tag{B.4}$$

Equation (B.3) can then be written as:

$$I(i,j=i) = \int_0^{\alpha} \int_0^{r_{23}(\theta)} \{1 - \frac{r\cos\theta}{S_{12}} - [\frac{1}{S_{13}\sin\alpha} - \frac{\cos\alpha}{S_{12}\sin\alpha}] r\sin\theta\} \frac{1}{r} dS, \tag{B.5}$$

where

$$dS = r dr d\theta\,, \tag{B.6}$$

$$r_{23}(\theta) = \frac{c}{a\cos\theta + b\sin\theta}\,, \tag{B.7}$$

and

$$a = S_{13}\sin\alpha\,, \tag{B.8}$$

$$b = S_{12} - S_{13}\cos\alpha\,, \tag{B.9}$$

$$c = S_{12}S_{13}\sin\alpha\,, \tag{B.10}$$

and S_{12}, S_{23} and S_{23} are the length of the three sides of panel q, (see Fig. B.1), which can be calculated directly through the coordinate of the three vertices of panel q.

Substituting equation (B.6) into equation (B.5) gives

$$I(i,j=i) = \int_0^{\alpha}\int_0^{r_{23}(\theta)}[1 - \frac{r\cos\theta}{S_{12}} - (\frac{1}{S_{13}\sin\alpha} - \frac{\cos\alpha}{S_{12}\sin\alpha})r\sin\theta]dr d\theta\,. \tag{B.11}$$

Performing the integration with respect to dr gives

$$I(i,j=i) = -\frac{c^2}{2S_{12}}I_I - \frac{c^2}{2}(\frac{1}{S_{13}\sin\alpha} - \frac{\cos\alpha}{S_{12}\sin\alpha})I_{II} + cI_{III}\,, \tag{B.12}$$

where I_I, I_{II} and I_{III} are three integrals with respect to $d\theta$, they are

$$I_I = \int_0^{\alpha}\frac{\cos\theta}{(a\cos\theta + b\sin\theta)^2}d\theta\,; \tag{B.13}$$

$$I_{II} = \int_0^{\alpha}\frac{\sin\theta}{(a\cos\theta + b\sin\theta)^2}d\theta\,; \tag{B.14}$$

$$I_{III} = \int_0^{\alpha}\frac{1}{(a\cos\theta + b\sin\theta)}d\theta\,. \tag{B.15}$$

Performing the integration for the above three integrals gives

$$I_I = \frac{-b^2\sin\alpha}{d^2(d^2\sin^2\alpha - a^2)} + \frac{-ab\cos\alpha}{d^2(d^2\cos^2\alpha - b^2)} + \frac{b}{d^2a} + \frac{a}{2d^3}V_{6n}\,; \tag{B.16}$$

$$I_{II} = \frac{a^2 \cos\alpha}{d^2(d^2\cos^2\alpha - b^2)} + \frac{ab\sin\alpha}{d^2(d^2\sin^2\alpha - a^2)} - \frac{1}{d^2} + \frac{b}{2d^3} V_{\ell n}\,; \quad \text{(B.17)}$$

$$I_{III} = \frac{1}{2d} V_{\ell n}\,. \quad \text{(B.18)}$$

In the above equations

$$V_{\ell n} = \ln\left(\frac{d\cos\alpha - b}{d\cos\alpha + b}\frac{d + b}{d - b}\frac{a + d\sin\alpha}{a - d\sin\alpha}\right). \quad \text{(B.19)}$$

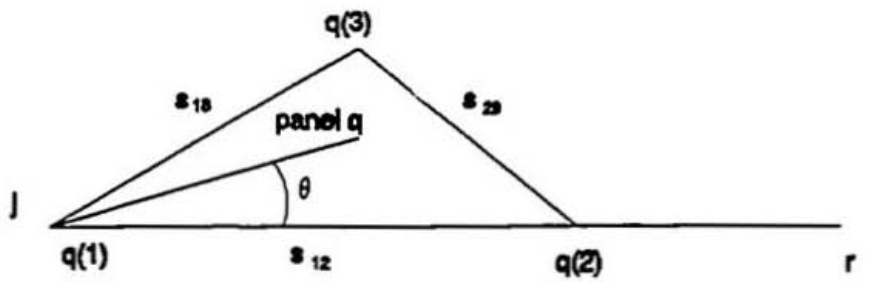

Fig. B.1 Local polar coordinate system

C. Free Surface Panelization

In applying the indirect algorithm developed in the present study to solve a submerged body generated wave problem, the fluid free surface is discretized into triangular panels which are bounded by the streamlines. Prior to the generation of the streamlines, the size of the surface mesh and the size of the panels have to be determined. The size of the surface mesh and the size of the panels are determined as the function of the size and the velocity of the body under consideration. The length of the surface mesh is determined by the wave length generated by the moving body. The wave length is a function of the Froude number F_n which is defined as: $F_n = U/\sqrt{gL}$, with L the characteristic length of the body. The length of the surface mesh is calculated by the following equation:

$$L_m = \alpha L_w, \tag{C.1}$$

where L_m is the length of the surface mesh; α is a coefficient representing the number of waves modelled by the mesh on the free surface; and L_w is the length of the wave which is determined by the Froude F_n, in the form :

$$L_w = 2\pi F_n L. \tag{C.2}$$

The element size S_x in the x direction, is considered uniformly through the mesh. The size of an element in this direction is proportional to the wave length. From the numerical tests it is found that S_x between $L_w/20$ to $L_w/12$ would be suitable for submerged object cases.

The element size in the y direction determines the location of the streamlines. The element size in that direction, at the leftmost edge of the surface mesh must

be determined before generating the streamlines. In the present computations, to save computational resources and increase the accuracy, the element size in y direction is arranged in a way so that closer to the body the size of elements is relatively smaller than the size of those elements away from the body. On the leftmost edge of the surface mesh the element size in y direction is calculated by

$$y_i = (i-1)[\Delta y + \beta \Delta y(i-1)]\,, \tag{C.3}$$

where $\Delta y = 1.5 L_w/(n_s - 1)$ and n_s is the number of streamlines; β is a constant controlling the size increment along y.

The location of the surface mesh relative to the body, which is defined by the distance between the leftmost edge of the mesh and the front of the body D_f, is also needed to be determined. Numerical tests show that $D_f \geq L_w$ would be suitable for the submerged object cases. In the present computations the relation $D_f = L_w$ is used. Numerical experiments also show that the location of the front of the wave generated by the body does not depend on the location of the mesh as long as D_f is chosen large enough, (see Baddour, Pawlowski and Song 1991).

D. Finite Difference Operators

D.1 Three-point centered finite difference operator

The finite difference operators used in the present study are obtained through a general finite difference approximation formulation which is expressed in terms of Lagrange coefficient polynomial. The formula is given as:

$$f'(x_k) = \sum_{j=1}^{n+1} f(x_j) L'_j(x_k) + \frac{f^{(n+1)}(\xi(x_k))}{(n+1)!} \prod_{j=1, j\neq k}^{n+1} (x_k - x_j), \qquad (D.1)$$

where $L'_j(x_k)$ denotes the first order derivative of the $(k-1)th$ Lagrange interpolating polynomial for function $f(x)$ at $x_1, x_2, ...x_{n+1}$. The $(k-1)th$ Lagrange interpolating polynomial is given as:

$$L_j(x_k) = \frac{(x-x_1)(x-x_2)...(x-x_{k-1})(x-x_{k+1})...(x-x_{n+1})}{(x_k-x_1)(x_k-x_2)...(x_k-x_{k-1})(x_k-x_{k+1})...(x_k-x_{n+1})},$$
$$for\ each\ k = 1, 2, ...(n+1). \qquad (D.2)$$

Equation (D.1) is called an $(n+1)$-point formula to approximate $f'(x_k)$, since a linear combination of the $(n+1)$ values $f'(x_j)$ is used for $j = 1, 2, ..., (n+1)$.

In general, using more evaluation points in equation (D.1) produces greater accuracy, although the number of functional evaluations and growth of rounding error discourages this somewhat. The most common formulas are those involving three and five evaluation points. In the present study, both the three and five points formulas are used in the algorithm.

To obtain a three-point formula the three-point Lagrange coefficient polynomial and its first order derivatives at the three points are need to be derived, which is given as:

$$L_1(x) = \frac{(x-x_2)(x-x_3)}{(x_1-x_2)(x_1-x_3)}; \qquad (D.3)$$

$$L_2(x) = \frac{(x-x_1)(x-x_3)}{(x_2-x_1)(x_2-x_3)}\,; \tag{D.4}$$

$$L_3(x) = \frac{(x-x_1)(x-x_2)}{(x_3-x_1)(x_3-x_2)}\,; \tag{D.5}$$

$$L_1'(x) = \frac{(x-x_2)+(x-x_3)}{(x_1-x_2)(x_1-x_3)}\,; \tag{D.6}$$

$$L_1'(x) = \frac{(x-x_1)+(x-x_3)}{(x_2-x_1)(x_2-x_3)}\,; \tag{D.7}$$

$$L_1'(x) = \frac{(x-x_1)+(x-x_2)}{(x_3-x_1)(x_3-x_2)}\,. \tag{D.8}$$

Hence, from equation (D.1)

$$\begin{aligned} f'(x_j) = {} & f(x_1)[\frac{(x_j-x_2)+(x_j-x_3)}{(x_1-x_2)(x_1-x_3)}] \\ & +f(x_2)[\frac{(x_j-x_1)+(x_j-x_3)}{(x_2-x_1)(x_2-x_3)}] \\ & +f(x_3)[\frac{(x_j-x_1)+(x_j-x_2)}{(x_3-x_1)(x_3-x_2)}]\,. \end{aligned} \tag{D.9}$$

To obtain a centered three-point operator j is set to be equal to 2 and write $f'(x)$ in a general form with respect to the center point i

$$f'(\bar{x}_i) = F3D1(i)f(\bar{x}_{i-1}) + F3D2(i)f(\bar{x}_i) + F3D3(i)f(\bar{x}_{i+1})\,, \tag{D.10}$$

where $\bar{x}_i = (x_i, y_i, z_i)$, and

$$F3D1(i) = S_{i,(i+1)}/[S_{(i-1),i}S_{(i-1),(i+1)}]\,; \tag{D.11}$$

$$F3D2(i) = 1/S_{i,(i-1)} + 1/S_{i,(i+1)}\,; \tag{D.12}$$

$$F3D3(i) = S_{i,(i-1)}/[S_{(i+1),(i-1)}S_{(i+1),i}]\,; \tag{D.13}$$

$$S_{(i-1),i} = -\sqrt{(x_{i-1}-x_i)^2+(y_{i-1}-y_i)^2+(z_{i-1}-z_i)^2}\,;$$

$$
\begin{aligned}
S_{(i-1),(i+1)} &= -\sqrt{(x_{i-1}-x_{i+1})^2+(y_{i-1}-y_{i+1})^2+(z_{i-1}-z_{i+1})^2}\,; \\
S_{i,(i-1)} &= \sqrt{(x_i-x_{i-1})^2+(y_i-y_{i-1})^2+(z_i-z_{i-1})^2}\,; \\
S_{i,(i+1)} &= -\sqrt{(x_i-x_{i+1})^2+(y_i-y_{i+1})^2+(z_i-z_{i+1})^2}\,; \\
S_{(i+1),(i-1)} &= \sqrt{(x_{i+1}-x_{i-1})^2+(y_{i+1}-y_{i-1})^2+(z_{i+1}-z_{i-1})^2}\,; \\
S_{(i+1),i} &= \sqrt{(x_{i+1}-x_i)^2+(y_{i+1}-y_i)^2+(z_{i+1}-z_i)^2}\,.
\end{aligned}
$$

In the above equations $(x_{i-1}, y_{i-1}, z_{i-1})$, (x_i, y_i, z_i) and $(x_{i+1}, y_{i+1}, z_{i+1})$ are the coordinates of the three points.

D.2 Five-point centered finite difference operator

Following the way as explained in the three-point operator, the five-point centered finite difference operator is obtained as:

$$
\begin{aligned}
f'(\bar{x}_i) &= F5D1(i)f(\bar{x}_{i-2}) + F5D2(i)f(\bar{x}_{i-1}) + F5D3(i)f(\bar{x}_i) \\
&\quad + F5D4(i)f(\bar{x}_{i+1}) + F5D5(i)f(\bar{x}_{i+2}),
\end{aligned} \tag{D.14}
$$

where

$$
\begin{aligned}
F5D1(i) &= S_{i,(i-1)}S_{i,(i+1)}S_{i,(i+2)}/[S_{(i-2),(i-1)}S_{(i-2),i}S_{(i-2),(i+1)}S_{(i-2),(i+2)}]\,; \\
F5D2(i) &= S_{i,(i-2)}S_{i,(i+1)}S_{i,(i+2)}/[S_{(i-1),(i-2)}S_{(i-1),i}S_{(i-1),(i+1)}S_{(i-1),(i+2)}]\,; \\
F5D3(i) &= 1/S_{i,(i-2)} + 1/S_{i,(i-1)} + 1/S_{i,(i+1)} + 1/S_{i,(i+2)}\,; \\
F5D4(i) &= S_{i,(i-2)}S_{i,(i-1)}S_{i,(i+2)}/[S_{(i+1),(i-2)}S_{(i+1),(i-1)}S_{(i+1),i}S_{(i+1),(i+2)}]\,; \\
F5D5(i) &= S_{i,(i-2)}S_{i,(i-1)}S_{i,(i+1)}/[S_{(i+2),(i-2)}S_{(i+2),(i-1)}S_{(i+2),i}S_{(i+2),(i+1)}]\,.
\end{aligned}
$$

And

$$
S_{(i-2),(i-1)} = -\sqrt{(x_{i-2}-x_{i-1})^2+(y_{i-2}-y_{i-1})^2+(z_{i-2}-z_{i-1})^2}\,;
$$

$$
\begin{aligned}
S_{(i-2),i} &= -\sqrt{(x_{i-2}-x_i)^2+(y_{i-2}-y_i)^2+(z_{i-2}-z_i)^2}\,;\\
S_{(i-2),(i+1)} &= -\sqrt{(x_{i-2}-x_{i+1})^2+(y_{i-2}-y_{i+1})^2+(z_{i-2}-z_{i+1})^2}\,;\\
S_{(i-2),(i+2)} &= -\sqrt{(x_{i-2}-x_{i+2})^2+(y_{i-2}-y_{i+2})^2+(z_{i-2}-z_{i+2})^2}\,;\\
S_{(i-1),(i-2)} &= \sqrt{(x_{i-1}-x_{i-2})^2+(y_{i-1}-y_{i-2})^2+(z_{i-1}-z_{i-2})^2}\,;\\
S_{(i-1),i} &= -\sqrt{(x_{i-1}-x_i)^2+(y_{i-1}-y_i)^2+(z_{i-1}-z_i)^2}\,;\\
S_{(i-1),(i+1)} &= -\sqrt{(x_{i-1}-x_{i+1})^2+(y_{i-1}-y_{i+1})^2+(z_{i-1}-z_{i+1})^2}\,;\\
S_{(i-1),(i+2)} &= -\sqrt{(x_{i-1}-x_{i+2})^2+(y_{i-1}-y_{i+2})^2+(z_{i-1}-z_{i+2})^2}\,;\\
S_{i,(i-2)} &= \sqrt{(x_i-x_{i-2})^2+(y_i-y_{i-2})^2+(z_i-z_{i-2})^2}\,;\\
S_{i,(i-1)} &= \sqrt{(x_i-x_{i-1})^2+(y_i-y_{i-1})^2+(z_i-z_{i-1})^2}\,;\\
S_{i,(i+1)} &= -\sqrt{(x_i-x_{i+1})^2+(y_i-y_{i+1})^2+(z_i-z_{i+1})^2}\,;\\
S_{i,(i+2)} &= -\sqrt{(x_i-x_{i+2})^2+(y_i-y_{i+2})^2+(z_i-z_{i+2})^2}\,;\\
S_{(i+1),(i-2)} &= \sqrt{(x_{i+1}-x_{i-2})^2+(y_{i+1}-y_{i-2})^2+(z_{i+1}-z_{i-2})^2}\,;\\
S_{(i+1),(i-1)} &= \sqrt{(x_{i+1}-x_{i-1})^2+(y_{i+1}-y_{i-1})^2+(z_{i+1}-z_{i-1})^2}\,;\\
S_{(i+1),i} &= \sqrt{(x_{i+1}-x_i)^2+(y_{i+1}-y_i)^2+(z_{i+1}-z_i)^2}\,;\\
S_{(i+1),(i+2)} &= -\sqrt{(x_{i+1}-x_{i+2})^2+(y_{i+1}-y_{i+2})^2+(z_{i+1}-z_{i+2})^2}\,;\\
S_{(i+2),(i-2)} &= \sqrt{(x_{i+2}-x_{i-2})^2+(y_{i+2}-y_{i-2})^2+(z_{i+2}-z_{i-2})^2}\,;\\
S_{(i+2),(i-1)} &= \sqrt{(x_{i+2}-x_{i-1})^2+(y_{i+2}-y_{i-1})^2+(z_{i+2}-z_{i-1})^2}\,;\\
S_{(i+2),i} &= \sqrt{(x_{i+2}-x_i)^2+(y_{i+2}-y_i)^2+(z_{i+2}-z_i)^2}\,;\\
S_{(i+2),(i+1)} &= -\sqrt{(x_{i+2}-x_{i+1})^2+(y_{i+2}-y_{i+1})^2+(z_{i+2}-z_{i+1})^2}\,.
\end{aligned}
$$

In the above equation $(x_{i-2}, y_{i-2}, z_{i-2})$, $(x_{i-1}, y_{i-1}, z_{i-1})$, (x_i, y_i, z_i), $(x_{i+1}, y_{i+1}, z_{i+1})$, and $(x_{i+2}, y_{i+2}, z_{i+2})$ are the coordinates of the five points.

D.3 Four-point centered finite difference operator

The coefficients of the four-point finite difference formula are given as:

$$F4D4(i) = [S_{(i-1),i}]^2[S_{(i-2),i}]^2 S_{(i-2),(i-1)}[S_{(i-2),i} + S_{(i-1),i}]/D_i ; \quad (D.15)$$

$$F4D3(i) = [S_{(i-1),i}]^2[S_{(i-3),i}]^2 S_{(i-3),(i-1)}[S_{(i-3),i} + S_{(i-1),i}]/D_i ; \quad (D.16)$$

$$F4D2(i) = [S_{(i-2),i}]^2[S_{(i-3),i}]^2 S_{(i-3),(i-2)}[S_{(i-3),i} + S_{(i-2),i}]/D_i ; \quad (D.17)$$

$$F4D1(i) = -(F4D2(i) + F4D3(i) + F4D3(i))/D_i ; \quad (D.18)$$

$$D_i = -[S_{(i-1),i}S_{(i-2),i}S_{(i-3),i}S_{(i-3),(i-1)}S_{(i-2),(i-1)}S_{(i-3),(i-2)} (S_{(i-3),i} + S_{(i-2),i} + S_{(i-1),i})] , \quad (D.19)$$

where

$$S_{(i-1),i} = \sqrt{(x_{i-1} - x_i)^2 + (y_{i-1} - y_i)^2 + (z_{i-1} - z_i)^2} ;$$

$$S_{(i-2),(i-1)} = \sqrt{(x_{i-2} - x_{i-1})^2 + (y_{i-2} - y_{i-1})^2 + (z_{i-2} - y_{i-1})^2} ;$$

$$S_{(i-3),(i-2)} = \sqrt{(x_{i-3} - x_{i-2})^2 + (y_{i-3} - y_{i-2})^2 + (z_{i-3} - z_{i-2})^2} ;$$

$$S_{(i-2),i} = S_{(i-1),i} + S_{(i-2),(i-1)} ;$$

$$S_{(i-3),i} = S_{(i-3),(i-2)} + S_{(i-2),(i-1)} + S_{(i-1),i} ;$$

$$S_{(i-3),(i-1)} = S_{(i-3),(i-2)} + S_{(i-2),(i-1)} .$$

And $(x_{(-3}, y_{i-3}, z_{i-3})$, $(x_{i-2}, y_{i-2}, z_{i-2})$, $(x_{i-1}, y_{i-1}, z_{i-1})$, and (x_i, y_i, z_i) are the coordinates of the four points.